

SIZING AND SCHEDULING SOLAR PHOTOVOLTAIC BATTERY SYSTEMS FOR  
PEAK ELECTRICAL DEMAND MANAGEMENT

A Dissertation

by

HUSSEIN SALEH SULAIMAN SHARADGA

Submitted to the Graduate and Professional School of  
Texas A&M University  
in partial fulfillment of the requirements for the degree of

DOCTOR OF PHILOSOPHY

Chair of Committee,	Bryan Rasmussen
Committee Members,	Richard Malak
	Ying Li
	Juan Carlos Baltazar
Head of Department,	Guillermo Aguilar

August 2022

Major Subject: Mechanical Engineering

Copyright 2022 Hussein Sharadga

## ABSTRACT

For Texas commercial and industrial customers, peak electrical demand charges are largely based on the highest 15-minute monthly peak. By storing energy from photovoltaic cells in batteries for use during high-demand times, electrical utility customers can shave the electrical demand peak by load-shifting. The potential for this type of load shifting strategy is demonstrated in this study using data from commercial buildings located in Texas.

Shaving the monthly peak demand is a challenging optimization problem due to the long scheduling horizon of one month. Moreover, the initial and the operation costs of both the photovoltaic system and battery storage are significant; thus, the sizes of these systems need to be optimized. To optimize a photovoltaic battery system, the sizing and the scheduling problems are solved in tandem. One year's worth of data is usually considered for sizing energy systems, but scheduling the load over one year is computationally intensive. Consequently, sizing a photovoltaic battery system for peak shaving under Texas's electricity tariff is a complex optimization problem.

In its most basic form, shaving peak electrical demand is achieved by judiciously scheduling battery storage, assuming knowledge of photovoltaic and load profiles. Forecasting errors of the photovoltaic and load profiles to construct the schedule might lead to higher peaks. Therefore, scheduling a photovoltaic battery system for peak shaving requires a real-time control mechanism to manage the PV power and load uncertainties.

In this work, a framework based on convex optimization is developed for sizing combined photovoltaic battery systems under different pricing policies. In addition, a

control scheme is established to shave the electrical site demand peak with long control-horizon and propagated uncertainty based on stochastic dual-dynamic programming. Also, the sophisticated prediction methods are replaced by simple estimation methods based on imitating the patterns as well as the sub-optimality decision-making.

Overall, this research has led to great contributions to grid-connected energy storage sizing and scheduling. The results show that reformulating the optimization problem reduces the problem complexity significantly. Furthermore, the effectiveness of scheduling battery storage in shaving the demand peak under the uncertainty of prediction for different buildings was investigated in this study.

## DEDICATION

To my parents and my only sister, Rahmeh Sharadgah

## ACKNOWLEDGEMENTS

I would like to thank my research advisor, Dr. Bryan Rasmussen for his advising and assistance at every stage of my Ph.D. I would also like to express my gratitude to Dr. Richard Malak, Dr. Ying Li, and Dr. Juan Carlos Baltazar, for serving on my committee and for their insightful comments and suggestions.

I would like to thank all my research team, for their help and friendship. I also want to extend my thanks to all my friends and colleagues in College Station, for making these years a great experience.

Finally, thanks to my parents, my five brothers, my only sister Rahmeh Sharadgah, my nephews, Hamzeh and Zain, for their love, encouragement, and emotional support. My appreciation also goes out to all the support I received from the rest of my relatives in Jordan (my elder uncle Abdallah, Mo'men Sharadga, Odai Nawafleh, Basheer Mugdadi,to name a few).

## CONTRIBUTORS AND FUNDING SOURCES

### **Contributors**

This work was supervised by a dissertation committee consisting of Dr. Bryan Rasmussen, Dr. Richard Malak and Dr. Ying Li of the Department of Mechanical Engineering, and Dr. Juan Carlos Baltazar of the Department of Architecture. All work conducted for the dissertation was completed by Hussein Sharadga, under the advisement of Dr. Bryan Rasmussen.

### **Funding Sources**

This study was supported by the Graduate Teaching Assistantship and the Continuing Student Fellowship from the J. Mike Walker '66 Department of Mechanical Engineering. The contents, views, and opinions portrayed in this work are solely the responsibility of the authors and do not necessarily represent the official views of any funding resources.

## NOMENCLATURE

$B$	binary variable
$C_{Bat}$	battery capacity [kWh]
$C_{PV}$	PV system capacity [W]
$DHI$	diffuse horizontal irradiance [W/m <sup>2</sup> ]
$DNI$	direct normal irradiance [W/m <sup>2</sup> ]
$E_{Bat}$	battery energy [kWh]
$E_L$	load energy [kWh]
$E_G$	grid energy [kWh]
$E_{PV}$	PV system energy [kWh]
$E_s(t)$	energy stored in the battery at time $t$ [kWh]
$E_s(t_0)$	initial energy stored in the battery [kWh]
$F$	linearization variable
$f$	linearization variable
$GHI$	global horizontal irradiance [W/m <sup>2</sup> ]
$I_m$	current at the maximum power point [A]
$I_{n,r}$	interest rate
$I_{f,r}$	inflation rate
$K(x_T)$	final cost which is a function of the final state ( $x_T$ )
$L$	life of a component in years
$L_t$	current cost
$LCC$	life cycle cost [\$/year]

$M$	big-M value
$N$	life of the system in years
$N_p$	number of modules connected in parallel
$N_{PV}$	total number of PV modules
$N_s$	number of modules connected in series
$P_G$	grid power [kW]
$P_m$	maximum PV power [W]
$P_{m, array}$	maximum PV power generated by PV array [W]
$P_{m, module}$	maximum PV power generated by one PV module [W]
$POA$	plane-of-array irradiance [W/m <sup>2</sup> ]
$Q$	the energy charged or discharged [kWh]
$S_{IC}$	the initial capital cost of the system [\$]
$S_{O\&M}$	the operation, and the maintenance cost [\$]
$S_{Rep}$	the replacement cost [\$]
$S_{Hardware}$	the price of the system's components [\$]
$S_{Civil}$	the civil/labor cost [\$]
$S_{O\&M,0}$	the operation and maintenance cost for the first year [\$]
$T$	control horizon
$T_a$	ambient temperature [K]
$T_c$	cell temperature [K]
$T_m$	module temperature [K]
$U_{PV}$	PV unit cost [\$/W]

$U_{Bat}$	battery unit cost [\$/kWh]
$U_{\text{salvage}}$	per unit salvage value
$u$	charging/discharging rate [1/hr.]
$u_t$	control decision, battery charging rate
$V$	expected future cost
$V_m$	voltage at the maximum power point [V]
$W$	exogenous discrete noise
$W_s$	wind speed [m/s]
$x_T$	final state
$x_t$	system state at time $t$
$X$	system states
$y$	linearization variable
$Z$	linearization variable

### Greek Letters

$\eta$	battery charging/discharging efficiency
$\theta$	angle of incidence
$\theta_z$	solar zenith angle
$\beta$	title angle of array
$\gamma$	azimuth angle of array
$\gamma_s$	solar azimuth

## **Abbreviations**

AR	autoregressive model
ARIMA	autoregressive integrated moving average model
CVX	convex optimization algorithm
GA	genetic algorithm
MPC	model predictive control
MPP	maximum power point
NN	neural network
PSO	particle swarm optimization
PV	photovoltaic
R	correlation coefficient
RMSE	root mean square error
ROI	return on investment
SDDP	stochastic dual dynamic programming
SDP	stochastic dynamic Programming
TOU	time of use

## TABLE OF CONTENTS

	Page
ABSTRACT .....	ii
DEDICATION .....	iv
ACKNOWLEDGEMENTS .....	v
CONTRIBUTORS AND FUNDING SOURCES.....	vi
NOMENCLATURE.....	vii
TABLE OF CONTENTS .....	xi
LIST OF FIGURES.....	xv
LIST OF TABLES .....	xx
1. INTRODUCTION.....	1
1.1. Current Status of Electricity Production .....	3
1.2. Energy Storage Technologies.....	5
1.3. Demand Management Programs .....	7
1.3.1. Demand Management Strategies.....	7
1.3.2. Electricity Pricing Models.....	8
1.4. Electrical Demand Database .....	8
1.5. Motivation of the Dissertation.....	11
1.6. Objective of the Dissertation.....	12
1.7. Organization of the Dissertation .....	13
2. SUMMARY OF CONTRIBUTIONS.....	15
2.1. Sizing PV-battery Systems for Peak Shaving Applications.....	18
2.1.1. Sizing Challenges .....	18
2.1.2. Solution Techniques .....	19
2.2. Real-time Peak Shaving Controller.....	25
2.2.1. Uncertainty of Prediction .....	26
2.2.2. Time Frame of the Decision.....	30
2.2.3. Different Prediction Methods .....	33

<b>3. PAPER A: SIZING PV-BATTERY GRID-CONNECTED SYSTEM UTILIZING THE CONVEX OPTIMIZATION ALGORITHM FOR PEAK SHAVING APPLICATION.....</b>	<b>39</b>
3.1. Synopsis .....	39
3.2. Introduction .....	40
3.2.1. A General Coupling of PV-Battery-Grid System.....	44
3.2.2. Contributions .....	44
3.3. Modeling and Problem Formulation .....	46
3.3.1. Life Cycle Cost.....	46
3.3.2. Electricity Cost Optimization.....	48
3.3.2.1. Approach #1: Nested Solution .....	49
3.3.2.2. Approach #2: Simultaneous Solution.....	64
3.3.3. Scenarios and Approaches Summary .....	71
3.3.4. CVX Solver Selection and Peak Shaving Example .....	74
3.3.5. Case Study .....	77
3.4. Results and Discussion.....	77
3.4.1. School Results .....	78
3.4.1.1. The Effect of The Initial Costs of PV and Battery Storage Systems ...	78
3.4.1.2. Solution Check .....	83
3.4.1.3. The Peaks and the Effect of The Charging Efficiency .....	84
3.4.1.4. PV-Only System and Battery-Only System .....	85
3.4.1.5. The Effect of Battery Charging Time-Step .....	87
3.4.2. The Effect of Different Facility Type.....	88
3.4.3. Scenarios Comparison .....	90
3.4.4. Energy Shares.....	93
3.4.5. Adaptive Pricing.....	98
3.4.6. Battery Aging Cost.....	100
3.5. Conclusion.....	102
<b>4. PAPER B: DEMAND PEAK SHAVING USING PV-BATTERY SYSTEM UNDER PV POWER AND LOAD PREDICTION-UNCERTAINTY .....</b>	<b>103</b>
4.1. Synopsis .....	103
4.2. Introduction .....	104
4.2.1. The Proposed Study.....	114
4.2.1.1. Method Selection.....	114
4.2.1.2. Case Studies .....	115
4.3. Problem Formulating and Implementation .....	116
4.3.1. Reformulating the Peak Shaving Problem .....	116
4.3.2. Stochastic Dual Dynamic Programming .....	121
4.3.3. Forecasting and Scenarios Generation .....	125
4.3.4. Forecasting with Receding Horizon .....	131
4.3.5. SDP and SDDP Libraries .....	134

4.3.6. SDDP Library Validation .....	135
4.3.7. System Sizing and Inputs Parameters .....	137
4.3.8. Controller Design .....	138
4.4. Results and Discussion.....	140
4.4.1. Comparison Between SDDP and Forecast for 15-Minute Daily Peak Shaving.....	141
4.4.2. Full-Year 15-Minute Monthly Peak Shaving.....	152
4.4.2.1. Monthly-based and Daily-based Shaving .....	153
4.4.2.2. Receding and no Receding Forecasting, Different Time-of-Realization, and Different Time-of-Scheduling.....	156
4.4.3. Two-layer Forecasting Versus Single-layer Forecasting .....	158
4.4.4. Different Facilities.....	162
4.5. Conclusion.....	166
 5. PAPER C: TIME SERIES FORECASTING OF SOLAR POWER GENERATION FOR LARGE-SCALE PHOTOVOLTAIC PLANTS .....	167
5.1. Synopsis .....	167
5.2. Introduction .....	167
5.3. Predictive Models.....	172
5.3.1. Dataset .....	172
5.3.2. Description of Models .....	173
5.3.3. Models Implementation.....	176
5.3.4. Time Series Cross-validation .....	178
5.4. Results and Discussion.....	179
5.4.1. Comparison of the Two NNs Models.....	179
5.4.2. NNs Forecasting with 2 and 3 Hours Ahead Horizon.....	186
5.4.3. Statistical Models Results .....	187
5.4.4. Removing Outliers .....	197
5.5. Conclusion.....	197
5.6. Acknowledgment .....	198
 6. PAPER D: COMPARISON OF FORECASTING METHODS FOR PEAK SHAVING CONTROL OF SITE ELECTRICAL DEMAND .....	199
6.1. Synopsis .....	199
6.2. Introduction .....	199
6.3. Peak Shaving Controller Design .....	202
6.3.1. Battery Scheduling .....	202
6.3.2. Prediction Methods.....	205
6.3.3. Data Availability and Processing .....	207
6.3.4. Pricing Scheme.....	207
6.3.5. Control Horizon.....	208
6.4. The Effectiveness of Peak Shaving Based on Different Prediction Methods .....	208

6.4.1. PV-battery System.....	208
6.4.2. Battery-only System.....	213
6.5. Prediction Performance Metrics.....	214
6.6. Conclusion.....	214
<b>7. CONCLUSIONS AND FUTURE WORK .....</b>	<b>216</b>
7.1. Summary of the Dissertation.....	216
7.2. Suggestions for Future Work .....	218
7.2.1. Aging-aware Sizing and Scheduling Model.....	218
7.2.2. Economics for Different Generation and Storing Technologies .....	219
7.2.3. Inverse-based Design .....	219
<b>REFERENCES .....</b>	<b>221</b>
<b>APPENDIX A SOLAR SYSTEM MODELING AND CALCULATIONS.....</b>	<b>232</b>
A.1. PV Array Diode-modeling .....	232
A.2. PV Array Configuration .....	235
A.3. Maximum Power Point Estimation .....	236
A.4. Plane-of-array (POA) Irradiance .....	237
A.5. Cell Temperature .....	239
A.6. Solar Calculations Flow Chart .....	240
<b>APPENDIX B CVX APPLICATION.....</b>	<b>242</b>

## LIST OF FIGURES

	Page
Figure 1.1. The projections of the US electricity generation shares from [5]. Left: most common sources. Right: renewable sources. ....	4
Figure 1.2. Number of each type of building in the available database. From [18].....	9
Figure 1.3. Median years of available data for each type of building (with quartiles and extrema). From [18]. .....	10
Figure 1.4. Electrical load for a single school, sample of two weeks. ....	10
Figure 2.1. Demand peak shaving for a school for one arbitrary day using (a) battery- only system (b) PV-battery system. Figure 2.1 (b) is presented in Chapter 6..	17
Figure 2.2. Demand forecasting for one-day ahead. Presented in Chapter 6. ....	27
Figure 2.3. PV-generation forecasting for one-day ahead (a) one-time forecasting (b) with receding horizon. Presented in Chapter 6. ....	27
Figure 2.4. Controller flow chart for monthly peak shaving with receding horizon. Presented in Chapter 4. ....	29
Figure 2.5. Monthly peak values before and after shaving using (1) Forecast, and (2) SDDP methods. Presented in Chapter 4. ....	33
Figure 2.6. Results of PV power prediction for 1 hour ahead forecasting for sunny days using (a) neural network (b) statistical method. Presented in Chapter 5..	34
Figure 2.7. The effectiveness of peak shaving using PV-battery system for different facilities based on different prediction methods. ....	38
Figure 3.1. Schematic of PV-Battery-Grid system. ....	41
Figure 3.2. Code representation of the proposed combined optimization algorithm. ....	60
Figure 3.3. Convergence of Fmincon and surrogate optimization algorithm with 600 maximum iterations, the first 30 to 40 iterations are zoomed for clarity. ....	63
Figure 3.4. School demand peak shaving for one random day using (a) SDPT3 and (b) MOSEK solvers. ....	76
Figure 3.5. School full results, the legend is given at the top. ....	80

Figure 3.6. The effect of battery capacity on the electricity cost at a given PV array size ( $N_{PV} = 2469$ ) .....	83
Figure 3.7. The effect of the number of PV modules at a given battery size, $C_{Bat} = 950$ .....	84
Figure 3.8. Peak before and after installing the PV-battery system.....	84
Figure 3.9. The effect of battery charging/discharging efficiency on the electricity cost reduction.....	85
Figure 3.10. The effect of size on the electricity cost with (a) PV-only system (b) Battery-only system.....	86
Figure 3.11. The electricity cost reduction with different charging time-step .....	87
Figure 3.12. Different facility load profile.....	89
Figure 3.13. Energy shares schematic.....	93
Figure 3.14. Energy shares for (a) scenario #1 (see Table 3-3) (b) scenario #2 (c) scenario #3.....	96
Figure 3.15. Initial cost of solar system. ....	99
Figure 3.16. The reduction in the electricity cost percentage for different bandwidths. (100, 85, and 70 are the upper bands [%]).....	101
Figure 4.1. SDD calculations flow chart.....	122
Figure 4.2. The real values versus the forecasted values for school load prediction with multi-step (15 steps (hours) ahead prediction). .....	127
Figure 4.3. The ratios between the real values to the forecasted values of school load for one-day ahead (multi-step prediction with 15 steps ahead) (a) the second step out of 15 steps (b) step number 6 out of 15 steps (c) step number 10 out of 15 steps (d) step number 14 out of 15 steps. ....	128
Figure 4.4. The percentiles for the ratios between the real values to the forecasted values of the school load (multi-step prediction with 15 steps ahead) (a) the second step out of 15 steps (b) step number 6 out of 15 steps (c) step number 10 out of 15 steps (d) step number 14 out of 15 steps.....	129
Figure 4.5. The ratio between the real values to the forecasted values of PV generation (multi-step prediction with 13 steps ahead) for (a) the first step	

out of 13 steps (b) step number 5 out of 13 steps (c) step number 9 out of 13 steps (d) step number 13 out of 13 steps.....	130
Figure 4.6. Uncertainty propagation (theoretical) of AR model. ....	131
Figure 4.7. Forecasting the school hourly-average load with receding horizon. ....	133
Figure 4.8. Forecasting the hourly-average PV generation with receding horizon.....	134
Figure 4.9. Controller flowchart for monthly peak shaving without receding horizon..	140
Figure 4.10. Controller flow chart for monthly peak shaving with receding horizon of Table 4-7.....	145
Figure 4.11. Hourly-demand peak shaving (a) using Forecast (b) using SDDP (c) the ideal case.....	148
Figure 4.12. 15-minute average demand Peak shaving (a) using the schedule obtained by hourly-based Forecast (b) using the schedule obtained by hourly-based SDDP (c) the ideal case. ....	150
Figure 4.13. Day #1 (a) forecasting hourly load results (b) the hourly and 15-minute load profiles (figure (b) timescale = 15 minutes). ....	152
Figure 4.14. Monthly peak values before and after shaving using (1) Forecast, and (2) SDDP methods.....	155
Figure 4.15. The monthly shaved peak power using (1) Forecast, and (2) SDDP methods.....	155
Figure 4.16. The daily peak values with receding monthly-based peak shaving using SDDP. ....	156
Figure 4.17. Peak shaving for one random day using (a) two-layer and (b) one-layer forecasting using the Forecast method. ....	161
Figure 4.18. Load and PV generation prediction. ....	162
Figure 4.19. Peak shaving for (a) church (b) theater (c) hotel. ....	164
Figure 4.20. Daily peaks after shaving for theater. ....	165
Figure 5.1. Architecture of (a) LSTM cell (b) Bi-directional LSTM.....	175
Figure 5.2. Schematic of the time series cross-validation procedure.....	178

Figure 5.3. Feedforward neural network structure used to predict the PV power output .....	179
Figure 5.4. Result of BI-LSTM forecast versus observed power production (a) sunny days (b) cloudy days (c) rainy days .....	183
Figure 5.5. Results of BI-LSTM for validation attempt number 4 for PV power prediction (a) Error histogram figure (real - forecast), (b) Regression plot ..	185
Figure 5.6. (a) ACF and (b) PACF of power output. ....	189
Figure 5.7. (a) ACF and (b) PACF of first differenced power output.....	190
Figure 5.8. Quantile-Quantile plot for SARIMA model. ....	191
Figure 5.9. Results of SARIMA model for PV power prediction, one hour ahead: (a) sunny days (b) cloudy days.....	194
Figure 5.10. Results of SARIMA model for PV power prediction, one hour ahead for validation attempt number 4: (a) Error histogram figure (real - forecast), (b) Regression plot. ....	196
Figure 6.1. Schematic of grid-connected PV-Battery system. ....	200
Figure 6.2. Demand peak shaving for a school using PV-Battery system for one random day. ....	203
Figure 6.3. Hourly-average demand forecasting for one-day ahead. ....	204
Figure 6.4. PV-generation forecasting for one-day ahead (a) one-time forecasting (b) receding horizon. ....	205
Figure 6.5. The effectiveness of peak shaving for different facilities based on different prediction methods (PV-battery system). ....	209
Figure 6.6. Results for shaving the demand peak for one year for (a) school, (b) theater, (c) church, and (d) hotel.....	211
Figure 6.7. The daily peaks after shaving for theater for one year based on NN and the common optimal strategy. ....	212
Figure 6.8. The effectiveness of peak shaving for different facilities based on different prediction methods (battery-only system). ....	213
Figure A.1. Power versus voltage curves of arrays of similar sizes but of different configurations, each array consists of eight modules. ....	235

Figure A.2. Sun angles (zenith and azimuth) are obtained by SAM software [45] and calculated using solar book equations [44] for August 20. ....	238
Figure A.3. The solar radiation components and the angle of incidence for August 20. ....	239
Figure A.4. PV-power calculations (one-time calculation). ....	241

## LIST OF TABLES

	Page
Table 2-1. The effectiveness of different methods in shaving the 15-minute monthly peak for a school for 5 years of historical data with different time-of-realization and time-of-scheduling, and with receding and non-receding horizons. Presented in Chapter 4. ....	32
Table 3-1. Financial data of the system's hardware [31], [50], [51].....	48
Table 3-2. General financial data of the system [31], [50]. .....	48
Table 3-3. Scenarios summary. ....	49
Table 3-4. Solution's feasibility and cost for different scenarios and solving approaches. ....	72
Table 3-5. Number of variables and constraints for different scenarios and solving approaches, $J$ = vector of optimization variables (size = $365 \times 24 \times 4$ ). ....	73
Table 3-6. Equations for different scenarios and solving approaches.....	73
Table 3-7. Parameters.....	77
Table 3-8. Electricity cost reduction for different systems. ....	86
Table 3-9. Optimization results for different facilities.....	90
Table 3-10. Scenario #1-3 comparison (see the parameter description in Table 3-11)....	92
Table 3-11. The parameter description of Table 3-10.....	92
Table 3-12. Equation (3.84) constraints update corresponding to the value of B.....	97
Table 4-1. Summary of the previous published work. ....	111
Table 4-2. Calculating the future expected cost ( $V$ ) using SDD, assuming that $E_s$ is the only state variable of the system just to simplify the concept. ....	122
Table 4-3. Hourly-average peak shaving percentage [%] for one day using SDP and SDDP for 10 random days.....	136
Table 4-4. Hourly-average peak shaving percentage [%] for one day with different numbers of iterations for 10 random days. ....	136

Table 4-5. Design inputs. ....	138
Table 4-6. Daily hourly-average demand peak shaving percentage [%] for different methods.....	142
Table 4-7. Daily 15-minute demand peak shaving percentage [%] utilizing the schedule construed for the hourly demand peak shaving. ....	143
Table 4-8. The Effectiveness [%] of the schedule in shaving the daily peak. ....	144
Table 4-9. Comparison of different methods in shaving the 15-minute monthly peak for five years of historical data. ....	154
Table 4-10. The effectiveness of different methods in shaving the 15-minute monthly peak with different time-of-realization and time-of-scheduling and with receding and non-receding horizons. ....	158
Table 4-11. Forecast method for 10 random days with one-layer forecasting and two-layer forecasting with receding forecasting horizon and with 15-minute realization and scheduling. ....	159
Table 4-12. Two-layer forecasting with receding horizon, 15-minute realization and scheduling, and with Forecast and SDDP methods. ....	160
Table 4-13. Effectiveness of Forecast method in shaving the 15-minute monthly peaks for different facilities. ....	163
Table 5-1 Number of layers and neurons of NNs. LM and BR stand for trainlm and trainbr, respectively. ....	177
Table 5-2. One hour ahead forecasting using various NNs with 8-time delays (model 1), LM and BR stand for trainlm and trainbr, respectively. ....	181
Table 5-3. One hour ahead forecasting using various NNs with 4-time delays (model 2), LM and BR stand for trainlm and trainbr, respectively. ....	182
Table 5-4. Two hours ahead forecasting using various NNs, 8-time delays.....	186
Table 5-5. Three hours ahead forecasting using various NNs, 8-time delays.....	187
Table 5-6. AIC and BIC values of available ARMA models.....	191
Table 5-7. Results of PV power prediction using ARMA, ARIMA, and SARIMA, one hour ahead.....	193

Table 5-8. Results of PV power prediction using ARMA, ARIMA, and SARIMA, two and three hours ahead. ....	193
Table 5-9. The effect of removing outliers on BI-LSTM accuracy. ....	197
Table 6-1. The effect of the window size on the effectiveness of school and theater demand peak shaving (church and hotel are removed for brevity). ....	210

## 1. INTRODUCTION

The demand for electricity has been growing due to overpopulation, electrification of both heating systems and transport, and indoor climate control. The high demand for electricity puts the electricity grid under stress, requiring upgrade of utility infrastructures and subsequent increase in the cost of electricity. Consequently, reducing the electricity peak demand became critical to avoid the necessity of building additional infrastructure to satisfy peak demand. Electricity demand-management efforts are often based on educating and incentivizing the consumers to reduce the electricity demand peak.

Demand over an interval can be typically reduced by (1) use of alternative energy sources, (2) installation of energy storage systems, and (3) shifting of the electrical load. Energy storage systems, such as batteries, can shave the peak by charging the storage devices during the off-peak period then setting them on the discharge mode during the peak period. The flexibility of shifting the load relies on the building type. For instance, the load of residential and commercial applications cannot be easily shifted, as the activities in these buildings are typically uncontrolled. Therefore, to reduce the peak demand of a school, for example, energy storage systems or alternative energy sources might be used. The load of industrial applications might be shifted by changing working hours or work patterns. Of course, the energy storage systems and alternative energy sources can be used to reduce the demand of industrial applications during critical times.

Renewable energy sources are the most sustainable alternative solutions to concurrently secure the grid operation and to reduce carbon emissions. Advances in both the renewable energy sector and the energy storage technologies encourage users to rely

on them as cost-effective solutions to reduce the bill amount. Photovoltaic technologies have experienced a sharp drop in the manufacturing cost, a significant improvement in conversion efficiency, and remarkable market penetration [1]. Photovoltaic technologies are on the track to be the worldwide leading source of renewable energy [2].

There are different methods for storing electricity. For example, the hydropower storage system is the utility choice for storing surplus electricity in the United States [3]. For commercial and residential applications, the electric battery is the most commonly used energy storage option, used for grid peak shaving, outage prevention, voltage balancing, and frequency regulation [4].

The electric battery storages and the PV systems can be combined and used to reduce the peak demand and the energy costs: (1) PV power systems reduce reliance on grid-sourced energy, (2) The battery saves the excess PV energy to meet the demand partially or completely during the night, (3) The battery storage can be also used to shave the facility peak by constructing a charging and discharging schedule, (4) Shaving the peak reduces energy costs significantly and leads to a better grid operation.

The status of electricity generation is discussed in Section 1.1. Energy storage technologies and demand management programs are reviewed briefly in Sections 1.2 and 1.3, respectively. The database of historical electrical load demands used to conduct this study is described in Section 1.4. Finally, the dissertation motivation, objective, and structure are laid out in Sections 1.5, 1.6, and 1.7, respectively.

## **1.1. Current Status of Electricity Production**

Fossil fuels are the primary source of energy for electricity production due to their low cost as well as the maturity of the fossil-fuel electricity-generation technologies. On the other hand, fossil fuels are nonrenewable sources of energy and the largest source of global greenhouse gas emissions. Their depletion and their contribution to climate change drive the motivation to replace them with clean renewable energy sources. Renewable energy research aims to create new technologies and improve the current renewable energy systems in terms of conversion efficiency, cost, and lifespan.

Natural gas is the most commonly used fossil fuel. The projections of the proportion of electricity generation from natural gas, renewable energy sources, and other sources for the United States (Figure 1.1) were taken from the annual energy report provided by US Energy Information Administration [5].

The renewable energy sources, ranked in order of overall power generated, hydroelectric and wind energy are followed by solar photovoltaic energy (Figure 1.1). Solar photovoltaic energy, however, has the highest growth rate among renewable energy sources. PV energy is on course to become the leading alternative energy source. These different energy technologies are discussed below:

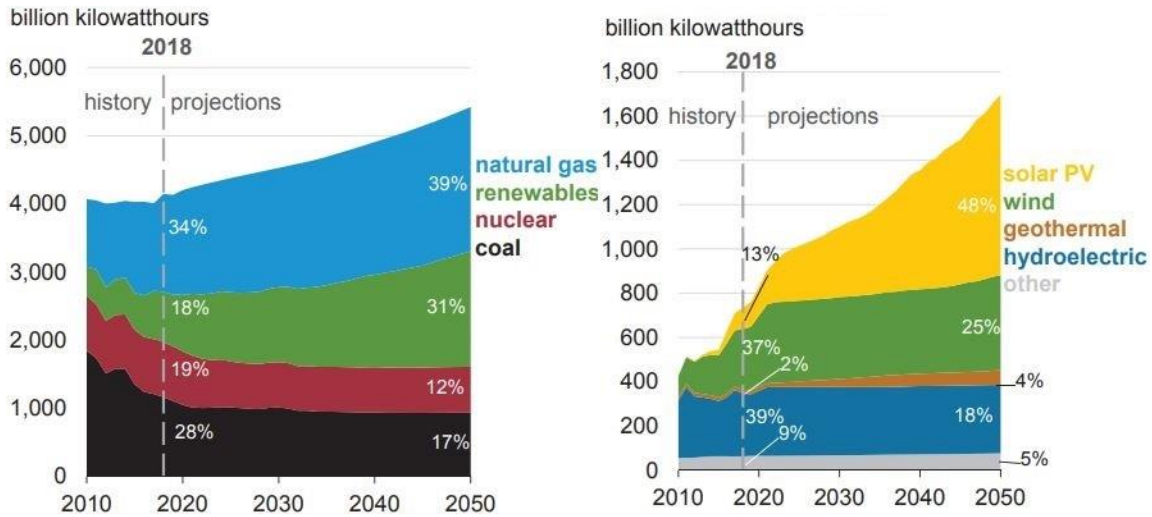


Figure 1.1. The projections of the US electricity generation shares. Left: most common sources. Right: renewable sources. Adapted from [5].

### A) Solar Photovoltaic

Solar photovoltaic (PV) cells are semiconductor devices that convert the sun's radiation into electricity. PV technology is gaining attention due to the significant increase in efficiency, drop in the PV market price, and the almost-ubiquitous availability of solar energy [2]. Furthermore, solar PV systems are the most portable of large energy sources and can be scaled for almost any application.

### B) Wind Turbine

Wind turbines harness the kinetic energy of moving air and convert it into electricity or other forms of energy. Most of the worldwide wind energy is produced by large wind turbines that feed the electricity grid. The manufacturing of small wind turbines of a capacity less than 100 kW, however, has seen significant growth in the past two decades [6]. These small-capacity turbines are marketed for residential and small business

applications. The United States is taking the lead in the world for producing small wind turbines [6].

### **C) Hydroelectric Turbine**

hydroelectric turbines are typically used for large-scale generation. Large-scale hydroelectric turbines use the potential energy of rivers by damming rivers to create reservoirs. Water released from the dam spins turbine electric generators. Another method of hydroelectricity generation is by discharging pumped hydropower storage to drive small-scale electric turbines.

### **D) Gas Turbine**

Gas turbines are the most used electricity-generation schemes. Gas turbines can operate on different types of fuels. Most gas turbines utilize natural gas or liquefied natural gas due to their combustion efficiency. Gas turbines are typically used by utilities and a few industrial sectors. The typical gas turbine capacity is 500 kW to 350 MW [7]. Microturbine sizes, available and under development, range from 30 kW to 400 kW [7]. New research aims to reduce the weight of gas turbines for small scale use including residential applications [8].

## **1.2. Energy Storage Technologies**

Energy storage systems store the energy that will be useful when there is no on-site generation or when the electricity market is expensive. The storage systems bring cost saving to both the end-users and the utilities. The main five electricity storing technologies are summarized as follows:

- A) Battery:** The electricity stored in the form of chemical energy. Battery storage is available at almost any scale.
- B) Thermal:** Excess electricity is converted into thermal energy and stored, for example, in the form of molten salts or metals. The molten salt can be used as a heating source to drive a steam turbine to generate electricity as needed. Thermal storage is usually used for large-scale electricity generation. For household usage and low-demand applications, thermal storages are used for heating applications rather than electricity production.
- C) Mechanical:** The electricity is stored in the forms of kinetic or gravitational energy, for example, lifting massive weights up a height or spinning a flywheel. Researchers in France are developing flywheel storage systems to store the excess domestic PV energy [9]. In [10], a small-scale (100-kW) flywheel of novel design was proposed to be competitive with the lithium battery in terms of the cost per kWh storage capacity.
- D) Hydrogen:** Excess electricity is used to generate hydrogen via electrolysis. The hydrogen is combined with oxygen atoms to produce electricity as required. Hydrogen fuel cell electric car is an example of small-scale hydrogen storage systems.
- E) Pumped Hydropower:** Electricity is used to pump water to an upper reservoir. The water from the upper reservoir is released to a turbine electric generator during the electricity shortage or the peak period. Pumped hydropower is the storage

system most commonly used by utilities; in the United States, 95% of the grid excess energy is stored by this form [3]. Pumped hydropower storage systems are usually marketed in the scale of the grid utility.

### **1.3. Demand Management Programs**

Utilities enact demand management programs to make the energy supply process more effective by maintaining a balance between the electrical demand and the distribution system's supply. Several types of demand-management program schemes and pricing structures are implemented to achieve a demand-supply convergence.

#### **1.3.1. Demand Management Strategies**

An example of the demand management strategies is when the utility sets a high pricing rate for the electricity usage during the peak period. Demand management programs are classified into two categories [11]: incentive-based and price-based.

**A) Incentive-based:** Participating customers receive incentives, typically as a bill credit. In these programs, the utilities can remotely shut down the participants' equipment during the peak period. Examples of these pieces of equipment are water heaters, HVAC systems, and lights (turn off or dim the lights).

**B) Price-based:** Utilities reward participating customers with money based on the amount of reduction in the load during peak periods. Some of these pricing methods are discussed in Section 1.3.2.

### **1.3.2. Electricity Pricing Models**

Some factors the utilities consider when constructing the rating structures are cost of electricity generation, government regulations, taxes, and distribution infrastructures. Electricity rates (typically called electricity tariffs) can be also based on the building type and local weather patterns.

To motivate consumers to participate in shaving the grid's peak, modern utilities employ different pricing schemes. The most common are the time-of-use and the real-time pricing.

**A) Time-of-use pricing** [12], [13], [14]: Consumers are charged based on the time of the day. The utility charges more during the grid peak period to encourage the consumers to shift their load to the off-peak period. The rate structure is typically broken into three groups: off-peak, peak, mid-peak (the energy ramp up or down). The tariffs are fixed for months, seasons, or years at a time.

**B) Real-time pricing** [15], [16], [17]: The electricity price changes over short time intervals, even hourly. The utility rate structures are announced typically one day ahead. The prices are updated to reflect the contemporaneous supply costs and the status of the demand on electricity.

### **1.4. Electrical Demand Database**

A large repository [18] of 15-minute electrical demand data for buildings in Texas was used for this current study. The breakdown of facilities within each type is shown in Figure 1.2, with at least five years of historical data available for most buildings (Figure

1.3). The database is described in more detail in [18]. A sample of the electrical load for a single school is shown in Figure 1.4.

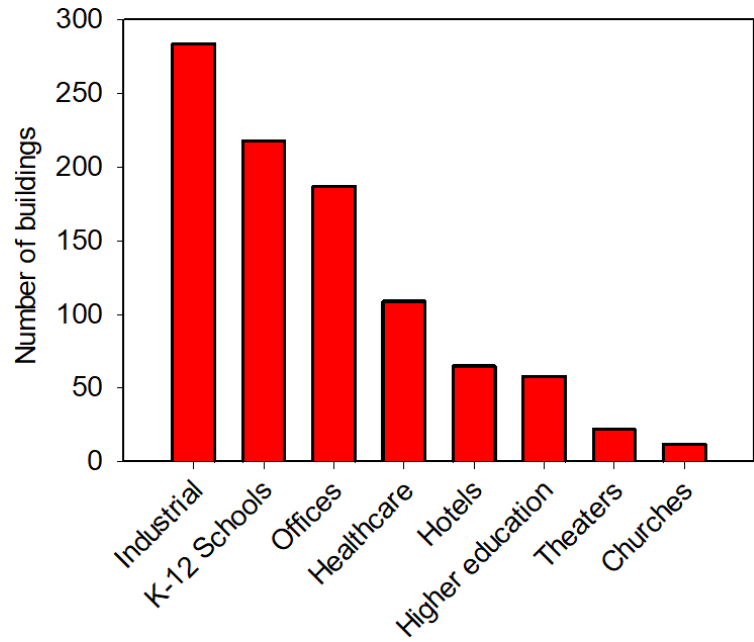


Figure 1.2. Number of each type of building in the available database. Adapted from [18].

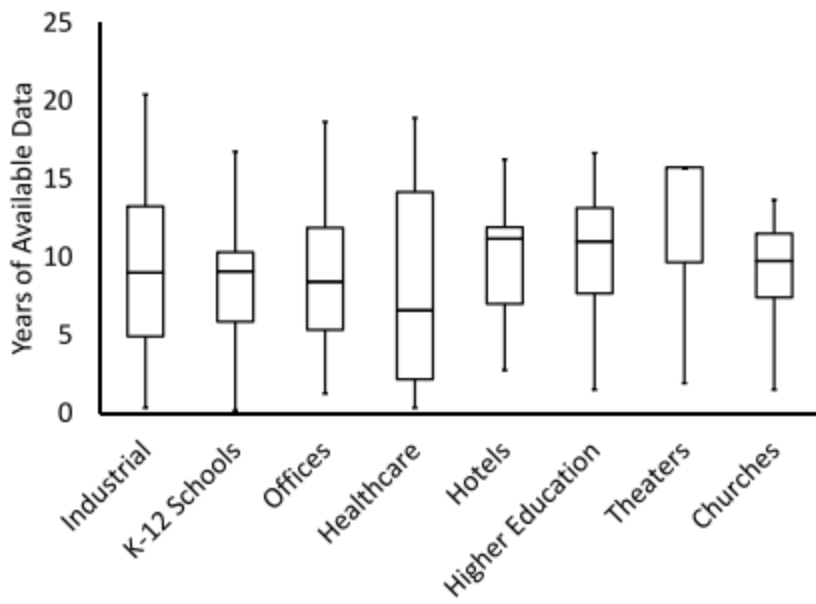


Figure 1.3. Median years of available data for each type of building (with quartiles and extrema). Adapted from [18].

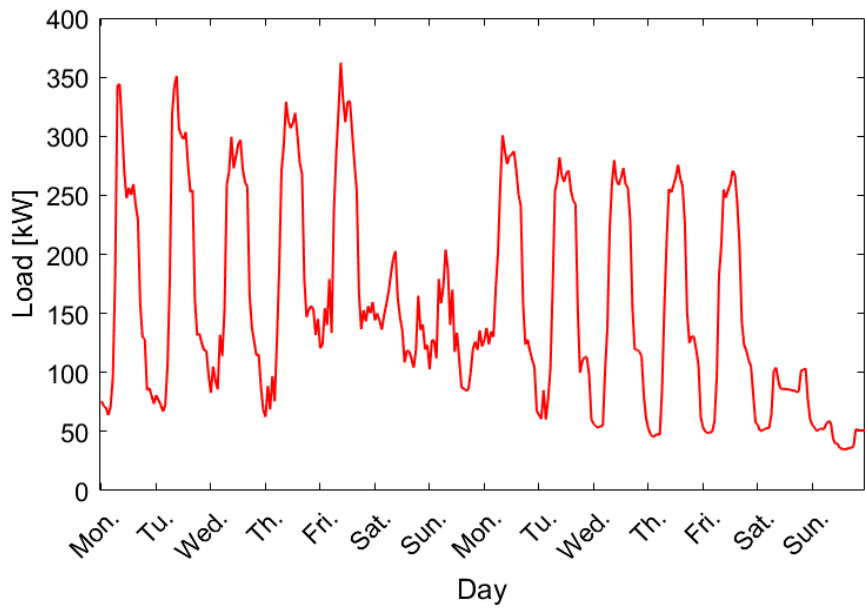


Figure 1.4. Electrical load for a single school, sample of two weeks.

## **1.5. Motivation of the Dissertation**

PV-battery system components are expensive. Capacities of these components need to be optimized for the system to give a positive return on investment (ROI). For instance, if the system is oversized, the life cycle cost of the system will be higher than the cumulative amount saved on electrical bills. Limited resources exist to determine the return on investment (ROI) and optimal sizing of PV-battery systems [1]. The studies in [1], [18], and [19] reveal that the battery systems, used to store the surplus PV energy for residential applications, might not achieve ROI over the lifetime of the system due to the cost of the battery, according to market price and battery aging characteristics. The battery market price is dropping, however, and there is ongoing research to enhance the battery life span. In the meantime, battery storage is used to provide energy during the night hours in standalone PV systems. On the other hand, in grid-connected PV systems, purchasing electricity from the grid to meet the demand deficiency is cheaper than installing expensive battery storage systems.

Another important application for PV-battery systems is to shave the site electrical demand peak. The fees on the peaks are expensive, thus installing batteries to shave the peak might give an attractive ROI. However, there is limited research on sizing the PV-battery systems that are applied for peak shaving. In this dissertation, a fast procedure to size the PV-battery system to shave the peaks with a long scheduling horizon is developed.

Despite a number of diverse strategies proposed to shave the end user's electrical demand peak, the research record is sparse on achieving this goal under uncertainty of

prediction. The real-time peak shaving control is based on realization of the current status and forecasting the electrical load and PV energy. However, the forecasting is uncertain. Therefore, the decision obtained by the peak shaving controller is not optimal. This dissertation also studies the effect of the uncertainty of prediction on the effectiveness of peak shaving. A method to handle the uncertainty of prediction based on stochastic dynamic programming is assessed. The study relies on historical data of electrical load [18].

Although artificial intelligence and statistical approaches have been widely used for prediction of electrical load and PV energy, these methods have not been yet validated for monthly peak shaving applications. In this dissertation, these prediction tools are tested for site electrical demand peak shaving. In addition, these sophisticated prediction tools are benchmarked with simple prediction methods.

### **1.6. Objective of the Dissertation**

The main objective of this dissertation is to develop a framework to optimally size and schedule combined photovoltaic-battery systems for the purpose of reducing the 15-minute monthly electrical peak demand for different commercial facilities located in Texas using historical data of load and solar photovoltaic generation. In this dissertation, the following technical questions are addressed:

- 1) How to reduce the computation cost of sizing combined solar photovoltaic battery storage systems used for 15-minute monthly electrical demand peak shaving?
- 2) How to reformulate the sizing problem so the optimization can be done faster?

- 3) How effective is the 15-minute monthly electrical demand peak shaving considering the uncertainty of prediction?
- 4) How to handle the uncertainty of prediction when shaving the electrical demand peak with a long control horizon of one month?
- 5) How reliable are state-of-art tools to predict the photovoltaic generation?
- 6) Can the complicated prediction tools be replaced with simple prediction algorithms for electrical demand peak shaving without sacrificing the peak shaving effectiveness?

### **1.7. Organization of the Dissertation**

The rest of the dissertation is organized as follows: Chapter 2 summarizes the contributions of this research. In Chapter 3, a rapid optimization model is developed to find the optimal sizes of combined solar photovoltaic battery systems for different pricing policies. Afterward, the proposed model is used to study the economic feasibility of the implementation of the solar photovoltaic battery systems for different commercial facilities. Chapter 4 details a control mechanism to shave the electrical demand peak with long control horizon and propagated uncertainties of prediction. The proposed procedure for peak shaving is validated using historical data. In Chapter 5, the prediction accuracy of different neural networks configurations and different statistical methods for photovoltaic power forecasting are compared. Chapter 6 is devoted to comparing different prediction methods when used for electrical demand peak shaving. The work in Chapter 6 studies the effectiveness of simple prediction methods for electrical demand peak

shaving rather than both the sophisticated neural networks and the complicated statistical approaches of prediction. Conclusions and suggestions for future work are outlined in Chapter 7.

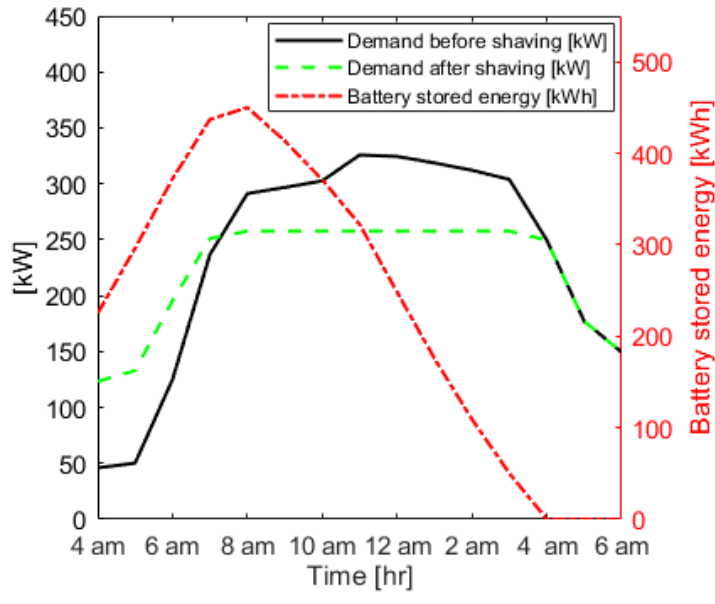
Questions 1 and 2 in Section 1.6 are addressed in Chapter 3. Chapter 4 addresses questions 3 and 4. Chapter 5 answers question 5. Finally, Chapter 6 answers question 6.

## 2. SUMMARY OF CONTRIBUTIONS

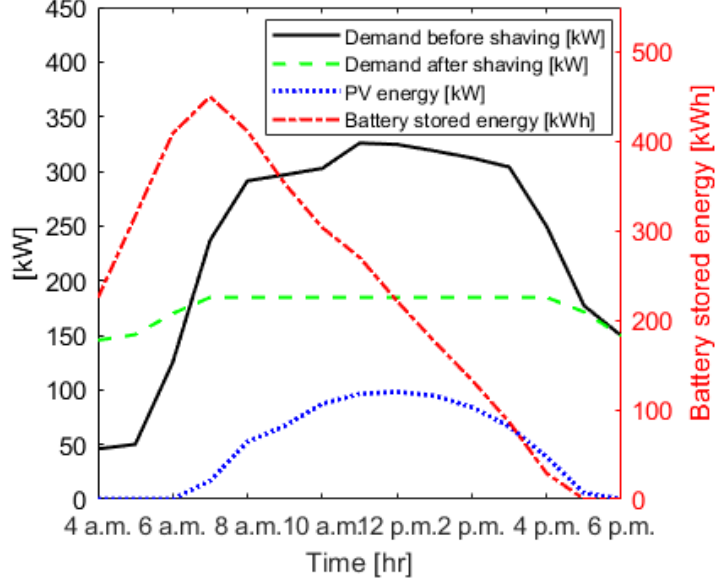
A fast optimization framework to size PV-battery system for monthly demand peak shaving application is developed in chapter 3. A brief summary of the sizing framework is given in Section 2.1. A real-time scheduling model is constructed to shave the monthly demand peak in Chapter 4. The scheduling model is based on forecasting the load and PV generation and on stochastic dual dynamic programming to handle the uncertainty of prediction. Different prediction methods are applied and their effectiveness in shaving the demand peak is compared in Chapters 5 and 6. The peak shaving controller design and the prediction algorithms are summarized in Section 2.2.

In an example of peak shaving (Figure 2.1 (a)), the daily peak is shaved for a Texas school building using a battery-only system (without a PV system). The school's significant load is between 4:00 a.m. and 6:00 p.m. Therefore, peak shaving is applied during this time interval. The demand peak is about 325 kW before shaving, compared with about 255 kW after shaving. The battery is charged between 4:00 a.m. and 8:00 a.m. by the utility-generated power. The battery's discharge mode is enabled at 8:00 a.m. to shave the peak. Most of the battery's energy is consumed by 4:00 p.m. In Figure 2.1 (b), the daily peak is shaved using PV-battery system. The peak is shaved from 325 to 180 kW. The battery is charged between 4:00 a.m. and 7:00 a.m. by utility-generated power. The battery is discharge mode is enabled at 7:00 a.m. to shave the peak. Most of the battery energy is consumed by 5:00 p.m. The power provided by the PV system between 6:00

a.m. and 5:00 p.m. is applied to shaving the demand peak alongside the energy discharged from the battery system.



(a)



(b)

Figure 2.1. Demand peak shaving for a school for one arbitrary day using (a) battery-only system (b) PV-battery system. Figure 2.1 (b) is presented in Chapter 6.

## **2.1. Sizing PV-battery Systems for Peak Shaving Applications**

The PV-battery system components are expensive. Therefore, the sizes of the system's components need to be optimized for the system to be economically effective and to deliver favorable return on investment. PV-battery systems are implemented to shave the demand peaks for commercial facilities to avoid the disincentive peak rates imposed by electrical utilities. Sizing PV-battery system for demand peak shaving is a complex optimization problem as illustrated in Section 2.1.1. The proposed solving techniques are discussed in Section 2.1.2.

### **2.1.1. Sizing Challenges**

Texas electric utilities charge the consumers a per-unit tariff based on the 15-minute monthly peak usage; however, shaving the 15-minute monthly peak is a computationally intensive scheduling problem, as the schedule of one month with 15-minute time step is a very lengthy vector. For clarification: one day contains 96 time-steps; the time-step is 15-minute length. One month contains about 3,000 time-steps. Solving an optimization problem with about 3,000 optimization variables is challenging. Moreover, historical data of one year is usually used for sizing so the sizes will be optimal over working conditions that occur over a year. Therefore, the number of variables that need to be optimized for one year is around 30,000. To size a photovoltaic battery system, the sizing and the scheduling problems are solved together.

### **2.1.2. Solution Techniques**

If system sizes are given, the problem of determining the charging/discharging rate vector of the battery for peak shaving is a convex problem (as shown in [21] and [22]) that can be solved using a convex optimization algorithm. The convex optimization is very fast, especially when solving for a huge number of optimization variables. The sizing problem in its simple format, however, cannot be handled using convex optimization; the sizing problem needs to be reformulated properly to be in compliance with the rules of the convex optimization algorithm.

Several techniques are utilized in this study to enable convex optimization to solve the sizing problem for different pricing policies and different constraints on the operation. These techniques include problem decoupling, the method of binary variables and big-M value, linearization, and problem mathematical-reformulation.

Pricing policies considered in this work are reformulated, using the techniques mentioned in the previous paragraph, to be solvable using convex optimization. These different pricing scenarios are listed as follows:

- 1) The utility prohibits the consumers from providing excess power to the grid to prevent unstable oscillations in grid frequency that could lead to major electrical grid failures.
- 2) The utility accepts excess PV energy without paying the PV system owner.
- 3) The utility charges the customers \$0.05 per kWh consumption but refunds them with a lower price, for example, \$0.01 per kWh feed-in.

- 4) The utility charges the consumers \$0.05 per kWh consumption and refunds them \$0.05 per kWh that is supplied to the grid, i.e., net metering.

Scenario # 3 is discussed briefly in this section. Other scenarios are discussed in detail in Chapter 3. Scenario # 3 can be written as follows:

$$\begin{aligned} \text{If } E_G \geq 0, \text{ Energy rate} &= 0.05 \text{ [$/kWh]} \\ \text{If } E_G < 0, \text{ Energy rate} &= 0.01 \text{ [$/kWh]} \end{aligned} \quad (2.1)$$

where  $E_G$  is grid energy and given below:

$$E_G = E_L - E_{PV} + E_{Bat} \quad (2.2)$$

where  $E_G$  is positive if the energy is provided by the grid to the customers.  $E_G$  is negative if the energy is supplied by the customers to the grid, i.e., PV energy is supplied to the grid.  $E_L$  is the load energy and  $E_{PV}$  is the energy produced by the solar photovoltaic array.

$E_{Bat}$  is the battery energy and given below (See [21], [22]):

$$E_{Bat} = C_{Bat} \max(\eta u, 1/\eta u) \quad (2.3)$$

where  $C_{Bat}$  is the battery capacity,  $u$  is the charging/discharging rate and  $\eta$  is the charging/discharging efficiency.

$E_{PV}$  is given below:

$$E_{PV} = N_{PV} P_{m, module} \quad (2.4)$$

where  $N_{PV}$  is the number of PV modules and  $P_{m, module}$  is the maximum power generated by one PV module which can be calculated as shown in Appendix A. Therefore,  $C_{Bat}$ ,  $u$  and  $N_{PV}$  are the optimization variables.

The if statement in Equation (2.1) cannot be handled using convex optimization algorithm. Thus Equation (2.1) needs to be reformulated. Two methods are suggested in

this work to reformulate Equation (2.1). One of these two methods is based on binary-variable scheme and the second one is based on using max function. These two methods are discussed as follows:

### i. Binary-variable scheme

The if statement of Equation (2.1) is replaced using binary-variable scheme as follows:

$$\text{Energy rate} = (0.04 B + 0.01) [\$/kWh] \quad (2.5)$$

where  $B$  is a binary variable such that if  $B = 0$  the energy rate will be  $0.01 [\$/kWh]$  and if  $B = 1$  the energy rate equals  $0.05 [\$/kWh]$ .

The first constraint of Equation (2.1) is updated as follows:

$$\begin{aligned} E_G &\geq 0 \\ E_L - E_{PV} + C_{Bat} \max(\eta u, \frac{1}{\eta} u) &\geq 0 \end{aligned} \quad (2.6)$$

Let's assume the charging/discharging process is ideal ( $\eta = 1$ ).

$$E_L - E_{PV} + C_{Bat} u(t) \geq 0 \quad (2.7)$$

Also, we will assume in this section that the only variable needing to be optimized is the charging/discharging rate vector  $u$ . We rewrite Equation (2.7) in terms of  $u$ , which is the optimization variable, and we assume a new constant ( $C$ ):

$$u \geq C \quad (2.8)$$

$$C = \frac{E_{PV} - E_L}{C_{Bat}} \quad (2.9)$$

Using Big-M value and a binary variable ( $B$ ) to replace the if statement of Equation (2.1) by updating Equation (2.8):

$$u \geq C - M(1 - B) \quad (2.10)$$

$$u < C + MB \quad (2.11)$$

$M$  is a very large number. In Equations (2.10) and (2.11):

- If  $B = 0$ , the constraint of Equation (2.10) will be always right and the constraint of Equation (2.11) needs to be satisfied.
- If  $B = 1$ , the constraint of Equation (2.11) will be always right and the constraint of Equation (2.10) needs to be satisfied.

## ii. Using max function

For scenario # 3, there might be an easier way to solve it without the need to use binary variables. Solving for binary variables is computationally intensive more than solving for continuous variables. The max function can be used to find the positive and the negative components of a variable as proposed in [23] without using if statements or binary variables:

$$E_G^+ = \max(E_G, 0) = \max(E_L - E_{PV} + Q, 0) \quad (2.12)$$

$$E_G^- = \max(-E_G, 0) = \max(-(E_L - E_{PV} + Q), 0) \quad (2.13)$$

where  $Q$  is the battery energy.  $Q$  is positive for charging and negative for discharging.

The bill amount can be given as follows:

$$\begin{aligned} \text{bill amount} &= E_G^+ [\text{kWh}] \times \text{Energy rate } [\$/\text{kWh}] \\ &+ E_G^- [\text{kWh}] \times \text{Refunding rate } [\$/\text{kWh}] \\ &+ \max(E_G [\text{kW}]) \times \text{Peak rate } [\$/\text{kW}] \end{aligned} \quad (2.14)$$

Energy rate is 0.05 [\$/kWh] and the Refunding rate is -0.01 [\$/kWh]. However, Equation (2.14) does not comply with convex optimization (CVX, CVX is given in Appendix B) algorithm rules; {convex} + {concave} is illegal operation as illustrated below:

- A. The function  $(E_G^+ \text{ [kWh]} \times \text{Energy rate [$/kWh]})$  is convex;  $E_G^+$  is convex because the max function is convex.
- B. The refunding rate, in Equation (2.14), is negative and the  $E_G^-$  is convex thus the function  $(E_G^- \text{ [kWh]} \times \text{Refunding rate [$/kWh]})$  is a concave.

To handle this issue, the max functions of Equations (2.12) and (2.13) are linearized and replaced by two constraints as follows:

$$\begin{aligned} E_G^+ &\geq E_G \\ E_G^+ &\geq 0 \end{aligned} \tag{2.15}$$

$$\begin{aligned} E_G^- &\geq -E_G \\ E_G^- &\geq 0 \end{aligned} \tag{2.16}$$

The constraints of Equations. (2.15) and (2.16) to replace max function are justified as follows:

- A. Since the purpose of optimization is to minimize the bill amount, the  $E_G^+$  will need to be minimized (see Equation (2.14)). The minimum possible value of  $E_G^+$  is  $E_G$  or zero according to Equation (2.15). To satisfy the two constraints of Equation (2.15),  $E_G^+$  will equal the maximum value ( $\max(E_G, 0)$ ). Therefore, the max function is satisfied.

B. An issue arises of the new two constraints of Equation (2.16): the optimization algorithm minimizes the bill amount, and since increasing the  $E_G^-$  will reduce the bill amount (see Equation (2.14)), the optimization algorithm will maximize the  $E_G^-$ . Therefore,  $E_G^-$  value will go to infinity as the constraints of Equation (2.16) are unbounded. To address this issue, the following constraint is enforced:

$$E_G^+ - E_G^- \geq E_G \quad (2.17)$$

C. The constraint of Equation (2.17) is justified as follows:

**a) Case 1:  $E_G$  is positive**

If the  $E_G$  is positive, the first constraint of Equation (2.15) is dominant and the second constraint is not dominant. If the  $E_G$  is positive, the second constraint of Equation (2.16) is the dominant constraint. Thus, the dominant constraints of Equations (2.15), (2.16), and (2.17) are summarized as follows:

$$\begin{aligned} E_G^+ &\geq E_G \\ E_G^- &\geq 0 \\ E_G^+ - E_G^- &\geq E_G \end{aligned} \quad (2.18)$$

To minimize the cost, the optimization algorithm minimizes  $E_G^+$  as much as possible. To satisfy the first constraint of Equation (2.18), the minimum possible value of  $E_G^+$  is  $E_G$ :

$$E_G^+ = E_G \quad (2.19)$$

Now replace the  $E_G^+$  with  $E_G$  in the third constraint of Equation (2.18) and remove the first constraint of Equation (2.18):

$$\begin{aligned} E_G^- &\geq 0 \\ E_G - E_G^- &\geq E_G \end{aligned} \quad (2.20)$$

Rewrite the second constraint of Equation (2.20), Equation (2.20) is updated as follows:

$$\begin{aligned} E_G^- &\geq 0 \\ E_G^- &\leq 0 \end{aligned} \quad (2.21)$$

The two constraints of Equation (2.21) can be satisfied simultaneously if and only if

$$E_G^- = 0:$$

$$E_G^- = 0 \quad (2.22)$$

To sum up, if the  $E_G$  is positive (Case 1), the following two equations (copied from Equations (2.19) and (2.22)) are satisfied:

$$\begin{aligned} E_G^+ &= E_G \\ E_G^- &= 0 \end{aligned} \quad (2.23)$$

### b) Case 2: $E_G$ is negative

If  $E_G$  is negative, the following equations are satisfied (That can be checked in a similar way to what stated in the analysis of Case 1):

$$\begin{aligned} E_G^+ &= 0 \\ E_G^- &= E_G \end{aligned} \quad (2.24)$$

Scenario # 3 is now convex after the reformulation and can be solved with the constraints of Equations (2.15), (2.16), and (2.17).

Solving the sizing problem for different pricing policies, and with and without the effect of charging/discharging efficiency is discussed with full details in Chapter 3.

## 2.2. Real-time Peak Shaving Controller

To shave the demand peak, the load and PV generation are forecasted and then the battery charging and discharging schedule is constructed accordingly. The prediction is not ideal. Thus, PV-battery implementation for peak shaving requires a real-time control scheme to manage the PV power and load uncertainties.

The controller aims to shave the 15-minute monthly demand peak, however, the schedule is constructed for only one-day ahead by forecasting the load and PV generation for the coming day. Then, the monthly peak target is updated every day, by realization of the daily peak value, to keep the monthly peak as low as possible. The uncertainty of prediction is handled in the following two sections (Sections 2.2.1 and 2.2.2). Different forecasting algorithms are compared when applied for shaving the 15-minute monthly demand peak in Section 2.2.3.

### **2.2.1. Uncertainty of Prediction**

Forecasting the PV and load profiles to construct a charging and discharging schedule might lead to higher peak values due to the potential of a significant forecasting error. To handle the uncertainty of prediction, the battery schedule is continuously updated (i.e., with receding horizon). Two situations arise in which the schedule can be updated every time step: (1) the demand peak status is being realized every time step (2) the forecasted profiles of the load and PV generation are being updated every time step. The load for a school is forecasted for one day ahead (Figure 2.2) where the real value and the forecasted values are very close. In Figure 2.3 (a), the PV generation is forecasted for one day ahead, but the prediction was not accurate. To enhance the accuracy of predicting the PV generation, the predicted profile is continuously updated with a receding horizon as shown in Figure 2.3 (b).

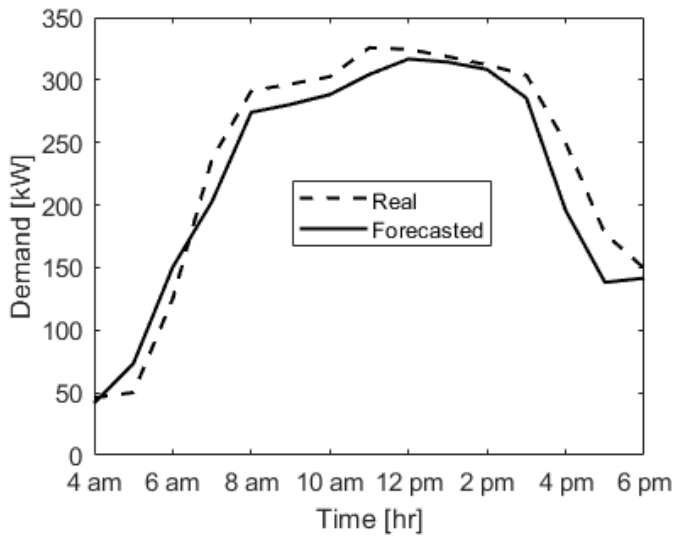


Figure 2.2. Demand forecasting for one-day ahead. Presented in Chapter 6.

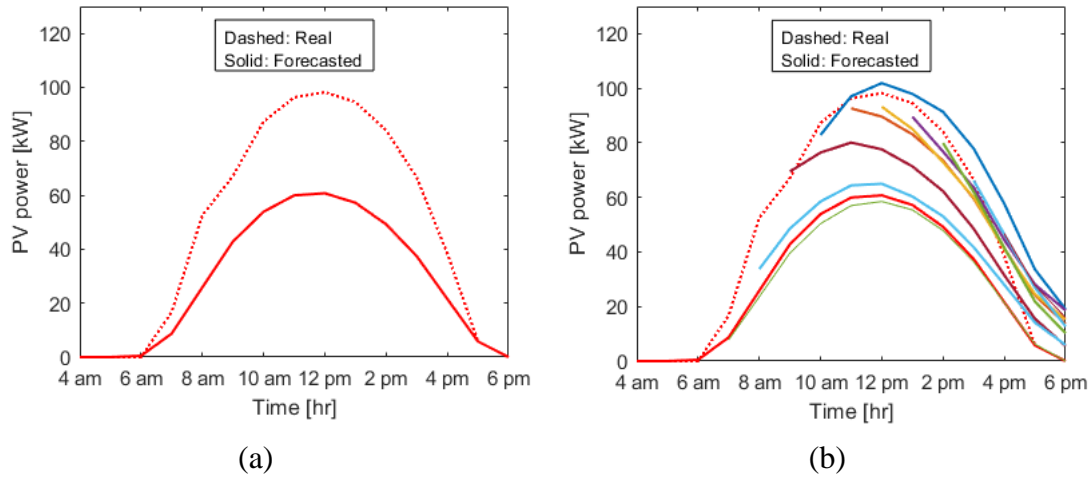


Figure 2.3. PV-generation forecasting for one-day ahead (a) one-time forecasting (b) with receding horizon. Presented in Chapter 6.

Also, stochastic dynamic programming (SDP) can be used to make a decision that takes into account the uncertainty of prediction. SDP is based on generating a solution of the highest probability to lead to the minimum peak value over different expected

scenarios of given probabilities. To generate these scenarios, the prediction tool is tested over historical data of one year. Then the ratios between the real values to the forecasted values are calculated. These ratios with their probability distributions are used to generate scenarios. These scenarios are fed to SDP which will make a decision that considers that the predictions are uncertain. The peak shaving problem is reformulated to be acceptable by SDP as shown in Section 4.3.1.

Figure 2.4 shows control mechanism to shave the monthly peak of a school. The school significant load takes place between 4:00 a.m. and 6:00 p.m. Thus, peak shaving is applied during this time interval. ARIMA model is used to predict the hourly electrical load and the hourly PV generation between 4:00 a.m. and 6:00 p.m. Then the schedule is constructed. There are two options to construct the schedule:

1) **Forecast:** The forecast is assumed to be certain, i.e., the uncertainty is neglected.

The schedule is optimized using convex optimization.

2) **SDDP:** The uncertainty of forecasting is handled using stochastic dual dynamic programming (SDDP).

Then the demand is measured for the coming hour and the peak value recorded thus far will be stored as the target peak ( $\text{Peak}_{\text{Target}}$ ). After 1 hour has elapsed, ARIMA model updates the hourly forecasted load and PV generation (see Figure 2.3 (b) on updating the PV generation profile every one hour). Then the schedule can be updated with two options as mentioned in the previous paragraph after the target peak is updated. The process is repeated every hour all day long. The battery is charged during the low-load period, i.e.,

between 6:00 p.m. and 4:00 a.m. The target peak is set back to zero at the beginning of each month to shave the monthly peak as much as possible.

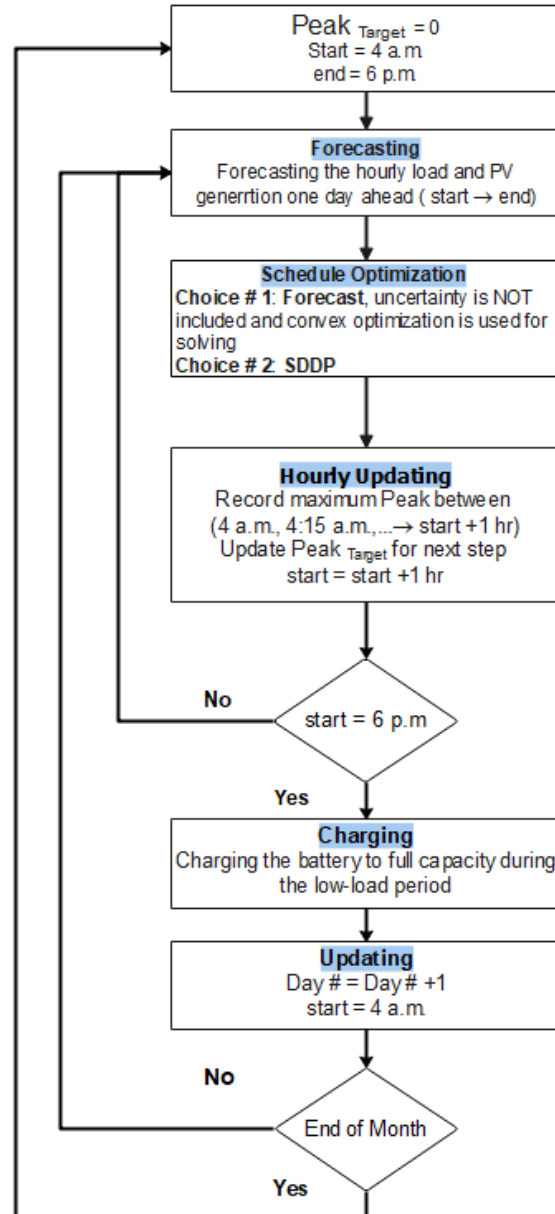


Figure 2.4. Controller flow chart for monthly peak shaving with receding horizon.  
Presented in Chapter 4.

### **2.2.2. Time Frame of the Decision**

The electrical load in the available data was recorded as 15-minute average. The controller is intended to shave the 15-minute monthly peak; however, the forecasting tool is trained in the current work to predict the hourly load and PV generation. The 15-minute load and PV profiles are noisy, thus difficult to use prediction. As mentioned, the prediction is not ideal. Thus, to enhance the accuracy of prediction, the forecasted profiles can be updated every hour. Then the schedule can be updated according to the new forecasted profiles. Although the forecast is hourly-based, the schedule can be updated with two options: 15-minute or hourly. A peak shaving controller with different combinations of time frames for forecasting, realization, and scheduling is established and tested. The results summary for 5 years is given in Table 2-1. It is found that scheduling without accounting for the uncertainty of prediction (Forecast) is more effective in shaving the monthly peak than SDDP as shown in Table 2-1.

The schedule effectiveness in shaving the demand peak is defined as follows:

$$\text{Effectiveness} = \frac{\text{Shaving [%]}}{\text{Ideal shaving [%]}} \times 100 \% \quad (2.25)$$

where Shaving [%] is the peak shaving percentage [%], calculated as follows:

$$\text{Shaving [%]} = \frac{\text{Peak without shaving} - \text{Peak after shaving}}{\text{Peak without shaving}} \times 100 \% \quad (2.26)$$

Ideal shaving [%] is peak shaving percentage if the forecasting is 100% accurate.

In Figure 2.5, the monthly peaks for one whole year are shown for different methods:

**Daily-based:** the peak is shaved for every day in one month; shaving the daily peak will shave the monthly peak.

**Monthly-based:** the peak of the first day in the month is shaved and the peak after shaving is used as a target ( $\text{Peak}_{\text{Target}}$ ) to shave the peak of the next day. The target peak is updated daily.

**Receding:** the schedule is updated every one step by realizing the peak demand and/or by updating the forecasted load and PV generation.

**Non-Receding:** the load and PV generation are forecasted one time at the beginning of the day, the schedule for one day ahead is constructed and is kept fixed during the day.

Table 2-1. The effectiveness of different methods in shaving the 15-minute monthly peak for a school for 5 years of historical data with different time-of-realization and time-of-scheduling, and with receding and non-receding horizons. Presented in Chapter 4.

#	<b>Hourly Forecasting</b>	realization	scheduling	<b>Effectiveness [%]</b>	
				Forecast	SDDP
1	One-time forecasting	no realization	One-time hourly based	46.63	36.82
2	receding horizon	hourly	Hourly based and receding	46.33	44.61
3	receding horizon	15-minute	Hourly based and receding	43.73	14.85
4	receding horizon	15-minute	15-minute based and receding	50.64	36.67
5	One-time forecasting	hourly	Hourly based and receding	41.92	35.86
6	One-time forecasting	15-minute	Hourly based and receding	40.13	40.09
7	One-time forecasting	15-minute	15-minute based and receding	46.03	34.33

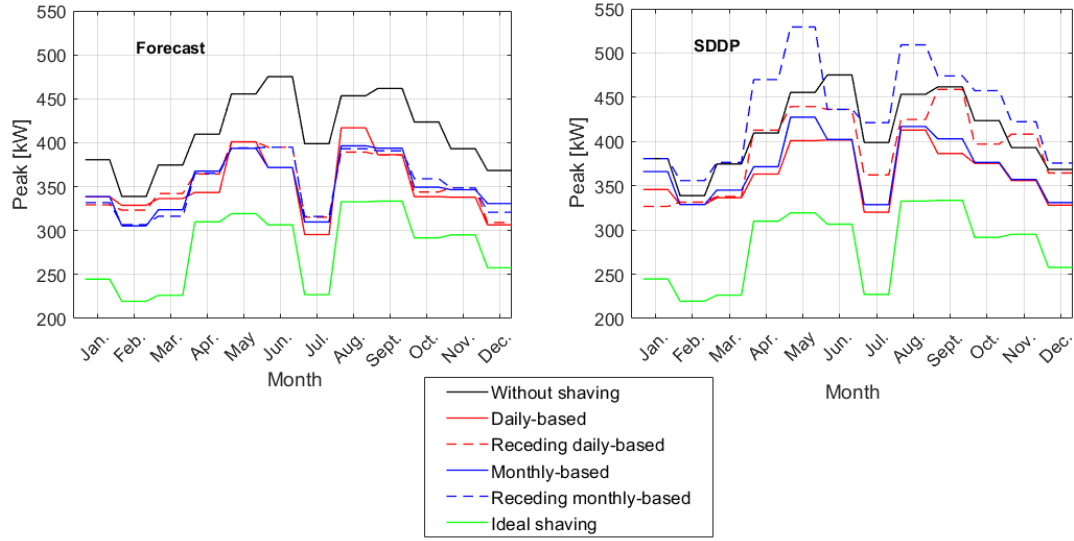
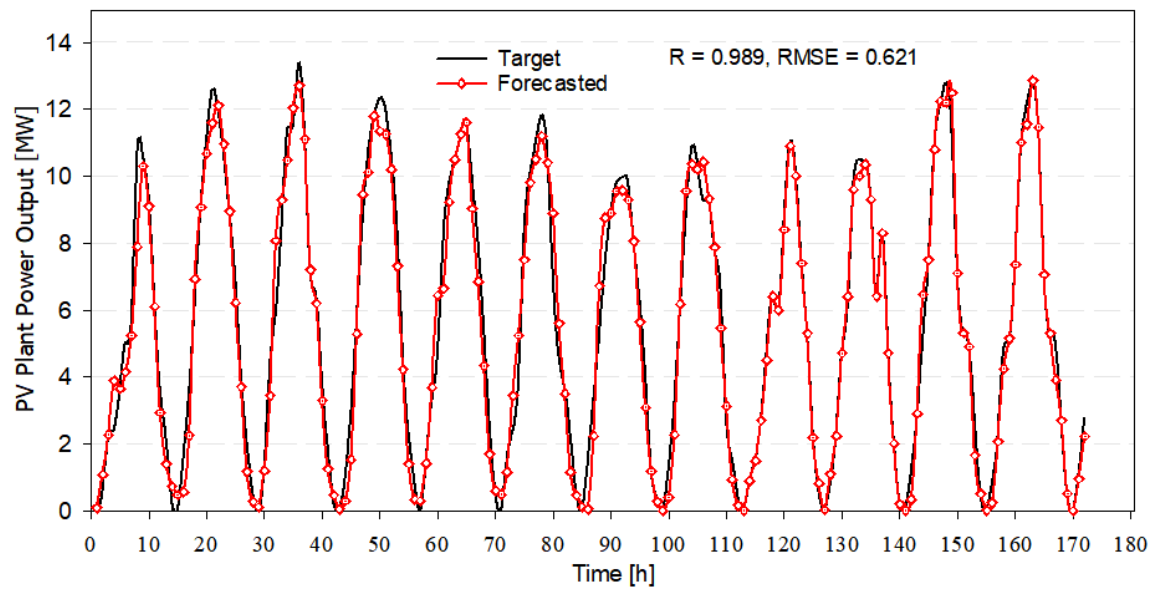


Figure 2.5. Monthly peak values before and after shaving using (1) Forecast, and (2) SDDP methods. Presented in Chapter 4.

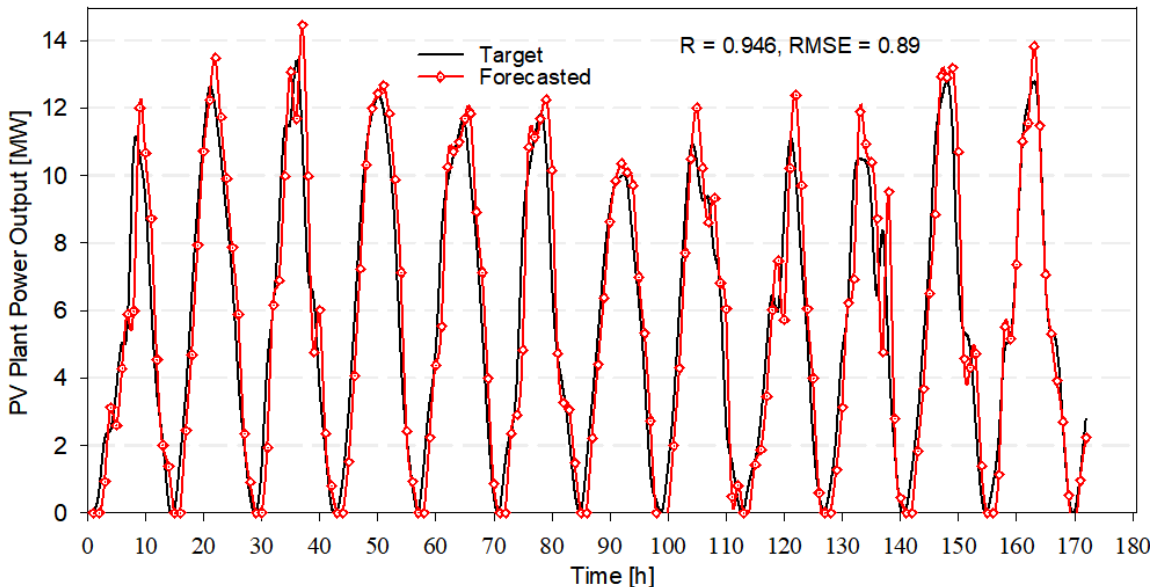
The results shown in this section are for a single school. The result for different commercial facilities are given in Chapter 4.

### 2.2.3. Different Prediction Methods

Different neural network configurations and different statistical approaches are compared in predicting the photovoltaic generation in Chapter 5. Neural networks are found to be more efficient in predicting the PV generation than the statistical approaches. Figure 2.6 shows the prediction results for sunny days using Neural networks and statistical approaches. Neural networks recorded a higher correlation coefficient ( $R$ ) and lower root mean square error (RMSE) when compared to statistical approaches.



(a)



(b)

Figure 2.6. Results of PV power prediction for 1 hour ahead forecasting for sunny days using (a) neural network (b) statistical method. Presented in Chapter 5.

The effectiveness of simple prediction tools is compared against the neural network and the most well-known statistical model (ARIMA model) in shaving the demand peak in Chapter 6. The proposed methods are based on a simple moving average concept, seasonality of the energy profiles, and suboptimality-based decision making. The methods are summarized, and they are assigned numbers as follows:

1. Common optimal strategy (Moving): A historical data of given window size is utilized in this method. The window size is expressed by the number of days in the moving window. The method is based on extracting the daily schedule that can be the optimal schedule across all days in the moving window. The extracted schedule is then used to shave the peak for the coming day. For example, we can take historical data of the last five days and optimize a one fixed daily schedule that if used to shave the peak of the last five days, the peak of the past five days will be the minimum.
2. Day-name-based common optimal strategy: A historical data of one year is used for example. The days of the same name are grouped (e.g., Monday). Then the optimal daily schedule across all days in one group is extracted. The controller will select a schedule out of seven pre-constructed schedules, based on the day name.
3. Moving average: The energy profiles for a predefined number of days (rolling window) for the load and PV generation are averaged. The average profiles will be used as a prediction to optimize the schedule of the coming day.

4. Day-name-based average: The days of the same name are grouped. Then we take the average of the energy profiles for all days in one group. Then the averaged energy profiles (demand and PV) for each group are used to optimize seven different schedules for these seven groups. The schedule will be then selected out of seven pre-optimized schedules, based on the day of the week.
5. Year average: The energy profiles (load and PV) are averaged across all days of the previous year. The average profiles will be used to optimize a schedule. The schedule is then adopted for the next full year's peak shaving.
6. Naive Forecasting: The electrical load and PV profiles for the next day are assumed to be the same as the preceding day. The schedule is constructed accordingly.
7. Neural Network: The neural network is used to predict the load and PV generation for one day ahead. The prediction in this work was based on time series forecasting, i.e., the sequential data of electrical load/ PV Power is used for prediction without using any other inputs. Historical data of one year was used to train NN: 70% of the data is used for training and 30% of the data is used for validation. The validation aims to optimize the NN parameters using the trial-and-error method.
8. ARIMA model: ARIMA model is one of the well-known statistical models used for time-series forecasting. ARIMA model parameters were optimized in a way similar to the optimization process of NN parameters.

Figure 2.7 shows the effectiveness of the proposed forecasting tools when used for shaving the demand peak of different facilities. The following conclusion can be drawn from Figure 2.7:

- Common optimal strategy (method #1) recorded the highest effectiveness when used to shave the peak of school, theater, and hotel if the window size is optimized.
- Common optimal strategy with optimized window size outperforms NN prediction in shaving the peak for all considered facilities.
- The NN outperformed ARIMA model in shaving the peak of school, theater, and hotel.
- Naive forecasting in general is the least efficient.
- The profiles of a school and a theater are easier for peak shaving under the prediction uncertainty than church and hotel. The peaks of school and theater can be shaved with effectiveness around 50%. The best effectiveness of peak shaving of church and hotel was about 35% and 32%, respectively.

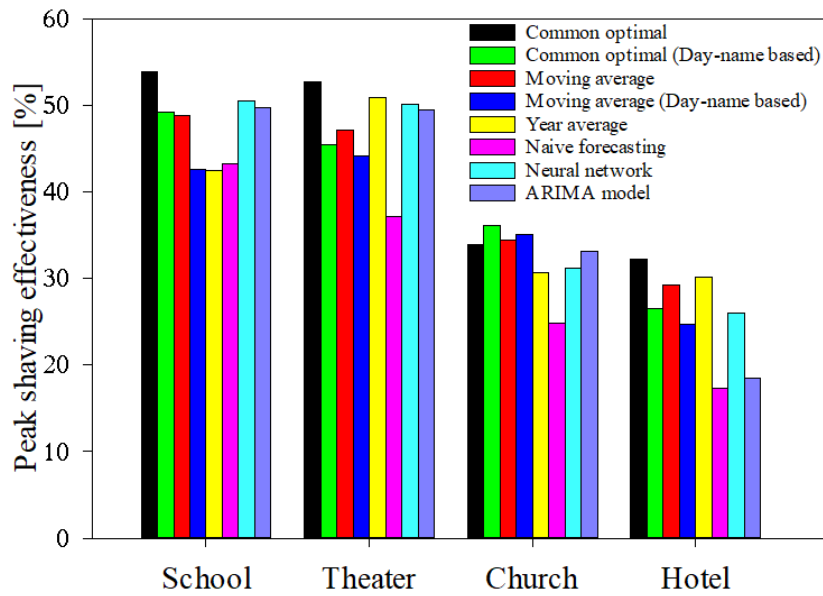


Figure 2.7. The effectiveness of peak shaving using PV-battery system for different facilities based on different prediction methods.

In summary, simple forecasting tools have proven to be competitive with the artificial intelligence and ARIMA model when used to predict the energy profiles to schedule PV-battery systems for peak shaving applications.

3. PAPER A: SIZING PV-BATTERY GRID-CONNECTED SYSTEM UTILIZING  
THE CONVEX OPTIMIZATION ALGORITHM FOR PEAK SHAVING  
APPLICATION<sup>1</sup>

### 3.1. Synopsis

This work introduces a framework to find the optimal sizes of combined photovoltaic (PV) and battery systems used to reduce the overall electricity cost of commercial buildings. Many electric utilities charge consumers based on both total energy consumption and the monthly peak demand. Monthly peak rates are intended to disincentivize large peaks in electrical demand for individual clients, and thus lower grid peak demand; however, shaving the monthly peak is a challenging optimization problem due to the long scheduling horizon of one month. Furthermore, data for at least one year is usually considered for sizing energy systems. Scheduling the battery storage over one year is computationally intensive. To optimize a photovoltaic battery system, the sizing and the scheduling problems need to be solved in tandem. Consequently, sizing a photovoltaic battery system for peak shaving under common electricity tariff structures is a complex optimization problem.

In the current work, a sequence of methods, including convex optimization algorithm, problem decoupling, binary variables and big-M value, linearization, surrogate optimization algorithm, and problem reformulation, are used to decrease the complexity

---

<sup>1</sup> Hussein Sharadga, Bryan Rasmussen, “Sizing PV-battery Grid-connected System Utilizing the Convex Optimization Algorithm for Peak-shaving Application”.

of the sizing problem. Different scenarios and pricing policies are considered and formulated to be convex. The economic feasibility of peak shaving using optimized photovoltaic battery systems is then analyzed using the actual load profiles from four different facilities located in Texas.

### **3.2. Introduction**

Commercial facilities powered by photovoltaic (PV) systems are usually connected to an electrical grid. The grid covers the facility's energy deficiency in case the produced power by the PV system is less than the facility's demand. Standalone PV systems (i.e., those not connected to the electrical grid) can be installed with or without batteries. In systems with batteries, these storage devices will be on charge mode if the PV system generates energy in excess of the facility's needs. The battery provides some electricity when the power produced by the PV system does not meet the facility's demand. Large-capacity batteries are required to meet the facility's demand in case of extreme conditions, such as during long stretches of rainy conditions. The capital cost of standalone PV systems with large batteries might be a deterrent to installation without an attractive return on investment. In terms of reliability, it is preferable to connect PV systems with batteries to the grid. Grid utilities, however, have policies to secure the grid operation. Optimizing and sizing the PV-battery system is a complex endeavor due to the constraints and pricing schemes imposed by the utilities. Figure 3.1 shows the general components and the coupling of PV-battery grid-connected system.

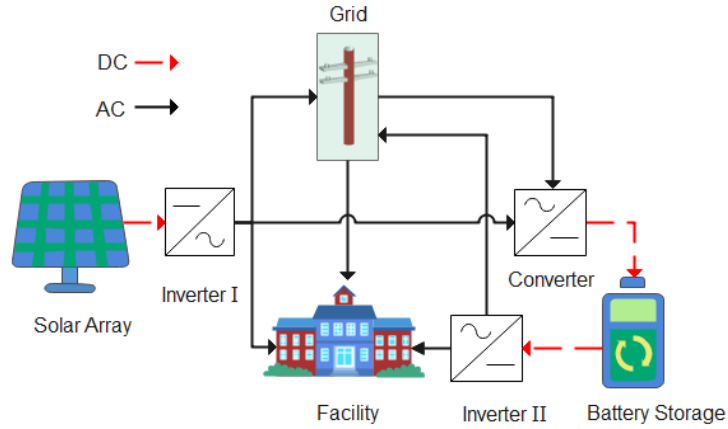


Figure 3.1. Schematic of PV-Battery-Grid system.

Maintaining the stability of an electrical grid involves reducing the grid's peak demand [24], accomplished by motivating consumers to reduce the electricity consumption during the grid's peak period by shifting the load to the off-peak period, often by using an energy storage system. Time-of-use pricing [12] and real-time pricing [15] are pricing schemes intended to motivate consumers to participate in the utility's peak shaving. In Texas, electrical utilities charge consumers based on the total amount of consumed electricity and the facility's monthly peak demand (i.e., the largest 15 minutes average of electrical demand measured in kW). If present, the energy storage system is set on the charge mode during the facility's off-peak demand and on discharge mode during the facility's peak demand.

In [22], the possibility of reducing the peak demand by using batteries for grid-connected commercial facilities in Texas is discussed. While the primary purpose of peak demand shaving is to enhance grid stability, reducing the billed amount for electricity is still the main motivation for the consumers to participate in grid's peak shaving.

Motivational pricing approach in Texas helps to reduce the facilities' peaks more than shaving the grid's peak. For instance, some commercial consumers might charge their batteries during the grid's peak in such a way that reduces their facility's peak. Automated demand management could reduce the bill amount for end-users significantly but might affect the grid stability negatively. In [21], a novel pricing scheme is proposed. The proposed management program encourages Texas commercial consumers, using a battery system, to shift their facilities' demands in an efficient way that shaves the peak demand of the grid. The proposed scheme aligns the objective of reducing consumer's bill amount with the grid's peak shaving.

Several studies using different methods and different cost functions have been conducted to shave the demand peak using a battery storage system of a given size. Nguyen et al. implemented game theory to reduce peak demand of facilities equipped with batteries in [25]. In [26], a battery system owned by the utility company is proposed to shave the grid's peak. In [27], it has been shown that the battery storage system, used to shave the peak, when used for two different applications promotes lower bill amount. The decision-tree algorithm consumes less computational time compared to other optimization techniques when used for peak shaving application for islanded microgrids equipped with batteries in [28]. In [29], the depth of discharge and the charge-discharge cycles of the battery system were constrained to increase the lifespan of batteries used for peak shaving. In [30], convex optimization was used to design a controller to schedule the battery charging and discharging of a PV-battery system used to reduce the electricity consumption

and to shave electricity peak demand. The controller includes the battery capacity-loss cost in the cost function using a convex battery-aging model.

Determining the optimal schedule for charging and discharging the battery is a challenging problem because of the long time horizons. Additionally, the sizes of the energy storage systems need to be optimized as part of the initial design process. Undersized battery systems age quickly, thus incur a higher replacement cost; however, oversized systems do not achieve a better cost-benefit ratio due to the high initial cost of large batteries [19]. Limited resources exist to determine the return on investment and optimal size of PV-battery storage systems [1]. In [31], [32], the size of the standalone PV system equipped with batteries is optimized with two objectives: reducing energy deficiency and reducing life cycle cost. The proposed work returned candidate solutions of optimal sizes of both the PV array and battery energy storage. In [33], the leveledized cost of electricity is estimated to evaluate the fitness of PV-battery grid-connected system. In [34], the size of the battery for grid-connected PV-battery system is optimized with two objective functions: the bill amount and the battery capacity loss. The size of the battery is obtained by flow decisions. In [35], the battery size for a given PV system was optimized to reduce the bill amount and the battery aging cost. The study was for a country adopting the time of use (TOU) pricing scheme. Therefore, the battery is used to reduce high consumption of grid electricity during the high-price period. The objective function with the time-of-use pricing scheme is linear, thus the mixed-integer linear programming was proposed to find the optimal charging and discharging schedule. The optimal size of PV system was obtained by tabulating the return on investment for different PV system sizes with

corresponding optimal battery capacity. In [36], the sensitivity analysis was implemented to find the optimal size of the grid-connected PV-battery system. In [37], the day is broken into six intervals. The battery state of charge through the year is obtained based on the time of the day. The study was accomplished under the time-of-use electricity tariff. The genetic algorithm was employed to optimize eight values: PV system size, battery maximum capacity, and other six values representing the optimal battery state of charge corresponding to the time-of-day slot.

### **3.2.1. A General Coupling of PV-Battery-Grid System**

The solar array produces power in the form of DC electricity. An inverter is used to convert power produced by the PV system into AC power (see Figure 3.1); however, the battery system stores the energy in the form of DC electricity.

The power produced by the solar array after being converted to AC can be then used to run our home applications, feed the grid, or can be passed to a converter that transforms the power back into the DC form for storing in the battery. The converter also converts the AC power coming from the grid to DC electricity to charge the battery. To use the electricity stored in the battery, a second inverter transforms the DC electricity of the battery into AC, which can be used to run our houses or feed the grid.

### **3.2.2. Contributions**

In the current work, the size of PV-battery systems connected to the grid is optimized to reduce electricity cost for commercial facilities whose electric utility rates include monthly peak demand costs. The battery collects excess PV energy and shaves the facility's demand peak by shifting the load. Shaving the 15-minute monthly demand peak

reduces the billed amount while not reducing the total energy consumption. The resulting scheduling problem is a computationally-intensive optimization problem due to the long scheduling horizon of one month. However, to effectively size a PV-battery system for peak shaving application, the scheduling problem and the sizing problem are solved together.

The proposed methods are demonstrated using actual electricity usage profiles from various types of commercial buildings located in Texas. A complete case study is performed for a school. Then the effect of the load profile of additional Texas commercial facilities is investigated: theater, church, and hotel. Different pricing scenarios are introduced and the formulations for these scenarios using convex optimization are provided. The convex optimization algorithm is very fast, especially when a large number of variables (or a large vector) needs to be optimized. The complexity of the current optimization is reduced by the following techniques:

- A. Breaking the optimization problem into two problems: (1) Sizing the PV-battery system (2) optimizing the charging/discharging schedule. Decoupling the problem enables using the convex optimization algorithm for sizing the system.
- B. Using binary variables and big-M value method to convexify the scheduling problem.
- C. linearization and reformulation of the charging/discharging schedule for a given PV-battery capacity.

### 3.3. Modeling and Problem Formulation

In this section, the optimization problem is reformulated to be accepted by the convex optimization algorithm. The objective function is to minimize electricity cost, which includes the bill amount and the life cycle cost. The life cycle cost estimation model is given in the following section. The mathematical model to extract PV array parameters is provided in Appendix A. The proposed PV system is equipped with a maximum power point (MPP) tracking controller. The methods for estimating the MPP, the effect of the array configuration, estimating the cell temperature, and solar radiation calculations are discussed in detail in Appendix A.

#### 3.3.1. Life Cycle Cost

The life cycle cost ( $LCC$ ) is the summation of the initial capital cost ( $S_{IC}$ ), the operation, and the maintenance cost ( $S_{O\&M}$ ) as well as the replacement cost ( $S_{Rep}$ ), as shown in [31]. In this section, the  $LCC$  is \$ per the life span of the system in years. The life span of the current system,  $N$ , in years is 20 years. Otherwise,  $LCC$  is given as [\$/year] in the rest of the paper.

$$LCC \text{ [\$]} = S_{IC} + S_{O\&M} + S_{Rep} \quad (3.1)$$

The initial capital cost of the system, ( $S_{IC}$ ), is the price of the system's components ( $S_{Hardware}$ ) as well as the civil/labor cost ( $S_{Civil}$ ):

$$S_{IC} = S_{Hardware, PV} + S_{Hardware, Bat} + S_{Hardware, Inv} + S_{Hardware, Conv} + S_{Civil} \quad (3.2)$$

where “PV” stands for photovoltaic modules, “Bat” is the storage battery, “Inv” is the inverter and “Conv” is the converter. Equation (3.2) can be written as follows [31]:

$$S_{IC} = C_{PV} \times U_{PV} + C_{Bat} \times U_{Bat} + C_{Inv} \times U_{Inv} + C_{Conv} \times U_{Conv} + S_{Civil} \quad (3.3)$$

where “ $C$ ” stands for the capacity, for example [W], of the hardware and the “ $U$ ” is the unit cost, [\$/W] for example. The  $S_{\text{Civil}}$  includes the cost of installation, engineering, and management. The capacity of a solar photovoltaic system ( $C_{PV}$ ) is array’s maximum power ( $P_m, \text{array}$ ) as defied in Appendix A, Equation (A.15). The  $S_{\text{Civil}}$  is about 0.4 of the total hardware’s cost as given in [49]:

$$S_{\text{Civil}} = 0.4 \times [S_{\text{Hardware, PV}} + S_{\text{Hardware, Bat}} + S_{\text{Hardware, Inv}} + S_{\text{Hardware, Conv}}] \quad (3.4)$$

The operation and maintenance cost ( $S_{O\&M}$ ) is obtained as follows [50]:

$$S_{O\&M} = \begin{cases} S_{O\&M,0} \times \left[ \frac{1 + I_{f,r}}{I_{n,r} - I_{f,r}} \right] \left[ 1 - \left( \frac{1 + I_{f,r}}{1 + I_{n,r}} \right)^N \right], & I_{n,r} \neq I_{f,r} \\ S_{O\&M,0} \times N, & I_{n,r} = I_{f,r} \end{cases} \quad (3.5)$$

where  $N$  is the life of the system in years,  $I_{n,r}$  is the interest rate and  $I_{f,r}$  is the inflation rate. The parameter  $S_{O\&M,0}$ is the operation and maintenance cost for the first year and is obtained as follows:

$$\begin{aligned} S_{O\&M,0} = & R_{O\&M, \text{PV}} \times S_{\text{Hardware, PV}} + R_{O\&M, \text{Bat}} \times S_{\text{Hardware, Bat}} \\ & + R_{O\&M, \text{Inv}} \times S_{\text{Hardware, Inv}} \\ & + R_{O\&M, \text{Conv}} \times S_{\text{Hardware, Conv}} \end{aligned} \quad (3.6)$$

where  $R_{O\&M}$  is the ratio of the operation and maintenance cost of the first year to the hardware cost.

The replacement cost ( $S_{Rep}$ ) of a component is given below [50] :

$$S_{Rep} = S_{\text{Hardware}} \times (1 - U_{\text{Salvage}}) \times \sum_{i=1}^{N_{\text{Replace}}} \left( \frac{1 + I_{f,r}}{1 + I_{n,r}} \right)^{N \times i / (N_{\text{Replace}} + 1)} \quad (3.7)$$

where  $U_{\text{salvage}}$  is per unit salvage value.  $N_{\text{Replace}}$  is the number of replacement of a component and is calculated as follow [50]:

$$N_{\text{Replace}} = \text{Integer} \left( \frac{2N - 1}{2L} \right) \quad (3.8)$$

where  $L$  is the life of a component in years.

The financial data are summarized in Table 3-1 and Table 3-2.

Table 3-1. Financial data of the system's hardware. Adapted from [31], [50], [51].

Component	Unit cost ( $U$ )	Life ( $L$ ) in years	$O\&M_{ratio}$	$(N_{\text{Replace}})$ using Equation (3.8)
PV module	1 [\$/W]	20	1%	0
Battery	125 [\$/kWh]	5	5%	3
Inverter	0.5 [\$/W]	10	0%	1
Converter	0.5 [\$/W]	10	0%	1

Table 3-2. General financial data of the system. Adapted from [31], [50].

Parameters	Value
$N$	20
$I_{f,r}$	0.08
$I_{n,r}$	0.04
$U_{\text{Salvage}}$	0.1

### 3.3.2. Electricity Cost Optimization

As mentioned before, to size a PV-battery system for peak shaving applications, the scheduling problem and the sizing problem are solved together. The current problem is solved using two approaches. In approach #1 (Nested Solution), the sizing and scheduling problems are decoupled and solved. In approach #2 (Simultaneous), the problem is reformulated to be solvable using convex optimization without Solution decoupling. Different scenarios are also introduced and formulated to be convex. Three scenarios are investigated in the current study. The scenarios are given in Table 3-3. Historical data of one year is considered for the sizing problem. Thus, the scheduling problem is solved with a one-year scheduling horizon.

Table 3-3. Scenarios summary.

<b>Scenario #</b>	<b>Scenario description</b>
1	no-supply-to-grid constraint
2	the grid receives the access PV energy for free
3	the consumer can sell the electricity to the grid but for a low price

### 3.3.2.1. Approach #1: Nested Solution

The problem is decoupled into two problems: scheduling (3.3.2.1.1) and sizing (Section 3.3.2.1.2). The scheduling problem is solved using convex optimization. The algorithm to solve the sizing problem is discussed in Section 3.3.2.1.3.

#### 3.3.2.1.1. Scheduling

The primary objective function is to minimize the bill amount as shown below:

$$\text{minimize} \left[ \begin{array}{l} \text{Total grid energy [kWh] } \times \text{Energy rate [$/kWh]} \\ + \sum_{n=1}^{12} \text{Peak (n) [kW] } \times \text{Peak rate [$/kW]} \end{array} \right] \quad (3.9)$$

Subject to:

$$\begin{aligned} u(t) &\geq -1 \\ u(t) &\leq 0.4 \\ 0 \leq E_S(t) &\leq C_{Bat} \end{aligned} \quad (3.10)$$

where:

$$E_S(t) = E_S(t_0) + C_{Bat} \int_{t_0}^t u(\tau) d\tau \quad (3.11)$$

where Peak is the monthly peak and is given below:

$$\text{Peak (n)} = \max [E_G (t = [n - 1] \times N_i + 1 : n \times N_i)] \quad (3.12)$$

where  $E_G$  is the grid energy and given below,  $n$  is the month's number (out of 12),  $N_i$  is the number of metered intervals within one month ( $N_i = 96 \frac{15-\text{min. intervals}}{\text{day}} \times$

$30 \text{ days} = 2880$  intervals). The  $u$  is the charging rate (positive for charging and negative for discharging),  $C_{Bat}$  is the capacity of the battery,  $E_S(t)$  is the energy stored in the battery at time  $t$ , and  $E_S(t_0)$  is the initial energy stored in the battery (at time = 0). The constraints, given in Equation (3.10), are applied on every time step. The maximum charging rate ( $u_{max}$ ) is assumed to be 0.4 and the maximum discharging rate ( $u_{min}$ ) is assumed to be one (see Equation (3.10)).

The grid energy is given below:

$$E_G = E_L - E_{PV} + E_{Bat} \quad (3.13)$$

The battery energy is given below (See [21], [22]) :

$$E_{Bat} = C_{Bat} \max(\eta u, \frac{1}{\eta} u) \quad (3.14)$$

where  $E_G$  is the grid energy,  $E_L$  is the load energy,  $E_{PV}$  is the PV energy ( $E_{PV}$  is the maximum PV power generated by an array ( $P_{m, array}$ ) and can be calculated as shown in Appendix A),  $E_{Bat}$  is the battery charging energy, and  $\eta$  is the battery charging/discharging efficiency. In Equations (3.13) and (3.14),  $C_{Bat}$  and  $u$  need to be optimized. Equation (3.14) does not comply with the convex optimization rule since the two variables are multiplied by each other. If the battery capacity ( $C_{Bat}$ ) is given, the problem of determining the charging/discharging rate vector is a convex optimization problem (as shown in [4] and [5]), thus can be solved using convex optimization algorithm. The convex optimization algorithm is fast, especially when solving for a huge number of variables or a large vector like  $u$ . In Nested Solution, the scheduling problem is solved with  $C_{Bat}$  given by decoupling the problem as shown in Section 3.3.2.1.2.

Three scenarios are investigated in the current study (Table 3-3). Formulating these scenarios to be accepted by the convex optimization algorithm, CVX (CVX is given in Appendix B), and the complexity of handling these scenarios are shown below:

**A) Scenario #1 and assuming the charging/discharging efficiency is one ( $\eta = 1$ )**

In this scenario (see Table 3-3), the consumer is not allowed to supply the grid with any electricity. In this case, we add a constraint on the grid energy ( $E_G$ , Equation (3.13)) to be nonnegative ( $E_G \geq 0$ ). We write the constraint  $E_G \geq 0$  in terms of  $u$  which is the CVX optimization variable (CVX is given in Appendix B):

$$\max(\eta u, 1/\eta u) \geq (E_{PV} - E_L)/C_{Bat} \quad (3.15)$$

Assuming that the charging/discharging efficiency is one.

$$u \geq (E_{PV} - E_L)/C_{Bat} \quad (3.16)$$

**B) Scenario #2 with both  $\eta = 1$  and  $\eta \neq 1$**

In this scenario, we assume that the grid utility will accept to receive energy from the PV system of the consumers but for free. That takes place in case the consumers need to get rid of the excess PV energy. To represent this, we add a simple statement as follow:

$$E_{G,new} = \max(E_{G,old}, 0) \quad (3.17)$$

In this scenario, if the consumer withdraws energy from the grid, i.e., the grid energy is positive, the utility will charge the consumers. If grid energy is negative, the optimization algorithm will read it as zero which means the utility receives this excess power and does not refund the consumers. However, the optimization algorithm is smart thus it will try to utilize the energy for the consumer's sake and not supply energy to the grid. However, in case the power produced by the PV system is high and the battery size

is small or is fully charged, the excess PV energy will provide to the grid for zero benefits.

Max function of Equation (3.17) is convex thus it can be used with convex optimization algorithm without reformulation.

### C) Scenario #3 with $\eta = 1$

Assuming the grid utility accepts to purchase electricity generated by the consumers but for a low price. Below is an example:

$$\begin{aligned} \text{If } E_G \geq 0, \text{ Energy rate} &= 0.05 \text{ [$/kWh]} \\ \text{If } E_G < 0, \text{ Energy rate} &= 0.01 \text{ [$/kWh]} \end{aligned} \quad (3.18)$$

The “if” statement is not accepted by the convex optimization algorithm. The “if” statement is replaced using binary-variable scheme as follows:

$$\text{Energy rate} = (0.04B + 0.01) \text{ [$/kWh]} \quad (3.19)$$

where  $B$  is a binary variable such that if  $B = 0$  the energy rate will be 0.01 [\$/kWh] and if  $B = 1$  the energy rate equals 0.05 [\$/kWh]. The “if” statement is then rewritten as follows:

The first constraint of Equation (3.18) is updated as follows:

$$\begin{aligned} E_G &\geq 0 \\ E_L - E_{PV} + C_{Bat} \max\left(\eta u, \frac{1}{\eta} u\right) &\geq 0 \end{aligned} \quad (3.20)$$

For  $\eta = 1$ :

$$E_L - E_{PV} + C_{Bat} u(t) \geq 0 \quad (3.21)$$

We rewrite Equation (3.21) in terms of  $u$ , which is the optimization variable, and to make the equation shorter, we assume a new constant ( $C$ ):

$$u \geq C \quad (3.22)$$

$$C = \frac{E_{PV} - E_L}{C_{Bat}} \quad (3.23)$$

Using Big-M value and a binary variable ( $B$ ) to replace the “if” statement of Equation (3.18):

$$u \geq C - M(1 - B) \quad (3.24)$$

$$u < C + MB \quad (3.25)$$

$M$  is a very large number. In Equations (3.24) and (3.25):

- If  $B = 0$ , the constraint of Equation (3.24) will be always right and the constraint of Equation (3.25) needs to be satisfied.
- If  $B = 1$ , the constraint of Equation (3.25) will be always right and the constraint of Equation (3.24) needs to be satisfied.

The new optimization problem will be:

$$\begin{aligned} \text{minimize} \quad & \left[ (E_L - E_{PV} + C_{Bat} u) (0.04 B + 0.01) \right. \\ & \left. + \sum_{n=1}^{12} \text{Peak}(n) \times \text{Peak rate} \right] \end{aligned} \quad (3.26)$$

The Variables are  $u$  and  $B$ ,  $B$  is the binary variable.

Subject to:

$$\begin{aligned} u &\geq -1 \\ u &\leq 0.4 \\ u &\geq C - M(1 - B) \\ u &< C + MB \end{aligned}$$

The  $E_L$  and  $E_{PV}$  are constants for the CVX optimization algorithm. An issue will arise due to the multiplication of two optimization variables  $u$  and  $B$  in Equation (3.26). The multiplication of two optimization variables does not comply with CVX algorithm. To linearize the problem, we assume a new variable ( $y = u B$ ) and the new optimization problem will be:

$$\begin{aligned} \text{minimize} & \left[ (E_L - E_{PV})(0.04 B + 0.01) + 0.01 C_{Bat} u + 0.04 C_{Bat} y \right. \\ & \left. + \sum_{n=1}^{12} \text{Peak}(n) \times \text{Peak rate} \right] \end{aligned} \quad (3.27)$$

The variables are  $u$ ,  $y$ , and the binary variable  $B$ .

The new constraints after linearization are updated as instructed in [52] and shown below:

$$\begin{aligned} y &\geq -B \\ y &\leq 0.4 B \\ u - y &\geq -1 + B \\ u - y &\leq 0.4(1 - B) \\ u &\geq C - M(1 - B) \\ u &< C + M B \\ 0 \leq E_S(t_0) + C_{Bat} \int_{t_0}^t u(\tau) d\tau &\leq C_{Bat} \end{aligned} \quad (3.28)$$

#### D) Scenario #1 but with $\eta \neq 1$

Scenario #1 with  $\eta \neq 1$  is maintained using the constraint of Equation (3.20). The grid energy ( $E_G$ ) with the max function is convex function (see Equation (3.20)) as max function is convex. The convex algorithm does not accept having a constraint on a convex function (such as  $E_G$ ) to be higher than a constant (the constant is zero in this work as  $E_G \geq 0$ ). As we know, the battery energy will be “ $C_{Bat} \eta u$ ” in case of discharging and “ $C_{Bat} 1/\eta u$ ” in case of charging.

The following equation needs to be rewritten:

$$E_{Bat} = C_{Bat} \max(\eta u, \frac{1}{\eta} u) \quad (3.29)$$

Equation (3.29) can be rewritten in terms of binary variables to remove the max function:

$$\begin{aligned} C_{Bat} \max(\eta u, \frac{1}{\eta} u) &= C_{Bat} u f \\ f &= B_1 \frac{1}{\eta} + B_2 \eta \end{aligned} \quad (3.30)$$

where  $B_1$  and  $B_2$  are binary variables. In the case of charging ( $u \geq 0$ ), the  $f$  will be “ $1/\eta$ ” and will be “ $\eta$ ” in the case of discharging ( $u < 0$ ). That can be satisfied as follows:

$$\begin{aligned} \text{if } u \geq 0, \quad B_1 = 1, B_2 = 0 \\ \text{if } u < 0, \quad B_1 = 0, B_2 = 1 \end{aligned} \quad (3.31)$$

The “if” statement in Equation (3.31) does not comply with convex optimization so it is replaced by (1) assuming that  $B_1 \neq B_2$ , and (2) the following new two constraints:

$$u \geq -M(1 - B_1) - M B_2 \quad (3.32)$$

$$u < M B_1 + M(1 - B_2) \quad (3.33)$$

- If  $B_1 = 1$  and  $B_2 = 0$ , the constraint of Equation (3.32) needs to be satisfied (which will be equivalent to  $u \geq 0$ ) and the constraint of Equation (3.33) will be always right.
- If  $B_1 = 0$  and  $B_2 = 1$ , the constraint of Equation (3.33) needs to be satisfied (which will be equivalent to  $u < 0$ ) and the constraint of Equation (3.32) will be always right.

To define that the two parameters ( $B_1$  and  $B_2$ ) do not equal each other, we use the following constraint:

$$B_1 \leq B_2 - 1 \quad \text{or} \quad B_1 \geq B_2 + 1 \quad (3.34)$$

The logical operator (or) is not accepted by CVX optimization thus we use another binary variable  $B_3$  and the big-M value to rewrite Equation (3.34) as follows:

$$\begin{aligned} B_1 &\leq B_2 - 1 + B_3 M \\ B_1 &\geq B_2 + 1 - M(1 - B_3) \end{aligned} \quad (3.35)$$

The battery energy formula needs to be linearized as follows:

$$\begin{aligned} E_{Bat} &= C_{Bat} u f \\ E_{Bat} &= C_{Bat} u \left( B_1 \frac{1}{\eta} + B_2 \eta \right) \\ E_{Bat} &= C_{Bat} Z_1 \frac{1}{\eta} + C_{Bat} Z_2 \eta \end{aligned} \quad (3.36)$$

We have new two variables ( $Z_1 = u B_1$  and  $Z_2 = u B_2$ ). The first two constraints of Equation (3.10) will be updated in new eight constraints as follows (see [52] on how to update the constraints after linearization):

$$\begin{aligned} Z_1 &\geq -B_1 \\ Z_1 &\leq 0.4 B_1 \\ Z_2 &\geq -B_2 \\ Z_2 &\leq 0.4 B_2 \\ u - Z_1 &\geq -1 + B_1 \\ u - Z_1 &\leq 0.4 (1 - B_1) \\ u - Z_2 &\geq -1 + B_2 \\ u - Z_2 &\leq 0.4 (1 - B_2) \end{aligned} \tag{3.37}$$

To sum up, the new optimization algorithm will be:

$$\begin{aligned} \text{minimize} \left[ & (E_L - E_{PV} + C_{Bat} Z_1 \frac{1}{\eta} + C_{Bat} Z_2 \eta) \times \text{Energy rate} \right. \\ & \left. + \sum_{n=1}^{12} \text{Peak}(n) \times \text{Peak rate} \right] \end{aligned} \tag{3.38}$$

The grid energy is given as follows:

$$E_G = E_L - E_{PV} + C_{Bat} Z_1 \frac{1}{\eta} + C_{Bat} Z_2 \eta \tag{3.39}$$

The variables are  $u$ ,  $Z_1$ ,  $Z_2$ , and the binary variables are  $B_1$ ,  $B_2$ , and  $B_3$ .

Subject to the following constraints:

$$\begin{aligned}
B_1 &\leq B_2 - 1 + B_3 M \\
B_1 &\geq B_2 + 1 - M(1 - B_3) \\
u &\geq -M(1 - B_1) - M B_2 \\
u &\leq M B_1 + M(1 - B_2) \\
Z_1 &\geq -B_1 \\
Z_1 &\leq 0.4 B_1 \\
Z_2 &\geq -B_2 \\
Z_2 &\leq 0.4 B_2 \\
u - Z_1 &\geq -1 + B_1 \\
u - Z_1 &\leq 0.4(1 - B_1) \\
u - Z_2 &\geq -1 + B_2 \\
u - Z_2 &\leq 0.4(1 - B_2) \\
0 &\leq E_S(t_0) + C_{Bat} \int_{t_0}^t u(\tau) d\tau \leq C_{Bat} \\
\left( E_L - E_{PV} + C_{Bat} Z_1 \frac{1}{\eta} + C_{Bat} Z_2 \eta \right) &\geq 0
\end{aligned} \tag{3.40}$$

### E) Scenario #3 but with $\eta \neq 1$

Including the effect of charging/discharging efficiency ( $\eta \neq 1$ ), using the binary variables, big-M value, and linearizing the multiplication of CVX variables to overcome the convex optimization algorithm rules, the new optimization problem will be as follows. The full steps are not shown for the sake of brevity.

The new objective function is:

$$\begin{aligned}
\text{minimize} \quad & \left[ (E_L - E_{PV}) \times (0.01 + 0.04 B_0) + 0.04 C_{Bat} \left( F_1 \frac{1}{\eta} + F_2 \eta \right) \right. \\
& \left. + 0.01 C_{Bat} \left( Z_1 \frac{1}{\eta} + Z_2 \eta \right) + \sum_{n=1}^{12} \text{Peak}(n) \times \text{Peak rate} \right] \tag{3.41}
\end{aligned}$$

The grid energy is given as follows:

$$E_G = E_L - E_{PV} + C_{Bat} Z_1 \frac{1}{\eta} + C_{Bat} Z_2 \eta \tag{3.42}$$

The continuous variables are  $u$ ,  $Z_1$ ,  $Z_2$ ,  $F_1$ , and  $F_2$ . The binary variables are  $B_0$ ,  $B_1$ ,  $B_2$ ,  $B_3$ ,  $B_{01}$ , and  $B_{02}$ .

Subject to the following constraints:

$$\begin{aligned} F_1 &\geq -B_{01}, & F_1 &\leq 0.4 B_{01} \\ F_2 &\geq -B_{02}, & F_2 &\leq 0.4 B_{02} \end{aligned} \quad (3.43)$$

$$\begin{aligned} Z_1 - F_1 &\geq -B_1 + B_{01}, & Z_1 - F_1 &\leq 0.4 B_1 - 0.4 B_{01} \\ Z_2 - F_2 &\geq -B_2 + B_{02}, & Z_2 - F_2 &\leq 0.4 B_2 - 0.4 B_{02} \end{aligned}$$

$$\begin{aligned} u - Z_1 &\geq -1 + B_1, & u - Z_1 &\leq 0.4 (1 - B_1) \\ u - Z_2 &\geq -1 + B_2, & u - Z_2 &\leq 0.4 (1 - B_2) \end{aligned}$$

$$\begin{aligned} Z_1 \frac{1}{\eta} + Z_2 \eta &\leq C + M B_0 \\ Z_1 \frac{1}{\eta} + Z_2 \eta &\geq C - M (1 - B_0) \end{aligned}$$

$$\begin{aligned} B_1 &\leq B_2 - 1 + B_3 M \\ B_1 &\geq B_2 + 1 - M (1 - B_3) \\ u &\geq -M (1 - B_1) - M B_2 \\ u &\leq M B_1 + M (1 - B_2) \end{aligned}$$

$$\begin{aligned} B_{01} &\leq B_0 \\ B_{01} &\leq B_1 \\ B_{01} &\geq B_0 + B_1 - 1 \\ B_{02} &\leq B_0 \\ B_{02} &\leq B_2 \\ B_{02} &\geq B_0 + B_2 - 1 \end{aligned}$$

$$0 \leq E_S(t_0) + C_{Bat} \int_{t_0}^t u(\tau) d\tau \leq C_{Bat}$$

As we can see, to solve scenario #3 (with  $\eta \neq 1$ ) using convex optimization, we needed to generate 10 new variables (4 continuous and 6 binary) and we needed to add 19 new constraints. Solving for this number of variables and constraints is complex even with convex optimization as these variables and constraints are vectors of one-year length.

### 3.3.2.1.2. Sizing and Problem Decoupling

If the capacity of the battery ( $C_{Bat}$ ) is not given, the problem cannot be solved using the convex optimization algorithm due to the multiplication of  $u$  and  $C_{Bat}$  (see

Equations (3.13) and (3.14)). The convex algorithm is fast, so it is utilized to solve the current optimization problem.

The problem is decoupled: we use two optimization algorithms, one inside the other (See Figure 3.2). The external optimization algorithm is used to update values for the sizes of the battery ( $C_{Bat}$ ) and the PV system ( $N_{PV}$ ) while the convex optimization (the internal optimization algorithm) is used to optimize the charging rate vector. The charging vector ( $u$ ) is one year thus decoupling the problem and using the convex optimization to optimize lengthy vector eases the complexity. The external algorithm used here is ‘surrogateopt’ optimization algorithm, an open-source algorithm written in MATLAB Library. The  $P_{m, module}$  in Figure 3.2 is the maximum power generated by one PV module (See Appendix A).

It is worth mentioning that the value of  $u$ , the speed of charging and discharging, determines the size (cost) of the inverter and the converter. The value  $u$  in the scheduling problem (scheduling problem is marked red in Figure 3.2 ) is not optimized with only the bill amount as the objective function; the life cycle cost of the system’s components, including the inverter and converter, are also included in the objective function (see Figure 3.2).

```

Inputs:  $P_{m, \text{module}}$  profile, Load profile

Start Surrogate algorithm: Optimize  $N_{PV}$ ,  $C_{\text{Bat}}$ 

 $E_{PV} = N_{PV} \times P_{m, \text{module}}$ 

Start Convex optimization: Optimize  $u(t)$ 

    Subject to:  $u(t) \geq -1$   

 $u(t) \leq 0.4$   

 $0 \leq E_S(t_0) + C_{\text{Bat}} \int_{t_0}^t u(\tau) d\tau \leq C_{\text{Bat}}$   

    Objective: Minimize (yearly bill amount + yearly life cycle cost)

End Convex optimization

    Objective: Minimize (yearly bill amount + yearly life cycle cost)

End Surrogate algorithm

```

Figure 3.2. Code representation of the proposed combined optimization algorithm.

### 3.3.2.1.3. Optimization Algorithms Selection

Three different optimization algorithms are utilized to solve the external optimization problem given in Figure 3.2:

#### 1. Genetic algorithm

The genetic algorithm (GA) is one of the most well-known heuristic algorithms. The algorithm consumes a lot of time without generating an acceptable solution for the current problem: it gets stuck far away from the optimal solution. Referring to the GA workflow: the GA keeps generating a new population (the population is more than one candidate solution) and evaluating the objective function for every candidate in the new generation. It is worth mentioning that the objective function in the current problem is relatively time-consuming: the convex optimization consumes 3 minutes to optimize the

schedule for one year. Therefore, the evaluation of one candidate solution consumes 3 minutes, thus the GA is not an efficient algorithm for the current optimization problem in terms of the optimization cost. For example, if the population of GA consists of 30 candidate solutions, 90 minutes is needed to evaluate all candidate solutions in every new population.

## **2. Fmincon algorithm**

Fmincon was implemented previously for load shifting problems, for example in [35] and [36]. However, Fmincon is not efficient in optimizing a charging rate vector of one-year length with that the rate changes every 15 minutes. The charging rate vector is obtained by the convex optimization algorithm in the current work. However, Fmincon can be used here to return the sizes of the PV system and the battery storage. The total number of PV modules is an integer variable. Fmincon does not allow integer constraints thus, the solution is rounded to the nearest integer. Fmincon algorithm requires an initial guess. The results of the Fmincon algorithm with different initial guesses are shown in Figure 3.3.

## **3. Surrogate optimization algorithm**

The surrogate optimization algorithm is recommended for problems in which the objective function is time-consuming or, in other words, when there is a need to reduce the number of objective function evaluations. In surrogate optimization, we do not use the objective function to evaluate all the new samples as genetic algorithm does, but we use the surrogate function, which is faster, to replace the objective function. The surrogate optimization algorithm is a built-in MATLAB library.

The convergence of surrogate optimization is shown in Figure 3.3. Both algorithms (Fmincon and Surrogate) were executed with 600 maximum iterations. Both generate the best solution within the first 35 iterations. It is shown that Fmincon terminated the optimization before reaching the maximum function evaluations (600) because the solution within the tolerance was obtained. Surrogate optimization algorithm converges faster, allows for integer constraints, and does not need an initial guess.

To reduce the optimization cost, surrogate optimization is adopted for the current work with 30 maximum iterations (the computation time is less than 2 hours). The initial guesses used to initiate the Fmincon algorithm are (1) close initial guess of  $N_{PV} = 2000$  and  $C_{Bat} = 200$  and (2) far initial guess of  $N_{PV} = 1000$  and  $C_{Bat} = 100$ .

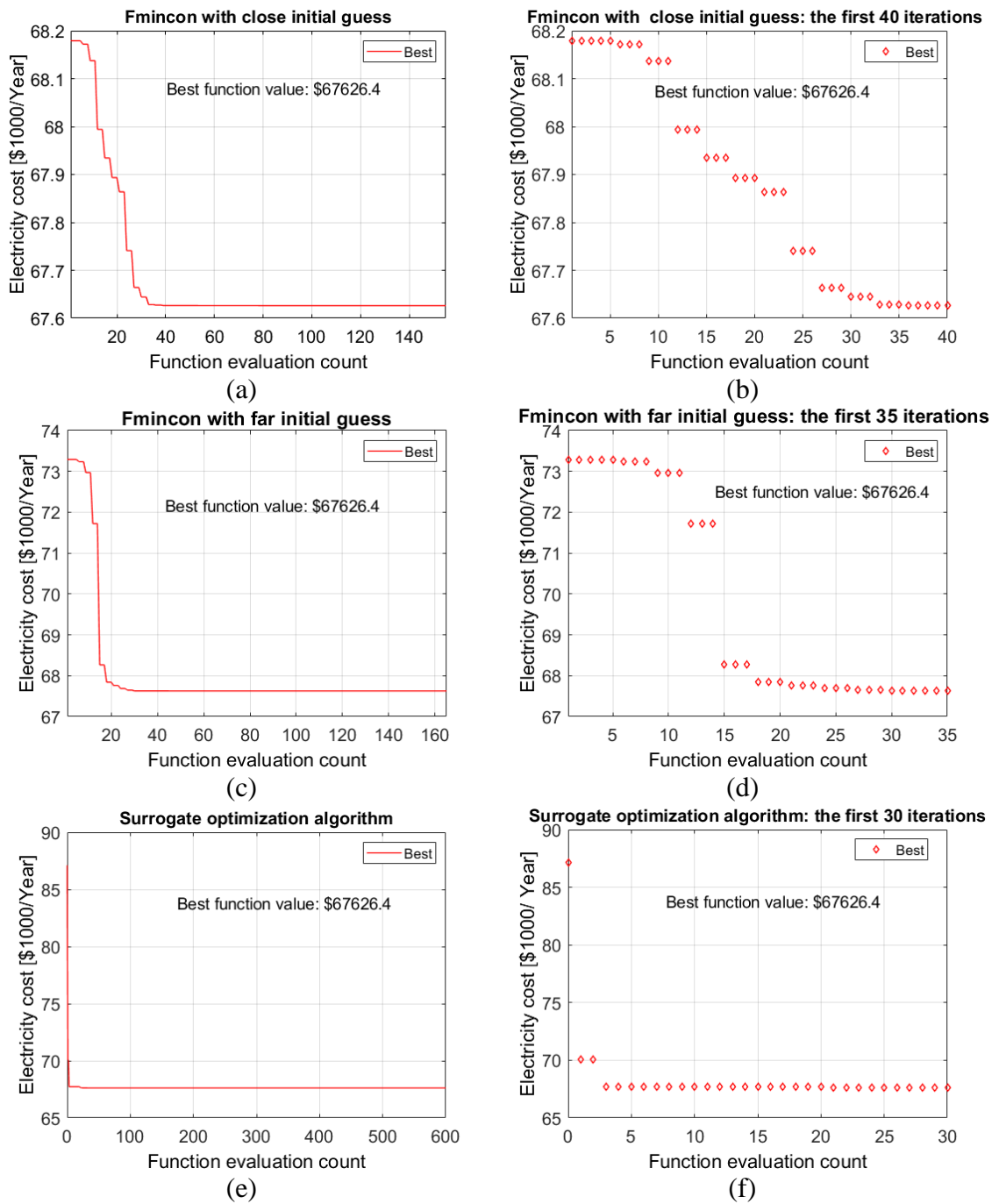


Figure 3.3. Convergence of Fmincon and surrogate optimization algorithm with 600 maximum iterations, the first 30 to 40 iterations are zoomed for clarity.

### 3.3.2.2. Approach #2: Simultaneous Solution

In this approach, the problem of sizing and scheduling is solved as one problem; the sizes and the charging rate vector is optimized together without decoupling. The problem is reformulated to be accepted by convex optimization algorithm.

Equation (3.14), the battery energy, which is given in [4] and [5] can be replaced by the following equation:

$$E_{Bat} = \max(\eta Q, \frac{1}{\eta} Q) \quad (3.44)$$

The grid energy is updated as given below:

$$E_G = E_L - E_{PV} + \max(\eta Q, \frac{1}{\eta} Q) \quad (3.45)$$

The new constraints are updated accordingly:

$$\begin{aligned} Q(t) &\geq -1 C_{Bat} \\ Q(t) &\leq 0.4 C_{Bat} \\ 0 \leq E_S(t_0) + \int_{t_0}^t Q(\tau) d\tau &\leq C_{Bat} \end{aligned} \quad (3.46)$$

where  $Q$  is the energy of charging or discharging.  $Q$  is positive if charging and negative if discharging.

The objective function will be:

$$\text{minimize } (\text{yearly bill amount} + \text{yearly life cycle cost}) \quad (3.47)$$

where the bill amount is given below:

$$\begin{aligned} \text{bill amount} &= E_G [\text{kWh}] \times \text{Energy rate} [\$/\text{kWh}] \\ &+ \sum_{n=1}^{12} \text{Peak (n)} [\text{kW}] \times \text{Peak rate} [\$/\text{kW}] \end{aligned} \quad (3.48)$$

The CVX variables are  $Q$ ,  $N_{PV}$ , and  $C_{Bat}$ . The problem is convex and can be solved by convex optimization without the need for decoupling (which was proposed in Nested Solution). Solving for the three different scenarios are summarized as follows:

#### A) The charging/discharging efficiency equals one ( $\eta = 1$ )

Scenarios #1 and #2 (see Table 3-3) can be solved directly using CVX optimization if the charging/discharging efficiency is assumed to be one ( $\eta = 1$ ). The Battery energy, Equation (3.44), and the grid energy, Equation (3.45), are updated as follows:

$$E_{Bat} = Q \quad (3.49)$$

$$E_G = E_L - E_{PV} + Q \quad (3.50)$$

For Scenario #2,  $E_G$  is updated as follows:

$$E_{G,new} = \max (E_{G,old}, 0) \quad (3.51)$$

For scenario # 3, there might be an easier way to solve it without the need to use binary variables. Solving for binary variables is more computation-intensive than solving for continuous variables. Binary variables were used to replace the “if” statement in Nested Solution. The max function can be used to find the positive and the negative components of a variable without using “if” statement or binary variables as proposed in [23]:

$$E_G^+ = \max (E_G, 0) = \max (E_L - E_{PV} + Q, 0) \quad (3.52)$$

$$E_G^- = \max (-E_G, 0) = \max (-(E_L - E_{PV} + Q), 0) \quad (3.53)$$

The bill amount is updated as follows:

$$\begin{aligned} \text{bill amount} &= E_G^+ [\text{kWh}] \times \text{Energy rate } [\$/\text{kWh}] \\ &+ E_G^- [\text{kWh}] \times \text{Refunding rate } [\$/\text{kWh}] \\ &+ \sum_{n=1}^{12} \text{Peak (n)} [\text{kW}] \times \text{Peak rate } [\$/\text{kW}] \end{aligned} \quad (3.54)$$

Energy rate is 0.05 [\$/kWh] and the Refunding rate is -0.01 [\$/kWh]. However, Equation (3.54) does not comply with CVX rules; {convex} + {concave} is illegal CVX operation as illustrated below:

-The function  $(E_G^+ \text{ [kWh]} \times \text{Energy rate [$/kWh]})$  is convex;  $E_G^+$  is convex because the max function is convex.

-The refunding rate, in Equation (3.54), is negative and the  $E_G^-$  is convex thus the function  $(E_G^- \text{ [kWh]} \times \text{Refunding rate [$/kWh]})$  is a concave.

To handle this issue, the max functions of Equations (3.52) and (3.53) are linearized and replaced by two constraints as follows:

$$\begin{aligned} E_G^+ &\geq E_G \\ E_G^+ &\geq 0 \end{aligned} \tag{3.55}$$

$$\begin{aligned} E_G^- &\geq -E_G \\ E_G^- &\geq 0 \end{aligned} \tag{3.56}$$

The constraints of Equations (3.55) and (3.56) to replace max function are justified as follows:

1) Since the purpose of optimization is to minimize the electricity cost, the  $E_G^+$  will need to be minimized. The minimum possible value of  $E_G^+$  is  $E_G$  or zero according to Equation (3.55). To satisfy the two constraints of Equation (3.55),  $E_G^+$  will equal the maximum value ( $\max(E_G, 0)$ ). Therefore, the max function is satisfied.

2) An issue rises of the new two constraints of Equation (3.56): the optimization algorithm minimizes the electricity cost, and since increasing the  $E_G^-$  will reduce the electricity cost, the optimization algorithm will maximize the  $E_G^-$ . Therefore  $E_G^-$  value will go to infinity

as the constraints of Equation (3.56) are unbounded. To address this issue, the following constraint is enforced:

$$E_G^+ - E_G^- \geq E_G \quad (3.57)$$

3) The constraint of Equation (3.57) is justified as follows:

**i. Case 1:  $E_G$  is positive**

If the  $E_G$  is positive, the first constraint of Equation (3.55) is dominant and the second constraint is not dominant. If the  $E_G$  is positive, the second constraint of Equation (3.56) is the dominant constraint. Thus, the dominant constraints of Equations (3.55), (3.56), and (3.57) are summarized as follows:

$$\begin{aligned} E_G^+ &\geq E_G \\ E_G^- &\geq 0 \\ E_G^+ - E_G^- &\geq E_G \end{aligned} \quad (3.58)$$

To minimize the cost, the optimization algorithm minimizes  $E_G^+$  as much as possible. To satisfy the first constraint of Equation (3.58), the minimum possible value of  $E_G^+$  is  $E_G$ .

$$E_G^+ = E_G \quad (3.59)$$

Now replace the  $E_G^+$  with  $E_G$  in the third constraint of Equation (3.58) and remove the first constraint of Equation (3.58):

$$\begin{aligned} E_G^- &\geq 0 \\ E_G - E_G^- &\geq E_G \end{aligned} \quad (3.60)$$

Rewrite the second constraint of Equation (3.60), Equation (3.60) is updated as follows:

$$\begin{aligned} E_G^- &\geq 0 \\ E_G^- &\leq 0 \end{aligned} \quad (3.61)$$

The two constraints of Equation (3.61) can be satisfied simultaneously if and only if

$$E_G^- = 0:$$

$$E_G^- = 0 \quad (3.62)$$

To sum up, if the  $E_G$  is positive (Case 1), the following two equations are satisfied:

$$\begin{aligned} E_G^+ &= E_G \\ E_G^- &= 0 \end{aligned} \quad (3.63)$$

### ii. Case 2: $E_G$ is negative

If  $E_G$  is negative, the following equations are satisfied (the reader might check in a similar way to what stated in the analysis of Case 1):

$$\begin{aligned} E_G^+ &= 0 \\ E_G^- &= E_G \end{aligned} \quad (3.64)$$

To sum up, scenario # 3 is now convex after the reformulation and can be solved with the constraints of Equations (3.55), (3.56), and (3.57).

## B) The charging/discharging efficiency is not one ( $\eta \neq 1$ )

For scenario #1, the max function of Equation (3.45) makes it unacceptable to have a constraint on  $E_G$  to be higher than zero ( $E_G \geq 0$ , the convex function  $E_G$  that is higher than constant as the constraint does not comply with the CVX algorithm rules). To remove the max function, the battery energy, Equation (3.44), and grid energy, Equation (3.45), are updated as follows:

$$\begin{aligned} E_{Bat} &= \frac{1}{\eta} Q_1 - \eta Q_2 \\ Q_1, Q_2 &\geq 0 \end{aligned} \quad (3.65)$$

$$E_G = E_L - E_{PV} + \frac{1}{\eta} Q_1 - \eta Q_2 \quad (3.66)$$

Now we have two vectors ( $Q_1$  for charging and  $Q_2$  for discharging). Solving for two vectors might be more computation-intensive than solving for one vector, but it is still better than using all of binary variables, big-M value, linearization, etc. To make sure the battery is not charged and discharged simultaneously, we can add the following constraint:

$$Q_1 Q_2 = 0 \quad (3.67)$$

The constraint of Equation (3.67) does not comply with convex optimization rules due to the multiplication of two optimization variables and needs to be linearized. However, according to Equation (3.66), there is a penalty on charging ( $1/\eta$ ) and a penalty on discharging ( $\eta$ ). To minimize the penalties, the CVX optimization will force one of the two variables ( $Q_1$  and  $Q_2$ ) to be zero, thus no need for the constraint of Equation (3.67). In [30], two vectors were used one for charging and one for discharging to construct the battery charging and discharging schedule. However, the problem of [30] can be solved using one vector (see Equation (3.44)). Optimizing one vector is usually faster than optimizing two vectors.

For scenario #2,  $E_G$  is calculated without any the need for any reformulation as follows:

$$E_G = E_L - E_{PV} + \max(\eta Q, \frac{1}{\eta} Q) \quad (3.68)$$

$$E_{G,new} = \max(E_{G,old}, 0) \quad (3.69)$$

For scenario #3, let's use Equation (3.52) and Equation (3.53) but with assuming  $\eta \neq 1$  as follows:

$$E_G^+ = \max(E_G, 0) = \max\left(E_L - E_{PV} + \max(\eta Q, \frac{1}{\eta} Q)\right), 0 \quad (3.70)$$

$$E_G^- = \max(-E_G, 0) = \max\left(-\left(E_L - E_{PV} + \max(\eta Q, \frac{1}{\eta} Q)\right), 0\right) \quad (3.71)$$

In Equation (3.71), the term “ $\left[E_L - E_{PV} + \max(\eta Q, \frac{1}{\eta} Q)\right]$ ” is convex. When this term is multiplied by a negative sign, it will be a concave function. The operation  $\max(\{\text{concave}\}, \{\text{constant}\})$  in Equation (3.71) does not comply with CVX rules. Thus, the max function is replaced by having  $Q_1$  as the charging vector and  $Q_2$  as the discharging

vector (using Equations (3.65) and (3.66)). Equations (3.70) and (3.71) are updated as follows:

$$E_G^+ = \max(E_G, 0) = \max\left(E_L - E_{PV} + \frac{1}{\eta} Q_1 - \eta Q_2, 0\right) \quad (3.72)$$

$$E_G^- = \max(-E_G, 0) = \max\left(-E_L + E_{PV} - \frac{1}{\eta} Q_1 - \eta Q_2, 0\right) \quad (3.73)$$

However, it still does not comply with CVX rules; the operation of {convex} + {concave} is illegal CVX operation as shown in Section A (See comments on Equation (3.54)). The five constraints (Equations (3.55), (3.56), and (3.57) can be used to find the positive and the negative components to replace max function of Equations (3.72) and (3.73), but the  $E_G$  in the formula of Equation (3.45) along with these constraints does not comply with convex optimization rules: in the first constraint of Equation (3.56), the CVX variable ( $E_G^-$ ) is greater than concave ( $E_G$  of Equation (3.45) is convex thus “ $-E_G$ ” is concave). The constraint of CVX variable greater than concave does not comply with CVX rules. Therefore, the max function of Equation (3.45) is replaced by two variables as suggested in Equation (3.65). The constraints used to solve for this scenario are summarized below:

$$E_G = E_L - E_{PV} + \frac{1}{\eta} Q_1 - \eta Q_2 \quad (3.74)$$

$$\begin{aligned} E_G^+ &\geq E_G \\ E_G^+ &\geq 0 \end{aligned} \quad (3.75)$$

$$\begin{aligned} E_G^- &\geq -E_G \\ E_G^- &\geq 0 \end{aligned} \quad (3.76)$$

$$E_G^+ - E_G^- \geq E_G \quad (3.77)$$

### **3.3.3. Scenarios and Approaches Summary**

Table 3-4, Table 3-5, and Table 3-6 summarize the scenarios and the solving approaches considered in the current study.

For Nested Solution: Scenario #1 can lead to termination of the optimization; the problem has no feasible solution if the PV system is large and the battery is small. That is caused by the constraint that the grid energy is nonnegative. Scenario #2 is easier to be handled. In scenario #2, the optimization algorithm will try to store all excess PV energy and not provide this power to the grid. The PV energy provided by the consumers to the grid will not be refunded. To store all of this excess PV energy, a larger battery is needed. However, if the cost of the battery is high, the optimization algorithm will choose to provide the excess PV power to the grid for free. Scenario #3 can make more sense. Scenario # 3, however, is difficult to handle using convex optimization with Nested Solution due to the complexity rising when the convex algorithm solves for binary variables. GROUBI solver might be helpful to solve scenario #3 as MOSEK solver simulation time goes to infinity.

For Simultaneous Solution: All scenarios are reformulated to be accepted by convex optimization and solved in a significantly short computation time.

Table 3-4. Solution's feasibility and cost for different scenarios and solving approaches.

<b>Scenario #</b>	<b>Description/Constraints</b>	<b>Solution status and the computation cost</b>	
		<b>Approach #1: Nested Solution</b>	<b>Approach #2: Simultaneous Solution</b>
<b>1</b>	no-supply-to-grid constraint: $E_G \geq 0$	Non-feasible if the battery size is small and there is a high excess PV power thus the simulation keeps getting terminated	- MOSEK solver consumes around 4 minutes if $\eta=1$ - MOSEK solver consume 20 minutes if $\eta\neq1$ *
<b>2</b>	the grid receives the access PV energy for free: $E_{G,new} = \max(E_{G,old}, 0)$	<ul style="list-style-type: none"> <li>-The internal problem (see Figure 3.2) is solved using MOSEK solver (3 minutes simulation time to return the vector <math>u</math>). The internal problem consumes 7 hours if solved with SDPT3 solver. Thus, MOSEK solver is adopted.</li> <li>-The external problem consumes around 20 iterations.</li> <li>- The whole problem consumes around one hour for both cases (<math>\eta=1</math> and <math>\eta\neq1</math>): 20 iterations with 3 minutes per one iteration</li> </ul>	MOSEK solver consumes around 3 minutes for both cases ( $\eta=1$ and $\eta\neq1$ )
<b>3</b>	the consumer can sell the electricity to the grid but for a low price: Energy rate = 0.05 [\$/kWh] if $E_G \geq 0$ , Energy rate = 0.01 [\$/kWh] if $E_G < 0$	MOSEK solver run forever if used for data vector of length higher than 50 due to the complexity of solving for binary variables	<ul style="list-style-type: none"> <li>- MOSEK solver consumes 5 minutes if <math>\eta=1</math></li> <li>- MOSEK solver consume 22 minutes if <math>\eta\neq1</math> *</li> </ul>

\* solving for two vectors ( $Q_1, Q_2$ ) consumes more time compared to solving for one vector ( $Q$ )

Table 3-5. Number of variables and constraints for different scenarios and solving approaches,  $J$  = vector of optimization variables (size =  $365 \times 24 \times 4$ ).

Scenario #	# of variables and constraints (both are vectors of year-length)	
	$\eta = 1$	$\eta \neq 1$
<b>Approach #1: Nested Solution</b>		
<b>1</b>	$1 \times J$ variable and $4 \times J$ constraints	$6 \times J$ variables ( $3 \times J$ binary and $3 \times J$ continues) and $13 \times J$ constraints
<b>2</b>	$1 \times J$ variable and $3 \times J$ constraints	$1 \times J$ variable and $3 \times J$ constraints
<b>3</b>	$3 \times J$ variables ( $1 \times J$ binary and $2 \times J$ continues) and $6 \times J$ constraints	$11 \times J$ variables ( $6 \times J$ binary and $5 \times J$ continues) and $24 \times J$ constraints
<b>Approach #2: Simultaneous Solution</b>		
<b>1</b>	$1 \times J$ variable and $4 \times J$ constraints	$2 \times J$ variables and $4 \times J$ constraints
<b>2</b>	$1 \times J$ variable and $3 \times J$ constraints	$1 \times J$ variable and $3 \times J$ constraints
<b>3</b>	$5 \times J$ variables and $8 \times J$ constraints	$6 \times J$ variables and $8 \times J$ constraints

Table 3-6. Equations for different scenarios and solving approaches.

Scenario #	Equations	
	$\eta = 1$	$\eta \neq 1$
<b>Approach #1: Nested Solution</b>		
<b>1</b>	equations (3.9)-(3.14) and (3.16)	equations (3.38)-(3.40)
<b>2</b>	equations (3.9)-(3.14) and (3.17)	equations (3.9)-(3.14) and (3.17)
<b>3</b>	equations (3.23), (3.27), and (3.28)	equations (3.41)-(3.43)
<b>Approach #2: Simultaneous Solution</b>		
<b>1</b>	equations (3.46)-(3.48) and (3.50)	equations (3.46)-(3.48), (3.65), and (3.66)
<b>2</b>	equations (3.46)-(3.48), (3.50), and (3.51)	equations (3.46)-(3.48), (3.68), and (3.69)
<b>3</b>	equations (3.46), (3.47), (3.50), and (3.54)-(3.57)	equations (3.46), (3.47), (3.54), and (3.74)-(3.77)

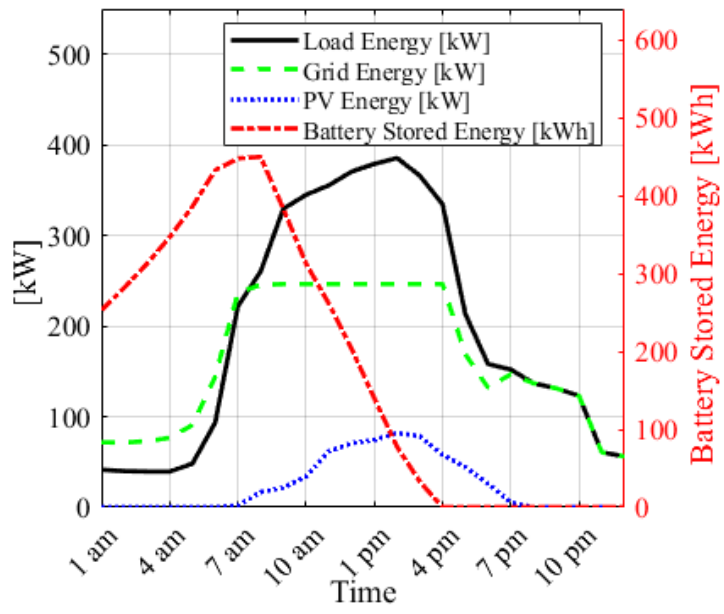
### 3.3.4. CVX Solver Selection and Peak Shaving Example

The CVX is a MATLAB library for convex optimization. The CVX library uses three solvers to solve: SDPT3, MOSEK, and GUROBI. SDPT3 is an academic solver that can solve only for continuous variables. MOSEK and GUROBI are commercial solvers which can be used to solve for both binary and continuous variables or mixed. For scenario #2, the variables are always continuous thus any solvers can be used. However, it is found that using MOSEK solver is faster than SDPT3: SDPT3 consumes about 7 hours while MOSEK solver consumes only 3 minutes to solve the problem. GUROBI solver requires a different MATLAB syntax; the problem should be rewritten in a different way. Many researchers claimed that GUROBI solver is the fastest solver for convex optimization. However, GUROBI solver was not used in the current work as MOSEK solver was found to be satisfying in terms of the computation cost.

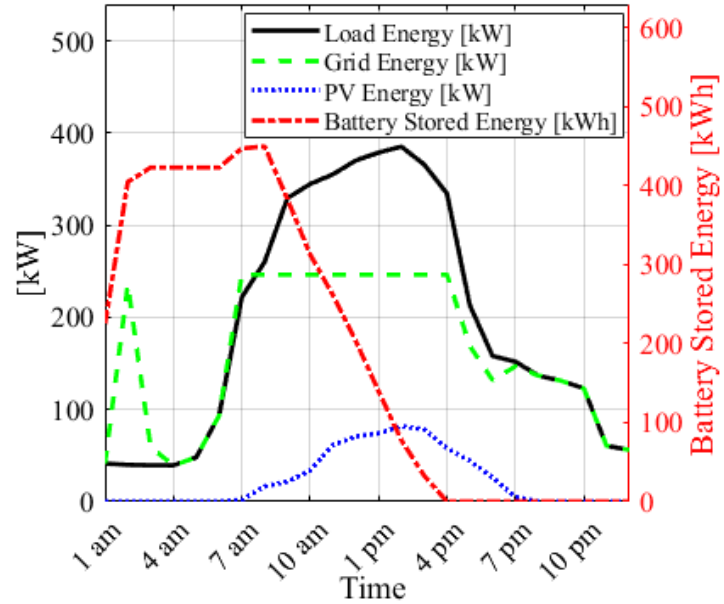
In Figure 3.4, one random day is selected, and the peak of that day is shaved using two different solvers. The PV-battery system's components are not optimized, for this example. The system is composed of 500 PV modules and a battery of a 450-kWh capacity. The battery is 50% charged at the beginning of the day. The battery schedule is optimized using convex optimization and the results are summarized as follows:

- A) The battery is on the charging mode between 1:00 a.m. and 7:00 a.m. (the off-peak period).
- B) The battery is set on the discharging mode Between 8:00 a.m. and 4:00 p.m.
- C) The battery discharging rate changes a little bit with time.

- D) The battery is fully discharged at 4:00 pm.
- E) The demand is shaved from about 385 to about 245 kW by the energy provided by both the solar modules and the battery.
- F) Both solvers (SDPT3, MOSEK) shave the peak from about 385 kW to about 245 kW. However, the solution is not unique.
- G) The signals of the battery stored energy and the grid energy obtained by SDPT3, between 1 am and 7 am, are smoother than the one obtained by MOSEK solver.



(a)



(b)

Figure 3.4. School demand peak shaving for one random day using (a) SDPT3 and (b) MOSEK solvers.

### 3.3.5. Case Study

A large repository [18] of 15-minute electrical demand data for buildings in Texas was used for this current study with at least five years of historical data available for most buildings. The database is described in more detail in [18]. A full analysis is performed for a school in the current work. The effect of different facilities profiles is discussed with brevity in Sections 3.4.2 and 3.4.3. The staff and students at the school leave typically between 3 and 5 p.m. The electricity bill is issued monthly. The estimated electricity cost for the investigated school was \$87174 in 2014 without installing the PV-battery system. The utility charged the school an estimated \$54,918 for total consumption and an estimated \$32,256 (37% of the total bill amount) for the monthly peaks (12 peaks in a year) based on rates given in Table 3-7. Therefore, shaving the school's peak is of great interest. The relevant parameters used are summarized in Table 3-7. The current analysis is based on scenario # 2 (see Table 3-3).

Table 3-7. Parameters.

Parameters	Value
Energy rate	0.05 [\$/kWh] ([129])
Peak rate	7 [\$/kW] ([129])
Charging/discharging efficiency ( $\eta$ )	0.92

## 3.4. Results and Discussion

The full analysis for school is given in Section 3.4.1. A summary of different commercial buildings located in Texas is provided in Section 3.4.2. All results sections except Section 3.4.3 are based on scenario # 2 (scenario # 2 in Table 3-3) for the sake of brevity. The summary for different scenarios with different buildings is given in Section

3.4.3. The energy shares (solar- use vs. sell back to the grid, solar- use vs. battery charging, etc.) are calculated in section 3.4.4. There are limited resources to quote the initial prices for PV-battery system's components, especially with a huge number of providers. However, the system's initial prices usually decrease as the scale of the system increases, i.e., adaptive pricing. In Section 3.4.5, a method to solve an adaptive pricing optimization problem with convex optimization is discussed. The battery's lifespan is impacted by the operation strategy. Formulating the battery aging cost to be a compliance with convex optimization is discussed briefly in Section 3.4.6.

### **3.4.1. School Results**

The initial costs of the proposed system's components (PV module, battery, inverter, converter) are different from one provider to another and different at various system scales. The effect of the initial costs is evaluated in Section 3.4.1.1. The solution obtained by convex optimization is validated using the drawing method in Section 3.4.1.2. The peaks before and after shaving as well as the effect of the charging efficiency on the electricity cost reduction are shown in Section 3.4.1.3. The electricity cost reduction achieved using combined PV-battery, PV-only, and battery-only systems are compared in Section 3.4.1.4. The effect of battery charging time-step is shown in Section 3.4.1.5.

#### **3.4.1.1. The Effect of The Initial Costs of PV and Battery Storage Systems**

The parameters and the size of the optimal PV-battery system with a different unit cost for both PV system and battery storage system (Figure 3.5) shows that the unit cost of the PV system affects the economic feasibility of the system significantly. The reduction in the electricity cost can drop from 30% to about 11% in Figure 3.5 (a) if the

PV unit cost increase from 0.2 to 0.4 [\$/W] (with 25 [\$/kWh] for the battery unit cost).

The reduction in the electricity cost changes from 30% to 20% if the battery unit cost increase from 25 to 50 [\$/kWh] (with 0.2 [\$/W] for the PV unit cost). Shaving the peak can reduce the bill amount by up to 35% (see Figure 3.5 (b)). Looking at the system parameters at 0.2 [\$/W] and 25 [\$/kWh] unit costs for PV and battery system, respectively: the following conclusion can be drawn:

1. The optimization algorithm suggests installing a large PV system even it supplies the grid with 283,320 [kWh] excess energy per year (32% excess PV energy). The proposed large PV system produces useful energy that reduces the bill amount by about 45% (Figure 3.5 (c)) and also shaves the peaks which reduce the bill amount by about 25% as well (Figure 3.5 (b)). Using a large PV system is intended to shave the peak since the peak of the school occurs during daylight.
2. Most of the initial investment goes to the solar PV system (55% of the cost is for the solar PV system, and 45% of the cost is for the battery storage system).
3. The life cycle cost in general decreases as the unit cost increases (Figure 3.5 (h, i)).

That can be explained as follows: the optimization algorithm will choose to have a smaller system as equipment gets more expensive.

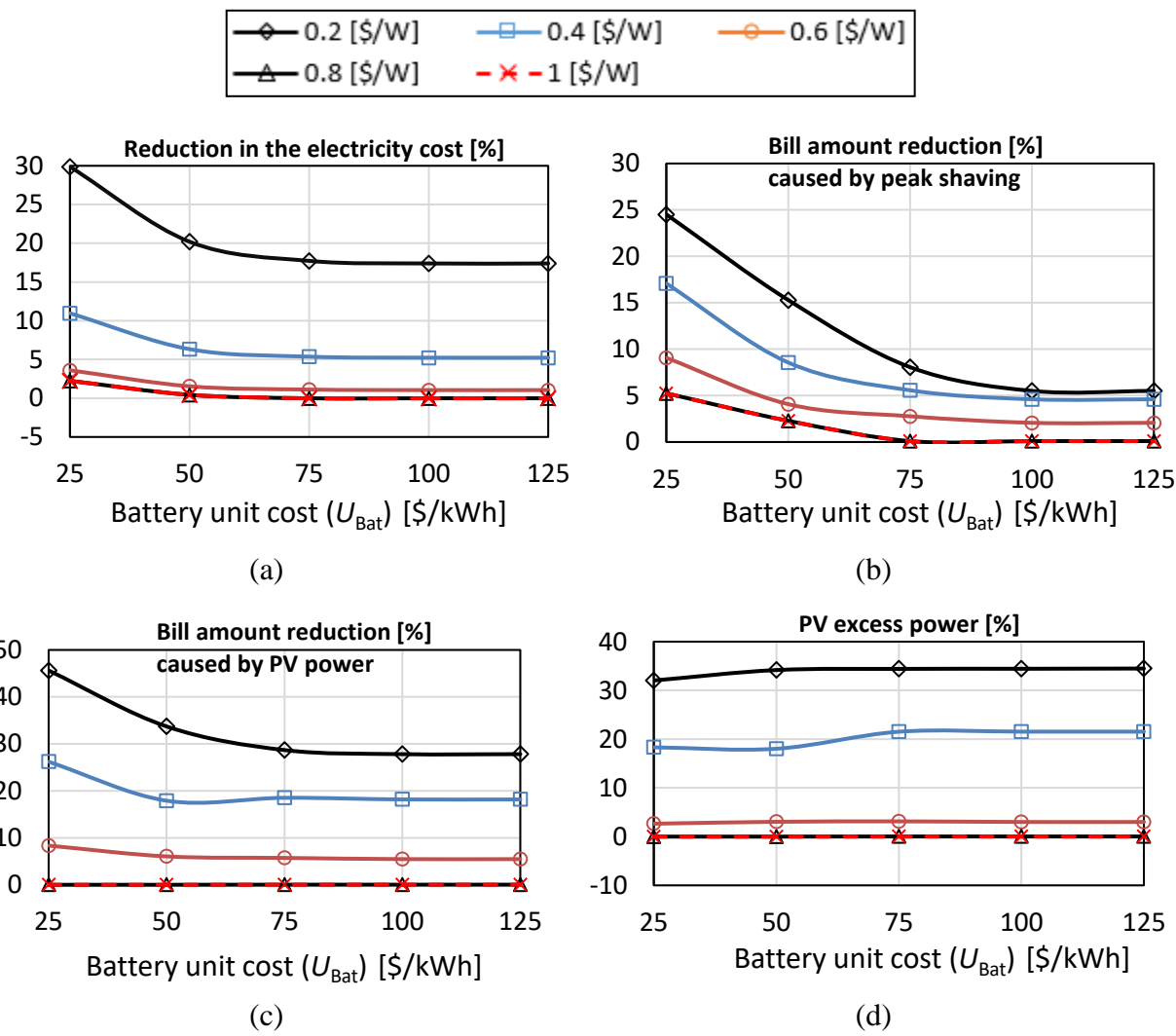


Figure 3.5. School full results, the legend is given at the top.

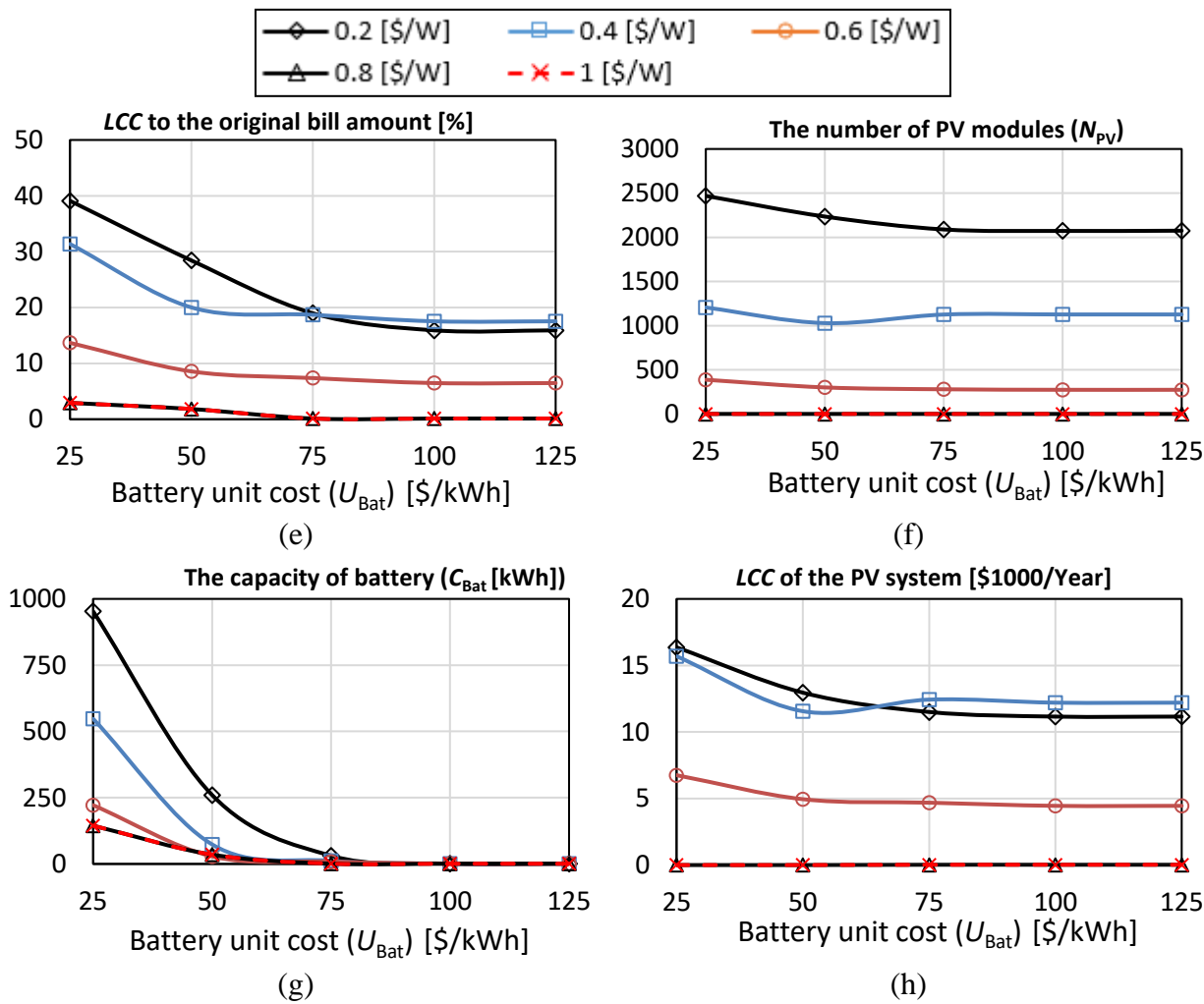


Figure 3.5. Continued.

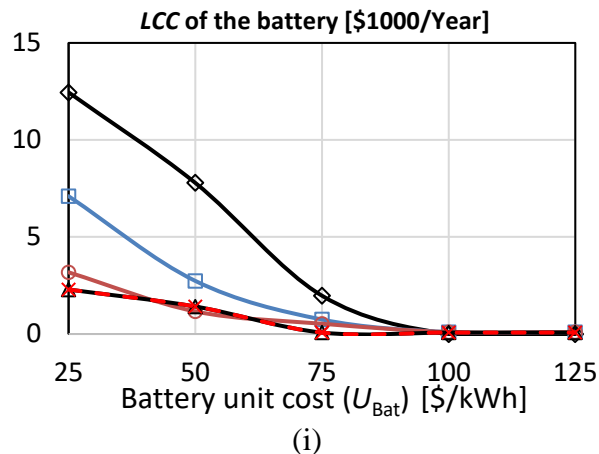
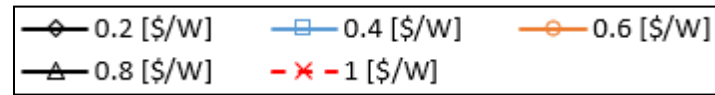


Figure 3.5. Continued.

### 3.4.1.2. Solution Check

The optimal solution obtained by the optimization algorithm is  $C_{\text{Bat}} = 950$  and  $N_{\text{PV}} = 2469$  (unit cost for battery is 25 [\$/kWh] and 0.2 [\$/W] for the PV system). Figure 3.6 shows the effect of the battery capacity on the electricity cost with  $N_{\text{PV}} = 2469$ . Figure 3.7 shows the effect of the PV array size on the electricity cost with  $C_{\text{Bat}} = 950$ . Figure 3.6 and Figure 3.7 show that the optimization algorithm works well locally. To make sure that the optimization algorithm works well globally, the algorithm can be compared with different optimization algorithms or solvers. In Figure 3.6, the life cycle increases with the increase in the battery capacity, and the bill amount decreases with the increases in battery capacity.

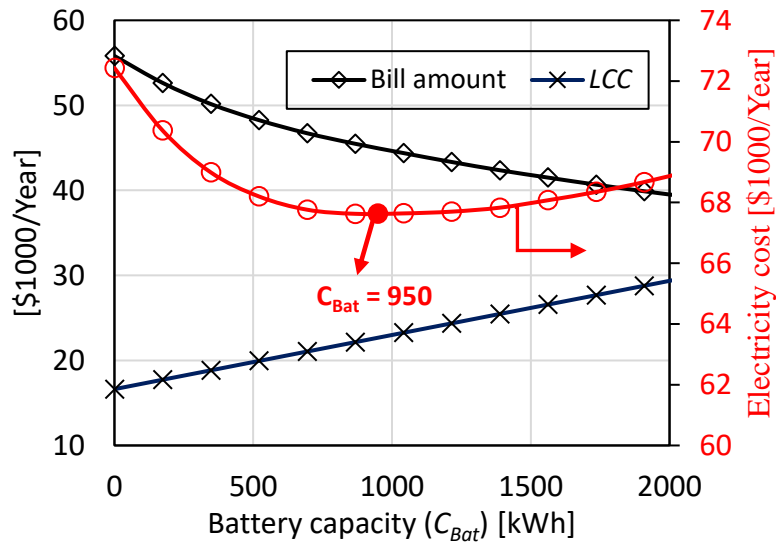


Figure 3.6. The effect of battery capacity on the electricity cost at a given PV array size ( $N_{\text{PV}} = 2469$ ).

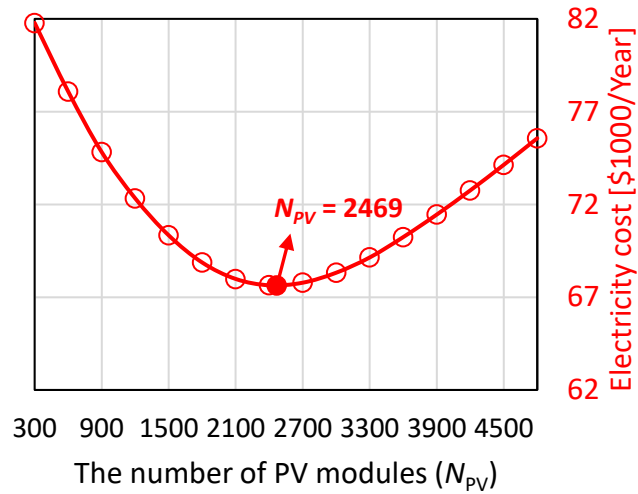


Figure 3.7. The effect of the number of PV modules at a given battery size,  $C_{Bat} = 950$ .

### 3.4.1.3. The Peaks and the Effect of The Charging Efficiency

The demand peak before and after installing the PV-battery system is shown in Figure 3.8. The system can shave the peak from about 350 kW to about 100 kW in July due to the fact that the peak is high in this month for a few days.

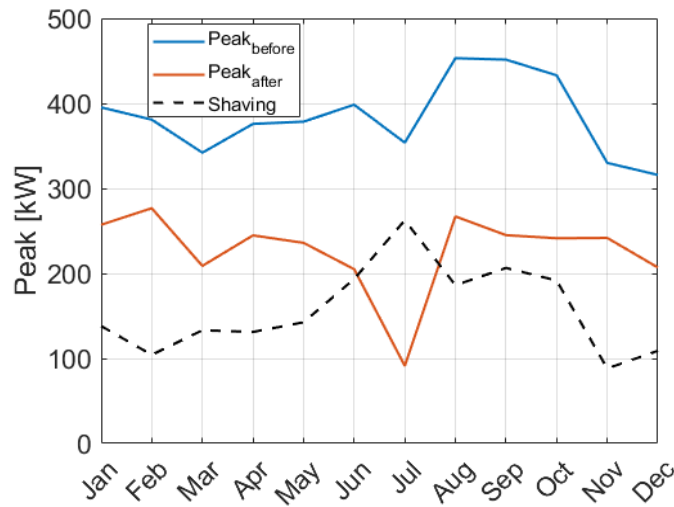


Figure 3.8. Peak before and after installing the PV-battery system.

The effect of battery charging/discharging efficiency on the electricity cost reduction is shown in Figure 3.9. The relation is found to be linear. The slope is not one; increasing the charging efficiency from 0.8 to one (increase by 25%) increases the electricity-cost reduction from 28.5% to 31% (increase by about 9%).

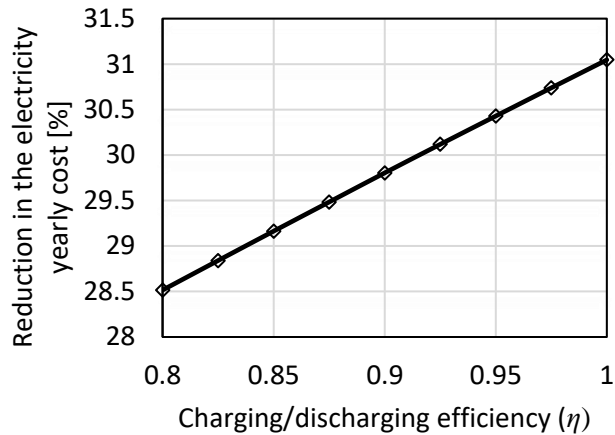
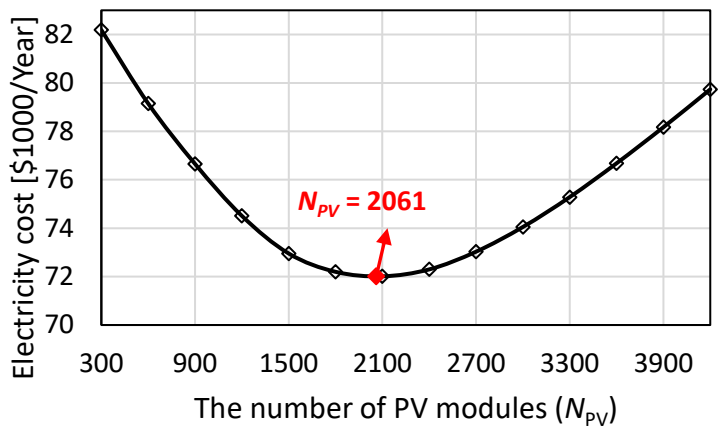


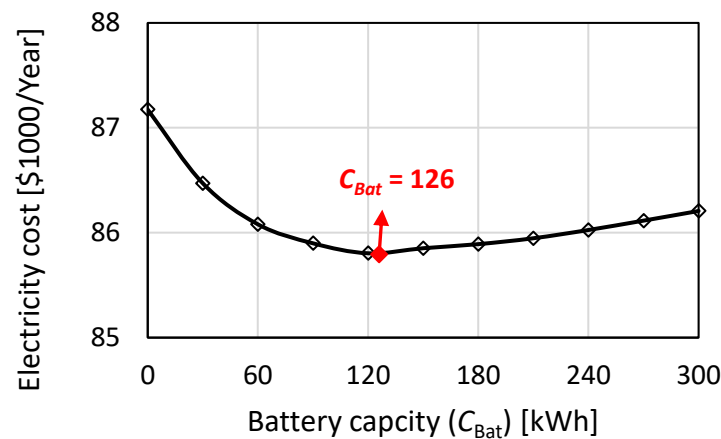
Figure 3.9. The effect of battery charging/discharging efficiency on the electricity cost reduction.

#### 3.4.1.4. PV-Only System and Battery-Only System

The electricity cost for PV-only system and battery-only system for different capacities is shown in Figure 3.10. The reduction in the electricity cost is summarized in Table 3-8. As shown in Table 3-8, the battery contribution in reducing the electricity cost is higher when used with PV system. The electricity cost is reduced by 29.8% when PV-battery system is used. When PV-only system is used, the electricity cost is reduced by 17.4%. Thus, adding the battery to the PV system can reduce the electricity cost by 12.4% more. The electricity cost is reduced by only 2.25% when battery-only system is used.



(a)



(b)

Figure 3.10. The effect of size on the electricity cost with (a) PV-only system (b) Battery-only system.

Table 3-8. Electricity cost reduction for different systems.

System	Reduction in the electricity cost [%]
PV-battery	29.8
PV-only	17.4
Battery-only	2.25

### 3.4.1.5. The Effect of Battery Charging Time-Step

The excess battery charging/discharging reduces the battery lifespan. Recall that the utility charges the consumers based on the total energy consumption and the maximum 15-minute energy in a month. To shave the peak, the battery charging/discharging status is updated every 15 minutes. However, the battery charging/discharging rate can be instead updated every 30 minutes, 45 minutes and so. The effect of battery charging time-step size is shown in Figure 3.11.

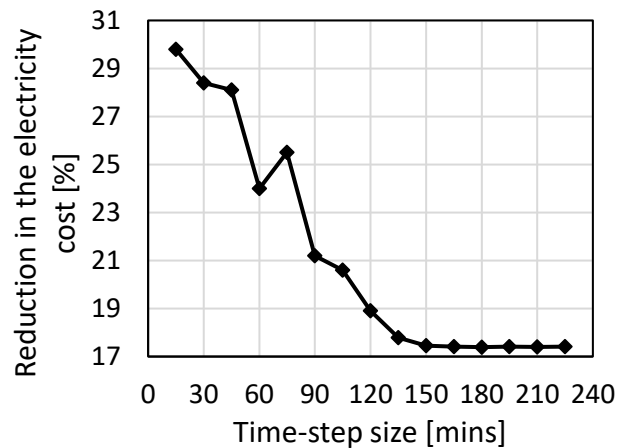


Figure 3.11. The electricity cost reduction with different charging time-step.

It is easier to shave the 15-minutes demand peak if the time-step is 15 minutes. The system with two and a half hour time-step can only reduce the electricity cost by 17.4% the same as the PV-only system can do. In other words, using a battery with 2.5 hour time-steps is useless in terms of the electricity cost reduction.

The change in the trend (compare the results with 60- and 75-minutes time-step) can be justified by:

1. The location of the peaks during the year
2. The system with a longer time step might have a smaller inverter and converter.

As mentioned before, the maximum rate of charging and discharging determines the initial capital costs of the inverter and the converter.

### **3.4.2. The Effect of Different Facility Type**

The load profiles for one random day for different commercial facilities in Texas are shown in Figure 3.12. The reduction in the electricity cost and the peak shaving, etc., are summarized in Table 3-9. The unit cost of the PV system and the battery are assumed to be 0.2 [\$/W] and 25 [\$/kWh], respectively. It has shown that it is more feasible to shave the peaks and reduce the electricity cost of both the school and church, compared to other facilities. That can be justified by that (1) the peak of school and church, and most of the electricity consumption occur during the daylight and (2) since the PV system is relatively cheap compared to the cost of the battery thus adding a large PV system to shave the peak and meet a large portion of demand is economically feasible. For theater and hotel, the peak occurs during the night. To shave the peak of the night, the peak of the hotel as an example, a large battery is needed and since the battery is relatively expensive compared to the kWh electricity purchase cost, the optimal system will be able to reduce the peak by only 6.3%.

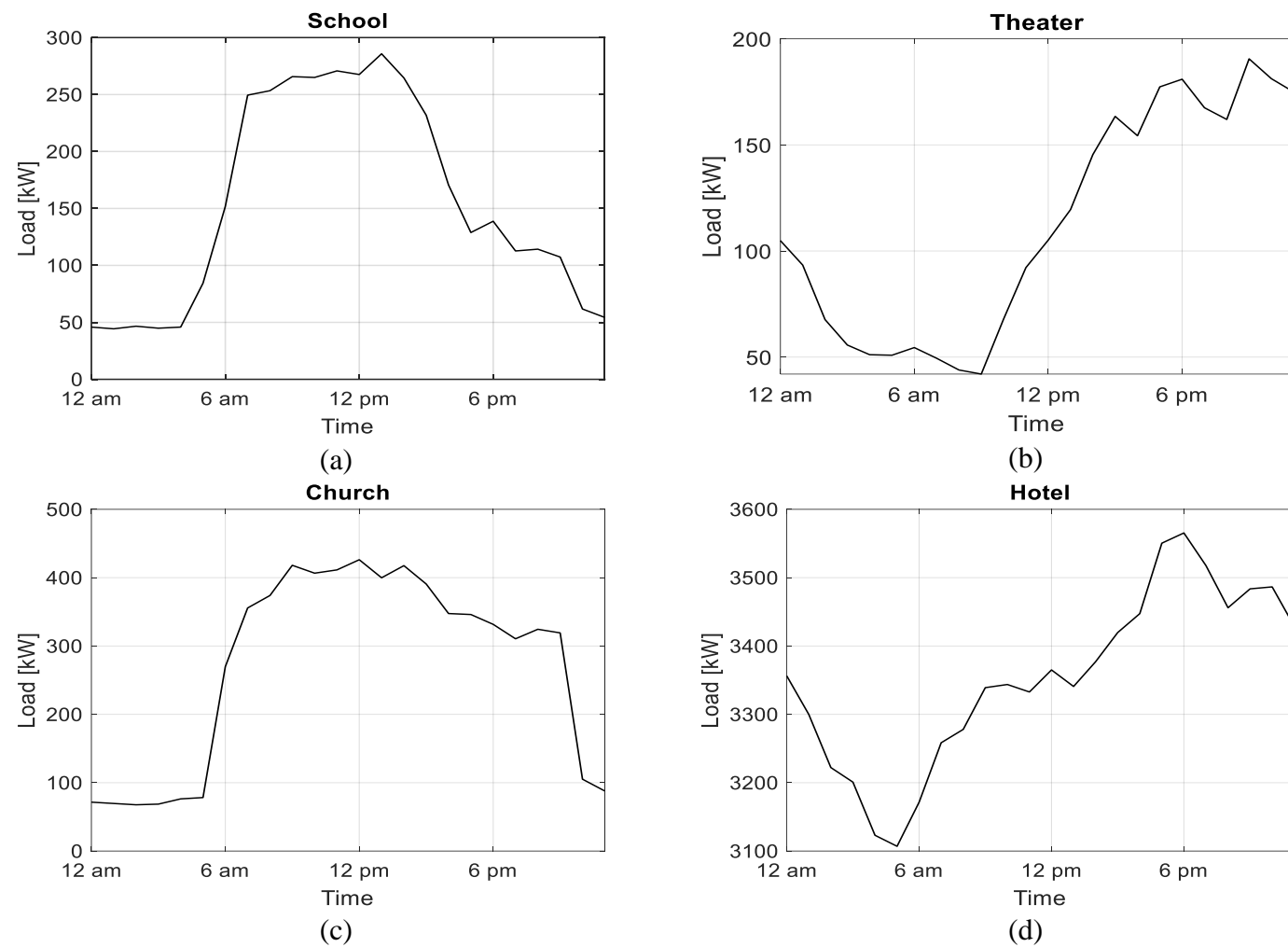


Figure 3.12. Different facility load profile.

Table 3-9. Optimization results for different facilities.

Parameters	School	Theater	Church	Hotel
	[%]			
Electricity cost reduction	30	22	29	17
Peak cost / original bill amount*	37	27	30	20
Bill amount reduction caused by peak shaving	24.5	16.1	19.6	6.3
Bill amount reduction caused by PV power	44.6	51.1	52.3	62.0
Excess PV energy	32.3	14.1	11.2	10.1
LCC / original bill amount*	38.9	45.2	42.9	51.3
LCC of PV system / original bill amount*	21.4	23.3	24.1	17.8
LCC of battery system / original bill amount*	17.5	21.9	18.8	12.5

### 3.4.3. Scenarios Comparison

The results for the optimized PV-battery system for scenarios # 1-3 (see Table 3-3) are summarized in Table 3-10 and Table 3-11. To prevent any excess energy in scenario #1, the PV array might be smaller, and/or the battery might be bigger to store all the excess PV energy. The PV is smaller in scenario #1, i.e., the required PV system is cheaper, thus the system cost-saving might be used to install a large battery.

The optimized PV-battery system with scenario #1 reduces the electricity cost of a school by only 15% compared to 30% with scenario #2. Restricting the consumers to not provide any power to the grid even for free as in scenario #1 will reduce the return-of-investment of the PV-battery system significantly.

However, the PV system of the current work is equipped with a maximum-power-point-tracking controller (see Appendix A). The PV-battery system obtained by solving for scenario #2 can be instead equipped with another controller that meets the requirements of scenario #1. The suggested controller will be adjusting the voltage of

\* the original bill amount is the bill amount before installing the PV-battery system

operation to make a balance between (1) the demand, (2) the power produced by the PV system, and (3) the battery state-of-charge to prevent any excess PV energy. The controller will reduce the power produced by the PV system by changing the voltage of operation if the energy produced by the PV system is higher than the summation of the demand and the available battery storing capacity (see a similar controller designed in [40]). To sum up, the system designed based on scenario #2 can meet the requirements of scenario #1 and scenario #2 by installing the right controller.

Table 3-10. Scenario #1-3 comparison (see the parameter description in Table 3-11).

Parameter	School			Theater			Church			Hotel		
	1	2	3	1	2	3	1	2	3	1	2	3
<b>a</b>	860	2469	3061	1028	2203	2708	3103	5532	6473	33347	58558	69390
<b>b</b>	1107	950	953	948	1069	1142	2264	2446	2172	26981	34285	33222
<b>c</b>	<b>15</b>	<b>30</b>	<b>34</b>	<b>15</b>	<b>22</b>	<b>28</b>	<b>18</b>	<b>29</b>	<b>35</b>	<b>8</b>	<b>17</b>	<b>22</b>
<b>d</b>	20.3	24.5	25.4	15.2	16.1	18.2	18.4	19.6	20.3	4.9	6.3	11.1
<b>e</b>	17.7	44.6	50.1	28.6	51.1	56.0	35.5	52.3	53.2	36.3	62.0	65.1
<b>f</b>	0	32.3	43.1	0	14.1	22.6	0	11.2	22.6	0	10.1	19.8
<b>g</b>	23.0	38.9	41.5	28.8	45.2	46.2	35.9	42.9	38.5	33.2	51.3	54.2

Table 3-11. The parameter description of Table 3-10.

Parameter	Parameter Description
<b>a</b>	Number of PV modules ( $N_{PV}$ )
<b>b</b>	Battery capacity ( $C_{Bat}$ ) [kWh]
<b>c</b>	Reduction in the electricity cost [%]
<b>d</b>	Bill amount reduction caused by peak shaving [%]
<b>e</b>	Bill amount reduction caused by PV power [%]
<b>f</b>	Excess PV energy (scenario 2)
	PV energy sold to the grid (scenario 3) [%]
<b>g</b>	LCC / original bill amount

### 3.4.4. Energy Shares

To reduce the computation time, the optimization problem was solved in this paper with the least possible number of variables. For example, the variables  $B, E$ , and  $D$  in Figure 3.13 were reduced to  $E_G$ . The variables A, E and F were reduced to  $E_B$ . In this section, the system of equations to find the energy shares (A - F) is presented and solved.

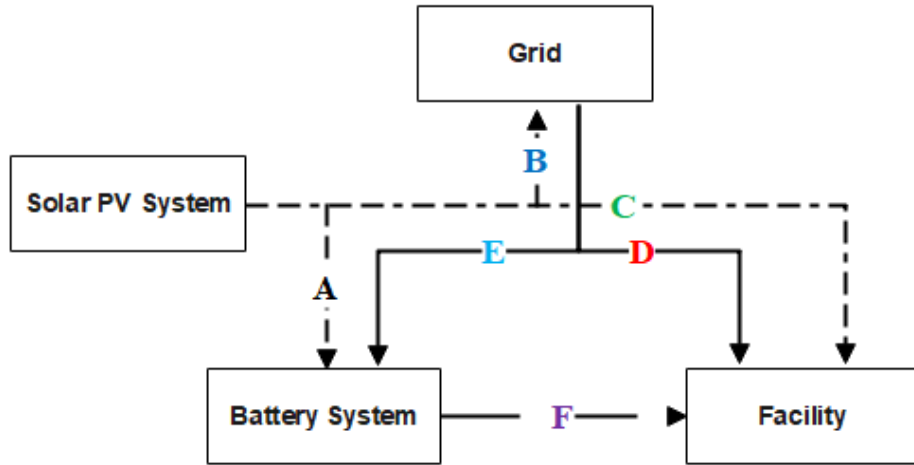


Figure 3.13. Energy shares schematic.

The system, shown in Figure 3.13, can be described by the following set of equations:

$$E_{PV} = A + B + C \quad (3.78)$$

$$E_G = D + E - B$$

$$E_{Bat} = A + E - F$$

$$B = E_G -$$

$$F = E_{Bat} -$$

$$E_L = C + D + F$$

In this system of equations, the unknown variables are the alphabetical symbols (A - F). The system is of 6 equations with 6 variables. However, the last equation is found to be redundant, which can be checked by the reduced augmented matrix, thus, the system has a free variable. To handle this issue, the system is solved case-by-case as shown below:

Case 1: discharging the battery and feeding the grid ( $E_{Bat} \leq 0$  and  $E_G \leq 0$ )

If the battery is being discharged, A and E are zeros. If the grid is being fed, E and D are zeros. The system of equations will be as follows:

$$\begin{aligned} E_{PV} &= A + B + C \\ E_G &= D + E - B \\ E_{Bat} &= A + E - F \\ A, E, D &= 0 \end{aligned} \tag{3.79}$$

Case 2: discharging the battery and the grid is providing power ( $E_{Bat} \leq 0$  and  $E_G \geq 0$ )

If the battery is being discharged, A and E are zeros. If the grid is providing power, B is zero. The system of equations will be as follows:

$$\begin{aligned} E_{PV} &= A + B + C \\ E_G &= D + E - B \\ E_{Bat} &= A + E - F \\ A, E, B &= 0 \end{aligned} \tag{3.80}$$

Case 3: charging the battery and grid is being fed ( $E_{Bat} \geq 0$  and  $E_G \leq 0$ )

If the battery is being charged, F is zero. If the grid is being fed, E and D are zeros. The system of equation will be as follows:

$$\begin{aligned} E_{PV} &= A + B + C \\ E_G &= D + E - B \\ E_{Bat} &= A + E - F \\ F, E, D &= 0 \end{aligned} \tag{3.81}$$

Case 4: charging the battery and grid is providing power ( $E_{Bat} \geq 0$  and  $E_G \geq 0$ )

If the battery is being charged, F is zero. If the grid is providing power, B is zero. The system of equation will be as follows:

$$E_{PV} = A + B + C \quad (3.82)$$

$$E_G = D + E - B$$

$$E_{Bat} = A + E - F$$

$$F, B = 0$$

However, the system is still missing one equation to be consistent. Case 4 can be broken into two subcases as follows:

- a) If the solar photovoltaic energy is higher than the load ( $E_{PV} \geq E_L$ ), D will be zero.
- b) If the solar photovoltaic energy is lower than the load ( $E_{PV} \leq E_L$ ), A will be zero.

The system is updated as follows:

$$E_{PV} = A + B + C \quad (3.83)$$

$$E_G = D + E - B$$

$$E_{Bat} = A + E - F$$

$$F, B = 0$$

$$D = 0 \text{ if case (a)}$$

$$A = 0 \text{ if case (b)}$$

The energy shares (A - F) are calculated for every time step in one year. The process is executed for all scenarios (see Table 3-3). The cumulative energy shares over one year (A` - F`) are shown in Figure 3.14.

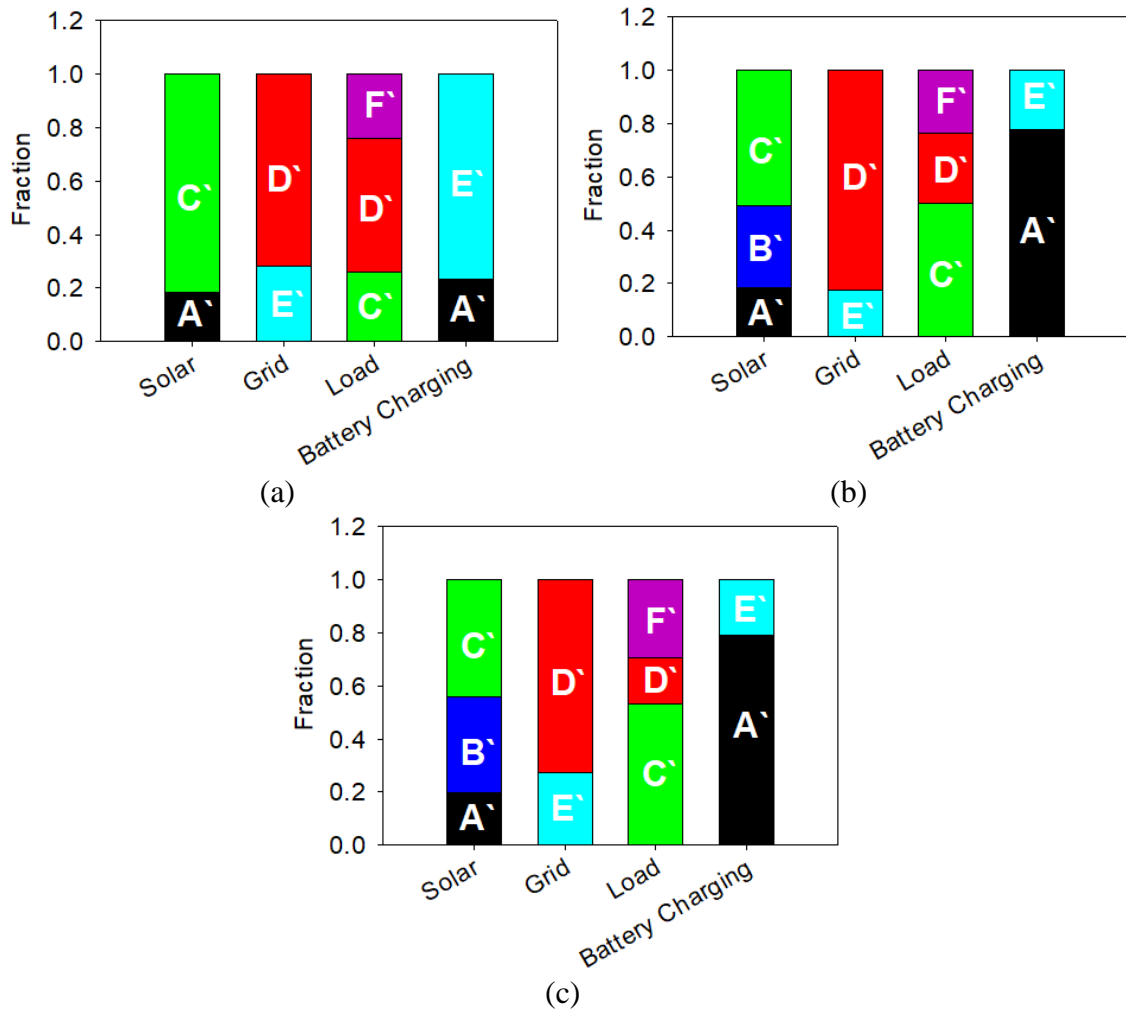


Figure 3.14. Energy shares for (a) scenario #1 (see Table 3-3) (b) scenario #2 (c) scenario #3.

The largest portion of PV energy is used in meeting the customer demand and around 20% of the PV energy is used to charge the battery. For scenarios #2 and #3 (see scenarios #1-3 in Table 3-3), about 31-35% of the PV energy is fed in the grid. For scenarios #2 and #3, the PV energy is the main source to charge the battery; about 75% of the energy used to charge the battery is PV-sourced. For scenario #1, about 75% of the

energy used to charge the battery is grid-sourced; the PV system is relatively small for scenario #1.

The equations of the four cases can be used in designing the demand management controller as the energy shares need to be calculated. However, the optimization problem solved in this paper can be also solved based on Figure 3.13 and the Equations (3.79)-(3.83), but solving the sizing problem based on the problem formulation of this section will be more resource-intensive. Below is a brief on how to formulate cases 2 and 3 to be acceptable by convex optimization:

$$E_{Bat} \leq 0 + M B \quad (3.84)$$

$$E_{Bat} \geq 0 - M (1 - B)$$

$$E_G \geq 0 - M B$$

$$E_G \leq 0 + M (1 - B)$$

$B$  in Equation (3.84) is a binary variable such that, if  $B = 0$ , the two constraints ( $E_{Bat} \leq 0$  and  $E_G \geq 0$ ) need to be satisfied. These two constraints represent case 2, while  $B = 1$  represents case 3. That is clarified in Table 3-12.

Table 3-12. Equation (3.84) constraints update corresponding to the value of  $B$ .

<b>Constraint #</b> <b>(see Equation (3.84))</b>	<b>If <math>B = 0</math></b>	<b>If <math>B = 1</math></b>
<b>1</b>	$E_{Bat} \leq 0$	Always right
<b>2</b>	Always right	$E_{Bat} \geq 0$
<b>3</b>	$E_G \geq 0$	Always right
<b>4</b>	Always right	$E_G \leq 0$

For case 2 where  $B = 0$ , the constraint  $(A, E, B = 0)$  need to be satisfied (see Equation (3.80)). Below is an example of how to formulate  $(A = 0)$  to be acceptable by CVX:

$$A \geq 0 - M B \quad (3.85)$$

$$A \leq 0 + M B$$

- If  $B = 0$ , the first and second constraint of Equation (3.85) will be updated in new two constraints  $(A \geq 0, A \leq 0)$ . These two constraints are satisfied if and only if  $A = 0$ .
- If  $B = 1$ , the first and second constraint of Equation (3.85) will be always right.

For case 3 where  $B = 1$ , the constraint  $(F, E, D = 0)$  need to be satisfied (see Equation (3.81)). Below is an example of how to formulate  $(F = 0)$ :

$$\begin{aligned} F &\geq 0 - M (1-B) \\ F &\leq 0 + M (1-B) \end{aligned} \quad (3.86)$$

### 3.4.5. Adaptive Pricing

As we know, the price of a solar system per W ( $U_{PV}$ ) decreases as the system size increases. Most of the PV system manufacturing companies provide their clients with a quote algorithm. In Figure 3.15, the initial prices of solar systems are shown in case the price per W is fixed (1 \$/W) and in case of a simple adaptive algorithm is used to adjust the cost when the size of the PV system goes up to encourage people to install more PV modules. The adaptive pricing curve in Figure 3.15 is concave thus cannot be solved in convex optimization. To handle this issue, a piecewise linear function can be used to convert the concave curve to a set of linear relations. Below is a simple example of how to handle it with convex optimization.

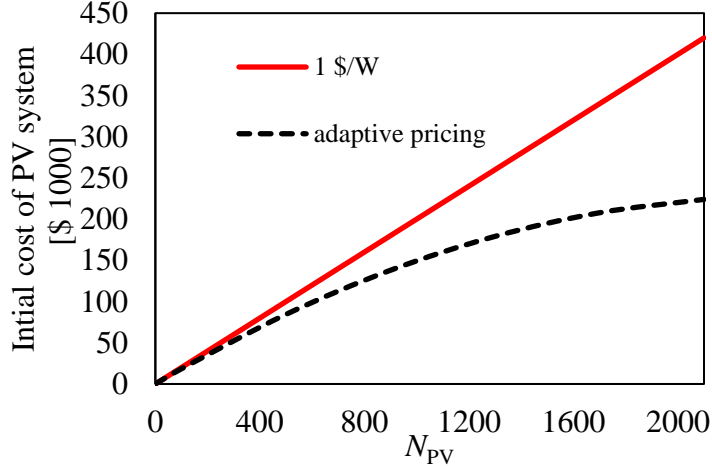


Figure 3.15. Initial cost of solar system.

Let's assume the following adaptive pricing scheme:

$$U_{PV} = 1 [\$/W] \text{ if } N_{PV} \leq 1000 \quad (3.87)$$

$$U_{PV} = 0.4 [\$/W] \text{ if } N_{PV} \geq 1000$$

where  $U_{PV}$  is the unit cost of the PV system as discussed in Section 3.3.1. To remove the

'if statement', the binary variable ( $B$ ) can be used as follows:

$$U_{PV} = 0.4 [\$/W] + 0.6 B [\$/W] \quad (3.88)$$

The constraints of Equation (3.87) are updated as shown below:

$$N_{PV} \geq 1000 - M B \quad (3.89)$$

$$N_{PV} \leq 1000 + M (1 - B)$$

Now Equation (3.3) is updated as follows:

$$IC_{cost} = C_{PV} \times 0.4 + C_{PV} \times 0.6 \times B + \dots \quad (3.90)$$

$IC_{cost}$  is the initial capital cost of the system. The capacity of solar photovoltaic system ( $C_{PV}$ ) is array maximum power ( $P_{m, array}$ ) defied in Equation (A.15), Appendix A.

Equation (3.90) is updated as follows:

$$IC_{cost} = P_{m, \text{module}} \times N_{PV} \times 0.4 + P_{m, \text{module}} \times N_{PV} \times 0.6 \times B + \dots \quad (3.91)$$

The binary variable ( $B$ ) and the size of the PV system ( $N_{PV}$ ) need to be optimized. These two optimization variables are multiplied by each other which does not comply with convex optimization. A new variable called  $y$  ( $y = N_{PV} \times B$ ) is used to linearize the multiplication of these two variables. The constraints before linearization are shown below:

$$\begin{aligned} N_{PV} &\geq 0 \\ N_{PV} &\geq 1000 - M B \\ N_{PV} &\leq 1000 + M (1 - B) \end{aligned} \quad (3.92)$$

The constraints after linearization are shown below (see [52] on how to linearize the multiplication of two variables):

$$\begin{aligned} y &\geq 0 \\ N_{PV} - y &\geq 0 \\ y &\geq 1000 B - M B \\ y &\leq 1000 B \\ N_{PV} - y &\geq 1000 - 1000 B \\ N_{PV} - y &\leq 1000 - 1000 B + M (1 - B) \end{aligned} \quad (3.93)$$

### 3.4.6. Battery Aging Cost

The battery's lifespan deteriorates gradually with the normal usage due to the irreversible physical and chemical changes. The excessive charging and discharging actions reduce the battery lifetime significantly thus the battery needs to be replaced frequently. The battery is relatively expensive thus the frequent replacements lead to a high operation cost and reduce the return on investment.

The bandwidth of the state-of-charge for the battery can be constrained, as one of the methods to enhance the battery life span. The effect of the bandwidth of the state-of-

charge on the electricity cost-reduction is shown in Figure 3.16, assuming the battery life span is fixed and equals 5 years.

The battery can stay for about 4000 cycles before it needs to be replaced if the temperature is maintained at 20° as shown in Figure 5 in [55]. For a school, the battery can be charged slowly during the off-peak hours (between 6 pm and 4 am see Figure 3.12 (a) and Figure 3.4). The battery is discharged during the daylight (see Figure 3.4), thus the number of discharging-charging cycles is one a day and about 260 a year (no charging/discharging during the weekends). In this study, the battery is assumed to have a 5-year lifespan (1300 cycles) which seems to be a sane assumption. However, battery-aging model can be utilized for more efficient sizing. The physical-based battery capacity loss model is a non-convex thus including the battery aging cost is associated with optimization challenges. Hence, Cai et al. [56] proposed replacing the non-convex degradation physical model with an approximate convex model using a set of piece-wise linear models. On the other hand, some empirical degradation models might be convex.

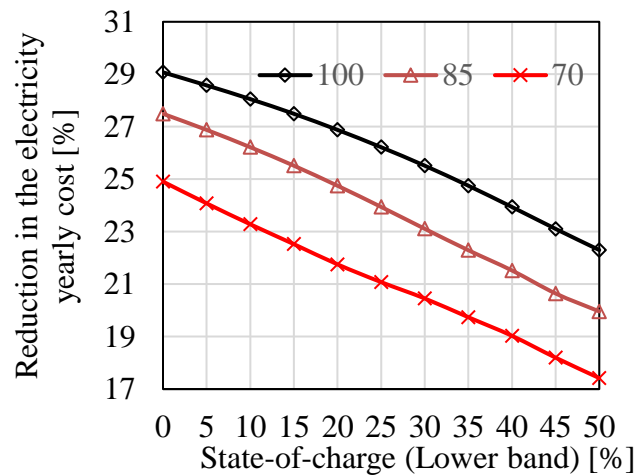


Figure 3.16. The reduction in the electricity cost percentage for different bandwidths. (100, 85, and 70 are the upper bands [%]).

### **3.5. Conclusion**

The PV-battery system is implemented to reduce the electricity cost for commercial applications in Texas. The battery has two functions: storing the excess PV energy and shaving the peak. The fees on the peaks are based on the highest monthly peak. Shaving the peak of one month is a complex optimization problem due to the long scheduling horizon. For energy system sizing, we usually consider data of one year. The scheduling problem for one year is computationally intensive. A fast algorithm to optimize the PV system size, battery capacity, and charging rate vector has been developed. The proposed algorithm can return the optimal solution in less than 1 hour of computation time for different pricing policies and sometimes less than 5 minutes. The study shows that problem reformulation can ease the complexity of the optimization problem significantly. Different scenarios have been introduced. These scenarios have been formulated to be solvable using convex optimization algorithm. The effects of different parameters have been investigated: the purchase cost of the PV-battery system's components, battery charging/discharging efficiency, facility type.

## 4. PAPER B: DEMAND PEAK SHAVING USING PV-BATTERY SYSTEM UNDER PV POWER AND LOAD PREDICTION-UNCERTAINTY<sup>1</sup>

### 4.1. Synopsis

Shaving of peak electrical demand using a photovoltaic-battery system is possible by optimally scheduling the battery charging and discharging using forecasts of the photovoltaic (PV) generation and facility load profiles. However, when using predictive control, forecasting errors can exacerbate peak electrical demand, rather than reducing them. Thus, improving forecast predictions can directly enhance the scheduling of energy storage to minimize facility peak demand costs. The PV generation and load profiles, however, cannot be perfectly predicted, especially with long control horizons. On the other hand, large battery storage systems can be utilized to shave the peaks in case of the worst scenarios. The initial and replacement costs of battery storage are significant, thus installing large and expensive batteries is not an economic option. PV-battery implementation for peak shaving requires a real-time control scheme to manage the PV power and load uncertainties.

In this work, a framework to schedule the battery charging and discharging under load and PV generation prediction-uncertainty for commercial facilities is proposed and verified. Many electric utilities charge the consumers based on the total consumption and the monthly 15-minute-average peak demand. The monthly peak shaving is a complex

---

<sup>1</sup> Hussein Sharadga, Bryan Rasmussen, “Demand Peak Shaving Using PV-battery System Under PV Power and Load Prediction-Uncertainty”.

problem due to the long control horizon. Furthermore, the 15-minute-average energy profiles are noisy signals, which are difficult to forecast especially with a long forecasting horizon. Shaving the end-user's demand peak under uncertainty, however, has not been addressed in the literature.

## 4.2. Introduction

Photovoltaic-battery systems, in which an integrated battery stores excess photovoltaic (PV) energy to meet future demand, are economical means of reducing total electricity cost for commercial and residential applications. The battery can be also used to shave the facility peak by shifting portion of the load to the off-peak period. The load is shifted by replacing portion of the grid-supplied electricity with stored electricity during peak demand times. Shaving the peak can reduce the billed amount significantly, by avoiding high rates for monthly demand peak, and contributes to more stable grid operation. Operationally, shaving the demand peak is accomplished by devising a battery charging and discharging schedule based upon the forecasted load and PV energy profiles. Forecasting error can be significant, especially in cases of continuously changing weather conditions and variable electricity-consumption patterns. For efficient battery scheduling, the PV and the load uncertainties need to be integrated into the control decision.

Several methods have been implemented to address the uncertainty when scheduling the PV-battery systems. These PV-battery systems have been also employed for different scheduling goals. In [57], chance-constrained programming is implemented for day-ahead scheduling for PV-battery systems under PV power uncertainty. The schedule aims to maintain a pre-defined power profile shape. The chance-constraint can

be mathematically converted from probabilistic to deterministic form by assuming that the uncertain parameters are following a given distribution [58], for example a Weibull probability distribution. The deterministic formula is easier to be solved. Another well-known method to address the uncertainty for energy planning with a control horizon is called scenario-based programming. In this method, different scenarios or expectations are generated. Then we find the optimal control decision for different scenarios and then averaging the control decisions of these different scenarios for the first time-step in the schedule. The process is repeated for each time-step in the schedule. To reduce the computation time of scenario-based programming, scenario-reduction methods are utilized. In [59], a system of PV panels and battery storage was scheduled to reduce the daily electricity purchase cost for residential complexes. The scenario-based programming was used to optimize the schedule. The uncertainty of each battery state of charge, load, solar irradiance components, and ambient temperature were modeled by 20 expected scenarios for each of them with their probability. In [60], scenario-based programming was utilized to dispatch PV-battery systems. The schedule was optimized to enhance the power self-consumption of PV-battery systems. They proposed to constrain the control decision for the first time-step in the schedule to be the same for the different scenarios. That was aiming to find the common optimal decision across all expectations for the first time-step in the receding control horizon. The authors in [60] also proposed replacing the PV power and the electricity load with net power to reduce the number of scenarios, thus reducing computation cost. Stochastic dynamic programming (SDP) is another well-known method for decision-making with future uncertainty. The SDP is based on breaking

the control horizon into stages and discretizing the system state. To reduce the computation time, the problem can be solved recursively with no need to ignore any expected scenario. In other words, all expected scenarios with their probabilities are considered when constructing the schedule. Abdulla et al. [23] proposed stochastic dynamic programming (SDP) to operate PV-battery storage systems. The SDP handled PV and load uncertainties. The proposed operational strategy aimed to maximize the utilization efficiency of the system but with the consideration of battery aging. For better scheduling efficiency, the realizations of the load and PV generation were used to update the schedule with a receding horizon.

The operation of different combined energy systems and battery storage systems of under the effect of uncertainty can be managed similarly to the applications implemented on PV-battery systems, above. Chance-constrained programming optimization was utilized to minimize the operational cost of an isolated microgrid in [61]. This method included the uncertainties of PV power, wind power, and load. Chance-constrained programming was proposed for day-ahead battery scheduling for PV-battery-based electric vehicle power stations in [13]. The uncertainties of load demand and PV power were simulated by their probabilistic behavior. The genetic algorithm was used to minimize the electricity purchase price. The chance constraint was used to find the reserve energy needed to trade off between the operation cost and the system reliability in meeting the demand. Similar studies were conducted in [14] and [62]. In [14], stochastic dual dynamic programming (SDDP) was proposed to reduce the daily electricity purchase cost under load and solar uncertainties. The work was based on constructing a charging

schedule coordinating between PV-battery system and plug-in electric vehicle. This study was performed for a country adopting the time of use (TOU) pricing method thus, it favored avoiding high-energy consumption during the high-pricing period. A resolution method based on SDP was implemented in [62] to coordinate between the PV system and the electric vehicle to improve the predictability of both the vehicle's availability and PV generation. The optimal energy flow satisfies both the grid commitment and the mobility needs and considers the battery aging and replacement cost. Luo et al. [63] used the scenario-based method to optimize the energy schedule for grid-connected microgrid systems. The microgrid is integrated with different renewable energy resources, such as PV-battery system, wind turbine, and full cell, as well as microturbine. The forecasting errors for PV energy, wind energy, and demand are used to generate scenarios. The scenario-reduction method reduces the computation time. The battery is charged during the low energy-price as the country adopts the time-of-use pricing mechanism. In [64], the scenario-reduction method was used to operate a microgrid system. The microgrid contains a PV system, wind turbines, gas turbines, and storage structures. An energy-management program was proposed to ensure that the supply of an integrated system meets the demand for household applications in [65]. The integrated system is composed of a solar PV system, battery, and hot-water tank for household applications. Stochastic dual dynamic programming treats the future uncertainties of the electrical and hot water demands. The operation of a power-plant system composed of solar panels, wind farm, and compressed air storage systems was managed by the SDP to minimize the cost of operation in [66].

The three most well-known methods to address uncertainty for energy planning are chance-constraint programming, scenario-based programming, and scenario-reduction methods, and stochastic dynamic programming; however, other methods have been put forward in the literature for energy management. In [67], a demand response program based on the point estimation method was implemented to optimize the electricity purchase cost for microgrids. The energy-flow management program considered the uncertainties of wind energy, PV power, load demand, and the electricity market price. An operational strategy for PV-battery and full cell hybrid grid-connected systems was proposed in [68]. The energy management mechanism was based on using the risk-based information gap decision theory method to model the demand load uncertainty. In [69], load shifting and energy storage control were optimized simultaneously to minimize the operational cost using Lyapunov optimization. The framework handles the stochastic behavior of the demand load, market price, and renewable energy generation. T. Li and M. Dong [69] showed that load shifting and energy storage management can be decoupled and solved sequentially. On the other hand, the online stochastic algorithm outperformed the Lyapunov optimization as shown in [16]. Tavakkoli et al. [70] proposed using the conditional-value-at-risk method to manage the operation of grid-connected PV-battery systems considering the uncertainty of the electricity price. The SARIMA model was used to predict the demand load and PV power generation. In [71], model predictive control was implemented to schedule the energy storage of grid-connected PV-battery systems. The schedule maximizes self-consumption but considers system degradation. The neural network was used to predict the load and PV generation. In [72], a robust optimization

method was used to schedule the thermal, cooling, and electrical loads under market price fluctuations; however, robust optimization is a very conservative method to handle uncertainty [17], as the problem is solved assuming the worst-case scenario. In [73], the adaptive probabilistic concept of the confidence interval method reduced the effect of prediction uncertainty of wind power on energy scheduling of micro-grid systems. The method is based on estimating the dependable level of the predicted wind power. Talari et al. [74] proposed using a stochastic variables computation module to operate a micro-grid system under the uncertainties of wind and PV generation. The micro-grid includes PV modules, wind turbines, battery energy storage, and responsive loads. A forecasting tool was used to predict the wind and PV energies. The variance of these energies was calculated using historical data. The output of forecasting was assumed to be the mean. The mean and the variance were used to generate scenarios fitting Weibull and beta distribution for the wind and PV energy, respectively. Then the scenario-reduction method was used to reduce the computation time.

A two-stage decision might be a good proposal to reduce the effect of uncertainty on the efficiency of planning. In [75], the effect of the uncertainties of renewable energy generation, and the electrical load of a residential building on energy dispatching effectiveness were counteracted using two-stage decision SDDP dispatching. The energy system is a standalone system that consists of a fuel cell, solar PV system, and solar thermal collector. The energy schedule is constructed based on expected hourly energy profiles, which are generated using the probability density function. The schedule in the

second stage is updated every 15 minutes after realizing the uncertainties to minimize the deviation in the battery energy profiles of the first and second stages.

Limited research has been conducted in the literature on the demand peak shaving under uncertainty. In [76], the model predictive control was used to shave the peak of both the electrical load and PV feed-in for the grid-connected PV-battery systems. PV generation was forecasted using the sun's position calculations, while the load was assumed to be previously given. The system stores the energy produced by the PV system in the battery only when PV energy, fed to the grid, exceeds the feed-in limits. In [16], the load was constrained to not exceed the maximum allowable rating to avoid any wiring failures.

The studies discussed in above are summarized in the following table:

Table 4-1. Summary of the previous published work.

<b>REF</b>	<b>Method</b>	<b>Optimization tool</b>	<b>Pricing scheme</b>	<b>Uncertain parameters</b>	<b>Consumer's peak shaving</b>
[57]	Chance-constrained programming	Nonlinear mixed-integer optimization (GUROBI solver)	Assumed to be constant	PV generation	No
[58]	Chance-constrained programming	Design space approach	Standalone PV system (no purchasing)	Wind speed	No
[59]	Scenarios-based method	Linear programming	TOU	Battery state of charge, electrical load, irradiance components, and ambient temperature	No
[60]	Scenarios-based method	Linear programming	TOU	Net power (electrical load - PV generation)	No
[23]	SDP	SDP	Two-part time-of-use tariff	PV generation and electrical load	No
[61]	Chance-constrained programming	Linear programming	No information	Wind energy, PV generation and electrical load	No
[13]	Chance-constrained programming	GA	TOU	Electrical load and PV generation	No
[14]	SDP	SDDP	TOU	PV generation and electrical load	No
[62]	SDP	SDDP	No information	PV generation	No
[63]	Scenarios-based method	Different heuristic algorithms (GA, PSO, etc.)	TOU	Wind energy, PV generation, and electrical load	No

Table 4-1. Continued.

<b>REF</b>	<b>Method</b>	<b>Optimization tool</b>	<b>Pricing scheme</b>	<b>Uncertain parameters</b>	<b>Consumer's peak shaving</b>
[64]	Scenario reduction method	Multiobjective optimization algorithm	Three-part time-of-use	Wind and PV generation	No
[65]	SDP	SDDP	Two-part time-of-use tariff	Electrical and the thermal demands	No
[66]	SDP	SDP	Two-part time-of-use tariff	No information	No
[67]	Point estimation method	Linear programming	Variable market price	PV, wind energy, market price and electrical load	No
[68]	Information gap decision theory	Information gap decision theory	Three-part time-of-use tariff	Electrical load	No
[69]	Stochastic optimization	Lyapunov optimization	Variable market price	Renewable energy (different sources), market price, and electrical load	No
[16]	Online stochastic algorithm	Online stochastic algorithm	Real-time pricing	Electricity market price	Yes, consumption limit assigned by the utility
[70]	Conditional value at risk method	Linear programming	No information	Electricity market price	No
[71]	MPC	No information	No information	Electrical load and PV prediction	No

Table 4-1. Continued.

<b>REF</b>	<b>Method</b>	<b>Optimization tool</b>	<b>Pricing scheme</b>	<b>Uncertain parameters</b>	<b>Consumer's peak shaving</b>
[72]	Robust optimization approach	Mixed-integer linear programming	TOU and real-time pricing	Electricity market price	No
[17]	Robust optimization approach	No information	Real-time pricing	PV and wind generations, and electrical load	No
[73]	Adaptive probabilistic concept of confidence interval	Non-dominated sorting genetic algorithm II	Real-time pricing	Wind power	No
[74]	Stochastic variables computation module	No information	Constant	PV and wind generation, and electrical Load	No
[75]	SDP	SDDP	Standalone system (no purchasing)	Solar energy, and thermal and electrical loads	No
[76]	Model predictive control	BM-CPLEX MATLAB solver	Single electricity-price scenario	PV generation	Yes
[77]	SDP	SDDP	No information	PV and wind energies	No

### **4.2.1. The Proposed Study**

In the current work, a scheduling model is proposed for grid-connected PV-battery systems used for demand peak shaving applications under the load and PV uncertainties. The system of the current work shaves the demand peak for facilities located in Texas. The Texas utility under study charges the consumers based on the total energy consumption and the 15-minute-average monthly demand peak. Shaving the peak reduces the bill amount significantly. The complexity of monthly peak shaving emerges due to the long control horizon of one month; thus, designing an efficient controlling mechanism is essential for the controller to be successful. In addition, forecasting the 15-minute-average energy profiles is a challenging problem requiring an accurate representation of the uncertainty of prediction.

#### **4.2.1.1. Method Selection**

The peak shaving problem can be formulated using chance-constraint programming. To convert the probabilistic formula of the chance constraint to deterministic, the amount of electricity generated by a photovoltaic array and the load need to be assumed following a given distribution, for example, a Gaussian distribution. In the current work, however, historical data is used to model the stochastic behavior of the load and PV generation for a more accurate representation, instead of assuming that they are following a defined distribution.

While uncertainties can be simulated using many scenarios (scenario-based programming), the optimal control decision obtained by averaging across all scenarios is computationally too intense to be implemented in practice. For example, the control

horizon for school is from 4:00 a.m. to 6:00 p.m., i.e., 15 steps. At each time step out of 15 steps, let us assume we have 10 expected values for load and 10 expected values for the PV generation. Therefore, at each time step, we have 100 different combinations of the expected values of the load and the PV generation. Having 100 different combinations at each step results in  $100^{15}$  different combinations of load and PV trajectories. The number of scenarios is  $100^{15}$ . Solving for one scenario consumes a millisecond, thus the total number of scenarios require  $3 \times 10^{19}$  year of computation time. As we are constructing a schedule for one day ahead, the schedule for one day ahead received after  $3 \times 10^{19}$  years is too late.

To reduce the simulation time, scenario-reduction methods are usually employed to reduce the number of scenarios; however, the scenario-reduction method reduces the accuracy of the uncertainty modeling.

In the current work, stochastic dual dynamic programming (SDDP) based on historical data handles the uncertainty of the current problem. Unlike the scenario-reduction method, the SDDP does not ignore any scenario. The SDDP mainly reduces the computation time when solving for a huge number of expected scenarios by breaking the control horizon into stages and solving the problem recursively with rapid solving methods.

#### **4.2.1.2. Case Studies**

The current case study was conducted for a school located in Texas, for which a full analysis is provided. The study also includes other facilities, a church, a theater, and a hotel, located in Texas, whose results are summarized for the sake of brevity.

### **4.3. Problem Formulating and Implementation**

In this section, a controller to shave the demand peak is designed while considering load and PV uncertainties. The peak shaving problem is reformulated to be acceptable by stochastic dual dynamic programming (SDDP) in Section 4.3.1. SDDP is used for decision-making under future uncertainty (See Section 4.3.2). The schedule constructed by the SDDP is intended to lead to the best cost with the highest probability. The statistical model, ARIMA, is used for hourly averages PV and load prediction. The probability distribution of the forecasting errors for historical data will be used to generate scenarios that are representations of the prediction uncertainty (See Section 4.3.3 ). The forecasted profiles are updated with receding horizon as shown in Section 4.3.4. The controller makes a decision with a receding horizon based on two main inputs: (A) the system states which are the stored energy in the battery and the peak value that has been recorded so far (B) the predicted hourly PV and Load profiles as well as the associated expected prediction errors.

The available libraries for stochastic dynamic programming and stochastic dual dynamic programming are discussed in Section 4.3.5. The adopted library is validated against in-house library in Section 4.3.6. The system sizes and the inputs parameters are given in Section 4.3.7. The controller design is depicted in Section 4.3.8.

#### **4.3.1. Reformulating the Peak Shaving Problem**

The objective function of peak shaving needs to be properly reformulated to be acceptable by the SDDP algorithm. More precisely, the max function, which is used to

find the peak value, needs to be linearized. The general formula of the optimization problem, which can be solved using stochastic dynamic programming, is discussed below.

The optimal control strategy with a finite horizon ( $T$ ) in discrete time for the deterministic case can be written as follows:

$$\min \sum_{t=0}^{T-1} L_t(x_t, u_t) + K(x_T) \quad (4.1)$$

The system dynamics can be described as:

$$x_t = f_t(x_{t-1}, u_t), \forall t \in \{0, 1, 2, \dots, T-1\}, x \in X \quad (4.2)$$

The current cost  $L_t(x_t, u_t)$  depend on the current state ( $x_t$ ) and the control decision ( $u_t$ ). The final cost of the system,  $K(x_T)$ , depends on the system's final state ( $x_T$ ). "T" is the control horizon. The optimal control strategy is a set of policy,  $\pi = (\pi_1, \pi_2, \dots, \pi_{T-1})$ , which provides the optimal control decision for any state ( $x$ ) and time ( $t$ ).

Equation (4.1) can be rewritten as:

$$\begin{aligned} \min [\sum_{t=0}^{T-1} L_t(x_t, u_t) + K(x_T)] &= \min [L_1(x_1, u_1) + L_2(x_2, u_2) + \\ &\quad L_3(x_3, u_3) + \dots + L_{T-1}(x_{T-1}, u_{T-1}) + K(x_T)] \end{aligned} \quad (4.3)$$

The problem of Equation (4.3) can be rewritten as a dual problem as follows:

$$\min [L_1(x_1, u_1) + V(x_1, u_1)] \quad (4.4)$$

where  $V(x_1, u_1)$  represents the expected future cost, given the system initial state ( $x_1$ ) and the control decision ( $u_1$ ). The future cost ( $V$ ) can be expressed as follows:

$$\begin{aligned} V(x_1, u_1) &= \min [L_2(x_2, u_2) + L_3(x_3, u_3) + \dots + \\ &\quad L_{T-1}(x_{T-1}, u_{T-1}) + K(x_T)] \end{aligned} \quad (4.5)$$

The electricity bill amount of a facility is given as follows:

$$\text{Bill amount} = \text{Cost (Total Grid energy)} + \text{Cost (Peak)} \quad (4.6)$$

where:

$$\text{Grid energy } (E_G) = E_L - E_{PV} + E_{Bat} \quad (4.7)$$

$$E_{Bat} = C_{Bat} \max(\eta u, \frac{1}{\eta} u)$$

$$E_s(t) = E_s(t-1) + C_{Bat} u(t)$$

$$\text{Peak} = \max(E_G)$$

where  $E_G$  is the grid energy,  $E_L$  is the electrical load of the facility,  $E_{PV}$  is the energy produced by the PV system,  $E_{Bat}$  is the battery charged/discharged energy,  $E_s$  is the energy stored in the battery in kWh,  $C_{Bat}$  is the maximum capacity of the battery,  $u$  is the charging/discharging rate, and  $\eta$  is the charging and discharging efficiency. The efficiencies of charging and discharging are assumed to be the same. The charging rate vector ( $u$ ) is positive for charging and negative for discharging. The penalty on charging is  $(1/\eta)$  and the penalty on discharging is  $(\eta)$ . Max function, in Equation (4.7), is used to determine the penalty based on the sign of  $u$ .

The charging/discharging rate ( $u$ ) of Equation (4.7) represents the control decision ( $u_t$ ) of Equation (4.1). The energy stored in the battery ( $E_s$ ) is the state of the system ( $x_t$ ). The final cost,  $K$  of Equation (4.1), for the current problem is the cost of the Peak. The Peak is the maximum grid power. The maximum grid power depends on all grid power values and thus on all the states ( $X$ ). However, the final cost,  $K$  in Equation (4.1), depends only on the final state. Thus, the problem needs to be reformulated for the SDDP to be applied. The problem is reformulated as follows:

Let's replace the variable Peak of Equations (4.6) and (4.7) with vector Peak (t) along with the following new two constraints:

$$\text{Peak}(t) \geq E_G(t) \quad (4.8)$$

$$\text{Peak}(t) \geq \text{Peak}(t-1) \quad (4.9)$$

The optimization algorithm using constraint (4.8) will force Peak (t) to be as close as possible to the grid energy at time t ( $E_G(t)$ ) to minimize the objective function. The second constraint (4.9) stores the highest peak that has been recorded so far in the control horizon as the last element in the vector Peak. The last element in the vector Peak will be used to calculate the cost of the system's final state.

The billed amount, given in Equation (4.6), is updated as follows:

$$\text{Bill amount} = \text{Cost}(\text{Total Grid energy}) + \text{Cost}(\text{Peak}(t=T)) \quad (4.10)$$

The problem now can be reformulated to be consistent with Equation (4.1) as follows:

$$\min \sum_{t=0}^{T-1} L_t(x_t, y_t, u_t, W_t) + K(y_T) \quad (4.11)$$

$$x_{t+1} = f_1(x_t, u_t, W_t), \quad \forall t \in \{0, 1, 2, \dots, T-1\}, x \in X$$

$$y_t = f_2(y_{t-1}, u_t, W_t), \quad \forall t \in \{0, 1, 2, \dots, T-1\}, y \in Y$$

where  $x$  is the energy stored in the battery ( $E_s$ ),  $y$  represents the Peak value,  $u$  is the charging rate, and  $W$  is the exogenous discrete noise, i.e., the uncertain values. The system has now two states: the energy stored in the battery ( $E_s$ ), and the peak value (Peak (t)). Now in Equation (4.10), the fees on the Peak are a function of the last element in vector Peak (the last element is Peak (t = T)). The final cost,  $K(y_T)$  of Equation (4.11), is

function of the final state ( $y_T$ ). The final state ( $y_T$ ) is Peak ( $t = T$ ). The problem now can be solved using SDDP.

Peak ( $t - 1$ ) of Equation (4.9) is defined as follows: The optimization problem starts at  $t = 0$  and starts with target value of the Peak being zero.

$$\text{Peak}(t - 1)|_{t=0} = \text{Peak}_{\text{Target}} = 0 \quad (4.12)$$

The utility in Texas charges consumers based on the monthly peak; thus  $T$  is one month. However, the control horizon for school is broken into stages of one-day length to reduce the complexity of scheduling for a long control horizon, as shown in Section 4.3.8. Therefore, the control horizon  $T$  is one day, and  $\text{Peak}_{\text{Target}}$  is updated daily.  $\text{Peak}_{\text{Target}}$  is the peak value the schedule is constructed to maintain.

The battery is fully charged at the  $t = 0$ :

$$E_s(t - 1)|_{t=0} = C_{\text{Bat}} \quad (4.13)$$

The max function in Equation (4.7) needs to be linearized for the problem to be acceptable by the library given in [78]. The library which is used to solve the current problem is discussed in Section 4.3.5:

$$E_{\text{Bat}} = C_{\text{Bat}} f \quad (4.14)$$

$$f \geq \eta u \quad (4.15)$$

$$f \geq \frac{1}{\eta} u$$

The max function is replaced by a new variable called  $f$  as we see in Equation (4.14), and we add new two constraints (see Equation (4.15)). We know that the output of

the max function of two values equals the higher value. In constraints of Equation (4.15),

the output of the max function ( $f$ ) can be higher or equal any of them. To explain this:

- A) If the battery is in charge mode ( $u$  is positive): the second constraint of Equation (4.15) is the dominant constraint. To minimize the Grid energy of Equation (4.7), the Battery energy of Equation (4.7) needs to be minimized. To minimize the Battey Energy, we minimize the  $f$  (see Equation (4.14)). The minimum possible value for the  $f$  that satisfies the second constraint of Equation (4.15) is “ $1/\eta u$ ”.
- B) If the battery is in discharge mode ( $u$  is negative): the first constraint of Equation (4.15) is the dominant constraint. To minimize the Grid energy of Equation (4.7), the Battery energy of Equation (4.7) needs to be minimized. To minimize the Battey Energy, we minimize the  $f$  (see Equation (4.14)). The minimum possible value for the  $f$  that satisfies the first constraint of Equation (4.15) is “ $\eta u$ ”.

### 4.3.2. Stochastic Dual Dynamic Programming

Stochastic dynamic problems can be solved by the backward recursion method (Figure 4.1). In backward recursion, the cost function ( $V$ ) is calculated for every possible state in the final stage ( $t = T$ ) by discretizing the state, where “ $V$ ” is the optimal (the minimum for example) expected future cost for a given stage and given system state. The costs ( $V$ ) associated with different states in the final stage ( $t = T$ ) are calculated and tabulated (Table 4-2). In Table 4-2 the system is assumed to have one state variable ( $E_s$ ) just to simplify the concept. After we calculate the cost function ( $V$ ) for stage  $T$  for

different states, we can move backward to the previous stage ( $t = T-1$ ) and find the cost function ( $V$ ) for different states in the stage ( $T-1$ ) (Figure 4.1). The cost function ( $V$ ) in stage ( $T-1$ ), (Figure 4.1), is the summation of (1) the current cost of the stage ( $T-1$ ),  $\text{Cost}(T-1)$ , and (2) the future expected cost of stage  $T$  ( $V(T)$ ). These two costs are a function of the control decision of stage ( $T-1$ ),  $u_{T-1}$ . The control decision being made in stage  $T-1$  is the one that will lead to the minimum  $V(T-1)$ . The process is repeated up to the first stage (stage 1 in Figure 4.1), and all cost functions ( $V$ ) for all stages are tabulated.

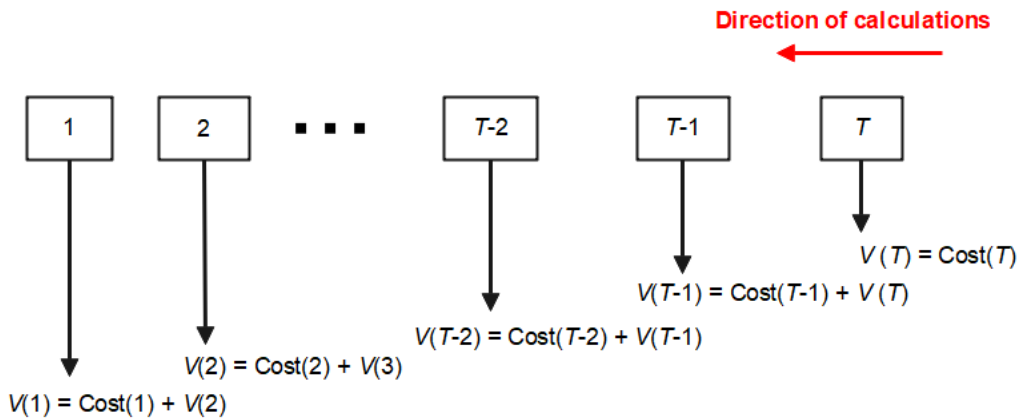


Figure 4.1. SDD calculations flow chart.

Table 4-2. Calculating the future expected cost ( $V$ ) using SDD, assuming that  $E_s$  is the only state variable of the system just to simplify the concept.

State ( $E_s$ )	$t = 1$	$t = 2$	...	$t = T$
$E_s = 1\%$	$V(1, 1\%)$	$V(2, 1\%)$	...	$V(T, 1\%)$
$E_s = 2\%$	$V(1, 2\%)$	$V(2, 2\%)$	...	$V(T, 2\%)$
...	...	...	...	...
$E_s = 100\%$	$V(1, 100\%)$	$V(2, 100\%)$	....	$V(T, 100\%)$

For clarification, the equation representing the cost function ( $V$ ) of stage  $T-1$  is discussed with in detail as follows:

$$V(T-1) = \text{Cost}(T-1) + V(T) \quad (4.16)$$

**i. Remark 1:**

$\text{Cost}(T-1)$  represents the current electricity cost at  $t = T-1$ .  $\text{Cost}(T-1)$  is a function of current control chosen ( $u_{T-1}$ ), and the Load and PV generation. The load and PV generation, uncertain parameters, are represented by  $W$ .

$$\text{Cost}(T-1) = f(u_{T-1}, W_{T-1}) \quad (4.17)$$

The control decision,  $u_{T-1}$ , affects the system states ( $x_{T-1}, y_{T-1}$ ). The energy stored in the battery ( $E_s$ ) and the current peak value are the states ( $x, y$ ) in the current work.

$$\begin{aligned} x_{T-1} &= f(x_{T-2}, u_{T-1}) \\ y_{T-1} &= f(y_{T-2}, u_{T-1}, W_{T-1}) \end{aligned} \quad (4.18)$$

**ii. Remark 2:**

$V(T)$  is the future cost given the current stage  $T-1$ , and the current states ( $x_{T-1}, y_{T-1}$ ).

$$V(T) = f(t = T, x_{T-1}, y_{T-1}) \quad (4.19)$$

**iii. Remark 3:**

- A. The future expected cost  $V(T)$  can be retrieved from Table 4-2 based on the future stage time ( $T$ ) and the current states ( $x_{T-1}, y_{T-1}$ ).
- B. The control chosen ( $u_{T-1}$ ) affects the current states ( $x_{T-1}, y_{T-1}$ ) as shown in Equation (4.18) and current cost ( $\text{Cost}(T-1)$ ) as shown in Equation (4.17). The current states ( $x_{T-1}, y_{T-1}$ ) determines the future cost ( $V(T)$ ) as shown in

Equation (4.19). Therefore, the chosen control “ $u_{T-1}$ ” affects the current cost ( $\text{Cost}(T-1)$ ) and future cost  $V(T)$ . Therefore, the value of “ $u_{T-1}$ ” needs to be optimized to minimize the total cost  $V(T-1)$  which is a summation of the current cost ( $\text{Cost}(T-1)$ ) and future cost  $V(T)$ .

- C. Consequently,  $V(T-1)$  represents the minimum expected future cost given stage T-2, assuming that the control decisions made in the future (at stage T-1 and stage T) are optimal.

Stochastic dynamic programming (SDP) assumes only a finite number of possible discrete states. We know that the battery can be charged/discharged by an arbitrary number smaller than the discrete step. The peak value (one of the system states) can also change by a number smaller than the discrete step. Therefore, the SDP formulation is an approximation. Furthermore, the backward recursion leads to a huge number of calculations in two cases: (1) many variables are used to represent the system state, and (2) in the case of small discretization step size. Stochastic dual dynamic programming (SDDP) is proposed to tackle the curse of dimensionality of the SDP. The SDDP is based on approximating the future cost instead of solving for a large state-space. Monte Carlo simulations, parallel computing, convex optimization, piecewise linear, modern solvers such as GUROBI, and cutting plane method are some of the methods to reduce the computation time.

### **4.3.3. Forecasting and Scenarios Generation**

In the current work, ARIMA model is used to predict hourly load and PV electricity generation. The ARIMA model available in MATLAB is used in the current work. The school loads on the weekend, holidays, and during the nights are low thus ignored. The days of low load are also removed from the data that is used for training. The new load signal, after ignoring the low-load hours, is smoother thus facilitates prediction by the forecasting tool. The signal is further smoothed using Hampel filter (Hampel filter is used in [79] for better prediction). Cleaning the data that is used for training remarkably enhanced the prediction. The new load signal is the school load between 4:00 a.m. to 6:00 p.m. While the load is low around 4:00 a.m., it is included in the new signals because we found that adding the load of the school at 4:00 a.m. enhances the prediction accuracy. The PV signal is the PV generation between 6:00 a.m. and 6:00 p.m.

The results of hourly load forecasting for the school for 15 steps (4 a.m. to 6 p.m.) ahead shown in Figure 4.2, which contains forecasting results for 20 days as a sample. The historical data of one year is divided into two subsets: one to tune the forecasting tool parameters (70%), and the second subset (30%) to generate scenarios to represent the prediction uncertainty.

The forecasting tool is tested on the second subset; the ratios between the real and predicted values are calculated. The number of workdays in one year is about 255 days. Of those, 75 days (30%) are used to generate Figure 4.3, which shows the ratio between the real and forecasted values for four step numbers out of 15 total steps. The probability distribution of the ratios for each step number of the 15 is used to generate scenarios to

represent the expected prediction errors for each step. The probability distribution is represented using the 10 percentiles for each step (Figure 4.4). It is shown in Figure 4.2 and Figure 4.3 (a) that, at the beginning of the day (4 a.m. to 5 a.m., during the low-load period) the prediction error is relatively high. The ratio between the real value and the forecasted is usually close to one (Figure 4.3 (b-d)). At each step in the forecasting horizon of 15 steps, the forecasted load value (the output of ARIMA model) with the 10 ratios, obtained in Figure 4.4, are used to generate 10 excepted values for the school load at each step.

The same process is applied to the prediction of PV generation. The ratio between the real and the predicted values for PV generation is shown in Figure 4.5. Forecasting the PV generation with a long forecasting horizon (more than three steps ahead) is a challenging problem [79]. Solar power generation can change significantly from one day to another due to the volatile nature of solar radiation. The PV power for a long trajectory is more difficult to be predicted as compared to the load prediction.

At each time step out of 15 steps, we have 10 expected values for load and 10 expected values for the PV generation. Therefore, at each time step, we have 100 different combinations of the expected values of the load and the PV generation. The control horizon is from 4 a.m. to 6 p.m., i.e., 15 steps. Having 100 different combinations at each step results in  $100^{15}$  different combinations of load and PV trajectories. The number of scenarios is  $100^{15}$ . Solving for one scenario consumes millisecond, thus the total number of scenarios require  $3 \times 10^{19}$  year of computation time. As we are constructing a schedule for one day ahead, the schedule received after  $3 \times 10^{19}$  years is considered to be too late.

The scenario-reduction method can be used to reduce the number of scenarios thus reducing the computation time. However, SDDP is proposed to solve the current problem without the need to ignore any scenarios and with a reasonable computation time of about 2 minutes.

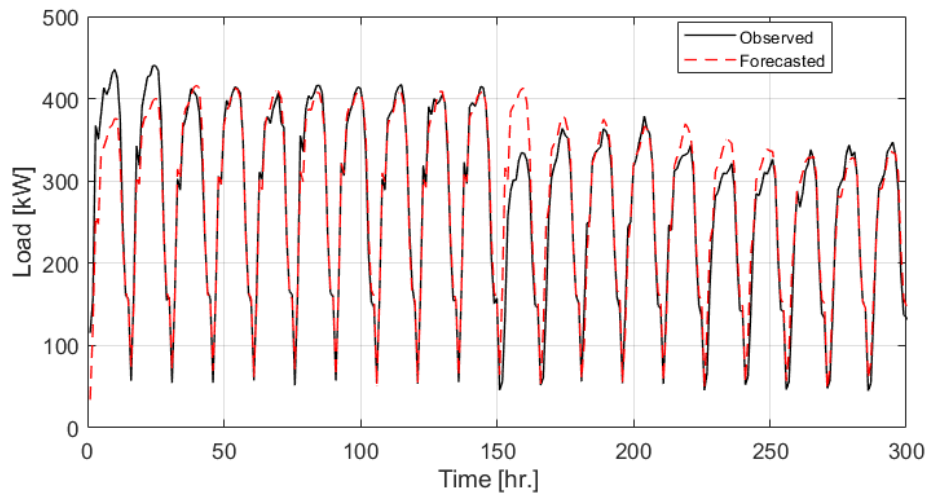


Figure 4.2. The real values versus the forecasted values for school load prediction with multi-step (15 steps (hours) ahead prediction).

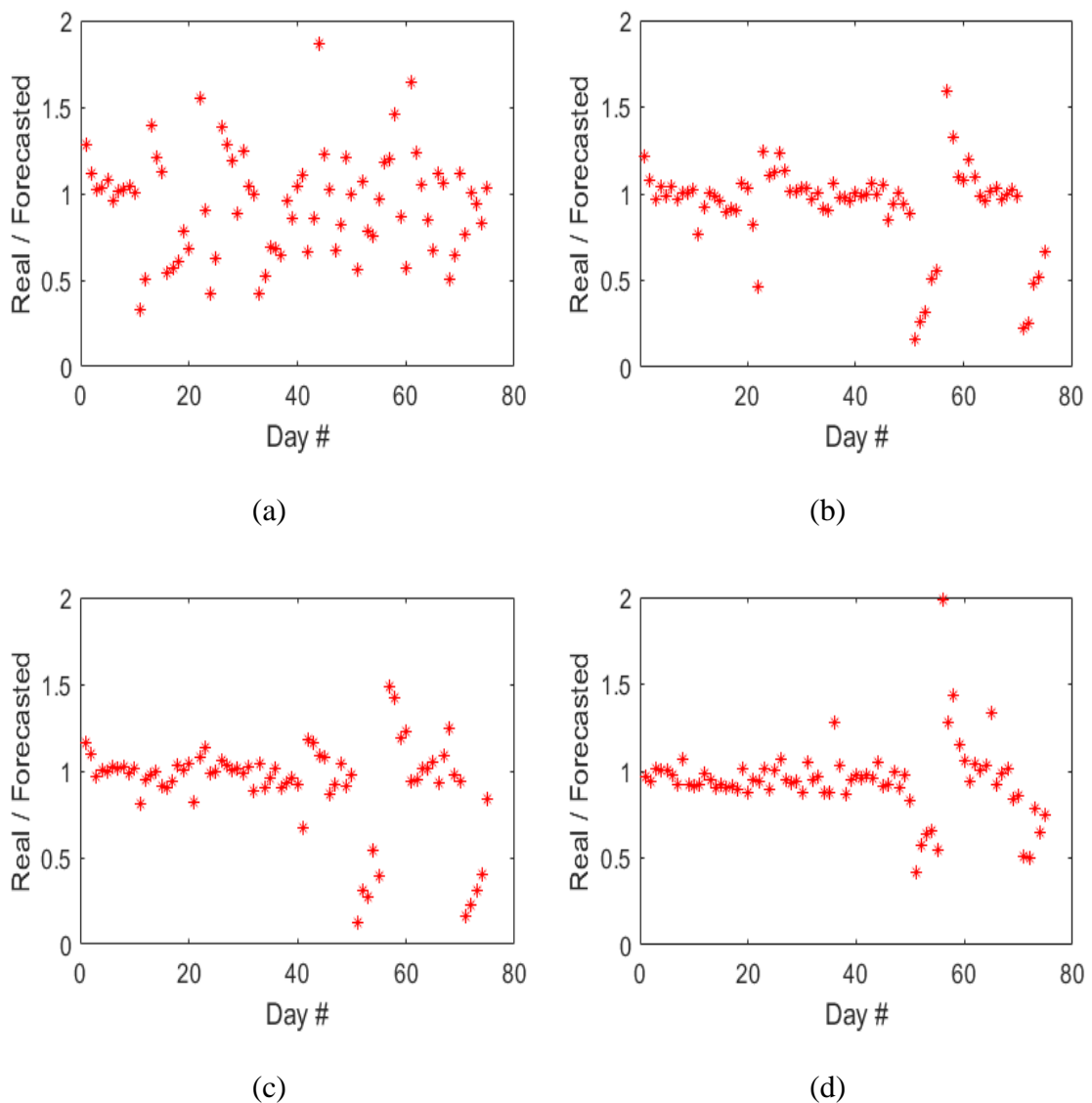


Figure 4.3. The ratios between the real values to the forecasted values of school load for one-day ahead (multi-step prediction with 15 steps ahead) (a) the second step out of 15 steps (b) step number 6 out of 15 steps (c) step number 10 out of 15 steps (d) step number 14 out of 15 steps.

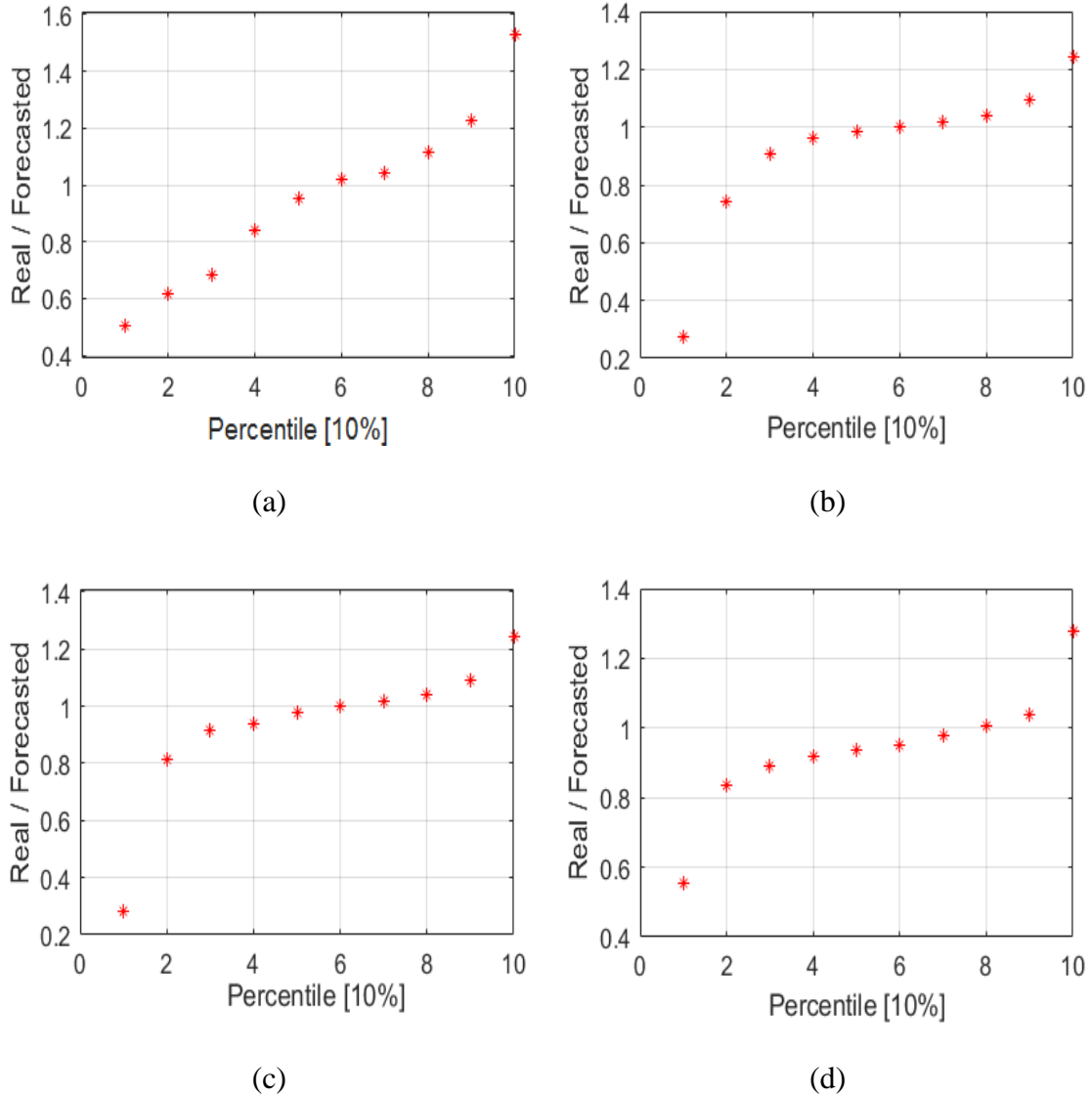


Figure 4.4. The percentiles for the ratios between the real values to the forecasted values of the school load (multi-step prediction with 15 steps ahead) (a) the second step out of 15 steps (b) step number 6 out of 15 steps (c) step number 10 out of 15 steps (d) step number 14 out of 15 steps.

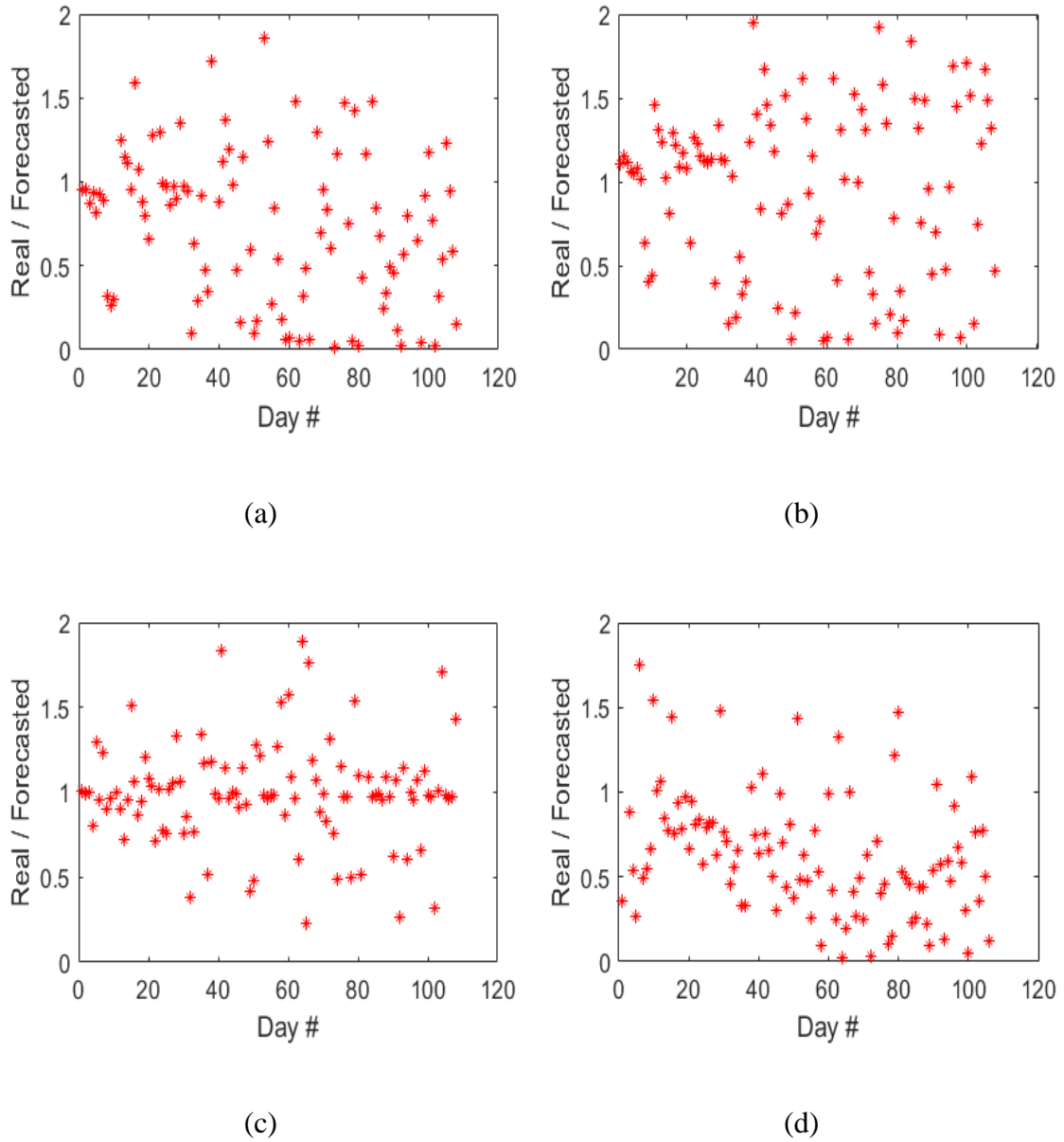


Figure 4.5. The ratio between the real values to the forecasted values of PV generation (multi-step prediction with 13 steps ahead) for (a) the first step out of 13 steps (b) step number 5 out of 13 steps (c) step number 9 out of 13 steps (d) step number 13 out of 13 steps.

In [77], the autoregressive (AR) model is used to predict multiarea renewable energy generation for real-time scheduling of a storage system. The uncertainty of

prediction using AR model in [77] is assumed to be propagating with time theoretically as proposed by Cabral [80]. The expected ratio between the real value and the forecasted is represented by 10 evenly spaced quantiles. Figure 4.6 shows the 1<sup>st</sup> and the 10<sup>th</sup> quantile (see Equations (4) and (5) in [77]). In the current work, the forecasting error for historical data simulates the uncertainty of prediction for a given horizon. Using available historical data gives a more accurate representation of the prediction uncertainty. On the other hand, Nair et al. [71] used the prediction error based on historical data to adjust the battery state of charge minimum limit to accommodate for the prediction uncertainty.

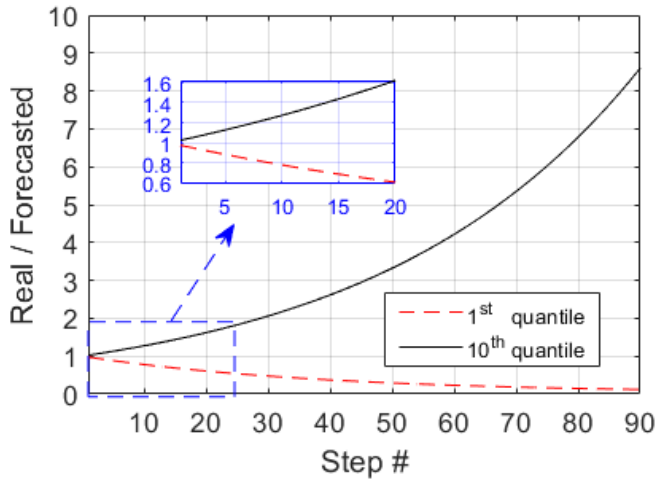


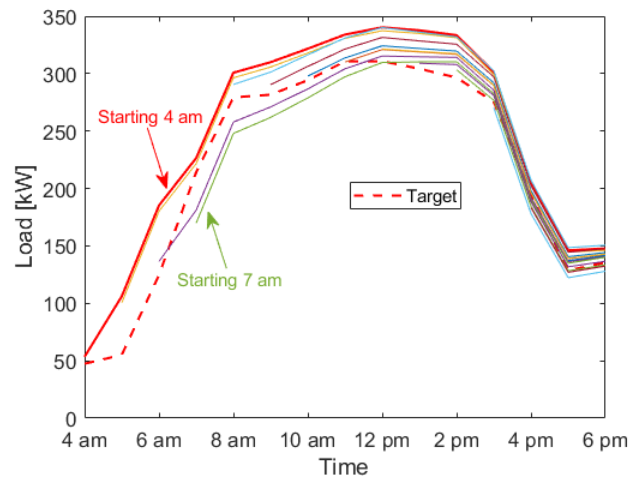
Figure 4.6. Uncertainty propagation (theoretical) of AR model.

#### 4.3.4. Forecasting with Receding Horizon

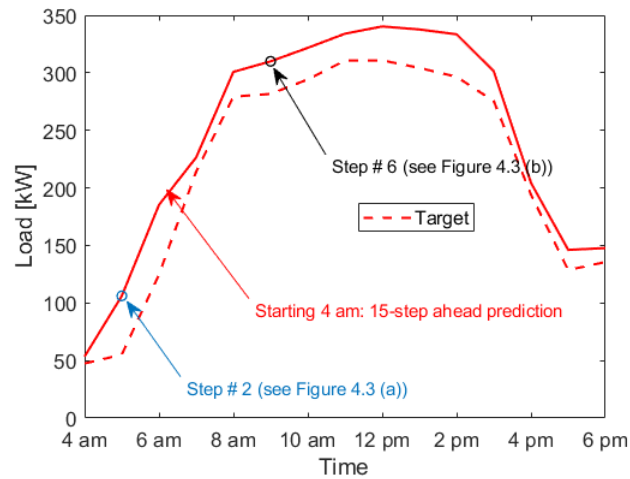
Figure 4.7 (a) shows the results of predicting the school's hourly load with a receding horizon for an arbitrary day. As we can see, updating the forecasted profile with a receding horizon can enhance prediction accuracy: the forecasted value is getting closer to the real value. However, that does not mean the peak shaving will not be always better

by updating the forecasted values with a receding horizon. For instance, at 8 a.m. the new forecasted value (as compared to the first forecast) is lower than the real value. If we charge the battery during this time interval and since we have already underestimated the load, a higher demand peak might occur at 8 a.m. Figure 4.7 (b) shows the forecasting with 15 steps ahead starting at 4 a.m. The ratio between the real value and the forecasted value for the different steps of the 15-step ahead prediction for different days is shown in Figure 4.3. Figure 4.7 (c) shows the forecasting with 12 steps (control horizon is 12 steps) ahead starting at 7 a.m. The ratio between the real values and the forecasted values for the different 12 steps for different days in the historical data is calculated. In the same way, as the horizon recedes, the ratios are calculated for different horizons and stored in a matrix and can be then called using the information of the new control horizon length and the step number in the new horizon. These ratios are used to generate scenarios as discussed in Section 4.3.3 for the new horizon of the new length.

Figure 4.8 shows the results of predicting the PV power with a receding horizon for an arbitrary day. The prediction tool significantly underestimates the PV generation the first five times of receding. Then, the forecasted value starts to be closer to the real value.



(a)



(b)

Figure 4.7. Forecasting the school hourly-average load with receding horizon.

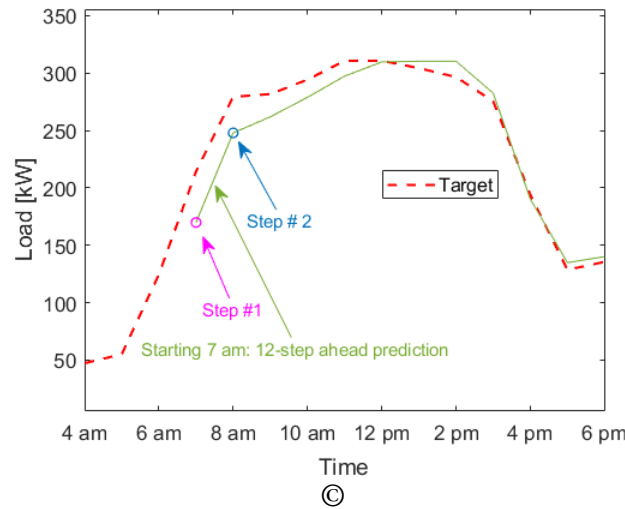


Figure 4.7. Continued.

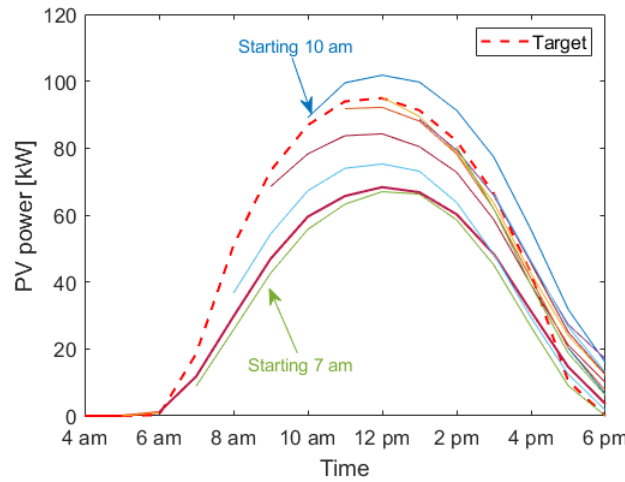


Figure 4.8. Forecasting the hourly-average PV generation with receding horizon.

#### 4.3.5. SDP and SDDP Libraries

FAST (Finally An SDDP Toolbox) [81] is the only open-library written in MATLAB language and could be found, used to solve stochastic problems. The library is user-friendly, but it is limited in that it does not support out-of-sample simulations, i.e.,

when the realization is not one of the defined scenarios. Limited open libraries for SDDP in python are available. The “SDDPY” [82] and “MSPPY” [83] are open libraries written in python for SDDP.

A library for the SDP written in Scilab language can be found in [22]. The library also uses the SDDP to solve stochastic problems using the cutting plane method. The library was rewritten in the current work using MATLAB language. However, the SDDP in this library only supports one state. In the current work, we have two states: (1) the energy stored in the battery, and (2) the peak value that has been recorded so far.

In the current work, an open library written in Julia language [78] is used to solve the current stochastic problem. The library supports out-of-sample simulations and systems with more than one state. The algorithm used to solve the stochastic problems in [78] is a new algorithm that was proposed in [84].

#### **4.3.6. SDDP Library Validation**

The proposed SDDP library of [78] is validated against the SDP that is given in [22]. The SDDP algorithm is found to be significantly faster than the SDP and provides a more efficient energy schedule (Table 4-3). SDP consumes 20 minutes for one-day peak shaving if the discretization step sizes are 1% for the energy stored in the battery and 10 kW for the peak. SDP consumes more time with smaller discrete sizes; smaller discrete sizes can be used to provide a better energy schedule. On the other hand, the SDDP library consumes less than one minute. SDP of [22] with receding horizon consumes 3 hours with the mentioned discrete step sizes while SDDP of [78] with receding horizon consumes only 5 minutes.

Table 4-3. Hourly-average peak shaving percentage [%] for one day using SDP and SDDP for 10 random days.

Day #	SDDP	SDP
1	41.6	40.7
2	33.6	35.8
3	13.7	15.1
4	37.2	36.1
5	12.6	11.7
6	27.1	22.4
7	43.2	42.4
8	38.6	36.2
9	35.6	32.2
10	30.4	28.2

Peak shaving percentage [%] (represented as Shaving [%] in this work) is calculated as follows:

$$\text{Shaving [%]} = \frac{\text{Peak}_{\text{without shaving}} - \text{Peak}_{\text{after shaving}}}{\text{Peak}_{\text{without shaving}}} \times 100 \% \quad (4.20)$$

The SDDP is trained with 300 iterations. Table 4-4 shows that the number of iterations of 300 is quite fair to solve the current stochastic problem.

Table 4-4. Hourly-average peak shaving percentage [%] for one day with different numbers of iterations for 10 random days.

Day #	Number of iterations				
	75	150	300	600	1200
1	34.26	35.77	<b>35.41</b>	35.48	35.47
2	41.81	41.41	<b>41.68</b>	41.56	41.72
3	22.23	28.07	<b>28.64</b>	26.88	28.4
4	13.74	13.74	<b>13.74</b>	13.73	13.72
5	36.67	36.72	<b>37.18</b>	37.0	37.07
6	38.53	38.58	<b>38.38</b>	38.26	38.40
7	43.11	43.66	<b>43.47</b>	43.13	43.31
8	33.25	34.04	<b>33.96</b>	33.66	33.84
9	32.93	33.06	<b>34.69</b>	35.63	33.78
10	36.84	36.72	<b>36.95</b>	36.98	37.14

#### **4.3.7. System Sizing and Inputs Parameters**

The initial, replacement, and maintenance costs of PV-battery systems are significant; thus, the capacities of the system components need to be optimized. The system components are PV modules, battery storage system, inverters, and converter. Convex optimization can be utilized to optimize the system components based on historical weather and load data. However, the purchase price of the system components can vary. The purchase price plays a significant role in sizing the system. The current system is equipped with 500 PV modules and battery storage of 450 kWh capacity. The efficiency of charging and discharging is assumed to be 92%. The PV module in the current work is a multi-crystalline (KC200GT) module with a maximum capacity of about 200 W, at the standard conditions. The utilities in Texas charge the consumers on average about \$ 0.05 per kWh and on average about \$ 7 per kW electrical demand peak. The peak rate is based on the highest 15-minute monthly electrical demand. Different pricing policies might be considered and listed as follows:

- 1) The utility charges the consumers \$0.05 per kWh consumption and refunds them \$0.05 per kWh that is supplied to the grid (net metering).
- 2) The utility accepts the excess PV energy without paying the PV system owner.
- 3) The utility charges the consumers \$0.05 per kWh but refunds them with a lower price, for example, \$0.01 per kWh feed-in.
- 4) The utility prohibits the consumers from providing excess PV power to the grid to prevent unstable oscillations in grid frequency that could lead to major electrical grid failures.

For the current study, pricing policy number 2 (see above) is adopted. However, all these scenarios can be reformulated to be acceptable by convex optimization (CVX) and stochastic dual dynamic programming (SDDP). Convex optimization is used to optimize the schedule if we do not account for the uncertainty, while SDDP is used to optimize the schedule if the uncertainty is included.

The PV system is assumed to be working on the maximum power point (MPP) by installing an MMP tracking controller. The maximum power generated by a solar system can be estimated using single diode model [85]. In the current work, the maximum power point is estimated using PV-LIB toolbox [41]-[42]. The PV-LIB library is based on Sandia laboratory's PV experimental model. The system's parameters are summarized in Table 4-5.

Table 4-5. Design inputs.

Parameter	Value
# PV modules	500
Battery capacity ( $C_{\text{Bat}}$ )	450 [kWh]
Charging/discharging efficiency ( $\eta$ )	92%
Electricity purchase cost	0.05 [\$/ kWh] ([129])
Peak fees	7 [\$/kW] ([129])

#### 4.3.8. Controller Design

The school load before 4 a.m. and after 6 p.m. is very low (low-load period) thus peak shaving is applied between 4 a.m. and 6 p.m. The low-load period is long enough to charge the battery until fully charged with a low charging rate. The low charging rate ensures the peak does not occur during the low-load period as the load in low-load period is not shaved. The maximum capacity of the battery is 450 kWh which can be charged

from empty to fully charged with a charging rate of 0.111 during the low-load period which means 50 kWh energy is added to the battery every one hour. The load during the low period will be raised by 50 kW to charge the battery. The load during the low-load period is about 50 kW. The load during the low-load period will rise from about 50 kW to 100 kW to charge the battery. The peak after shaving is about 200 kW in Figure 4.12 (the ideal case). The load of 100 kW is lower than the peak load of 200 kW. Therefore, the battery can be charged to full capacity without any risk.

The utility charges the consumers based on the monthly peak. Thus, the peak shaving horizon is one month. To ease the complexity, the horizon is broken into one-day-long stages. The forecasting tool forecasts the load and PV generation for one day ahead (between 4 a.m. and 6 p.m.). The new control horizon is one day ( $T = 1$  day, 1 day is 15 hours between 4 a.m. and 6 p.m.). The first-day energy profiles are predicted. Then a schedule to shave the peak of the first day is constructed. The real maximum peak value for that day is recorded and stored as  $\text{Peak}_{\text{Target}}$  for the next day. The battery is then charged in the period between 6 p.m. and 4 a.m. Then the forecasting tool predicts the load and PV generation of the next day. Then constructing a schedule to shave the peak value of the new day to be equal to or lower the peak value that has been recorded so far which is  $\text{Peak}_{\text{Target}}$  (See Equation (4.12)). The target peak value ( $\text{Peak}_{\text{Target}}$ ) is updated every day as shown in Equations (4.21) and (4.22). The process is repeated every day for one month. The flowchart of the control mechanism is shown in Figure 4.9.

$$\text{Peak}_{\text{Target}} = \max (\text{Peak}_{\text{Target}}, \text{maximum peak of the current day}) \quad (4.21)$$

$$\text{The maximum peak of the current day} = \text{Peak}(t = 6 \text{ p.m.}) \quad (4.22)$$

As shown in Equation (4.9), the maximum peak value is updated each time step, thus the Peak value at  $t = (\text{one month})$  equals the maximum peak recorded during that month.

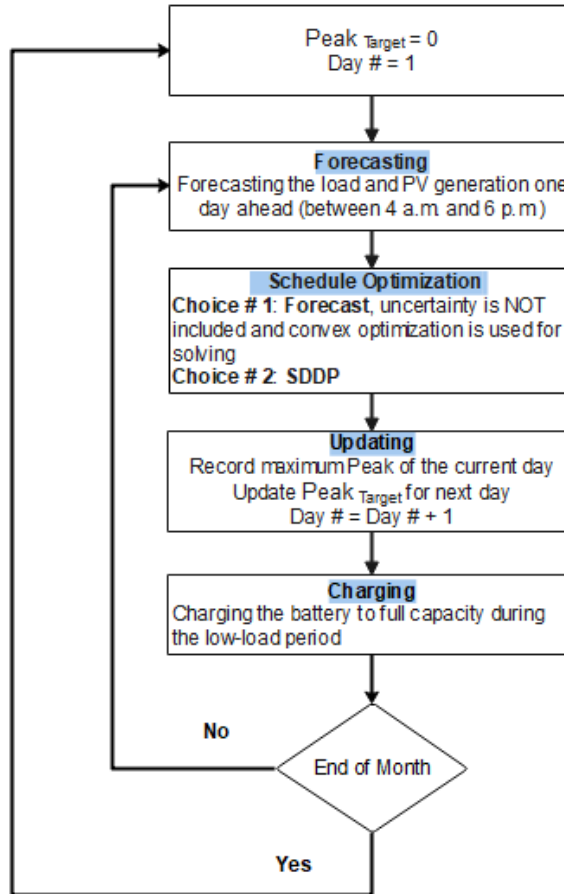


Figure 4.9. Controller flowchart for monthly peak shaving without receding horizon.

#### 4.4. Results and Discussion

A historical data of six years was used in the current work: one year for scenarios generation (see Section 4.3.3) and five years for the following analysis. The performance of SDDP in handling the uncertainty of the current problem is validated by comparing it with the base case (Forecast). In the Forecast method, the uncertainty is not included in

the energy scheduling. In Forecast, the load and PV energy trajectories are predicted and then an optimization tool is used to optimize the energy schedule. The scheduling problem for PV-battery system is convex [22], thus convex optimization algorithm is used for solving. However, the following work is based on hourly forecasting. The 15-minute load and PV signals are noisy and less effective to be predicted with long control horizon.

SDDP and Forecast are compared in shaving the 15-minute daily peak in Section 4.4.1. In Section 4.4.2, the results for shaving the 15-min monthly peaks for 5 full years are summarized. The scheduling problem is solved with different time-of-realization, and different time-of-scheduling, and with or without receding forecasting horizon. In Section 4.4.3, the forecasted profiles are updated with receding horizon and with two layers of forecasting: the first layer predicts the hourly profile for one day ahead, and the second layer predicts the 15-min profile for one hour ahead. The results for different facilities are summarized in Section 4.4.4.

#### **4.4.1. Comparison Between SDDP and Forecast for 15-Minute Daily Peak Shaving**

Table 4-6 shows the percentage for hourly demand peak shaving using Forecast and SDDP methods for 10 random days. The results are compared with the ideal case where we assume that we can predict the future with 100% accuracy. Scheduling with receding horizon and without receding horizon are compared in Table 4-6. In the receding-horizon-based scheduling, the forecasted energy trajectories (Load and PV) are updated every one step and the schedule is then reconstructed accordingly (see Section 4.3.4).

Table 4-6. Daily hourly-average demand peak shaving percentage [%] for different methods.

Day	Forecast		SDDP		Ideal
	No receding horizon	receding horizon	No receding horizon	receding horizon	
1	30	30	35	30	40
2	39	35	41	41	43
3	17	15	18	13	25
4	21	21	28	24	35
5	16	19	11	10	27
6	21	20	13	19	27
7	39	34	37	36	48
8	31	32	38	33	45
9	20	16	23	22	31
10	36	32	35	36	42

The following conclusions can be drawn from Table 4-6:

- Scheduling without receding horizon is most of the time more efficient than scheduling with receding horizon, for both Forecast and SDDP. As mentioned in Section 4.3.4, scheduling with receding horizon does not necessarily lead to a better peak shaving.
- SDDP is more efficient than Forecast for hourly demand peak shaving for 6 out of 10 days.

However, the utility in this case study charges the consumers based on the 15-minute monthly peak. The schedule constructed to shave the hourly demand peak is utilized in shaving the 15-minute demand peak, and the results are given in Table 4-7. Forecasting the Load and PV trajectories based on the hourly variations is easier than

forecasting based on 15-minute variations. The 15-minute load and PV signals are noisy thus more difficult to be predicted.

Table 4-7. Daily 15-minute demand peak shaving percentage [%] utilizing the schedule construed for the hourly demand peak shaving.

Day #	15-minute peak shaving using hourly-based Forecast		15-minute peak shaving using hourly-based SDDP		Ideal
	No receding horizon	receding horizon	No receding horizon	receding horizon	
1	19	19	24	19	42
2	33	30	32	22	44
3	16	12	3	4	27
4	16	6	8	3	44
5	9	15	2	-8	28
6	20	16	9	6	29
7	29	26	26	23	48
8	24	24	24	17	45
9	18	15	18	11	34
10	28	30	29	25	42

The following conclusions can be drawn from Table 4-7:

- Scheduling without receding horizon is most of the time more efficient than scheduling with receding horizon, for both Forecast and SDDP. The same conclusion was drawn from Table 4-6.
- Using the schedule constructed to shave the hourly peak by Forecast method for 15-minute demand peak shaving is more efficient than the one constructed by SDDP, most of the time.

The effectiveness of the schedule in shaving the peak when compared to the ideal case is calculated for SDDP of Table 4-6 and Forecast of Table 4-7, both methods without receding horizon. The results are given in Table 4-8. In general, shaving the hourly peak

is easier than shaving the 15-minute peak. The ideal case is the last column of Table 4-6 and Table 4-7.

The equation to calculate the effectiveness is given as follows:

$$\text{Effectiveness} = \frac{\text{Shaving [%]}}{\text{Ideal shaving [%]}} \times 100 \% \quad (4.23)$$

where peak shaving percentage [%] (Shaving [%]) is given in Equation (4.20).

Table 4-8. The Effectiveness [%] of the schedule in shaving the daily peak.

<b>Day #</b>	<b>Forecast of Table 4-7</b>	<b>SDDP of Table 4-6</b>
1	45.2	87.5
2	75	95.3
3	59.3	72
4	36.4	80
5	32.1	40.7
6	69.1	48.2
7	60.5	77.1
8	53.3	84.4
9	53.2	74.2
10	66.7	83.3

For the scheduling with receding horizon of Table 4-7, the Peak <sub>Target</sub> is updated every 15-minute and used to update the hourly-based schedule of receding horizon. The hourly-based schedule is applied to shave the 15-minute peak. The controller flow chart of receding horizon of Table 4-7 is shown in Figure 4.10.

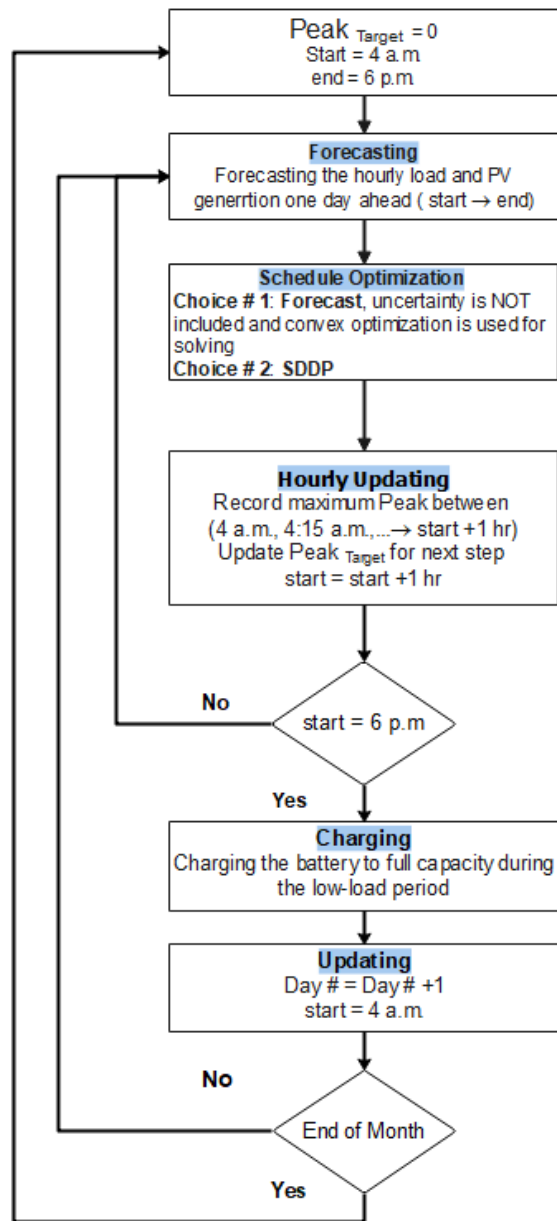


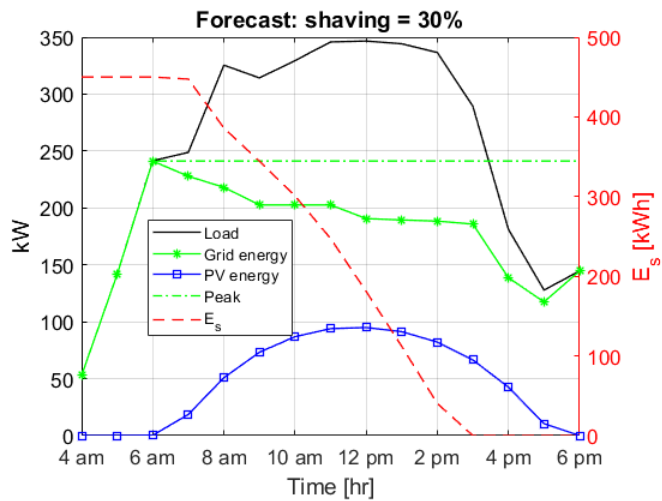
Figure 4.10. Controller flow chart for monthly peak shaving with receding horizon of Table 4-7.

Hourly average peak shaving for day #1 (Table 4-6) using Forecast and SDDP, without receding horizon, is shown in Figure 4.11. The schedule obtained by Forecast and SDDP shaves the hourly peak by 30% and 35%, respectively. In the ideal case in which

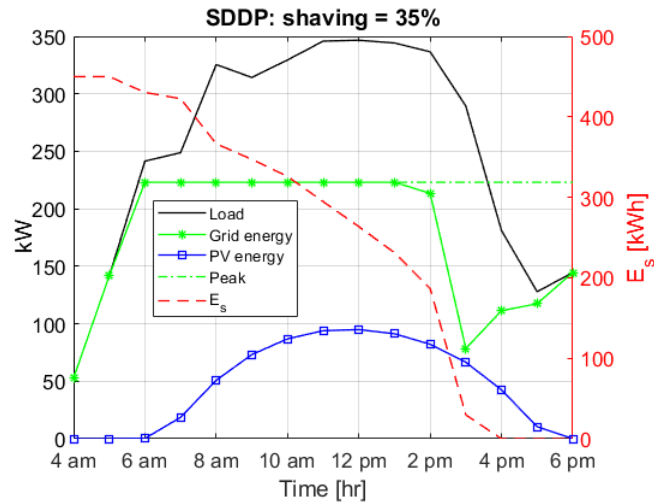
the forecasting is assumed to be 100% accurate, the schedule shaves the hourly demand peak by 40%. The Forecast started shaving the peak by discharging the battery at 7 a.m. which was slightly late, as the peak occurred at 6 a.m. (see Figure 4.11 (a)). In Figure 4.13 (a), the forecasting tool, ARIMA model, significantly underestimated the load at 6 a.m. which leaves the schedule constructed by Forecast with a higher demand peak at 6 a.m. The SDDP method started shaving the peak by setting the battery on the discharging mode at 5 a.m. In both the ideal case and the SDDP, the battery was on the discharging mode at 5 a.m. However, in the ideal case, the discharging rate at 5 a.m. was higher to keep the peak as low as possible.

Texas utility charges the consumers based on the 15-minute demand peak. The schedule based on shaving the hourly demand peak is used to shave the 15-minute demand peak, and the results for day #1 (see Table 4-7) are shown in Figure 4.12. The schedule obtained by hourly-based Forecast and hourly-based SDDP can shave the 15-minute demand peak by 19% and 24% without receding horizon, respectively. The most efficient schedule can shave the 15-minute demand peak by 42% (the ideal case, Figure 4.12 ©). The 15-minute variations given in Figure 4.13 (b) can be utilized to justify relatively the low shaving-effectiveness of the schedule obtained by Forecast with a higher peak at 6 a.m.: between 6:00 a.m. and 6:15 a.m., the school load is significantly higher than the hourly-average load between 6:00 a.m. and 7:00 a.m. In other words, the energy schedule based on the hourly average significantly underestimates the load between 6:00 a.m. and 6:15 a.m. for day #1.

For instance, in the ideal shaving (Figure 4.11 ©) at 8 a.m. the power produced by the PV system is about 50 kW and the battery discharged energy is about 70 kW. The demand is shaved by 120 kW ( $50\text{ kW} + 70\text{ kW}$ ). The grid energy at 8 a.m. is shaved from 325 to 205 kW.

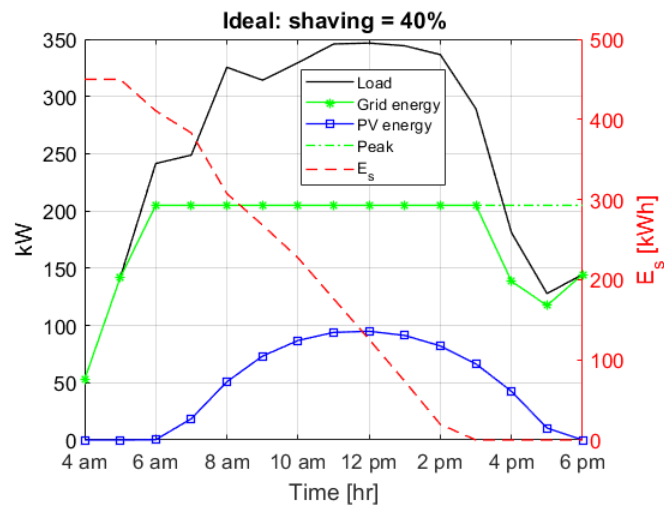


(a)



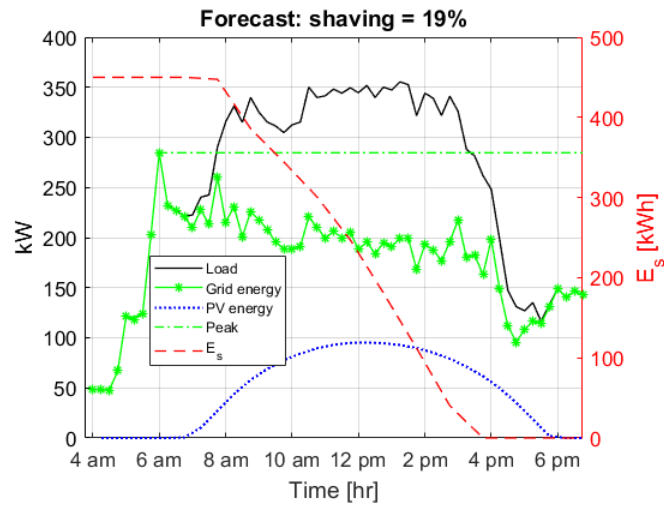
(b)

Figure 4.11. Hourly-demand peak shaving (a) using Forecast (b) using SDDP (c) the ideal case.

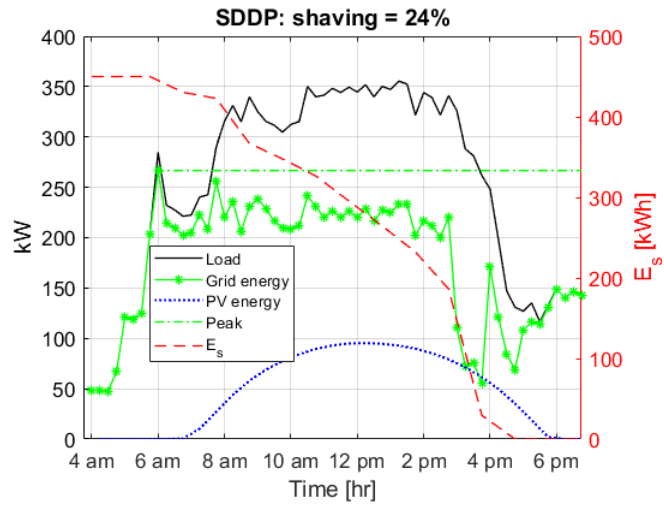


(c)

Figure 4.11. Continued.

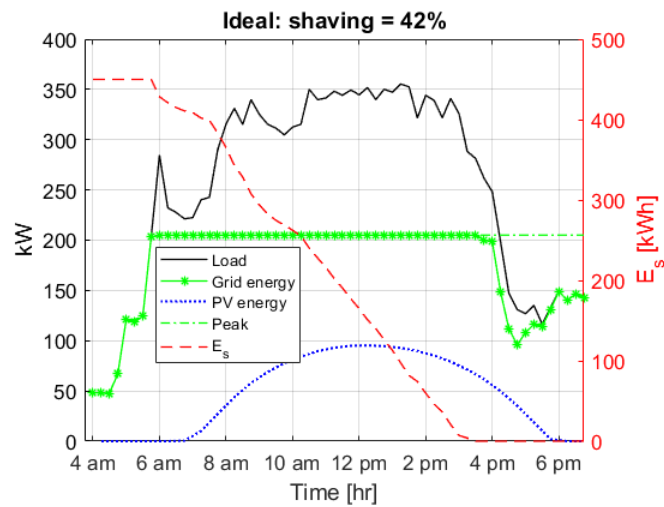


(a)



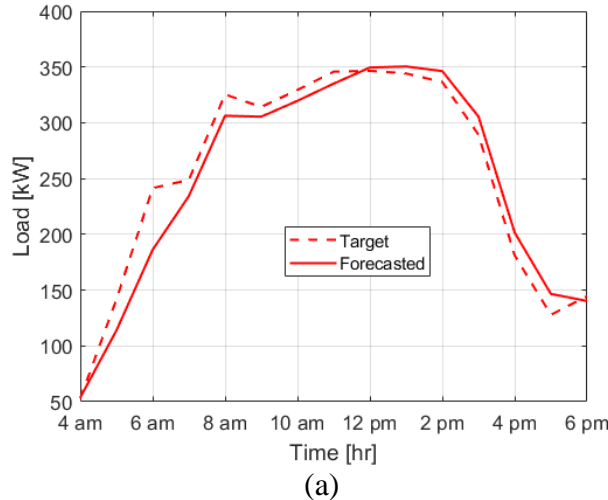
(b)

Figure 4.12. 15-minute average demand Peak shaving (a) using the schedule obtained by hourly-based Forecast (b) using the schedule obtained by hourly-based SDDP (c) the ideal case.

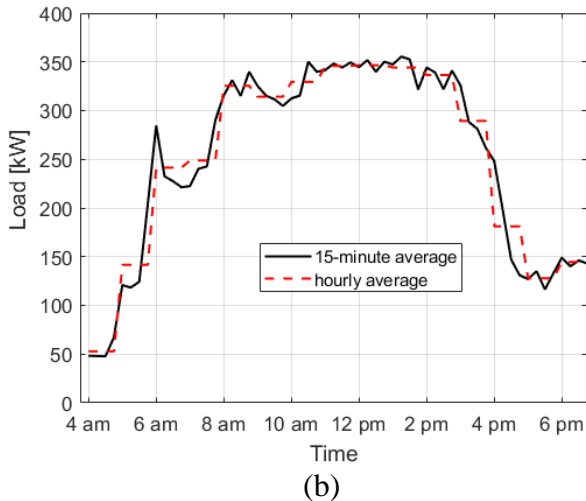


(c)

Figure 4.12. Continued.



(a)



(b)

Figure 4.13. Day #1 (a) forecasting hourly load results (b) the hourly and 15-minute load profiles (figure (b) timescale = 15 minutes).

#### 4.4.2. Full-Year 15-Minute Monthly Peak Shaving

In the following two sections, the SDDP and Forecast methods are validated for 15-minute monthly peak shaving over 5 years. In Section 4.4.2.1, the monthly-based and daily-based peak shaving are discussed and compared. Shaving the peak with different time scales of scheduling and realization, and with or without receding forecasting horizon is compared in Section 4.4.2.2.

#### **4.4.2.1. Monthly-based and Daily-based Shaving**

In the daily-based, the daily 15-minute peak is shaved every day in the month. In the monthly-based, the first day 15-minute peak is shaved and the new peak after shaving is used as a target for the next day 15-minute peak shaving. The target is updated every day in the month; the target is the maximum peak value that has been recorded so far in the current month. In other words, the scheduling is based on maintaining the new day's peak lower or equal to the maximum peak value that has been recorded so far in the current month.

The results of shaving the 15-minute monthly demand peak using monthly-based and daily-based shaving for 5 years are summarized in Table 4-9. The peak values and the shaved power for one random year out of 5 years are shown in Figure 4.14 and Figure 4.15.

The daily-based shaving is more harmful to the battery life span due to the excessive charging and discharging, compared to the monthly-based shaving. However, the daily-based shaving is more effective in shaving the monthly peak (see Table 4-9). The scheduling can be with receding or non-receding horizon. The scheduling with receding horizon was not a good suggestion, especially for SDDP, as shown in Table 4-9. Forecasting with receding horizon is explained in Section 4.3.4.

Forecast method is found to be better than SDDP method (at least about 10% better, see Table 4-9). Referring to the analysis: ARIMA prediction errors for historical data are extracted and then used as a representation of the prediction uncertainty. Including the uncertainty of prediction in the decision-making was not found to be effective.

As seen in Figure 4.14 and Figure 4.15, scheduling using SDDP with receding monthly-based peak shaving fails in shaving monthly peak in 10 out of 12 months. Based on Figure 4.14 and Figure 4.15, and Table 4-9, scheduling using SDDP with receding monthly-based peak shaving fails miserably. Figure 4.16 can justify this failure of SDDP. The month is 30 days and if the schedule obtained by SDDP fails in maintaining the peak value of one day in a month, the schedule of that month fails in shaving the monthly peak. For instance, in February (Figure 4.16) the peak in one day exceeded the monthly peak value that can be recorded without scheduling. For better understating of peaks signals of Figure 4.16: the load in the weekend is very low with a peak value of less than 100 kW which explains why the signal goes decreases to 100 kW periodically.

Table 4-9. Comparison of different methods in shaving the 15-minute monthly peak for five years of historical data.

#	Technique	Average Shaving net [kW/Year]	Average Saving net [\$/year]	Average Effectiveness [%]
<b>Forecast</b>				
1	Daily-based	735	5150	46.6
2	Daily-based (receding horizon)	686	4802	43.7
3	Monthly-based	708	4956	45.1
4	Monthly-based (receding horizon)	696	4872	44.3
<b>SDDP</b>				
1	Daily-based	562	3934	36.8
2	Daily-based (receding horizon)	233	1631	14.9
3	Monthly-based	479	3353	30.5
4	Monthly-based (receding horizon)	-275	-1925	-17.5
<b>Ideal</b>		<b>1569</b>	<b>10983</b>	<b>100%</b>

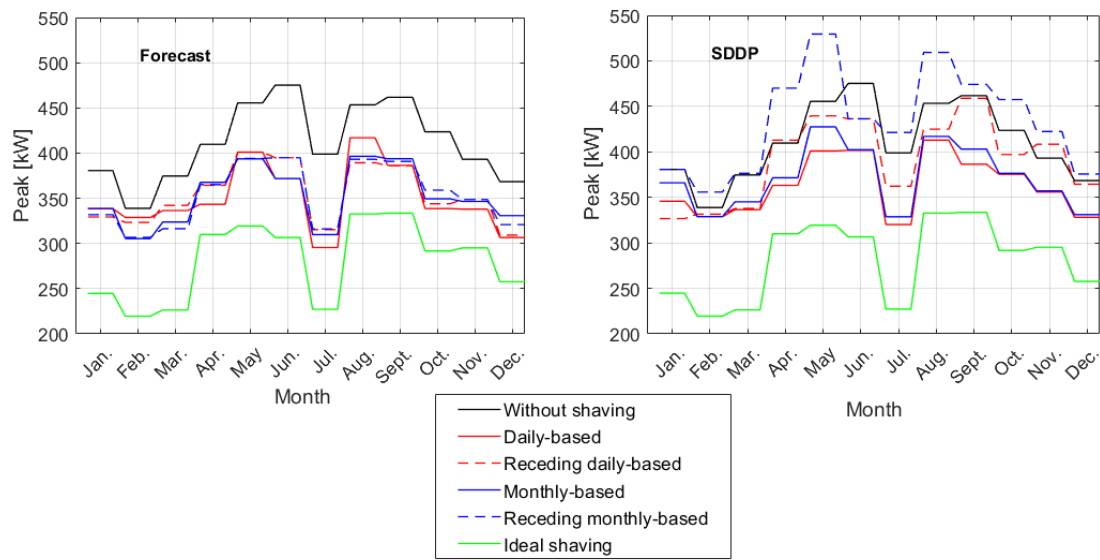


Figure 4.14. Monthly peak values before and after shaving using (1) Forecast, and (2) SDDP methods.

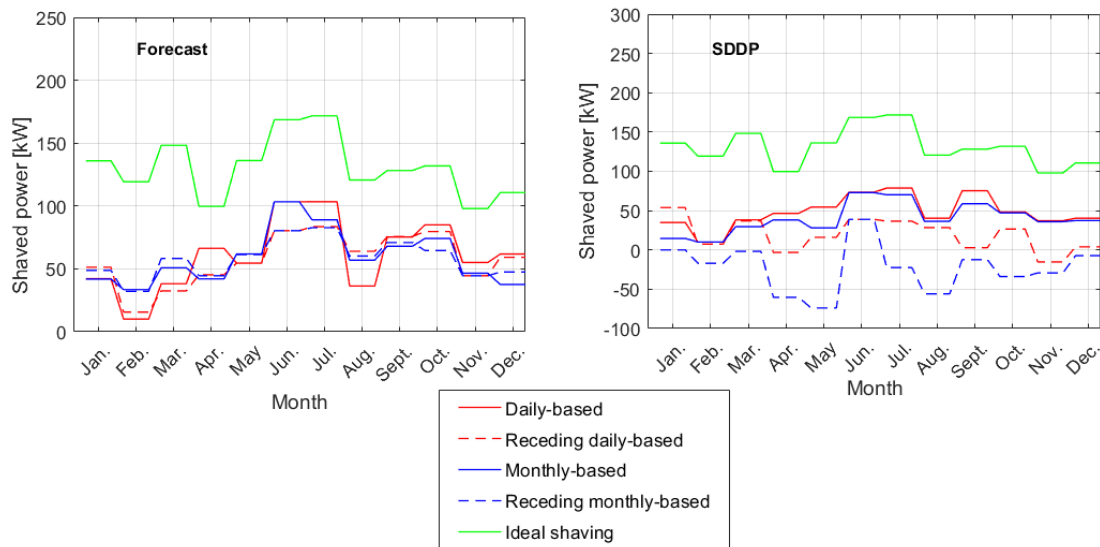


Figure 4.15. The monthly shaved peak power using (1) Forecast, and (2) SDDP methods.

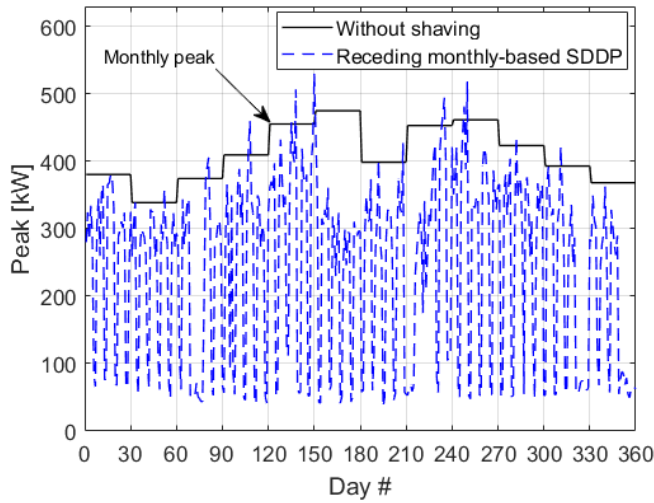


Figure 4.16. The daily peak values with receding monthly-based peak shaving using SDDP.

#### **4.4.2.2. Receding and no Receding Forecasting, Different Time-of-Realization, and Different Time-of-Scheduling**

In SDDP and Forecast methods, the forecasting tool predicts the hourly PV and load profiles for one day ahead. In the receding forecasting, the forecasted profiles are updated continuously every one hour and used to reconstruct the battery schedule. In non-receding forecasting, the profiles are forecasted only one time for one day ahead and adopted without any change. However, the schedule can be reconstructed if and only if the forecasted profiles and/or the peak target get updated. The peak target can be updated by realizing the highest demand recorded in the past time steps of the receding scheduling horizon. The realization can be accomplished by measuring and recording (1) the hourly-average demand or (2) 15-minute-average demand. The schedule is then updated accordingly. As mentioned, the forecasted profiles can be updated every one hour or can be left without updating. On other hand, the schedule can be updated with two options:

every 15 minutes or every one hour. If the peak target is updated every one hour (hourly realization), the schedule will be updated hourly. If the peak target is updated every 15 minutes (15-minute realization), the schedule will be updated with two options: 15-minute updating or hourly updating. In the hourly scheduling with 15-minute realization, the last four measurements in the last hour will be used to update the target peak and the target peak will be then used to update the hourly schedule. The effectiveness of different methods in the 15-minute-monthly-peak shaving, when tested on 5 full years, is summarized in Table 4-10. The Forecast and SDDP are tested with different combinations of (1) different time-of-realization, (2) different time-of-scheduling, and (3) with receding and non-receding horizons. The effectiveness is calculated (given in Equation (4.23)) based on the ideal shaving in which the forecasting tool is assumed to be perfect. The Forecast is found to be more efficient than SDDP in shaving the 15-minute monthly peak. Forecast with receding forecasting horizon, 15-minute realization, and 15-minute-based receding scheduling is the most effective in shaving the 15-minute monthly peak.

Table 4-10. The effectiveness of different methods in shaving the 15-minute monthly peak with different time-of-realization and time-of-scheduling and with receding and non-receding horizons.

#	<b>Hourly Forecasting</b>	realization	scheduling	<b>Effectiveness [%]</b>	
				Forecast	SDDP
1	One-time forecasting	no realization	One-time hourly based	46.63	36.82
2	receding horizon	hourly	Hourly based and receding	46.33	44.61
3	receding horizon	15-minute	Hourly based and receding	43.73	14.85
4	receding horizon	15-minute	15-minute based and receding	50.64	36.67
5	One-time forecasting	hourly	Hourly based and receding	41.92	35.86
6	One-time forecasting	15-minute	Hourly based and receding	40.13	40.09
7	One-time forecasting	15-minute	15-minute based and receding	46.03	34.33

#### 4.4.3. Two-layer Forecasting Versus Single-layer Forecasting

In this section, the energy profiles (load and PV generation) will be forecasted using two layers. In the first layer, the hourly profiles are forecasted for one day ahead and updated hourly with receding horizon. In the second layer, the 15-minute profiles are forecasted for 1 hour ahead and updated every 15-minute. The forecasted profiles for the load (hourly profiles of one day and 15-minute profiles of one hour) are combined in a single profile. The same is applied for PV generation forecasted profiles. The new profiles are then used to construct the battery schedule. The 15-minute profiles (load and PV

generation) for one hour ahead are updated every 15 minutes thus battery schedule is reconstructed every 15 minutes.

In Table 4-11, the scheduling effectiveness for one day 15-minute peak shaving using the Forecast method based on one-layer and two-layer forecasting is compared for 10 random days. It is found that the scheduling effectiveness in shaving the 15-minute peak for a day with one-layer forecasting is generally better than scheduling based on two-layer forecasting. The 15-minute profiles are so noisy thus, they are difficult to be predicated with reliable accuracy. In other words, the decision based on the hourly predicted profiles is more efficient than the decision based on the 15-minute predicted profiles for the current scheduling problem.

Table 4-11. Forecast method for 10 random days with one-layer forecasting and two-layer forecasting with receding forecasting horizon and with 15-minute realization and scheduling.

<b>Day #</b>	<b>Effectiveness [%]</b>	
	<b>Two-layer forecasting</b>	<b>One-layer forecasting</b>
1	69.4	75.5
2	57.6	57.6
3	51.6	54.8
4	41.2	61.8
5	39.1	43.5
6	69	58.6
7	63.6	69.7
8	48	60
9	38.6	38.6
10	62.5	50

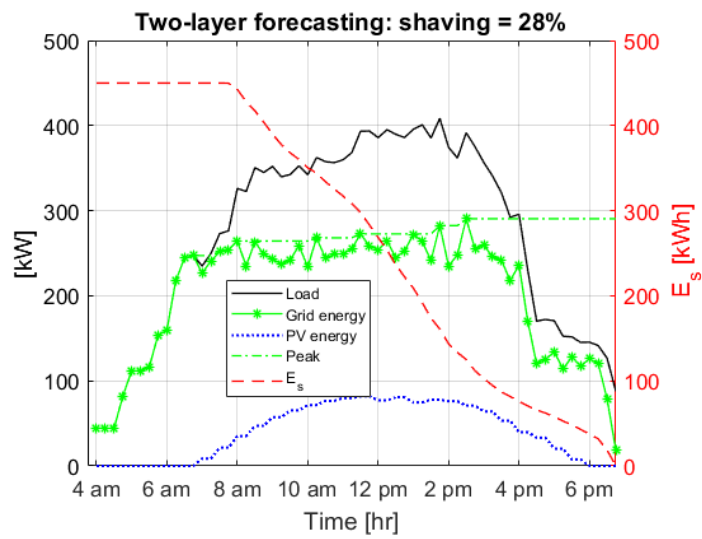
The effectiveness of scheduling for five years with two-layer forecasting with Forecast and SDDP methods is shown in Table 4-12. The Forecast is more efficient than

SDDP. However, Forecast with one-layer forecasting, given in Table 4-10 (row 4), is more efficient than the Forecast method based on two-layer forecasting.

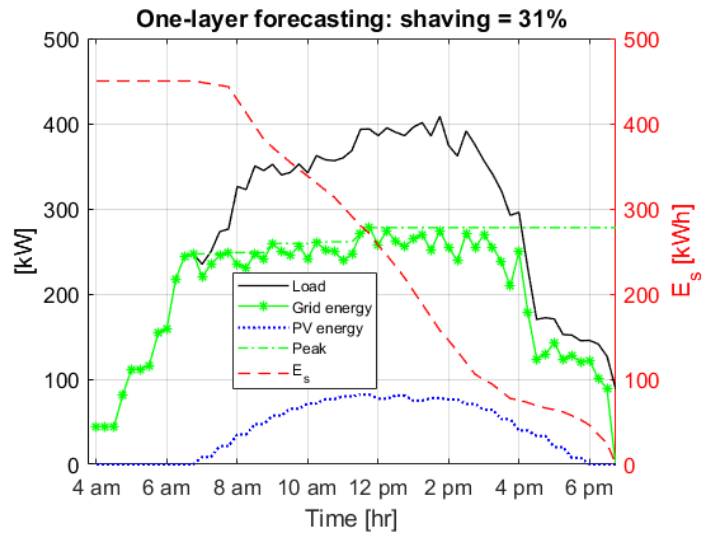
Table 4-12. Two-layer forecasting with receding horizon, 15-minute realization and scheduling, and with Forecast and SDDP methods.

Method	Effectiveness [%]
Forecast	49.08
SDDP	35.21

Figure 4.17 shows the energy scheduling using two-layer forecasting and one-layer forecasting for one random day. The prediction results are shown in Figure 4.18. At 1:45 p.m. and 2:30 p.m., the two-layer forecasting underestimates the load more than the one-layer forecasting does. The load peaks with two-layer forecasting occurred at these time points (Figure 4.17). However, two-layer is sometimes more efficient in prediction and peak shaving, but in general, the one-layer forecasting is better for shaving the peak of the current work.



(a)



(b)

Figure 4.17. Peak shaving for one random day using (a) two-layer and (b) one-layer forecasting using the Forecast method.

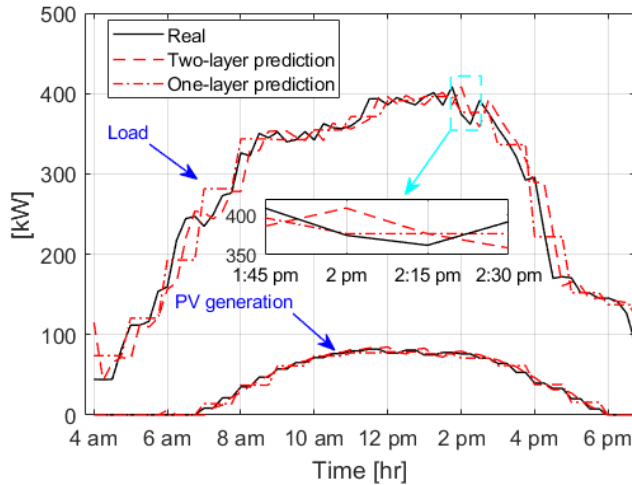


Figure 4.18. Load and PV generation prediction.

#### 4.4.4. Different Facilities

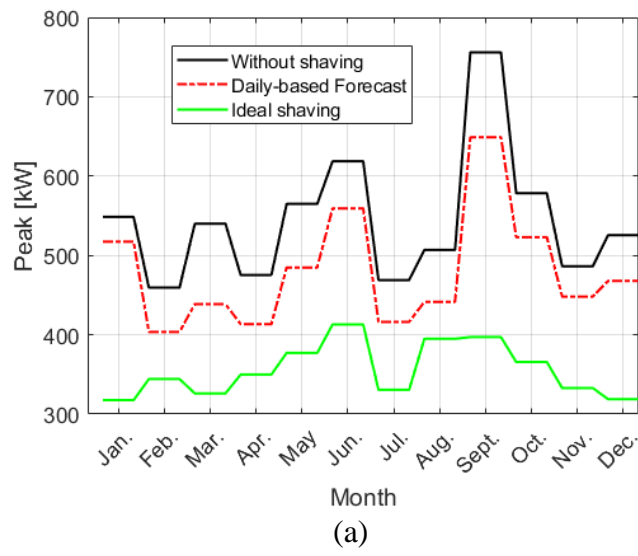
Electrical load data of 6 years for different Texas commercial buildings — churches, theaters, and hotels, as well as schools — was utilized in the current study. A complete case study is performed for a school in the previous sections. The other buildings, however, have different patterns of energy consumption; thus, the data cleaning and the scheduling horizon are different from those of a school.

The theater load signal, considered for shaving, is the load between 3 a.m. and 9 p.m., thus the load after 9 p.m. and before 3 a.m. is not included in the training, prediction, and scheduling process. The church significant load takes place between 3 a.m. and 8 p.m. The hotel load pattern is not predictable thus the data is not cleaned, and the scheduling is based on predicting the 24-hour profile. Therefore, hotel peak shaving is expected to be relatively more difficult due to the length of the control horizon and the propagated uncertainty of prediction. The results of shaving the 15-minute monthly peaks for different facilities and for 5 years are summarized in Table 4-13. The load signals before and after

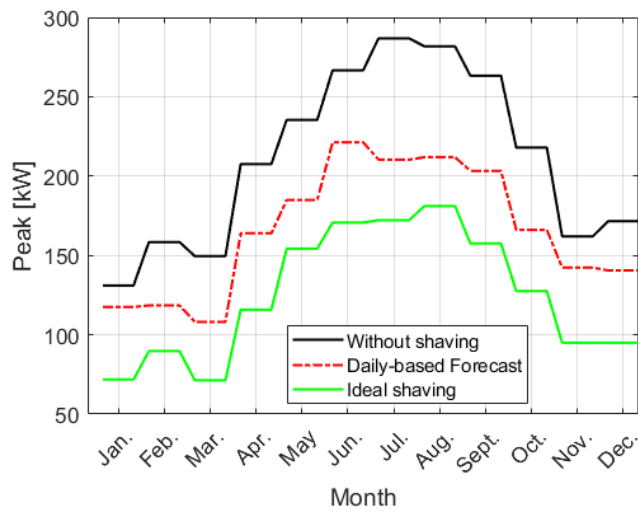
shaving for one random year for all these buildings are shown in Figure 4.19. The schools and theater loads profiles are easier to be shaved, compared to the load profiles of churches and hotels. The peak shaving for theater recorded the highest effectiveness. The daily peak after shaving for theater is shown in Figure 4.20. As mentioned, the hotel load is more difficult to shave under the uncertainty, compared with other considered facilities.

Table 4-13. Effectiveness of Forecast method in shaving the 15-minute monthly peaks for different facilities.

<b>Building type</b>	<b>Effectiveness [%]</b>
School	50.76
Church	31.25
Theater	53.18
Hotel	25.94



(a)



(b)

Figure 4.19. Peak shaving for (a) church (b) theater (c) hotel.

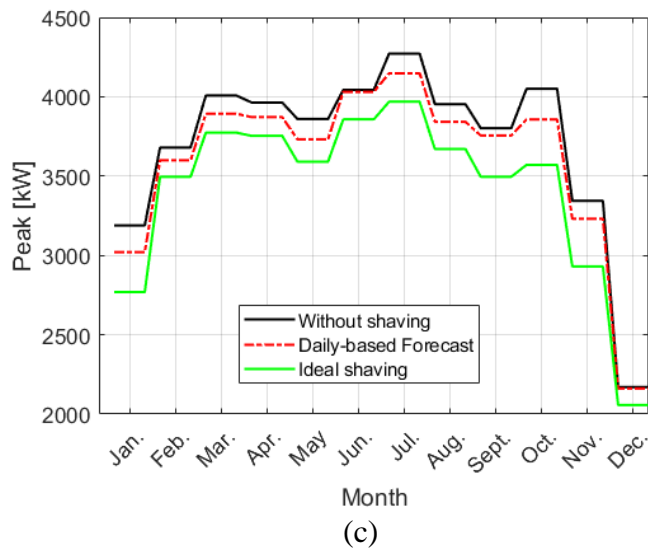


Figure 4.19. Continued.

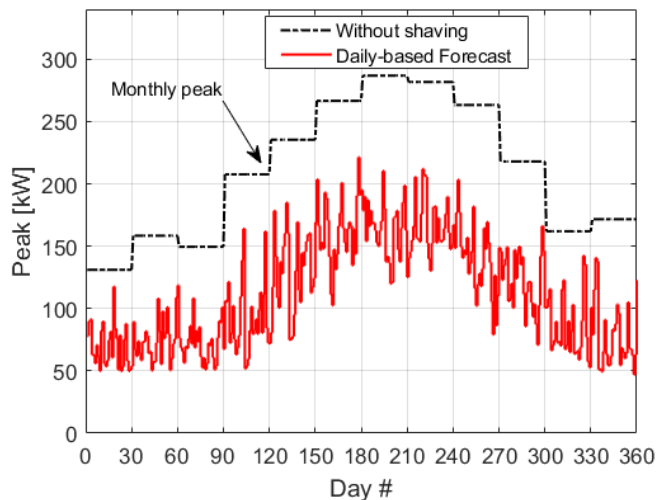


Figure 4.20. Daily peaks after shaving for theater.

#### **4.5. Conclusion**

A framework to schedule the battery storage of PV-battery system under prediction-uncertainty of PV generation and electrical demand is presented and tested. The framework shaves the 15-minute monthly peak demand for different commercial facilities. Shaving the end-user peak demand reduces the bill amount significantly and contributes to secure electrical grid operation. In the current work, the scheduling problem under the uncertainty of prediction is solved using stochastic dual dynamic programming. Scheduling with and without taking into consideration the uncertainty of prediction is compared rigorously. Shaving the peak with different time scales of scheduling and realization are compared. Scheduling with and without receding forecasting horizon and based on two-stage forecasting is studied.

## 5. PAPER C: TIME SERIES FORECASTING OF SOLAR POWER GENERATION FOR LARGE-SCALE PHOTOVOLTAIC PLANTS<sup>1</sup>

### 5.1. Synopsis

Accurate solar power forecasting is essential for grid-connected photovoltaic (PV) systems especially in case of fluctuating environmental conditions. The prediction of PV power output is critical to secure grid operation, scheduling and grid energy management. One of the key elements in PV output prediction is time series analysis especially in locations where the historical solar radiation measurements or other weather parameters have not been recorded. In this work, several time series prediction methods including the statistical methods and those based on artificial intelligence are introduced and compared rigorously for PV power output prediction. Moreover, the effect of prediction time horizon variation for all the algorithms is investigated. Hourly solar power forecasting is carried out to verify the effectiveness of different models. The data utilized in the current work comprises 3640 hours of operation data taken from a 20 MW grid connected PV station in China.

### 5.2. Introduction

The photovoltaic (PV) cells are one of the most widespread and desirable renewable energy systems due to their high energy productivity potential. Accurate

---

<sup>1</sup> Reprinted with permission from “Time series forecasting of solar power generation for large-scale photovoltaic plants” by Hussein Sharadga, Shima Hajimirza, Robert S. Balog, 2020. Renewable Energy Journal, 150, 797-807, Copyright 2020 by Elsevier Ltd.

prediction of PV power is important for the integration of PV systems with the smart grids. The prediction of PV power output is essential in cases where large scale PV systems are connected to the grid or when a large number of small scale PV systems are installed on the utility end.

The studies on PV-generated power forecasting is limited [86]. Most of the published work in this field focuses on solar radiation prediction. The output power of a PV module has more determining factors than just the solar irradiance, and includes the physical conditions of the cells, the type of solar cells and electrical circuit of the module, angle of incident, weather conditions and more. For example, the amount of produced power is largely influenced by the average temperature of the solar cell in a PV system [87]. The cell temperature is a function of the solar irradiance power, ambient temperature, wind speed and relative humidity. PV output power forecasting based on the principles of weather classification has been studied by several authors [88–92]. Shi *et al.* [88] introduced a novel prediction model to estimate the power output of PV plant of 20 MW capacity for a 24 hour time horizon by applying support vector machine for weather classification. Neural networks (NN) were adopted for a PV station output power short-term forecasting in [89]. The model was based on the solar radiation, seasonality and weather classification (*i.e.* sunny, cloudy or overcast). Mellit *et al.* [90] used two artificial neural networks to predict the power produced by a 50 W PV plant using more than one year of data. One network was trained for cloudy days one for sunny days, with three inputs to each network: cell temperature, solar radiation and PV voltage. In [91], a self-organized map was implemented to determine the day weather classifications: sunny,

cloudy and rainy, thus allowing to select the appropriate architecture and the training parameters for each day ahead of time. An accurate neural network has been developed for PV cells power estimation of large-scale grid-connected photovoltaic plants in [92]. The model takes three different types of days into account: sunny, partly cloudy and overcast. The network was trained using the data of solar radiation, PV cell temperature and electric power of one-Megawatt solar plant. Deep learning NNs have also been proposed for prediction and modeling. Long short-term memory (LSTM) architectures have been implemented in PV power forecasting due to the ability to preserve past time-series information using a memory architecture [93]. Auto-Encoders and LSTM have shown to be more efficient compared to multi-layer perceptron and physical prediction methods in power prediction when applied to 21 studied PV plants [94].

Different neural network architectures and combinations along with time-series filtering techniques have been introduced and applied for PV power estimation. Wavelet transform was used for data filtering of ill-behaved PV power and then combined with neural network for one-hour-ahead power forecasting in [95]. It was claimed that the proposed combination addressed inaccuracy issues with spikes and chaotic changes in the input time series. In [96] Focused Time delay NNs and Distributed Time delay NNs were compared and the former was proven superior when applied to the estimation of the output of a 5 kW PV power plant. Support vector machine (SVM) and seasonal auto-regressive integrated moving average (SARIMA) models were combined and employed for power forecasting of 20 kW grid-connected PV system in [97]. It was demonstrated that the proposed hybrid system can capture the nonlinearity behavior of time input time-series

better than both SVM and SARIMA models individually. In [98], support vector regression with the assistance of numerically predicted cloudiness was implemented to predict the PV plant power output. Numerical prediction of cloudiness was found to play an important role in the accuracy of the overall model. A hybrid system consisting of two numerical weather prediction models with different NNs of different configurations was used as an accurate short-term power prediction approach for photovoltaic plants in [99]. Support vector regression assisted with fuzzy inference was employed in [100] for one-day-ahead hourly prediction of power produced by PV systems. The data was classified based on the day type using learning vector quantization (LVQ) networks and self-organizing map prior to prediction.

In addition to those results, several other works have used NNs to predict the PV power output, though no solar radiation measurements have been used. A NARX network was used to predict the yield of grid-connected PV plant in [101]. The proposed model was based on air temperature measurements as well as the calculated clear-sky radiation incident using Hottel's radiation model. In [102] it was demonstrated that neural networks, assisted with a data of aerosol index and without any solar irradiance measurements, are more accurate than model based on conventional NNs that use solar irradiance measurements for PV power prediction.

Mellit et al. [103] proposed using recurrent neural network (RNN) to estimate the daily power production of PV power systems. The NN model was trained on 4 years of data and tested on another year. The model accepts the ambient temperature and daily global radiation ( $\text{W/m}^2 \text{ h}$ ) as inputs. Ashraf *et al.* [104] developed a NN to estimate the

electricity generation of grid-connected PV systems based on the clearness index. Two multi-layer perceptron (MLP)-based NNs were used to forecast the output power generated by the PV plants [105]. The first one uses solar irradiance and ambient temperate as input while the second model is based on the solar irradiance only. The plant used a maximum power point tracking controller and is a roof-mounted 20 kW capacity facility.

The prediction algorithms are also applied to different renewable energy technologies. In [106], the hybrid neuro-fuzzy was employed to predict the electrical power output of a wind turbine. To enhance the prediction accuracy, the data was divided into four subsets based on the seasons of year. Wong *et al.* [107] introduced a new prediction tool to estimate the performance of a biofuel engine. The new method was called sparse Bayesian extreme learning machine. The proposed algorithm can be competitive with different neural network configurations. Kavousi-Fard [108] used a hybrid prediction tool to estimate the speed and direction of tidal currents. The proposed forecaster was based on combining one machine-learning algorithm with a well-known statistical tool: the support vector regression and ARIMA model, respectively. In [109], the artificial neural network was applied to predict the power output of a small hydropower plant power.

In general, it is understood that when used properly, NNs do a better job of predicting output PV power than analytical models, standard time series forecasting techniques and polynomial and multiple linear regression models. Nevertheless, none of the mentioned previous studies have systematically compared the performance of the different approaches.

**Contributions.** In the current work, different time series forecasting models are compared for PV output power prediction. The methods include both statistical (persistent) methods and those based on artificial intelligence. The statistical models used in the current work belong to the category of persistence models including: Autoregressive moving average (ARMA), autoregressive integrated moving average (ARIMA) and seasonal autoregressive integrated moving average (SARIMA). Six different types of NN models are considered: Bi-directional long short term memory (Bi-LSTM), long short term memory (LSTM), fuzzy c-mean clustering, layer recurrent (LRNN), multi-layer perceptron (MLP) and feedforward NNs. In addition, the main novelties of the paper can be summarized as:

1. We propose a new deep learning BI-LSTM algorithm as an accurate power prediction model for large scale PV plants.
2. We assess and compare the performance of different NNs and statistical approaches for a time series forecasting of large scale PV systems.
3. We study the time horizons at which the studied predictive models work reliably.

### 5.3. Predictive Models

The data set used to conduct this study and the investigated prediction tools as well as the method of implantation and validation are discussed in this section.

#### 5.3.1. Dataset

The data belongs to a grid-connected PV power plant located in south China which was used in a previous study [3]. The tilt angle of the PV arrays is fixed. The system has a maximum capability of 20 MW and the data output power is recorded within the date range from 01/13/2010 to 10/29/2010. During this date range, the PV plant power output

is consistently zero between 8 P.M and 6 A.M. The power between 7 and 8 P.M is very low and is zero most of the time. Thus, we only consider the power between 6 A.M and 7 P.M in the simulations. The data is normalized, and the outliers and missing values are removed using Hampel filter with a window size of 14 hours, which is the maximum continuous daylight timeframe. The preprocessing procedure including outlier removals is described in Section 5.4.4.

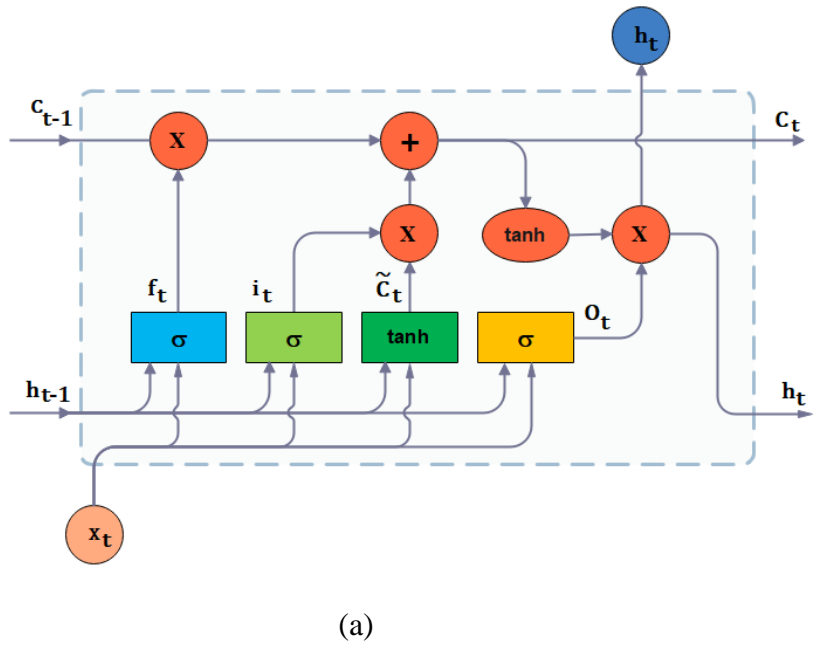
### **5.3.2. Description of Models**

The power produced by the solar photovoltaic system is predicted using artificial neural networks of different architectures and different statistical approaches. These different tools of prediction are described as follows:

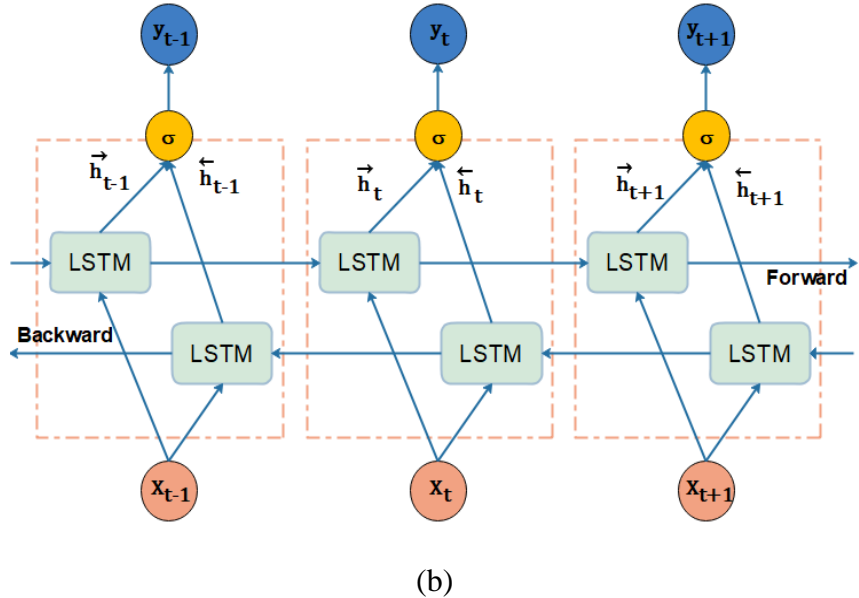
#### **a) Artificial Neural Network**

A neural network can learn complex dependencies between inputs and outputs. Artificial neural networks have been widely employed in different research disciplines for modeling nonlinear and complex functions. In a feedforward NN, the information is fed from the input layer to the output layer through the hidden layers. Layer recurrent neural networks are used in this study because they have dynamic responses to the input time series data. A layer recurrent neural network has the same architecture as a feedforward network, except that the layers have recurrent connections with associated tap delays. A multilayer perceptron network (MLP) belongs to the feedforward NN category. In MLP, the input layer consists of neurons that use an activation function. LSTM is a class of recurrent neural networks developed to overcome long-term dependency problems [110]. Unlike conventional NNs, LSTM has a memory block to store the temporal information

of the input data. The hidden layer of LSTM, also called LSTM cell, is shown in Figure 5.1 (a). The LSTM cell connects the layer input,  $X_t$ , to the layer output,  $h_t$ , using a gate structure. The LSTM cell has three gates: input gate ( $i_t$ ), output gate ( $O_t$ ) and forget gate ( $f_t$ ). The cell input state ( $\tilde{C}_t$ ) and the current cell output states ( $C_t$ ), as well as cell output states of the previous irritation ( $C_{t-1}$ ), are utilized in the training process. The cell input state, the cell output state and the gates can be calculated using the relations given in [111]. Bidirectional LSTM, which is shown in Figure 5.1 (b), is developed using two-time directions [112]. BI-LSTM is capable of learning more accurately than the unidirectional LSTM. BI-LSTM uses past and future information as inputs by connecting the neurons of two separate hidden layers to one output. The information is fed to every hidden layer from both the forward and backward layers. However, those neurons have no interactions in between. The output of BILSTM,  $y_t$ , is calculated by combining the two outputs ( $\overrightarrow{h}_t$ ,  $\overleftarrow{h}_t$ ) using the  $\sigma$  function. The  $\sigma$  function is the activation function in the artificial neuron that delivers an output based on inputs.



(a)



(b)

Figure 5.1. Architecture of (a) LSTM cell (b) Bi-directional LSTM.

### b) Statistical Models

Autoregressive (AR) and moving average (MA) models are commonly used for time series prediction. When Autoregressive (AR) and moving average (MA) models are

integrated, they result in a well-generalized time series forecasting model called ARMA. However, the ARMA model is inefficient for non-stationary time series analysis, which has led to the development of the ARIMA models which can handle non-stationarity [113]. The ARIMA model converts non-stationary time-series data to a stationary series via differencing. SARIMA model is a generalization of the ARIMA model developed by Box *et al.* [114] to handle the seasonal behavior of a time-series data. SARIMA model is often named with the associated parameters like SARIMA  $(p, d, q) \times (P, D, Q)^m$ , where  $p$  is the autoregressive order,  $d$  is the degree of integration,  $q$  is the moving average order and  $m$  is the seasonality order. For monthly and quarterly seasonal model,  $m$  equals 12 and 4, respectively. The capital letters ( $P$ ,  $D$  and  $Q$ ) refer to the seasonal part of the SARIMA formulation, *i.e.*  $P$  is the seasonal autoregressive order,  $D$  is the seasonal degree of integration and  $Q$  is the seasonal moving average order.

### **5.3.3. Models Implementation**

The NNs are trained using two functions: trainbr and trainlm. Trainbr (also known as Bayesian regularization) minimizes the combination of squared errors and weights. Trainlm uses Levenberg-Marquardt optimization to tune biases and weights. Trainlm is generally faster while trainbr is more likely to generalize the performance better and is thus more reliable out-sample. The appropriate number of layers and neurons in each hidden layer of NNs does not follow fixed theoretical guidelines [115]. In the current work, the number of layers and neurons is empirically chosen based on the mean squared error (MSE) as the performance measure [90]. The network configuration for each type of network for cross-validation attempt 5 (see Section 5.3.4) is listed in Table 5-1.

LSTM and BI-LSTM are trained by Adam solver. The maximum number of epochs is set to 100. To check the validation, the performance of prediction is guided using correlation coefficient ( $R$ ) and the root mean square error (RMSE).

Table 5-1 Number of layers and neurons of NNs. LM and BR stand for trainlm and trainbr, respectively.

Algorithm	Training method	#layers	# neurons
Feedforward	trainlm	1	16
Feedforward	trainbr	2	[7, 5]
MLP	trainlm	2	[5, 8]
MLP	trainbr	2	[8, 6]
Layer recurrent (LRNN)	trainlm	1	12
Layer recurrent (LRNN)	trainbr	2	[6, 9]
LSTM	Adam	1	11
BI-LSTM	Adam	2	[7, 8]

#### d) Statistical Models Implementation

We use the following statistical models: ARMA, ARIMA and SARIMA. Akaike's Information Criterion (AIC) is widely used to optimize the model parameters in those models [116]. AIC is an estimation of the likelihood of a model. However, AIC does not have any indication of the *absolute* quality. A similar criterion for model selection is the Bayesian Information Criterion (BIC). The AIC and BIC of the forecasting models are determined by [117]:

$$AIC(p + q) = T \log(r^2) + 2(p + q), \quad (5.1)$$

$$BIC(M) = T \log(rss) + (p + q) \log T, \quad (5.2)$$

Where  $p$  represents the autoregressive order,  $q$  is the moving average order, rss is residuals variance (sum squares) and  $T$  is the number of observations. Different combinations of parameters are investigated until the lowest AIC or BIC value is recorded.

Then the model with the minimum (AIC, BIC) is considered in the forecasting. The plots of auto correlation function (ACF) and partial autocorrelation function (PACF) are also considered to help in making parameters choices.

#### 5.3.4. Time Series Cross-validation

Cross-validation is a resampling procedure based on splitting the data into more than one training and testing subsets. Then, the overall performance of forecasters is basically obtained by looking at the prediction accuracy measures over all the testing subsets. Time series cross-validation is recommended as a key validation step in predictive models particularly in the case of small data samples. In the current work, the window sliding cross-validation method is implemented in the evaluation of the performance of predictors. The size of the training, validation and test sets is fixed while cross-validating: 2730 samples for training (%75), 364 samples for validation (%10) and 546 samples for testing (%15). Thus, the forecasters are tested on 2184 different samples ( $546 \times 4$ ). The performance measures are recorded for every cross-validation attempt and then used to estimate the overall prediction accuracy (Figure 5.2).



Figure 5.2. Schematic of the time series cross-validation procedure.

## 5.4. Results and Discussion

### 5.4.1. Comparison of the Two NNs Models

To predict the power production of PV plant, 8-time delays are applied and used as variables in the input layer of NNs, namely  $t - i$ ,  $i \in \{1,2,4,6,8,10,12,14\}$  hr (See Figure 5.3). The results are compared with those forecasted by a model of 4-time delays  $t - i$ ,  $i \in \{1,2,3,4\}$  for one hour ahead power prediction. The input matrix and the corresponding output matrix used to train and test the suggested model of 8 delays are given below:

$$\text{input} = \begin{bmatrix} X_1 & X_2 & \dots & X_{3626} \\ X_2 & X_3 & \dots & X_{3627} \\ X_4 & X_5 & \dots & X_{3629} \\ \dots & \dots & \dots & \dots \\ X_{14} & X_{15} & \dots & X_{3639} \end{bmatrix},$$

$$\text{output} = [X_{15} \quad X_{16} \quad \dots \quad X_{3640}]. \quad (5.3)$$

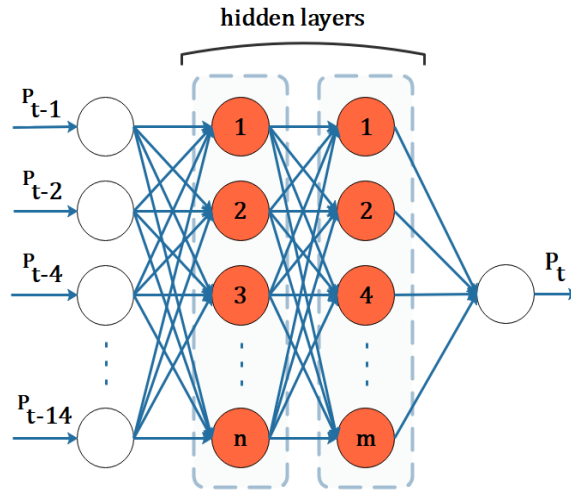


Figure 5.3. Feedforward neural network structure used to predict the PV power output.

The simulation results summarized in Table 5-2 and Table 5-3 show that the first model tracks the nonlinearity and the PV power dependency more reliably. Consequently, the first model is chosen as the model for the rest of work. In the following tables, LM and BR stand for trainlm and trainbr, respectively. The algorithms are sorted in the tables based on the correlation coefficient ( $R$ ) of the testing set in the descending order. Average computational time is mentioned in the tables and will be used for comparison to the statistical algorithms. Average computational time is the average time required for training, testing and results generation for one validation attempt. Recall that correlation coefficient ( $R$ ) and RMSE are defined as follows:

$$R = \frac{1}{N-1} \sum_{i=1}^N \left( \frac{O_i - \mu_O}{\sigma_O} \right) \left( \frac{P_i - \mu_P}{\sigma_P} \right), \quad (5.4) \quad RMSE = \sqrt{\frac{\sum_{i=1}^N (P_i - O_i)^2}{N}} \quad (5.5)$$

Where  $N$  is the number of samples,  $P$  is the predicted value,  $O$  is the observed value,  $\mu$  is the mean and  $\sigma$  is the standard deviation.. The Overall RMSE and the overall R are calculated by combining the results of every validation attempt in two columns: one for observed and one for forecasted and then using Equation (5.4) to calculate  $R$  and Equation (5.5) to calculate RMSE. However, The Overall RMSE can also be obtained using the following expression:

$$RMSE_{overall} = \sqrt{\frac{MSE_1 + MSE_2 + MSE_3 + MSE_4 + MSE_5}{5}} \quad (5.6)$$

Where the subscripts 1,2...,5 stand for the validation attempt number, and MSE is the mean square error.

BI-LSTM scored the highest correlation coefficient ( $R$ ) and the lowest root mean square error (RMSE) as shown in Table 5-2. Therefore, we can conclude that BI-LSTM with model 1 can be the most accurate forecasting algorithm when it is used for PV power prediction of the sample system. The Bi-directional LSTM can learn faster than the one-directional LSTM. BI-LSTM is found to be the most accurate model with a correlation coefficient ( $R$ ) of 98% and RMSE of 0.791. On the other hand, a multi-layer perceptron (MLP) trained by the two training functions is the fastest algorithm with an average computation time of 1-2 seconds. However, the correlation coefficient ( $R$ ) ranges between 93.4 and 98 % and RMSE ranges between 0.791 and 1.25 for different NNs with model 1.

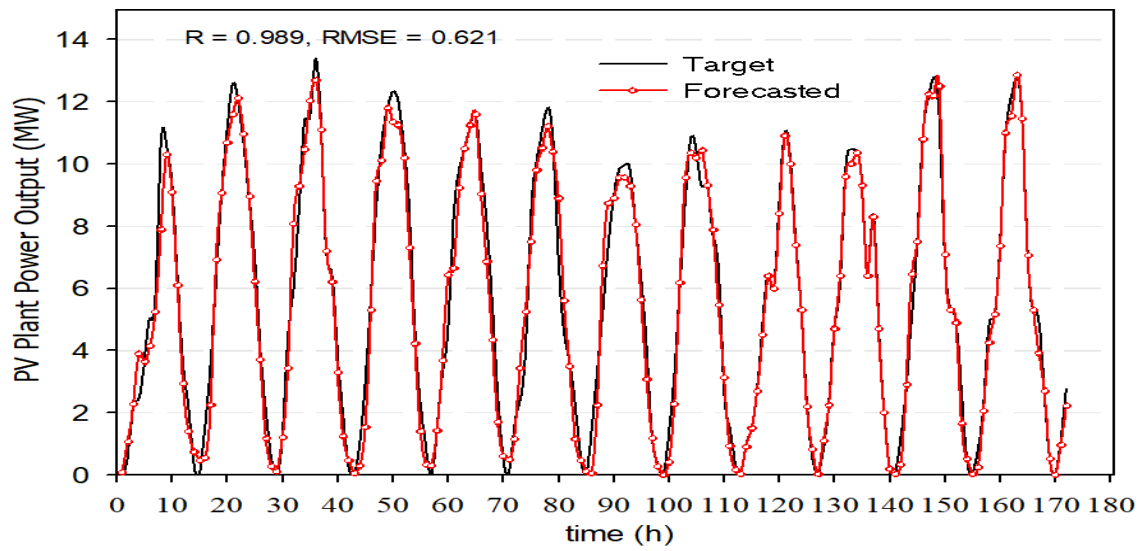
Table 5-2. One hour ahead forecasting using various NNs with 8-time delays (model 1), LM and BR stand for trainlm and trainbr, respectively.

<b>Algorithm</b>	<b><math>R</math> (test data)</b>	<b>RMSE (test data)</b>	<b>Average computation time (s)</b>
1 BI-LSTM	0.98	0.791	8.22
2 LSTM	0.965	0.841	8.61
3 LRNN-LM	0.959	0.961	2.54
4 LRNN- BR	0.953	0.995	8.21
5 FCM	0.95	1.11	22.1
6 FF- LM	0.947	1.05	5.43
7 MLP- LM	0.941	1.21	1.2
8 MLP- BR	0.936	1.16	1.85
9 FF-BR	0.932	1.27	6.11

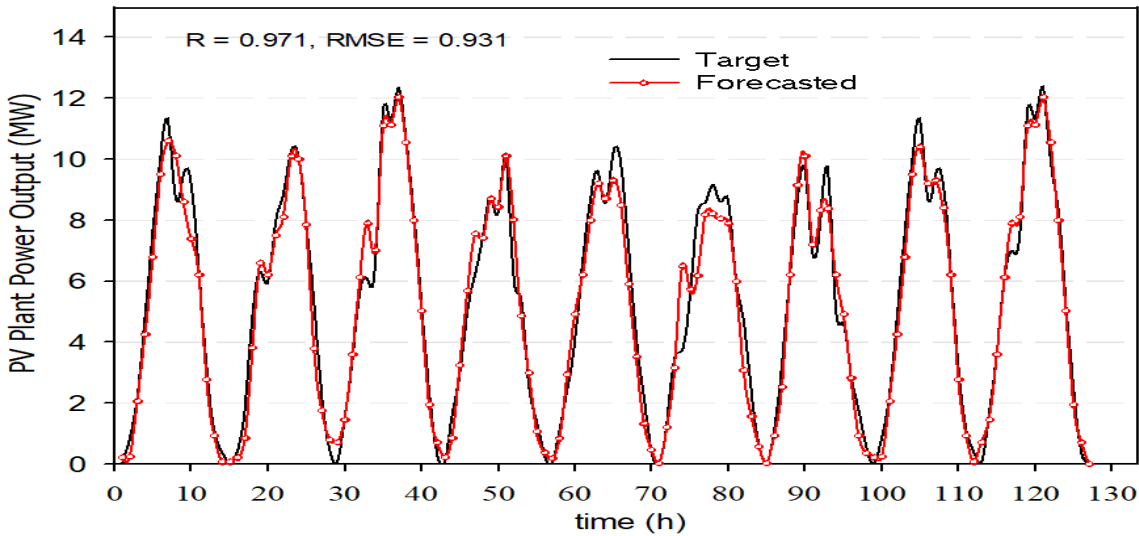
Table 5-3. One hour ahead forecasting using various NNs with 4-time delays (model 2), LM and BR stand for trainlm and trainbr, respectively.

	<b>Algorithm</b>	<b>R</b> <b>(test data)</b>	<b>RMSE</b> <b>(test data)</b>	<b>Average</b> <b>computation time (s)</b>
1	LSTM	0.935	1.591	8.73
2	LRNN-LM	0.931	1.421	3.04
3	BI-LSTM	0.925	1.456	10.02
4	LRNN-BR	0.919	1.621	8.22
5	MLP-LM	0.908	1.632	1.21
6	MLP-BR	0.88	1.694	1.99
7	FF- BR	0.865	1.681	6.79
8	FCM	0.841	1.675	19.95
9	FF- LM	0.835	1.791	6.85

Figure 5.4 presents the predicted PV power using BI-LSTM algorithm with 8-time delays (model 1) for different day types: sunny, cloudy and rainy. It is clear that the observations and the predictions are in good agreement. The result for validation attempt number 4 (see Section 5.3.4) is shown in Figure 5.5. As seen, most of error values range between 0 and 1. The predicted value of the PV power output is usually found to be less than the observed, i.e., the error is frequently positive. In addition, in 220 of the 546 samples the error is almost zero. We can conclude that BI-LSTM shows a strong potential to predict the PV output efficiently in short term time horizon of 1 hour ahead.

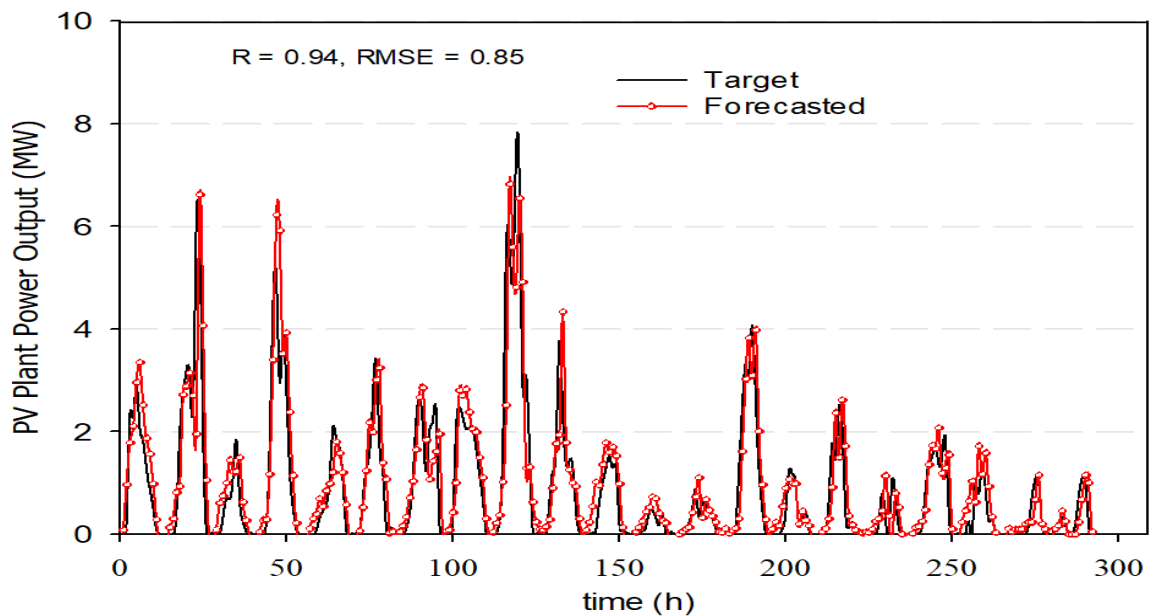


(a)



(b)

Figure 5.4. Result of BI-LSTM forecast versus observed power production (a) sunny days (b) cloudy days (c) rainy days.



(c)

Figure 5.4. Continued.

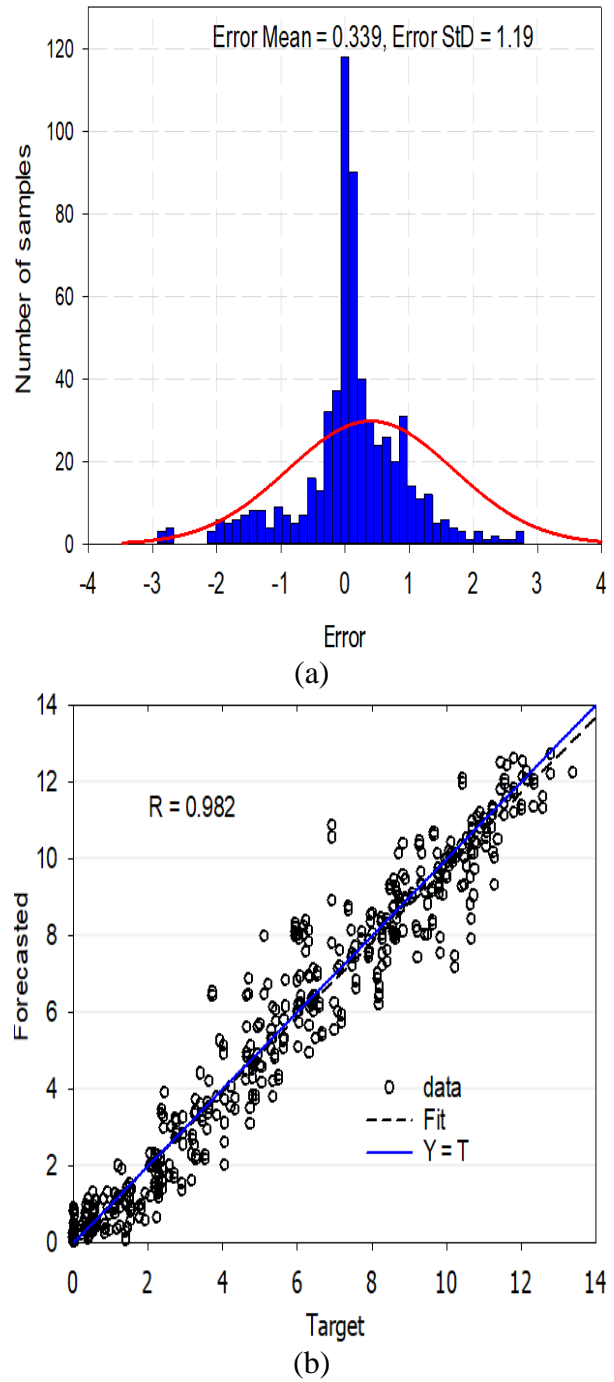


Figure 5.5. Results of BI-LSTM for validation attempt number 4 for PV power prediction (a) Error histogram figure (real – forecast), (b) Regression plot.

### 5.4.2. NNs Forecasting with 2 and 3 Hours Ahead Horizon

To evaluate the performance of different NNs for mid-term forecasting, 2 and 3 hours ahead forecasts are tested, and the findings are summarized in Table 5-4 and Table 5-5. BI-LSTM yields the most accurate prediction. The correlation coefficient ( $R$ ) of feedforward NN with trainbr changes from 93.2% to 78.5% when used for two hours ahead rather than one step (see Table 5-2 and Table 5-4). For time horizons of more than 2 hours ahead, the correlation coefficient ( $R$ ) falls under 90%. Therefore, the NNs are not recommended for time series forecasting of PV system power output for more than two steps ahead (hourly basis) without additional solar irradiance measurements or weather conditions. For the average computational time, the forecasters need less than 1 second more time to complete the two and three hours ahead prediction, compared to one hour ahead forecasting.

Table 5-4. Two hours ahead forecasting using various NNs, 8-time delays.

<b>Algorithm</b>	<b><math>R</math> (test data)</b>	<b>RMSE (test data)</b>	<b>Average computation time (s)</b>
1 LSTM	0.961	1.102	8.73
2 BI-LSTM	0.952	1.331	9.02
3 LRNN- LM	0.944	1.395	3.21
4 MLP- LM	0.927	1.365	1.42
5 LRNN- BR	0.915	1.423	8.92
6 FCM	0.902	1.591	22.9
7 FF- LM	0.896	1.571	6.21
8 MLP- BR	0.889	1.792	1.9
9 FF- BR	0.785	1.821	6.8

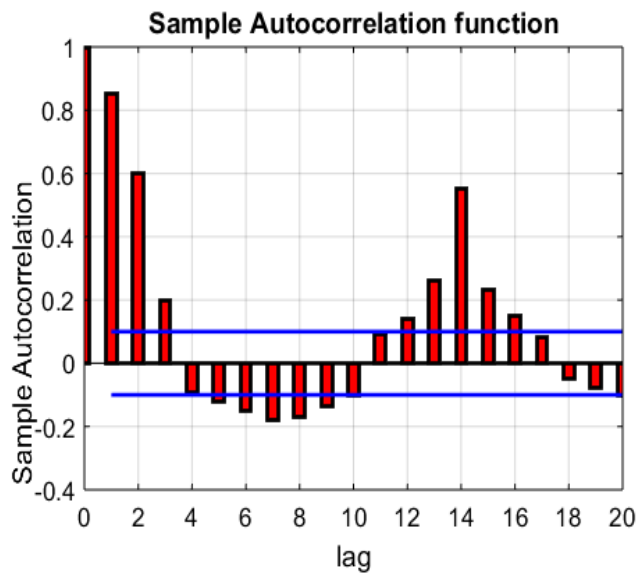
Table 5-5. Three hours ahead forecasting using various NNs, 8-time delays.

	<b>Algorithm</b>	<b>R</b> (test data)	<b>RMSE</b> (test data)	<b>Average computation time (s)</b>
1	LRNN- LM	0.895	1.805	3.41
2	LSTM	0.894	1.824	9.41
3	BI-LSTM	0.893	1.812	8.65
4	LRNN-BR	0.881	1.822	8.95
5	MLP- BR	0.861	2.105	1.91
6	MLP- LM	0.853	2.010	1.74
7	FF- LM	0.841	2.314	6.21
8	FCM	0.801	2.521	23
9	FF- BR	0.741	2.563	6.41

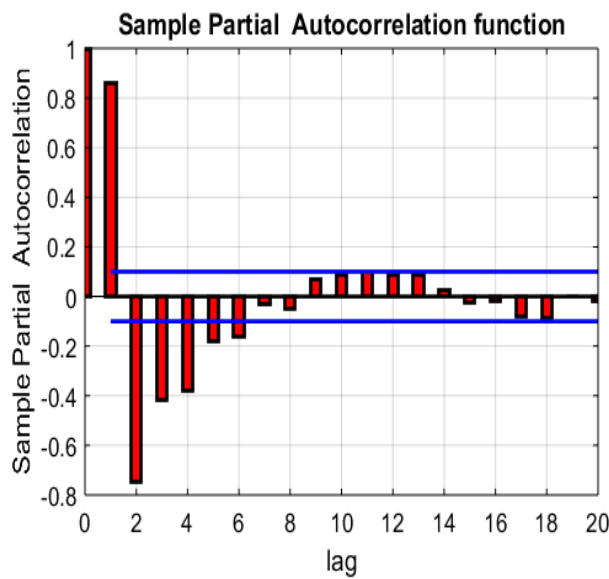
#### 5.4.3. Statistical Models Results

Sample autocorrelation and partial autocorrelation for produced power and for first differenced power output are plotted in Figure 5.6 and Figure 5.7, respectively. Based on the sample autocorrelation plot, the data has a seasonal pattern. The value of the seasonality index for SARIMA model is set at 14 since the data is recorded hourly with a period of 14 hours per day. Moreover, we can see from the sample autocorrelation plot that the pattern has a 14 hours periodicity. To optimize the models' parameters, different combinations of parameters are investigated and the models with the lowest AIC value are used in the prediction as the most reliable choices. ACF decays after the second lag while PACF decays after the third lag as seen in Figure 5.7. Therefore, we should theoretically use AR(2) of the SARIMA model. The possible candidate orders of the moving average of SARIMA model are 1 as shown in Figure 5.7 (b). However, AIC values are used to select the most appropriate models. The possible ARIMA and SARIMA models usually have a degree of integration equal to 1 [118]. The Phillips-Perron test was also applied in

this study to find h value for the first derivative of power output. The value of h was found to be 1 which indicated that the first difference can be used reliably to make the data stationary[119]. Thus, the degree of integration of SARIMA and ARIMA models in this study is set to 1. A one time use of SARIMA and ARIMA with a degree of integration more than 1 for forecasting was also conducted. Those models require a significant amount of computational time (see Table 5-7). ARMA (3, 4), ARIMA (2, 1, 3) and SARIM (2, 1, 3), (2, 0, 1)<sup>14</sup> have the lowest ACF values. Thus, they are considered as the best fit models in the current work. AIC and BIC values of ARMA models are given in Table 5-6. A similar table was generated for ARIMA and SARIMA. The residuals Q-Q plots of the SARIMA model is shown in Figure 5.8. The residuals have a linear trend.

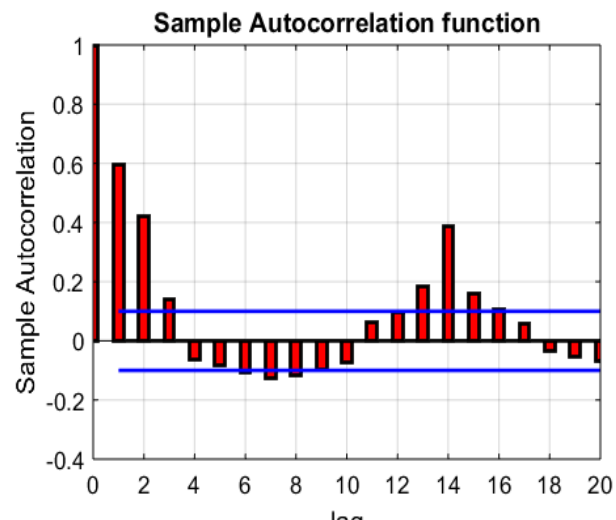


(a)

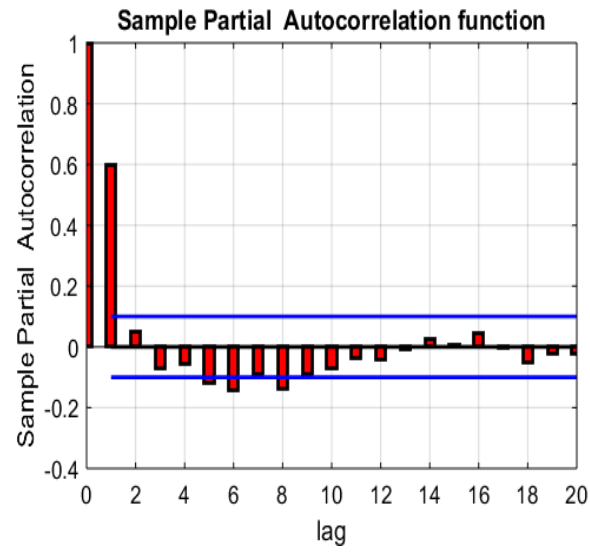


(b)

Figure 5.6. (a) ACF and (b) PACF of power output.



(a)



(b)

Figure 5.7. (a) ACF and (b) PACF of first differenced power output.

Table 5-6. AIC and BIC values of available ARMA models.

<b><i>p, q</i></b>	<b>AIC</b>	<b>BIC</b>
1, 1	5892.8	5899.7
1, 2	5865.5	5872.9
1, 3	5850.1	5857
1, 4	5833.2	5839.6
2, 1	5877.8	5884.9
2, 2	5450.9	5363.9
2, 3	5241.2	5267.4
2, 4	5332.2	5342.2
3, 1	5458.9	5471.2
3, 2	5359.4	5366.4
3, 3	5340.6	5359.2
<b>3, 4</b>	<b>5111.5</b>	<b>5204.8</b>
4, 1	5400.2	5412.9
4, 2	5342.9	5354.1
4, 3	5325.6	5341.5
4, 4	5335.1	5341.9

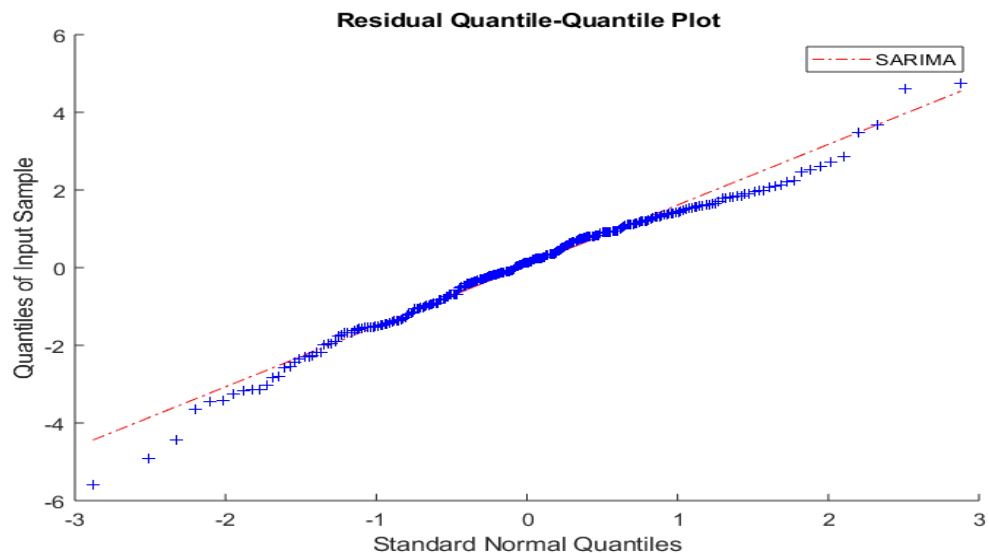


Figure 5.8. Quantile-Quantile plot for SARIMA model.

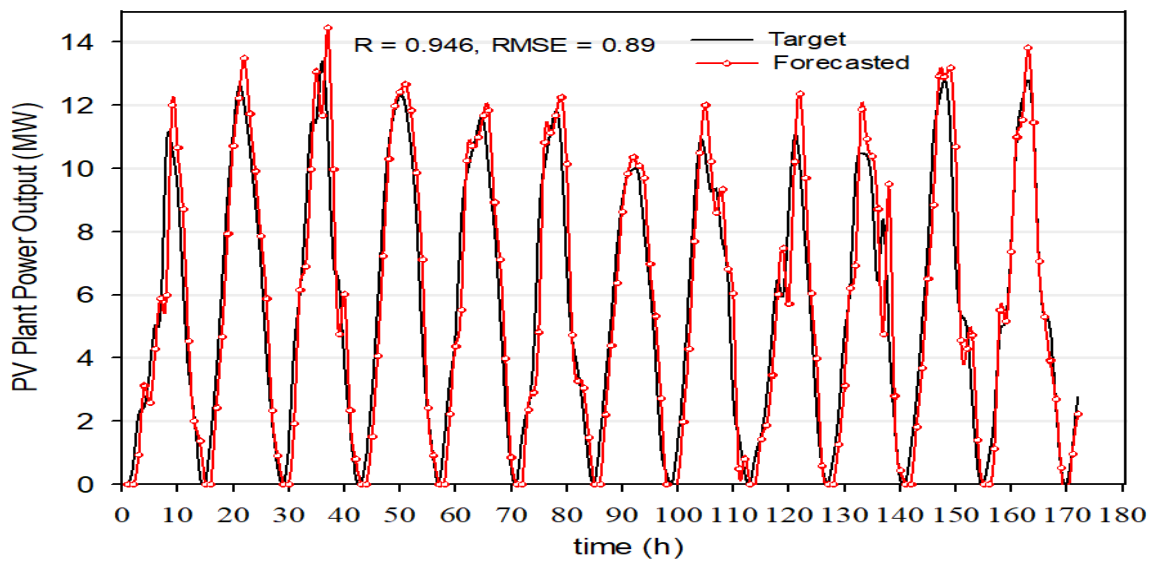
The models are listed in Table 5-7 and Table 5-8, and sorted based on the correlation coefficient ( $R$ ) in descending order using the test set. The SARIMA model scored the highest correlation coefficient ( $R$ ) and the lowest root mean square error (RMSE) for one and two hours ahead predictions. We conclude that identifying the time series pattern and accounting for the seasonality enhances the forecasting results. The predicted PV power using the SARIMA model with one hour ahead for different day types is plotted in Figure 5.9. The result for validation attempt 4 (see Section 5.3.4) is shown in Figure 5.10. It is noticed that the predicted value of PV power output using SARIMA is mostly higher than the true value. The opposite has been observed for BI-LSTM. It is concluded that the suggested statistical models consume more computation time and have an accuracy lower than most of the NNs. Artificial neural networks learn the complexity of time series data better than SARIM models. Thus, NNs are better than the suggested statistical models for PV power time series prediction. The average computation time for one hour ahead forecasting is given in Table 5-7. While two and three hours ahead prediction need about 1 or 2 more seconds for the forecasting to be accomplished, compared to one hour ahead forecasting (see Table 5-8).

Table 5-7. Results of PV power prediction using ARMA, ARIMA, and SARIMA, one hour ahead.

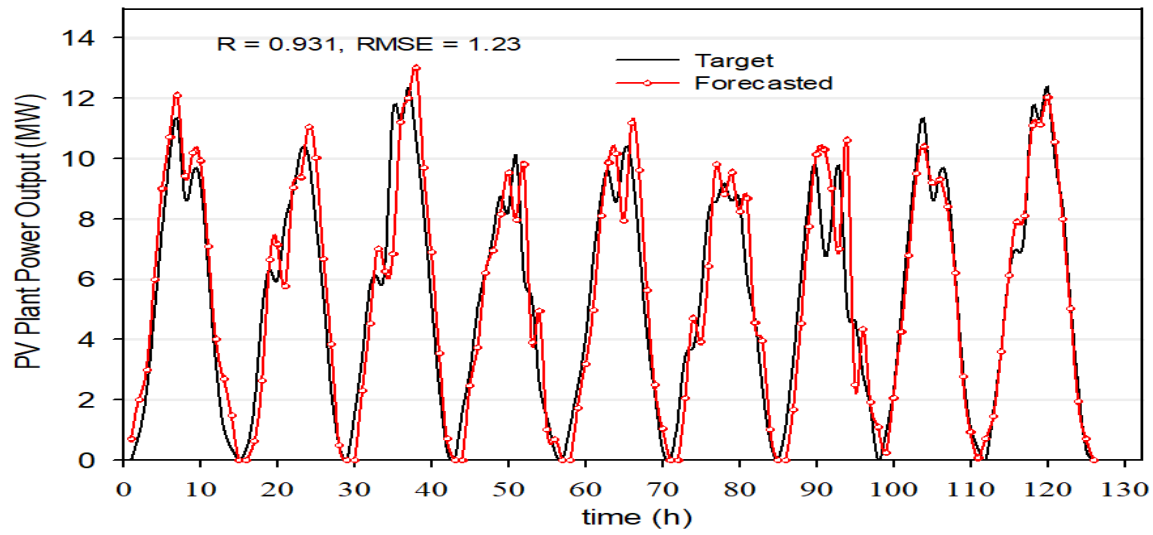
<b>Algorithm</b>	<b>R (test Data)</b>	<b>RMSE (test data)</b>	<b>Average computation time (s)</b>
1 SARIMA	0.929	1.183	84.14
2 ARIMA	0.912	1.318	37.55
3 ARMA	0.904	1.212	49.20

Table 5-8. Results of PV power prediction using ARMA, ARIMA, and SARIMA, two and three hours ahead.

<b>Algorithm</b>	<b>R (test data)</b>	<b>RMSE (test data)</b>	<b>Average computation time (s)</b>
Two hours ahead			
1 SARIMA	0.909	1.781	85.14
2 ARIMA	0.875	1.840	39.34
3 ARMA	0.864	1.914	50.75
Three hours ahead			
1 ARMA	0.819	2.212	85.63
2 SARIMA	0.801	2.314	39.54
3 ARIMA	0.742	2.604	51.02



(a)



(b)

Figure 5.9. Results of SARIMA model for PV power prediction, one hour ahead: (a) sunny days (b) cloudy days (c) rainy days.

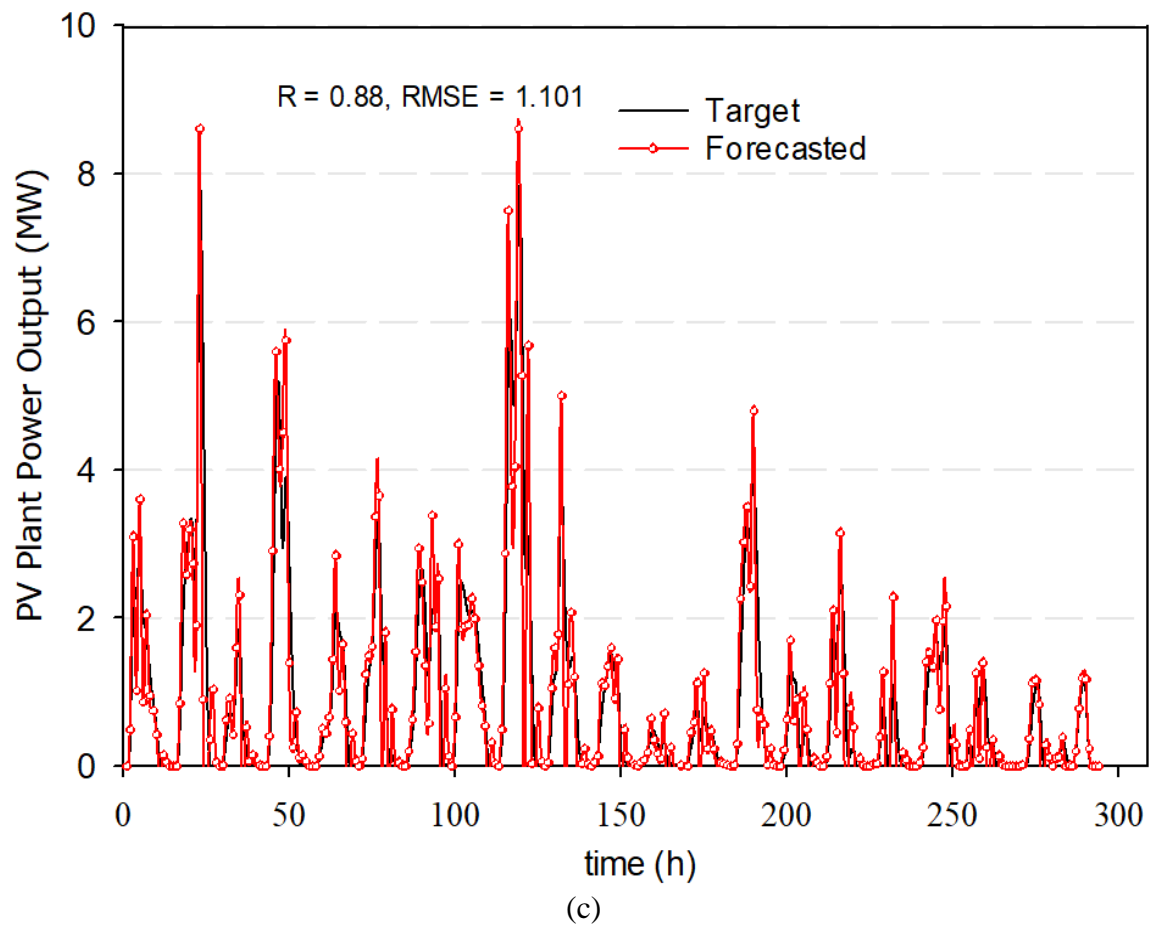


Figure 5.9. Continued.

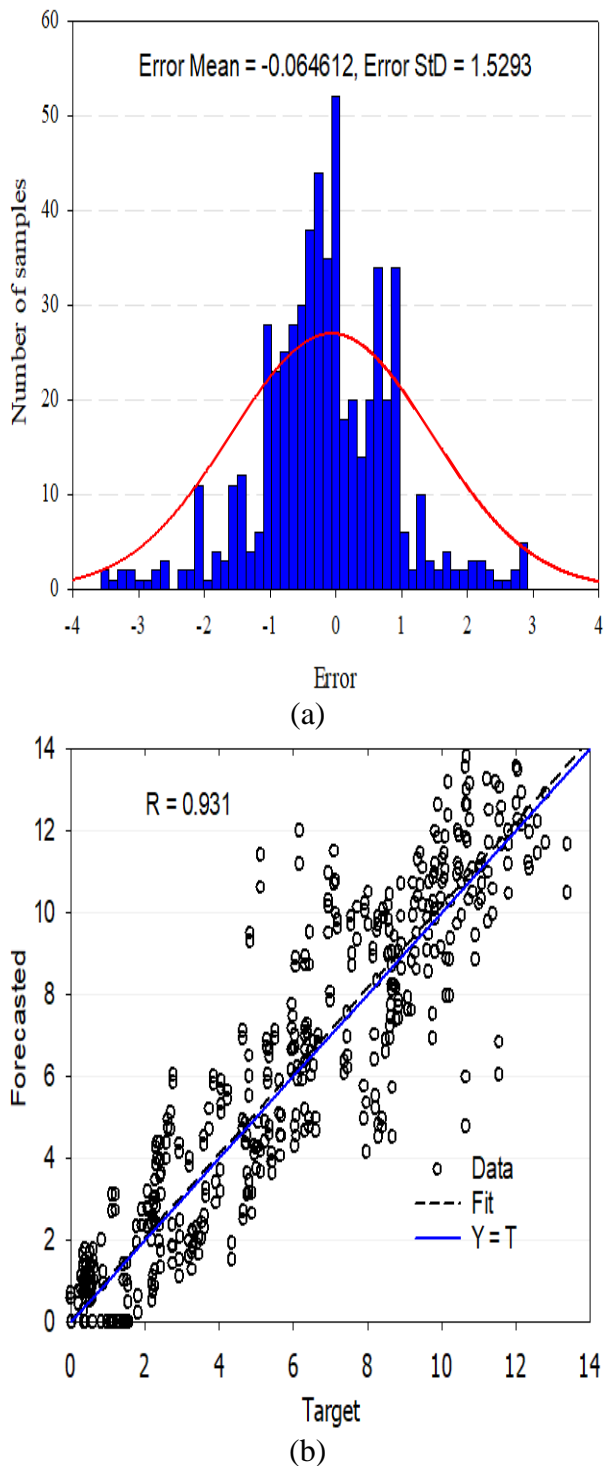


Figure 5.10. Results of SARIMA model for PV power prediction, one hour ahead for validation attempt number 4: (a) Error histogram figure (real – forecast), (b) Regression plot.

#### 5.4.4. Removing Outliers

Outlier removal is necessary to avoid poor fitting or overfitting especially in case of ill-behaved and very noisy training data. Overfitting occurs when the model falsely tunes to the random fluctuations of the training and generalizes the concept. For outlier detection, Hampel filter is utilized to remove the extreme values. Table 5-9 shows the effect of removing outliers on the correlation coefficient ( $R$ ) and RMSE of the BI-LSTM algorithm test results for different forecasting horizons. The enhancement in  $R$  and the reduction of RMSE are demonstrated in the same table. As demonstrated, removing the outliers improves the prediction results. The subscripts 1 and 2 refer to before and after removing the outliers, respectively.

Table 5-9. The effect of removing outliers on BI-LSTM accuracy.

Step	R <sub>1</sub>	R <sub>2</sub>	$\frac{R_2 - R_1}{R_1} \times 100\%$	MSER <sub>1</sub>	MSER <sub>2</sub>	$\frac{\text{MSER1} - \text{MSER2}}{\text{MSER1}} \times 100\%$
1	0.961	0.98	1.98%	0.881	0.791	10.2%
2	0.937	0.965	2.99%	1.16	1.092	5.86%
3	0.86	0.882	2.56%	1.95	1.831	6.1%

#### 5.5. Conclusion

Forecasting solar power is necessary for policy making, understanding the challenges and optimal integration of large-scale photovoltaic plants with the public power grid. In this paper, the performance of different NNs and simple statistical models such as ARMA, ARIMA, and SARIMA was evaluated in the time series forecasting of the power output of large-scale PV plants. The comparative study shows that neural networks are more accurate than the suggested statistical models when used for time series prediction

of PV power output and require less computation time. However, the NNs as well as the statistical models can be used to efficiently predict the produced power of PV plants for only one hour ahead without having access to solar irradiance measurements or any weather parameters. Thus, the time series forecasting for PV power plants is only reliable for one hour ahead prediction.

### **5.6. Acknowledgment**

The authors would like to thank Dr. Shi and Dr. Lee of the University of Jinan, China and the University of Texas at Arlington for providing us with the data.

## 6. PAPER D: COMPARISON OF FORECASTING METHODS FOR PEAK SHAVING CONTROL OF SITE ELECTRICAL DEMAND<sup>1</sup>

### 6.1. Synopsis

Peak shaving of electricity consumption is important for a stable grid operation. Shaving demand spike eliminates stress on the grid. The rates charged by electrical utilities on high peak demand are high; thus, shaving the peak reduces the bill amount significantly. In this work, the effectiveness of simple prediction tools is compared against the neural network and the ARIMA model in shaving the demand peak. The proposed methods are based on a simple moving average concept, seasonality of the energy profiles, and suboptimality-based decision making. Data from commercial buildings located in Texas is used to compare the prediction approaches.

### 6.2. Introduction

Battery storage systems are used for peak shaving applications by shifting the high demand to the off-peak period. The energy storage system is set on the charge mode during the facility's off-peak demand and on discharge mode during the facility's peak demand. The storage systems can be also integrated with different renewable energy technologies such as photovoltaic (PV) systems [16], wind turbines [120], fuel cells [121], etc. The energy produced by these alternative energy resources can further help in managing

---

<sup>1</sup> Hussein Sharadga, Bryan Rasmussen, "Comparison of Forecasting Methods for Peak Shaving Control of Site Electrical Demand".

expensive electricity cost. The study of the current work was conducted for a PV-battery system. The system components and coupling are shown in Figure 6.1.

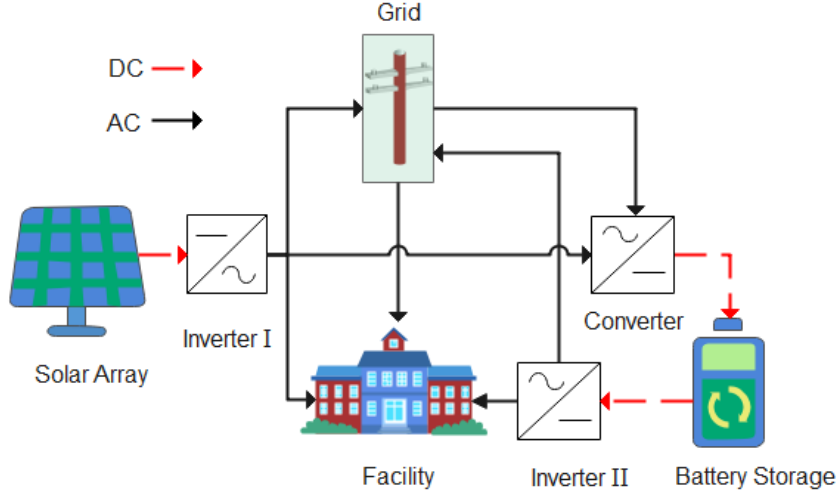


Figure 6.1. Schematic of grid-connected PV-Battery system.

Shaving the demand peak is accomplished by optimizing the battery schedule. A forecasting tool is used to predict the load and the PV generation so the schedule can be constructed ahead of time. Effectiveness of battery scheduling for shaving the demand peak is a function of the prediction accuracy.

Different prediction tools have been implemented in the management of different energy technologies. In [122], a neural network (NN) is proposed to replace the statistical approaches for time series forecasting of PV generation. The NN was found to achieve a higher correlation coefficient  $\mathbb{C}$  and a lower root mean square error (RMSE) when used for short-term prediction (from one to three steps ahead). In [123], the reliable horizon of prediction with NN is determined for PV power generation. Deep learning was employed to predict the cooling load for one day ahead in [124]. Deep learning is capable of

recognizing the complex patterns for big data. Nazaripouya et al. [125] proposed a hybrid prediction model for one-step-ahead PV power prediction. The model involves wavelet transform, ARMA model, and NN. Heterogeneous regression algorithm was implemented to predict the solar energy for a long horizon of 6 hours in [126]. The algorithm was found to be reliable to operate a smart grid.

On other hand, simpler forecast methods have been introduced and their reliability in prediction has been validated. In [127], a model based on simple concepts such as the moving average and exponential smoothing methods is proposed to predict solar radiation for one day ahead. In [128], nine prediction tools are compared against simple heuristic prediction tools for cooling-load forecasting. The predictions are used to optimize the operation of thermal energy storage. Seven of these tools are based on shallow learning such as linear regression, ARIMA model, support vector machine, and regression tree. Two of these tools are based on deep learning, for instance, long short-term memory. In the first heuristic method, the cooling load of the coming day is assumed to be exactly the same as the previous day and the schedule of the thermal storage for the coming day is optimized accordingly. In the second method, the next week's profile is assumed to be the same as that of the previous week. In the third method, a moving average of a given window size is used to estimate the average load profile and the result is used to schedule for the next day. They found that shallow and deep learning are more efficient than the heuristic algorithms. However, heuristic can be a very good choice for limited budget projects and in case of limited access to a historical data.

In this paper, simple estimation approaches are evaluated for peak shaving applications. These methods are compared against neural network and the well-known prediction statistical method, ARIMA model. The proposed methods are based mainly on the simple concept of the moving average and the repeated pattern of the electrical load and PV generation, as well as on the common optimal decision technique.

### **6.3. Peak Shaving Controller Design**

The method of optimizing the battery schedule to shave the demand peak is described in Section 6.3.1. Accurate forecasting is essential for effective scheduling. The proposed forecasting methods are discussed in Section 6.3.2. The data, used to conduct this study, and processing are described in Section 6.3.3. The pricing scheme is given in Section 6.3.4. The control horizon is broken into one day to reduce the scheduling complexity as discussed in Section 6.3.5.

#### **6.3.1. Battery Scheduling**

The schedule of the battery charging and discharging rates is supervised by a peak-shaving controller. The controlling mechanism is explained as follows:

- 1) The electrical demand and the PV generation for a predefined control horizon are forecasted using a prediction tool. The control horizon is one day in the current work.
- 2) This information is then fed to the controller to construct the initial schedule. The scheduling problem is convex [22]; thus convex optimization methods may be used for solving.
- 3) The load and PV generation are measured every one hour in the control horizon.

- 4) These measurements are then fed to the prediction tool to update the predictions of the future steps.
- 5) The schedule for the remaining time steps in the horizon is then updated accordingly based on the new predictions.

Figure 6.2 shows peak shaving for a school located in Texas. In this example, the demand and the PV generation are assumed to be previously given. The battery charging/discharging schedule is optimized using convex optimization. The demand peak is about 320 kW before shaving and is about 180 kW after shaving. The battery is charged between 4 a.m. and 6 a.m. by the utility. The battery is set to the discharging mode at 6 a.m. to shave the peak. Most of the battery energy is consumed at 4 p.m. The power provided by the PV system between 6 a.m. and 5 p.m. is used to shave the demand peak.

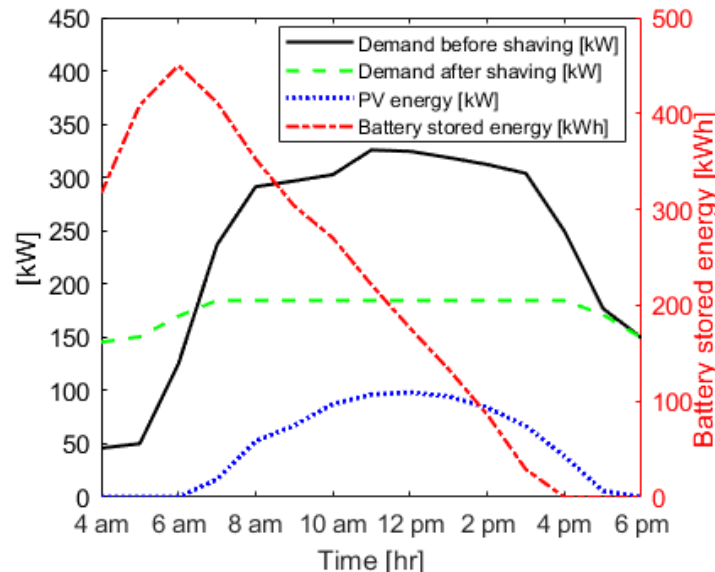


Figure 6.2. Demand peak shaving for a school using PV-Battery system for one random day.

Figure 6.3 shows the electrical load profile for one-day ahead prediction using a well-trained NN. Predicting PV generation is more difficult than forecasting electrical load (Figure 6.4). Prediction accuracy plays a significant role in the effectiveness of the battery schedule in shaving the demand peak. To enhance the accuracy of predicting the PV generation, the predicted profile is continuously updated with a receding horizon (Figure 6.4, (b)). The measurements of PV generation are used as input to continually update the forecasted profile. Then, updated forecasted PV and Load profiles are used to update the battery charging and discharging schedule.

The load predicted profile for the first-time forecasting is close to the real one as shown in Figure 6.3. However, the profile can be updated every one step in the control horizon to enhance the accuracy of prediction.

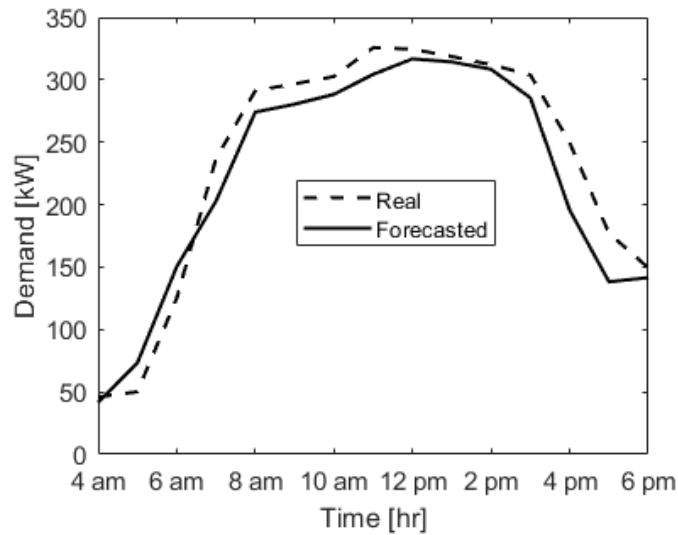


Figure 6.3. Hourly-average demand forecasting for one-day ahead.

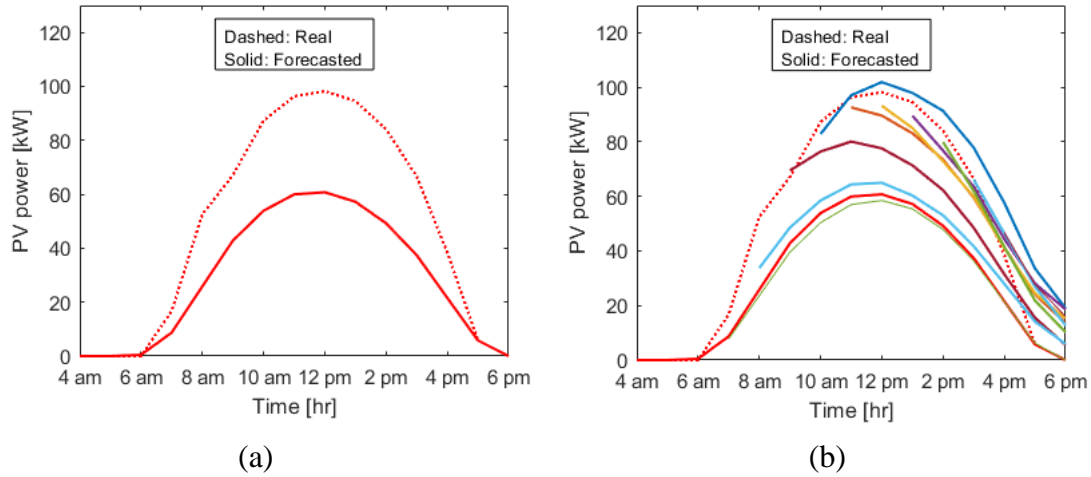


Figure 6.4. PV-generation forecasting for one-day ahead (a) one-time forecasting (b) receding horizon.

### 6.3.2. Prediction Methods

The proposed methods are based on suboptimality-based decision making, simple moving average concept, and seasonality of the energy profiles. The methods are summarized as follows:

**#1 Common optimal strategy (Moving):** Historical data of a given window size is used in this method. The window size is expressed by the number of days in the moving window. The method is based on extracting the daily schedule that can be the optimal schedule across all days in the moving window. The extracted schedule is then used to shave the peak for the coming day. For example, we can take historical data of the last five days and optimize a one fixed daily schedule such that, if used to shave the peak of the last five days, the peak of the past five days will be the minimum. The produced optimal schedule will be used to shave the peak of the coming day.

**#2** Day-of-the week common optimal strategy: Historical data of one year is used for example. Days of the same name are grouped. Then the optimal daily schedule across all days in one group is extracted. The controller will select a schedule out of 7 pre-constructed schedules, based on the day of the week.

**#3** Moving average: The energy profiles for a predefined number of days (rolling window) for the load and PV generation are averaged. The average profiles will be used as a prediction to optimize the schedule of the coming day.

**#4** Day-of-the week average: The days of the same name are grouped. Then we take the average of the energy profiles for all days in one group. Then the averaged energy profiles (demand and PV) for each group are used to optimize seven different schedules for these seven groups. The schedule will be then selected out of seven pre-optimized schedules, based on the day of the week.

**#5** Year average: The energy profiles (load and PV) are averaged across all days of the previous year. The average profiles are used to optimize a schedule. The schedule is then adopted for the next full year's peak shaving.

**#6 © Forecasting:** The electrical load and PV profiles for the next day are assumed to be the same as the preceding day. The schedule is constructed accordingly.

**#7 Neural Network:** The neural network is used to predict the load and PV generation for one day ahead. The prediction in this work was based on time series forecasting, i.e., the sequential data of electrical load/ PV Power is used for prediction without using any other inputs. A historical data of one year was used to train NN: 70% of the data is used for

training and 30% of the data is used for validation. The validation aims to optimize the NN parameters using the trial-and-error method.

**#8 ARIMA model:** ARIMA model is one of the well-known statistical models used for time series forecasting. ARIMA model parameters were optimized in a way similar to the optimization process of NN parameters.

### **6.3.3. Data Availability and Processing**

Data for 5 years for different types of facilities (public school, church, theater, and hotel) located in Texas were utilized for the current investigation. The data was cleaned to enhance prediction. The cleaning process was applied for all methods used in this study. The cleaning process is described as follows:

- 1) School: Weekends, holidays, and days of low demand were removed from the training data set. The demand data at the low-power periods (after 6 pm and before 4 am) was removed.
- 2) Theater and church: The demand data at the low-power periods (after 9 pm and before 3 am) was removed.
- 3) The full demand load is included for the hotel as the pattern is not predictable.
- 4) The PV energy data used for prediction or estimation is between 6 am and 6 pm.

### **6.3.4. Pricing Scheme**

The current investigation was applied for Texas facilities. Texas utilities charge consumers on average about \$ 0.05 per kWh consumption and on average about \$7 per kW electrical peak [129]. The peak rate is based on the highest 15-minute-average demand in one month.

### **6.3.5. Control Horizon**

The current controller is designed to shave the monthly peak. However, the one-month horizon is a challenging control. The control horizon in this work is broken into stages one day in length. Shaving the daily peak will shave the monthly peak. The 15-minute-average load and PV profiles are complex to be predicted using NN and ARIMA; thus, this work is based on predicting the hourly-average load and PV profiles as an alternative solution.

## **6.4. The Effectiveness of Peak Shaving Based on Different Prediction Methods**

The effectiveness of the proposed prediction tools in shaving the demand peak is estimated based on the ideal peak shaving (Equations (6.1) and (6.2)). In ideal peak shaving, the energy profiles (electrical load and PV generation) are previously given or can be predicted with 100% accuracy. However, perfect forecasting is not achievable. In this section, two systems, a PV-battery system and a battery-only system, are used to evaluate the proposed prediction methods.

$$\text{Shaving} = \frac{\text{Peak}_{\text{without shaving}} - \text{Peak}_{\text{after shaving}}}{\text{Peak}_{\text{without shaving}}} \quad (6.1)$$

$$\text{Effectiveness} = \frac{\text{Shaving}}{\text{Ideal shaving}} \times 100 \% \quad (6.2)$$

### **6.4.1. PV-battery System**

The system contains 500 PV panels with a maximum capacity of 100 kW and 450 kWh battery storage. Figure 6.5 shows the effectiveness of the proposed forecasting tools when used for shaving the demand peak of different facilities. Figure 6.6 shows the peak values that can be achieved with the ideal forecasting. The results in Figure 6.5 are the

average effectiveness across five years of historical data. The effect of the size of the rolling window on the effectiveness of methods #1 and # 3 is shown in Table 6-1. The rolling window size needs to be optimized. For instance, the rolling window size that can achieve the highest effectiveness for school peak shaving when method #1 is used is a window size of 20.

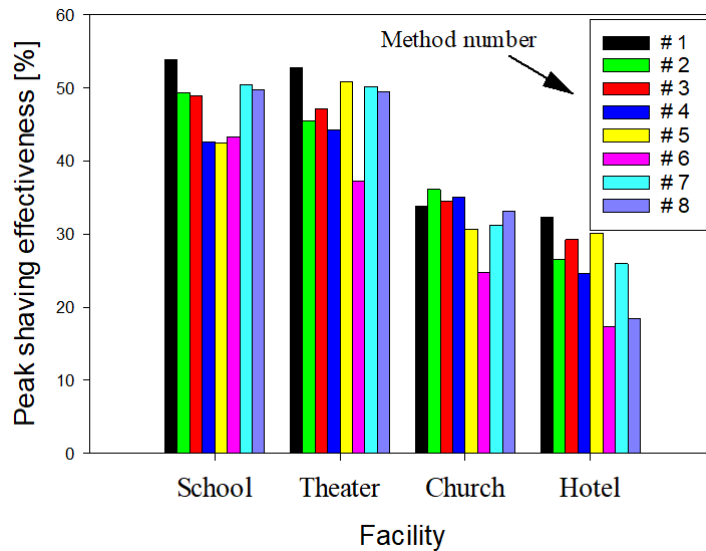


Figure 6.5. The effectiveness of peak shaving for different facilities based on different prediction methods (PV-battery system).

The following conclusion can be drawn from Figure 6.5:

- 1) Common optimal strategy (method #1) recorded the highest effectiveness when used to shave the peak of school, theater, and hotel if the window size is optimized.
- 2) Common optimal strategy with optimized window size outperforms NN prediction in shaving the peak for all considered facilities.
- 3) The NN outperformed ARIMA model in shaving the peak of school, theater, and hotel.

- 4) © forecasting in general is the least efficient.
- 5) The profiles of a school and a theater are easier for peak shaving under the prediction uncertainty than church and hotel. The peaks of school and theater can be shaved with effectiveness around 50%. The best effectiveness of peak shaving of church and hotel was about 35% and 32%, respectively. As we know, the effectiveness is a function of the predictability of the energy profiles' pattern and the severity of the noises.

Table 6-1. The effect of the window size on the effectiveness of school and theater demand peak shaving (church and hotel are removed for brevity).

# days	Effectiveness of methods		Effectiveness of methods	
	(School)	#1	(Theater)	#1
	#1	#3	#1	#3
2	46.65	44.39	39.03	41.25
3	47.57	45.98	39.31	41.41
4	49.16	46.75	37.96	40.01
5	48.57	45.65	37.00	40.87
6	47.32	45.70	40.44	41.65
7	48.05	45.53	45.04	43.84
8	47.35	45.53	46.44	45.00
9	49.84	45.19	45.63	44.36
10	48.02	45.85	45.28	45.00
20	53.88	48.38	49.35	45.89
30	51.63	48.86	51.06	46.55
90	48.77	41.55	52.74	47.09
150	51.98	45.12	51.45	47.20
200	49.51	42.33	50.57	47.18
360	49.02	42.11	50.00	47.03

The monthly peaks before and after shaving using (1) the common optimal strategy and (2) the NN prediction are shown in Figure 6.6. The monthly peaks before and after shaving are given for different types of facilities in Texas for one full year in Figure 6.6.

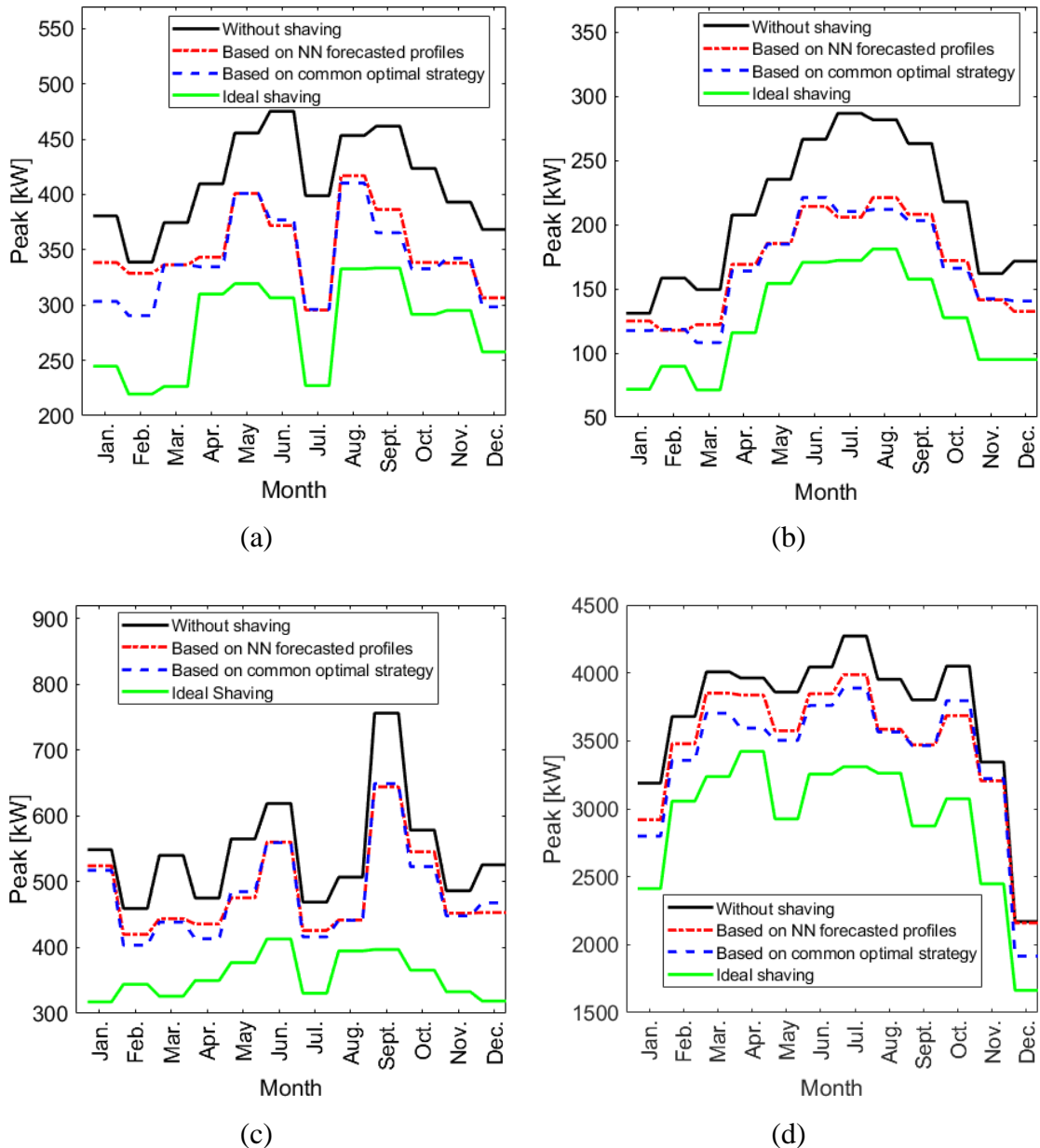


Figure 6.6. Results for shaving the demand peak for one year for (a) school, (b) theater, (c) church, and (d) hotel.

As mentioned in a previous section (Section 6.3.5), the control horizon of one month was broken into days to simplify the controlling problem complexity. The daily

peaks using a controller for a theater based on (1) the common optimal strategy and (2) using a controller based on NN prediction are shown in Figure 6.7 for one full year.

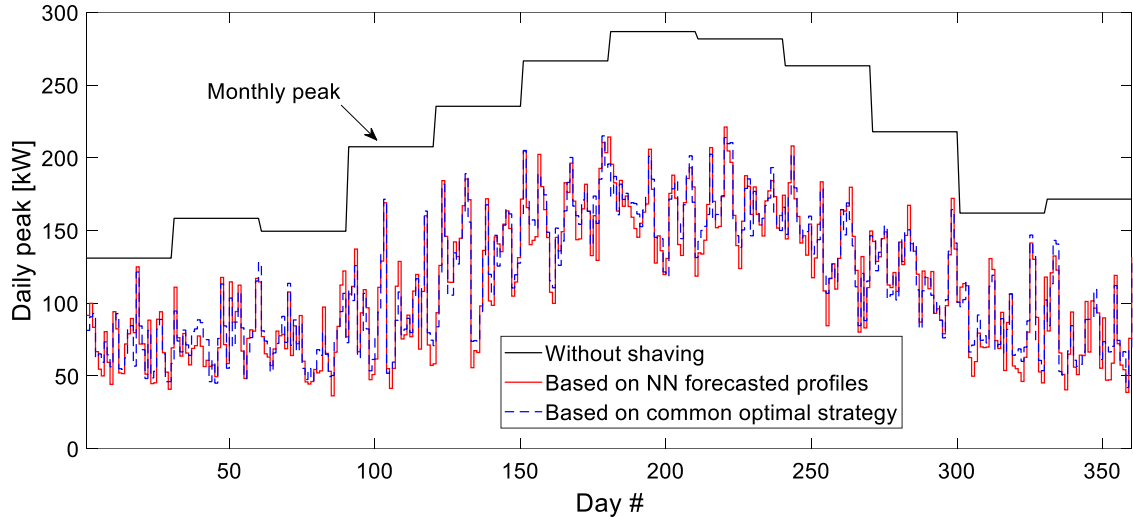


Figure 6.7. The daily peaks after shaving for theater for one year based on NN and the common optimal strategy.

Both controllers recorded an effectiveness of about 50% in shaving the demand peak. However, the one based on the common optimal strategy was found to be a slightly better (2.5% difference).

Predicting the energy profile for one day ahead is a challenging problem, especially for the PV generation. The results reveal that simple prediction tools can be competitive with complex prediction algorithms, such as artificial intelligence and the ARIMA model when applied for peak shaving applications.

### 6.4.2. Battery-only System

In this section, a scheduling controller is evaluated for shaving demand peak in a system with a battery but without a PV system. The effectiveness of the proposed prediction methods in shaving the demand peak is compared and given in Figure 6.8.

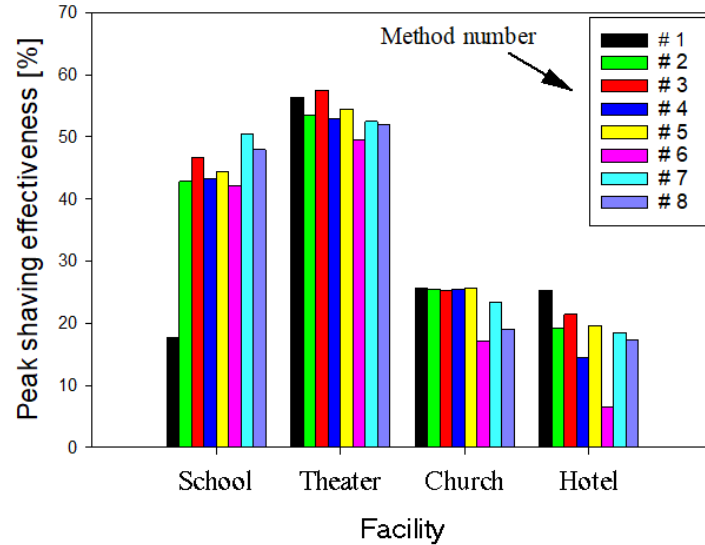


Figure 6.8. The effectiveness of peak shaving for different facilities based on different prediction methods (battery-only system).

The common optimal strategy using a battery-only system is the least efficient for shaving the school peak with an effectiveness of about 17.5% compared to more than 40% for other prediction methods. The naive forecasting even outperformed the common optimal strategy. The NN and ARIMA model recorded the highest effectiveness in shaving the school peak. The common optimal strategy with optimized rolling window size is the most effective for shaving the peaks of hotel and church. The moving average method outperformed other prediction tools in shaving the theaters' peak. The moving

average method is followed by the common optimal strategy in the effectiveness of shaving the theater's peak.

## **6.5. Prediction Performance Metrics**

Different prediction-performance metrics such as, but not limited to, root mean square error (RMSE) and correlation coefficient (R) can be used to compare different prediction methods. However, for peak shaving applications, the most important metric is how closely the shape of the predicted profile resembles the real profile.

The profile shapes of electric demand and PV generation play a significant role in the scheduling problem. The shape of the profile determines when the battery should be set on the charging or discharging mode as well as the rate of charging/discharging. As mentioned in Section 6.3.5, the scheduling horizon of one month is broken into days. For long control horizon of one day in length, the simple prediction methods were found to be competitive with the state-of-art prediction methods in imitating the patterns of electricity consumption and the PV generation. That finding applies to facilities of different types.

## **6.6. Conclusion**

Uncontrolled energy consumption can stress the electrical utility grid. One of the issues uncontrolled grids cause is the high demand short-term peaks. The peaks can be also costly to the consumers. However, different scheduling strategies have been implemented to reduce the demand peak. The demand peak can be also reduced by using alternative energy resources such as solar PV energy. The demand peak can be also reduced by shifting the high demand to the off-peak period, which can be accomplished using an energy storage system. To construct the schedule of the energy storage system, a

forecasting tool is used to predict the electrical load and PV generation profiles. In this work, simple forecasting tools are proven to be competitive with the artificial intelligence and ARIMA model when used to predict the energy profiles to schedule PV-battery systems or Battery-only systems for peak shaving applications. The current study is conducted for different types of commercial and public facilities located in Texas and for a sufficient number of years.

## 7. CONCLUSIONS AND FUTURE WORK

The following two sections provide a summary of the key findings of this study and detail suggestions for possible research directions related to the content of this work.

### 7.1. Summary of the Dissertation

In this dissertation, an optimization framework is proposed to size and schedule a combined solar photovoltaic battery system that is used to shave the demand peak under different pricing policies and by using historical data of load and solar generation.

In Chapter 3, convex optimization is employed to size the solar photovoltaic battery system. The problem is artfully reformulated to be convex for different pricing policies and under different working constraints. A summary of the key findings is listed below.

- Reformulating the optimization problem reduces the computation time significantly. For instance, the computation time, when solving for a binary large vector to handle one of the pricing scenarios, might go to infinity, but if the problem is rewritten using continuous variables, the simulation time decreases to 5 minutes.
- The sizing problem can be reformulated for different scenarios to comply with convex optimization. The convex optimization is very fast, especially when solving for large vectors of one-year length with a 15-minute time step.
- The combined PV-battery system is significantly more effective in reducing the electricity cost for the consumers than both the PV-only system and battery-only system.

In Chapter 4, a scheduling model is proposed to shave the monthly demand peak using a PV-battery system based on predicting load and PV energy. The uncertainty of prediction is handled using stochastic dual-dynamic programming. The key results of this study are summarized below.

- The effectiveness of shaving the monthly peak is around 50% for schools and theaters, and 25-30% for hotels and churches.
- Scheduling without including the effect of uncertainty was found to be more effective in shaving the monthly peak. More precisely, the proposed method of generating scenarios, which are extracted from the errors of prediction of a historical year of data with 10 scenarios for each the load and PV generation at each time step in the control horizon, was not found to be effective in handling the uncertainty of prediction for peak shaving application.
- Although forecasting with a receding horizon will enhance prediction, updating the schedule based on updated forecasts was not always found to be more effective than one-time scheduling of one-time forecasting. That is because that the ability of the forecasting tools to predict the shape of the profile is more important than how close the actual values to the forecasted values.
- Shaving the 15-minute monthly peak is more feasible if the forecasting is done based on the hourly average than on the 15-minute average. The hourly average forecasting is easier and more accurate than the 15-minute prediction as the 15-minute load and PV signals are noisy.

In Chapter 5, the state-of-art prediction methods (artificial neural network and statistical approaches) are compared in forecasting photovoltaic generation. In Chapter 6, simple prediction approaches are proposed and compared with the state-of-art prediction methods in shaving the monthly demand peak. These simple prediction methods are found to be competitive with artificial neural network and statistical approaches in shaving the 15-minute monthly electrical demand peak.

Overall, this research has led to great contributions in the field of energy storage sizing and dispatching. The sizing and scheduling schemes developed in this dissertation can be transferred to different energy technologies such as wind farms, hydroelectric power plants, different pricing policies, and different energy storage methods.

## **7.2. Suggestions for Future Work**

This section details suggestions for possible research directions related to the content of this work.

### **7.2.1. Aging-aware Sizing and Scheduling Model**

The battery's lifespan deteriorates gradually with the normal usage due to the irreversible physical and chemical changes. The excessive charging and discharging actions reduce the battery lifetime significantly, thus the battery needs to be replaced frequently. As batteries are relatively expensive, frequent replacements would mean a high operation cost, and by extension a low return on investment.

In this study, the battery is assumed to have a lifespan of five years. In other words, including the effect of scheduling pattern on the battery lifespan has not been considered in the current work. This study can be extended, however, to study the effect of battery

degradation on both the system sizing and the effectiveness of peak shaving. That can be accomplished by including the cost of battery degradation in the overall cost function. However, the physical-based battery capacity loss model is non-convex, thus including the battery aging cost is associated with optimization challenges. Cai et al. [56] proposed replacing the non-convex degradation physical model with an approximate convex model using a set of piece-wise linear models. In [129], a convex battery-degradation model based on the material fatigue process is proposed.

### **7.2.2. Economics for Different Generation and Storing Technologies**

Different on-site power generation systems and different storage technologies are available in the market. Examples of popular on-site power generation systems are diesel and natural gas engine generators, wind turbines, and fuel cells. Nevertheless, limited research has been undertaken to compare the economics of installing different systems for peak-shaving applications. The sizing procedure and the peak shaving control mechanism, proposed in this dissertation, however, can be applied to different energy systems and different energy storage methods.

### **7.2.3. Inverse-based Design**

As mentioned earlier, the costs of the battery and the solar system are decreasing. Also, there is currently substantial research into lifespan enhancement, as well as operation and conversion efficiency. However, limited resources are available to quote initial prices for PV-battery system components, despite a large number of providers. Also, system's initial prices usually decrease as the scale of the system increases. Owing to economies of

scale, the sizing problem can be solved inversely. The desired reduction in the electricity cost is predefined and then the initial prices are calculated accordingly.

## REFERENCES

- [1] H. C. Hesse, R. Martins, P. Musilek, M. Naumann, C. N. Truong, and A. Jossen, “Economic optimization of component sizing for residential battery storage systems,” *Energies*, vol. 10, no. 7, 2017.
- [2] M. Kaya, “Characterization and optimization of radiation at nano scale: applications in solar cell design,” Texas A&M University, 2020.
- [3] “National Renewable Energy Laboratory.” [Online]. Available: <https://www.nrel.gov/news/program/2020/psh-ensures-resilient-energy-future.html> [accessed 8 April 2022].
- [4] R. Khalilpour and A. Vassallo, “Planning and operation scheduling of PV-battery systems: A novel methodology,” *Renew. Sustain. Energy Rev.*, vol. 53, pp. 194–208, 2016.
- [5] U.S. Energy Information Administration, “Annual energy outlook 2019 with projections to 2050,” 2019.
- [6] Electricity from renewable resources: Status, prospects, and impediments. 2010.
- [7] “Understanding CHP.” [Online]. Available: <https://understandingchp.com/chp-applications-guide/4-2-microturbines/> [accessed 8 April 2022].
- [8] “The leads South Australia.” [Online]. Available: <https://theleadsouthaustralia.com.au/industries/renewables/micro-gas-turbine-could-help-take-homes-off-the-grid/> [accessed 8 April 2022].
- [9] “PV-magazine.” [Online]. Available: <https://www.pv-magazine.com/2021/06/21/concrete-flywheel-storage-system-for-residential-pv/> [accessed 8 April 2022].
- [10] X. Li, “Design and development of a next generation energy storage flywheel,” Texas A&M University, 2018.
- [11] M. H. Albadi and E. F. El-Saadany, “A summary of demand response in electricity markets,” *Electr. Power Syst. Res.*, vol. 78, no. 11, pp. 1989–1996, 2008.
- [12] R. De Sá Ferreira, L. A. Barroso, P. R. Lino, M. M. Carvalho, and P. Valenzuela, “Time-of-use tariff design under uncertainty in price-elasticities of electricity demand: A stochastic optimization approach,” *IEEE Trans. Smart Grid*, vol. 4, no. 4, pp. 2285–2295, 2013.
- [13] H. Liu, Y. Zhang, S. Ge, C. Gu, and F. Li, “Day-ahead scheduling for an electric vehicle PV-based battery swapping station considering the dual uncertainties,” *IEEE Access*, vol. 7, pp. 115625–115636, 2019.

- [14] F. Hafiz, A. R. De Queiroz, and I. Husain, “Coordinated control of PEV and PV-based storages in residential systems under generation and load uncertainties,” *IEEE Trans. Ind. Appl.*, vol. 55, no. 6, pp. 5524–5532, 2019.
- [15] C. Chen, S. Kishore, and L. V. Snyder, “An innovative RTP-based residential power scheduling scheme for smart grids,” *ICASSP, IEEE Int. Conf. Acoust. Speech Signal Process. - Proc.*, pp. 5956–5959, 2011.
- [16] A. S. Bedi, P. V. A. P., M. W. Ahmad, S. Swapnil, K. Rajawat, and S. Anand, “Online algorithms for storage utilization under real-time pricing in smartgrid,” *Electr. Power Energy Syst.*, vol. 101, 2018.
- [17] Y. Xiang, J. Liu, and Y. Liu, “Robust energy management of microgrid with uncertain renewable generation and load,” *IEEE Trans. Smart Grid*, vol. 7, no. 2, pp. 1034–1043, 2016.
- [18] A. P. Rogers and B. P. Rasmussen, “Opportunities for consumer-driven load shifting in commercial and industrial buildings,” *Sustain. Energy, Grids Networks*, vol. 16, pp. 243–258, 2018.
- [19] M. Naumann, R. C. Karl, C. N. Truong, A. Jossen, and H. C. Hesse, “Lithium-ion battery cost analysis in PV-household application,” *Energy Procedia*, vol. 73, pp. 37–47, 2015.
- [20] C. N. Truong, M. Naumann, R. C. Karl, M. Müller, A. Jossen, and H. C. Hesse, “Economics of residential photovoltaic battery systems in Germany: The case of tesla’s powerwall,” *Batteries*, vol. 2, no. 2, 2016.
- [21] A. Rogers and B. Rasmussen, “Consumer-driven shaving of grid demand using a strategically limited incentive,” in *Proceedings of the 2019 Industrial Energy Technology Conference*, 2019.
- [22] A. Rogers and B. Rasmussen, “A generalized approach for commercial and industrial load shifting control,” in *Proceedings of the ASME 2017 Dynamic Systems & Control Conference*, 2017.
- [23] K. Abdulla *et al.*, “Optimal operation of energy storage systems considering forecasts and battery degradation,” *IEEE Trans. Smart Grid*, vol. 9, no. 3, pp. 2086–2096, 2018.
- [24] S. Khemakhem, M. Rekik, and L. Krichen, “Double layer home energy supervision strategies based on demandresponse and plug-in electric vehicle control for flattening power load curves in a smart grid,” *Energy*, vol. 167, pp. 312–324, 2019.
- [25] H. K. Nguyen, J. Bin Song, and Z. Han, “Demand side management to reduce Peak-to-Average Ratio using game theory in smart grid,” *Proc. - IEEE INFOCOM*, pp. 91–96, 2012.

- [26] A. Rahimi, M. Zarghami, M. Vaziri, and S. Vadhva, “A simple and effective approach for peak load shaving using battery storage systems,” in *2013 North American Power Symposium (NAPS)*, 2013, pp. 1–5.
- [27] Y. Shi, B. Xu, D. Wang, and B. Zhang, “Using battery storage for peak shaving and frequency regulation: joint optimization for superlinear gains,” *IEEE Trans. Power Syst.*, vol. 33, no. 3, pp. 2882–2894, 2018.
- [28] C. F. Doc, D. Simply, W. The, and F. On, “A novel peak shaving algorithm for islanded microgrid using battery energy storage system,” *Energy*, vol. 196, p. 117084, 2020.
- [29] X. Dong, G. Bao, Z. Lu, Z. Yuan, and C. Lu, “Optimal battery energy storage system charge scheduling for peak shaving application considering battery lifetime,” in *Informatics in Control, Automation and Robotics*, 2011, pp. 211–218.
- [30] J. Cai, H. Zhang, and X. Jin, “Aging-aware predictive control of PV-battery assets in buildings,” *Appl. Energy*, vol. 236, no. August 2018, pp. 478–488, 2019.
- [31] H. M. Ridha, C. Gomes, H. Hizam, and S. Mirjalili, “Multiple scenarios multi-objective salp swarm optimization for sizing of standalone photovoltaic system,” *Renew. Energy*, vol. 153, pp. 1330–1345, 2020.
- [32] H. M. Ridha, C. Gomes, H. Hizam, and M. Ahmadipour, “Optimal design of standalone photovoltaic system based on multi-objective particle swarm optimization: A case study of Malaysia,” *Processes*, vol. 8, no. 1, 2020.
- [33] D. Magnor and D. U. Sauer, “Optimization of PV battery systems using genetic algorithms,” *Energy Procedia*, vol. 99, no. March, pp. 332–340, 2016.
- [34] A. R. Abul’Wafa, “Energy storage sizing for rooftop grid-connected PV system,” *Electr. Power Components Syst.*, vol. 45, no. 3, pp. 331–343, 2017.
- [35] U. G. K. Mulleriyawage and W. X. Shen, “Optimally sizing of battery energy storage capacity by operational optimization of residential PV-battery systems: An Australian household case study,” *Renew. Energy*, vol. 160, pp. 852–864, 2020.
- [36] J. Weniger, T. Tjaden, and V. Quaschning, “Sizing and grid integration of residential PV battery systems,” *8th Int. Renew. Energy Storage Conf. Exhib. (IRES 2013)*, pp. 1–15, 2013.
- [37] J. Li, “Optimal sizing of grid-connected photovoltaic battery systems for residential houses in Australia,” *Renew. Energy*, vol. 136, pp. 1245–1254, 2019.
- [38] H.-L. Tsai, C.-S. Tu, and Y.-J. Su, “Development of generalized photovoltaic model using MATLAB/SIMULINK,” in *Proceedings of the World Congress on Engineering and Computer Science 2008 WCECS 2008, October 22 - 24, 2008*,

*San Francisco, USA*, 2008, vol. 2008.

- [39] H. Sharadga, S. Hajimirza, and E. P. T. Cari, “A fast and accurate single-diode model for photovoltaic design,” *IEEE J. Emerg. Sel. Top. Power Electron.*, 2020.
- [40] A. Shafi, H. Sharadga, and S. Hajimirza, “Design of optimal power point tracking controller using forecasted photovoltaic power and demand,” *IEEE Trans. Sustain. Energy*, vol. 11, no. 3, pp. 1820–1828, 2020.
- [41] J. S. Stein, W. F. Holmgren, J. Forbess, and C. W. Hansen, “PVLIB: Open source photovoltaic performance modeling functions for Matlab and Python,” *Conf. Rec. IEEE Photovolt. Spec. Conf.*, vol. 2016–Novem, pp. 3425–3430, 2016.
- [42] “PV performance modeling collaborative.” [Online]. Available: <https://pvpmc.sandia.gov/applications/> [accessed 8 April 2022].
- [43] M. Lave, W. Hayes, A. Pohl, and C. W. Hansen, “Evaluation of global horizontal irradiance to plane-of-array irradiance models at locations across the United States,” *IEEE J. Photovoltaics*, vol. 5, no. 2, pp. 597–606, 2015.
- [44] J. A. Duffie, *Solar Engineering of Thermal Processes*, -John A. Duffie, William A. Beckman. 1991.
- [45] N. R. E. Laboratory, “System Advisor Model (SAM).” 2020.
- [46] M. A. Al-Nimr, S. Kiwan, and H. Sharadga, “Simulation of a novel hybrid solar photovoltaic/wind system to maintain the cell surface temperature and to generate electricity,” *Int. J. Energy Res.*, vol. 42, no. 3, pp. 985–998, 2018.
- [47] D. L. King, W. E. Boyson, and J. A. Kratochvil, “Photovoltaic array performance model, SANDIA Report SAND2004-3535,” *Sandia Rep. No. 2004-3535*, vol. 8, no. December, pp. 1–19, 2004.
- [48] M. C. Alonso García and J. L. Balenzategui, “Estimation of photovoltaic module yearly temperature and performance based on nominal operation cell temperature calculations,” *Renew. Energy*, vol. 29, no. 12, pp. 1997–2010, 2004.
- [49] A. Q. Jakhrani, A. R. H. Rigit, A. K. Othman, S. R. Samo, and S. A. Kamboh, “Life cycle cost analysis of a standalone PV system,” *Proceedings of the 2012 International Conference in Green and Ubiquitous Technology, GUT 2012*. IEEE, pp. 82–85, 2012.
- [50] P. P. Groumpos and G. Papageorgiou, “An optimal sizing method for stand-alone photovoltaic power systems,” *Sol. Energy*, vol. 38, no. 5, 1987.
- [51] D. H. Muhsen, T. Khatib, and H. T. Haider, “A feasibility and load sensitivity analysis of photovoltaic water pumping system with battery and diesel generator,” *Energy Convers. Manag.*, vol. 148, pp. 287–304, 2017.

- [52] “MIP formulations and linearizations.” [Online]. Available: <https://www.fico.com/en/resource-access/download/3217> [accessed 8 April 2022].
- [53] J.-Y. SHI, H.-M. KE, C. LI, and J.-J. SHAO, “A coordinated charging strategy for electric vehicles based on hierarchical optimization,” in *EDEP*, 2018.
- [54] Y. Farzambehboudi, O. Erdinc, A. Rifat Boynuerri, L. Ucun, and M. Alioz, “Economic impact analysis of load shifting in a smart household,” *2018 Int. Conf. Smart Energy Syst. Technol. SEST 2018 - Proc.*, 2018.
- [55] B. Xu, A. Oudalov, A. Ulbig, G. Andersson, and D. S. Kirschen, “Modeling of lithium-ion battery degradation for cell life assessment,” *IEEE Trans. Smart Grid*, vol. 9, no. 2, pp. 1131–1140, 2018.
- [56] J. Cai, H. Zhang, and X. Jin, “Aging-aware predictive control of PV-battery assets in buildings,” *Appl. Energy*, vol. 236, no. November 2018, pp. 478–488, 2019.
- [57] F. Conte, S. Massucco, S. Member, M. Saviozzi, F. Silvestro, and S. Member, “A stochastic optimization method for planning and real-time control of integrated PV-storage systems : design and experimental validation,” *IEEE Trans. Sustain. energy*, vol. 9, no. 3, pp. 1188–1197, 2018.
- [58] A. Roy, S. B. Kedare, and S. Bandyopadhyay, “Optimum sizing of wind-battery systems incorporating resource uncertainty,” *Appl. Energy*, vol. 87, no. 8, pp. 2712–2727, 2010.
- [59] S. Seyyedeh Barhagh, M. Abapour, and B. Mohammadi-Ivatloo, “Optimal scheduling of electric vehicles and photovoltaic systems in residential complexes under real-time pricing mechanism,” *J. Clean. Prod.*, vol. 246, p. 119041, 2020.
- [60] D. van der Meer, G. C. Wang, and J. Munkhammar, “An alternative optimal strategy for stochastic model predictive control of a residential battery energy management system with solar photovoltaic,” *Appl. Energy*, vol. 283, no. November 2020, p. 116289, 2021.
- [61] Y. Li, Z. Yang, G. Li, D. Zhao, and W. Tian, “Optimal scheduling of an isolated microgrid with battery storage considering load and renewable generation uncertainties,” *IEEE Trans. Ind. Electron.*, vol. 66, no. 2, pp. 1565–1575, 2019.
- [62] R. Le Goff Latimier, B. Multon, H. Ben Ahmed, F. Baraer, and M. Acquitter, “Stochastic optimization of an electric vehicle fleet charging with uncertain photovoltaic production,” *2015 Int. Conf. Renew. Energy Res. Appl. ICRERA 2015*, vol. 5, pp. 721–726, 2015.
- [63] L. Luo *et al.*, “Optimal scheduling of a renewable based microgrid considering photovoltaic system and battery energy storage under uncertainty,” *J. Energy Storage*, vol. 28, no. August 2019, p. 101306, 2020.

- [64] H. Li, H. Wang, J. Zhou, Z. Tan, J. Yang, and P. He, “Multiobjective optimization model considering demand response and uncertainty of generation side of microgrid,” *Math. Probl. Eng.*, vol. 2020, 2020.
- [65] P. Carpentier, J. Chancelier, and M. De Lara, “Stochastic optimal control of a domestic microgrid equipped with solar panel and battery,” *arXiv Optim. Control*, 2018.
- [66] V. Marano, G. Rizzo, and F. A. Tiano, “Application of dynamic programming to the optimal management of a hybrid power plant with wind turbines, photovoltaic panels and compressed air energy storage,” *Appl. Energy*, vol. 97, 2012.
- [67] S. Rajamand, “Effect of demand response program of loads in cost optimization of microgrid considering uncertain parameters in PV / WT , market price and load demand,” *Energy*, vol. 194, p. 116917, 2020.
- [68] S. Nojavan, M. Majidi, and K. Zare, “Performance improvement of a battery / PV / fuel cell / grid hybrid energy system considering load uncertainty modeling using IGDT,” *Energy Convers. Manag.*, vol. 147, pp. 29–39, 2017.
- [69] T. Li and M. Dong, “Real-time residential-side joint energy storage management and load scheduling with renewable integration,” *IEEE Trans. Smart Grid*, vol. 9, no. 1, pp. 283–298, 2018.
- [70] M. Tavakkoli, E. Pouresmaeil, R. Godina, I. Vechiu, and J. P. S. Catalão, “Optimal management of an energy storage unit in a PV-based microgrid integrating uncertainty and risk,” *Appl. Sci.*, vol. 9, no. 1, 2019.
- [71] U. Raveendrannair, M. Sandelic, A. Sangwongwanich, T. Dragicevic, R. Costa Castello, and F. Blaabjerg, “An analysis of multi objective energy scheduling in PV-BESS system under prediction uncertainty,” *IEEE Trans. Energy Convers.*, vol. 32, no. JULY 2020, pp. 1–10, 2021.
- [72] A. Najafi-Ghalelou, S. Nojavan, K. Zare, and B. Mohammadi-Ivatloo, “Robust scheduling of thermal, cooling and electrical hub energy system under market price uncertainty,” *Appl. Therm. Eng.*, vol. 149, no. April 2018, pp. 862–880, 2019.
- [73] J. Sarshar, S. S. Moosapour, and M. Joorabian, “Multi-objective energy management of a micro-grid considering uncertainty in wind power forecasting,” *Energy*, vol. 139, pp. 680–693, 2017.
- [74] S. Talari, M. Yazdaninejad, and M. R. Haghifam, “Stochastic-based scheduling of the microgrid operation including wind turbines, photovoltaic cells, energy storages and responsive loads,” *IET Gener. Transm. Distrib.*, vol. 9, no. 12, pp. 1498–1509, 2015.
- [75] S. Sharma, Y. Xu, A. Verma, and B. K. Panigrahi, “Time-coordinated

- multienergy management of smart buildings under uncertainties,” *IEEE Trans. Ind. Informatics*, vol. 15, no. 8, pp. 4788–4798, 2019.
- [76] D. Dongol, T. Feldmann, M. Schmidt, and E. Bollin, “A model predictive control based peak shaving application of battery for a household with photovoltaic system in a rural distribution grid,” *Sustain. Energy, Grids Networks*, vol. 16, pp. 1–13, 2018.
  - [77] A. Papavasiliou, Y. Mou, L. Cambier, and D. Scieur, “Application of stochastic dual dynamic programming to the real-time dispatch of storage under renewable supply uncertainty,” *IEEE Trans. Sustain. Energy*, vol. 9, no. 2, pp. 547–558, 2018.
  - [78] O. Dowson, “SDDP.jl.” [Online]. Available: <https://github.com/odow/SDDP.jl> [accessed 8 April 2022].
  - [79] H. Sharadga, S. Hajimirza, and R. S. Balog, “Time series forecasting of solar power generation for large-scale photovoltaic plants,” *Renew. Energy*, vol. 150, pp. 797–807, 2020.
  - [80] F. G. Cabral, “A proposal for a multiplicative autoregressive multivariate periodic model for the generation of inflow scenarios applicable to the planning model of the Brazilian electricity sector,” Federal Univ. Rio de Janeiro, 2016.
  - [81] L. Cambier, “FAST.” [Online]. Available: <https://github.com/leopoldcambier/FAST> [accessed 8 April 2022].
  - [82] Wanqiuchansheng, “SDDPY.” [Online]. Available: <https://github.com/wanqiuchansheng/sddpy> [accessed 8 April 2022].
  - [83] L. Ding, S. Ahmed, and A. Shapiro, “A Python package for multi-stage stochastic programming,” *Optim. Online*, pp. 1–45, 2019.
  - [84] A. Downward, O. Dowson, and R. Baucke, “Stochastic dual dynamic programming with stagewise-dependent objective uncertainty,” *Oper. Res. Lett.*, vol. 48, no. 1, pp. 33–39, 2020.
  - [85] H. Sharadga, S. Hajimirza, and E. P. T. Cari, “A Fast and accurate single-diode model for photovoltaic design,” *IEEE J. Emerg. Sel. Top. Power Electron.*, vol. 9, no. 3, pp. 3030–3043, 2021.
  - [86] S. K. H. Chow, E. W. M. Lee, and D. H. W. Li, “Short-term prediction of photovoltaic energy generation by intelligent approach,” *Energy Build.*, vol. 55, pp. 660–667, 2012.
  - [87] M. A. Al-Nimr, S. Kiwan, and H. Sharadga, “Simulation of a novel hybrid solar photovoltaic/wind system to maintain the cell surface temperature and to generate electricity,” *Int. J. Energy Res.*, vol. 42, no. 3, pp. 985–998, 2018.

- [88] J. Shi, W. J. Lee, Y. Liu, Y. Yang, and P. Wang, “Forecasting power output of photovoltaic systems based on weather classification and support vector machines,” *IEEE Trans. Ind. Appl.*, vol. 48, no. 3, pp. 1064–1069, 2012.
- [89] H. Jiang and L. Hong, “Application of BP neural network to short-term-ahead generating power forecasting for PV system,” *Adv. Mater. Res.*, vol. 608–609, pp. 128–131, 2013.
- [90] A. Mellit, S. Sağlam, and S. A. Kalogirou, “Artificial neural network-based model for estimating the produced power of a photovoltaic module,” *Renew. Energy*, vol. 60, pp. 71–78, 2013.
- [91] C. Chen, S. Duan, T. Cai, and B. Liu, “Online 24-h solar power forecasting based on weather type classification using artificial neural network,” *Sol. Energy*, vol. 85, no. 11, pp. 2856–2870, 2011.
- [92] A. Mellit, A. Massi Pavan, and V. Lughj, “Short-term forecasting of power production in a large-scale photovoltaic plant,” *Sol. Energy*, vol. 105, pp. 401–413, 2014.
- [93] H. Kalgude, V. Jadhav, S. Joshi, M. Joshi, G. Bharambe, and S. Walunj, “Forecasting the output power of solar panel using Lstm-Rnn,” *VJER-Vishwakarma J. Eng. Res.*, vol. 2, no. 1, pp. 113–121, 2018.
- [94] A. Gensler, J. Henze, B. Sick, and N. Raabe, “Deep learning for solar power forecasting – an approach using autoencoder and LSTM neural networks,” in *IEEE International Conference on Systems, Man, and Cybernetics*, 2016, pp. 2858–2865.
- [95] P. Mandal, S. T. S. Madhira, A. Ul haque, J. Meng, and R. L. Pineda, “Forecasting power output of solar photovoltaic system using wavelet transform and artificial intelligence techniques,” in *Procedia Computer Science*, 2012, vol. 12, pp. 332–337.
- [96] N. Al-Messabi, Y. Li, I. El-Amin, and C. Goh, “Forecasting of photovoltaic power yield using dynamic neural networks,” *Proc. Int. Jt. Conf. Neural Networks*, pp. 1–5, 2012.
- [97] M. Bouzerdoum, A. Mellit, and A. Massi Pavan, “A hybrid model (SARIMA-SVM) for short-term power forecasting of a small-scale grid-connected photovoltaic plant,” *Sol. Energy*, vol. 98, no. PC, pp. 226–235, 2013.
- [98] J. G. da S. Fonseca Jr., T. Oozeki, T. Takashima, G. Koshimizu, Y. Uchida, and K. Ogimoto, “Use of support vector regression and numerically predicted cloudiness to forecast power output of a photovoltaic power plant in Kitakyushu, Japan,” *Prog. Photovoltaics Res. Appl.*, vol. 20, pp. 874–882, 2011.
- [99] L. A. Fernandez-Jimenez *et al.*, “Short-term power forecasting system for

- photovoltaic plants,” *Renew. Energy*, vol. 44, pp. 311–317, 2012.
- [100] H.-T. Yang, C.-M. Huang, Y.-C. Huang, and Y.-S. Pai, “A weather-based hybrid method for 1-day ahead hourly forecasting of PV power output,” *IEEE Trans. Sustain. Energy*, vol. 5, no. 3, pp. 917–926, 2014.
- [101] T. Cai, S. Duan, and C. Chen, “Forecasting power output for grid-connected photovoltaic power system without using solar radiation measurement,” in *2nd International Symposium on Power Electronics for Distributed Generation Systems, PEDG 2010*, 2010, pp. 773–777.
- [102] J. Liu, W. Fang, X. Zhang, and C. Yang, “An improved photovoltaic power forecasting model with the assistance of aerosol index data,” *IEEE Trans. Sustain. Energy*, vol. 6, no. 2, pp. 434–442, 2015.
- [103] A. Mellit, “Recurrent neural network-based forecasting of the daily electricity generation of a photovoltaic power system,” *Ecol. Veh. Renew. Energy*, pp. 26–29, 2009.
- [104] I. Ashraf and A. Chandra, “Artificial neural network based models for forecasting electricity generation of grid connected solar PV power plant,” *Int. J. Glob. energy*, vol. 21, pp. 119–130, 2004.
- [105] A. Mellit and A. M. Pavan, “Performance prediction of 20 kW p grid-connected photovoltaic plant at Trieste ( Italy ) using artificial neural network,” *Energy Convers. Manag.*, vol. 51, no. 12, pp. 2431–2441, 2010.
- [106] A. E. Saleh, M. S. Moustafa, K. M. Abo-Al-Ez, and A. A. Abdullah, “A hybrid neuro-fuzzy power prediction system for wind energy generation,” *Electr. Power Energy Syst.*, vol. 74, pp. 384–395, 2016.
- [107] K. I. Wong, C. M. Vong, P. K. Wong, and J. Luo, “Sparse Bayesian extreme learning machine and its application to biofuel engine performance prediction,” *Neurocomputing*, vol. 149, pp. 397–404, 2015.
- [108] A. Kavousi-fard, “A hybrid accurate model for tidal current prediction,” *IEEE Trans. Geosci. Remote Sens.*, vol. 55, no. 1, pp. 112–118, 2017.
- [109] A. T. Hammid, M. H. Bin Sulaiman, and A. N. Abdalla, “Prediction of small hydropower plant power production in Himreen Lake dam (HLD) using artificial neural network,” *Alexandria Eng. J.*, vol. 57, no. 1, pp. 211–221, 2018.
- [110] S. Hochreiter and J. Schmidhuber, “Long short-term memory,” *Neural Comput.*, vol. 9, no. 8, pp. 1735–1780, 1997.
- [111] M. Abdel-Nasser and K. Mahmoud, “Accurate photovoltaic power forecasting models using deep LSTM-RNN,” *Neural Comput. Appl.*, vol. 31, no. 7, pp. 2727–2740, 2019.

- [112] A. Graves, N. Jaitly, and A. R. Mohamed, “Hybrid speech recognition with Deep bidirectional LSTM,” in *2013 IEEE Workshop on Automatic Speech Recognition and Understanding, ASRU 2013 - Proceedings*, 2013, pp. 273–278.
- [113] J. Flaherty and R. Lombardo, “Modelling private new housing starts in australia,” in *In A paper presented in the Pacific-Rim Real Estate Society conference*, 2000, pp. 24–27.
- [114] G. Box, G. Jenkins, G. Reinsel, and G. Ljung, *Time Series Analysis, Forecasting and Control*. John Wiley & Sons, 2015.
- [115] X. Zhang, Y. Liu, M. Yang, T. Zhang, A. A. Young, and X. Li, “Comparative study of four time series methods in forecasting typhoid fever incidence in China,” *PLoS One*, vol. 8, no. 5, 2013.
- [116] P. Chen, A. Niu, D. Liu, W. Jiang, and B. Ma, “Time series forecasting of temperatures using SARIMA: an example from Nanjing,” *IOP Conf. Ser. Mater. Sci. Eng.*, vol. 394, no. 5, 2018.
- [117] H. AKAIKE, “A Bayesian analysis of the minimum AIC procedure,” *Sel. Pap. Hirotugu Akaike*, pp. 275–280, 1998.
- [118] A. K. Mishra and V. R. Desai, “Drought forecasting using stochastic models,” *Stoch. Environ. Res. Risk Assess.*, vol. 19, no. 5, pp. 326–339, 2005.
- [119] M. H. Alsharif, M. K. Younes, and J. Kim, “Time series ARIMA model for prediction of daily and monthly average global solar radiation: the case study of Seoul, South Korea,” *Symmetry (Basel)*, vol. 11, no. 2, 2019.
- [120] G. Notton, D. Mistrushi, L. Stoyanov, and P. Berberi, “Operation of a photovoltaic-wind plant with a hydro pumping-storage for electricity peak-shaving in an island context,” *Sol. Energy*, vol. 157, pp. 20–34, 2017.
- [121] B. Liu, J. R. Lund, S. Liao, X. Jin, L. Liu, and C. Cheng, “Peak shaving model for coordinated hydro-wind-solar system serving local and multiple receiving power grids via HVDC transmission lines,” *IEEE Access*, vol. 8, pp. 60689–60703, 2020.
- [122] H. Sharadga, S. Hajimirza, and R. S. Balog, “Time series forecasting of solar power generation for large-scale photovoltaic plants,” *Renew. Energy*, vol. 150, 2020.
- [123] E. Izgi, A. Öztopal, B. Yerli, M. K. Kaymak, and A. D. Şahin, “Short-mid-term solar power prediction by using artificial neural networks,” *Sol. Energy*, vol. 86, no. 2, pp. 725–733, 2012.
- [124] C. Fan, F. Xiao, and Y. Zhao, “A short-term building cooling load prediction method using deep learning algorithms,” *Appl. Energy*, vol. 195, pp. 222–233,

2017.

- [125] H. Nazaripouya, B. Wang, Y. Wang, P. Chu, H. R. Pota, and R. Gadh, “Univariate time series prediction of solar power using a hybrid wavelet-ARMA-NARX prediction method,” *Proc. IEEE Power Eng. Soc. Transm. Distrib. Conf.*, vol. 2016–July, 2016.
- [126] M. R. Hossain, A. M. T. Oo, and A. B. M. S. Ali, “Hybrid prediction method of solar power using different computational intelligence algorithms,” *2012 22nd Australas. Univ. Power Eng. Conf. "Green Smart Grid Syst. AUPEC 2012*, 2012.
- [127] V. Prema and K. Uma Rao, “Development of statistical time series models for solar power prediction,” *Renew. Energy*, vol. 83, pp. 100–109, 2015.
- [128] Z. Wang, T. Hong, and M. A. Piette, “Building thermal load prediction through shallow machine learning and deep learning,” *Appl. Energy*, vol. 263, no. February, p. 114683, 2020.
- [129] “Industrial Assessment Centers.” [Online]. Available: <https://iac.university/#database> [accessed 24 June 2022].

## APPENDIX A

### SOLAR SYSTEM MODELING AND CALCULATIONS

The single-diode model is used in calculating the PV array parameters, determining the effect of the PV array configuration, and estimating the maximum power that can be produced by a solar PV system. The power produced by the solar PV system is affected by solar radiation and cell temperature. The sun angles and solar radiation calculations are given. A model to estimate the cell temperature is provided. Finally, a flowchart to calculate the maximum power generated by the solar PV system is depicted. The maximum power generated by one PV module will be used as inputs to the optimization framework.

#### A.1. PV Array Diode-modeling

The single-diode model is widely used in the design of solar PV systems. The general *I-V* equation used to describe the behavior of the solar cell, module, or array is given by [38]:

$$I = N_p \cdot I_{PV} - N_p \cdot I_o \left( e^{\frac{V}{a \cdot N_s}} + \frac{I R_s}{a \cdot N_p} - 1 \right) - \frac{\frac{N_p}{N_s} V + I R_s}{R_{sh}} \quad (\text{A.1})$$

where:

$$a = \frac{n k T}{q} \quad (\text{A.2})$$

$$\dot{N}_p = N_p \cdot N_{c-m-p} \quad (\text{A.3})$$

$$\dot{N}_s = N_s \cdot N_{c-m-s} \quad (\text{A.4})$$

where  $\dot{N}_p$  is the number of cells connected in parallel in the array,  $\dot{N}_s$  is the number of cells connected in series in the array,  $N_p$  is the number of PV modules connected in parallel

in the array,  $N_s$  is the number of PV modules connected in series in the array,  $N_{c-m-p}$  is the number of cells, in one module, connected in parallel, and  $N_{c-m-s}$  is the number of cells, in one module, connected in series.

The parameters-extracting model (model 1) developed in [39] was written for one module. This model has been rewritten here and modified to extract the characteristics and the  $I$ - $V$  curves of a solar array.

Equation (A.1) can be simplified, converted to explicit form, using Lambert W-function as given below:

$$I = \frac{-1}{C} W(X) - \frac{B}{A} \quad (\text{A.5})$$

$$A = -\frac{R_{sh} + R_s}{R_{sh} N_p I_o} \quad (\text{A.6})$$

$$B = \frac{-N_p I_{PV} - N_p I_o + \frac{V N_p}{R_{sh} N_s}}{-N_p I_o} \quad (\text{A.7})$$

$$C = \frac{R_s}{a N_p}, D = \frac{V}{a N_s} \quad (\text{A.8})$$

$$X = -\frac{C}{A} \exp(D - \frac{C B}{A}) \quad (\text{A.9})$$

The equations to estimate  $I_{PV,n}$ ,  $I_{o,n}$ ,  $I_o$ , and  $R_{sh,n}$ , given in [39], were written for one module. These equations have been updated here by adopting Equation (A.1) as shown below:

$$I_{PV,n} = I_{o,n} \left( e^{\frac{V_{oc,n}}{a_n N_s}} - 1 \right) + \frac{V_{oc,n}}{N_s R_{sh,n}} \quad (\text{A.10})$$

$$I_{o,n} = \frac{I_{sc,n} R_{s,n} - \frac{N_p}{N_s} V_{oc,n}}{N_p \left( e^{\frac{V_{oc,n}}{a_n N_s}} - e^{\frac{I_{sc,n} R_{s,n}}{a_n N_p}} \right)} \quad (\text{A.11})$$

$$I_o = \frac{(I_{sc,n} + K_I \Delta T) R_s - \frac{\dot{N}_p}{\dot{N}_s} (V_{oc,n} + K_V \Delta T)}{(I_{sc,n} + K_I \Delta T) + \frac{\dot{N}_p}{\dot{N}_s} R_{sh}} \quad (\text{A.12})$$

$$I_{sc,n} R_{s,n} - \frac{\dot{N}_p}{\dot{N}_s} V_{oc,n} + \frac{\frac{\dot{N}_p}{\dot{N}_s} V_{oc,n} - \frac{\dot{N}_p}{\dot{N}_s} V_m - I_m R_{s,n}}{\frac{V_{oc,n}}{e^{a_n \dot{N}_s}} - \frac{V_m}{e^{a_n \dot{N}_s}} + \frac{I_m R_{s,n}}{a_n \dot{N}_p}} \\ R_{sh,n} = \frac{I_m}{\frac{V_{oc,n}}{e^{a_n \dot{N}_s}} - \frac{V_m}{e^{a_n \dot{N}_s}} + \frac{I_m R_{s,n}}{a_n \dot{N}_p} - I_{sc,n}} \quad (\text{A.13})$$

$$R_{sh,n} = \frac{-V_m \frac{\dot{N}_p}{\dot{N}_s} \left( \frac{V_m}{\dot{N}_s} - \frac{I_m R_{s,n}}{\dot{N}_p} \right) \left( I_{sc,n} R_{s,n} - \frac{\dot{N}_p}{\dot{N}_s} V_{oc,n} \right) - \frac{\frac{V_m}{a_n \dot{N}_s} + \frac{I_m R_{s,n}}{a_n \dot{N}_p}}{a_n \left( \frac{V_{oc,n}}{e^{a_n \dot{N}_s}} - \frac{I_{sc,n} R_{s,n}}{a_n \dot{N}_p} \right)} + I_m R_{s,n}}{V_m I_{sc,n} \frac{\frac{V_m}{a_n \dot{N}_s} + \frac{I_m R_{s,n}}{a_n \dot{N}_p}}{a_n \left( \frac{V_{oc,n}}{e^{a_n \dot{N}_s}} - \frac{I_{sc,n} R_{s,n}}{a_n \dot{N}_p} \right)} - I_m \times \left( 1 + R_{s,n} I_{sc,n} \frac{\frac{V_m + I_m R_{s,n}}{a_n}}{a_n \left( \frac{V_{oc,n}}{e^{a_n \dot{N}_s}} - \frac{I_{sc,n} R_{s,n}}{a_n \dot{N}_p} \right)} \right)} \quad (\text{A.14})$$

As mentioned above, model 1 developed in [39] has been rewritten here and used to find the characteristics and the *I-V* curves for a PV array. Multi-crystalline (KC200GT) PV module is adopted in the current work. Some parameters of KC200GT are given in the manufacturer's datasheet. These parameters (short-circuit current, open-circuit voltage, etc.) are given in the datasheet for one PV module ( $N_s = 1$  and  $N_p = 1$ ) consisting of 54 cells connected in series ( $N_{c-m-s} = 54$ ,  $N_{c-m-p} = 1$ ). The modified model can be used, assuming  $N_s = 1$  and  $N_p = 1$ , to find the parameters at the standard conditions for one module:  $I_{PV,n}$ ,  $I_{o,n}$ ,  $I_o$ ,  $R_{sh,n}$ ,  $R_{s,n}$ , and  $n$ . To find these parameters at different operation

conditions we also assume  $N_s = 1$  and  $N_p = 1$ . The effect of  $N_s$ ,  $N_p$  of array is only applied on  $I$ - $V$  equations, Equations (A.1)-(A.9). To sum up, the parameters at the standard condition and different operation conditions are calculated for one module ( $N_s = 1$  and  $N_p = 1$ ). Equations (A.1)-(A.9) are then used to find the  $I$ - $V$  curves of an array.

## A.2. PV Array Configuration

The power-voltage curves of a solar array consisting of eight KC200GT modules but of different configurations are given in Figure A.1.

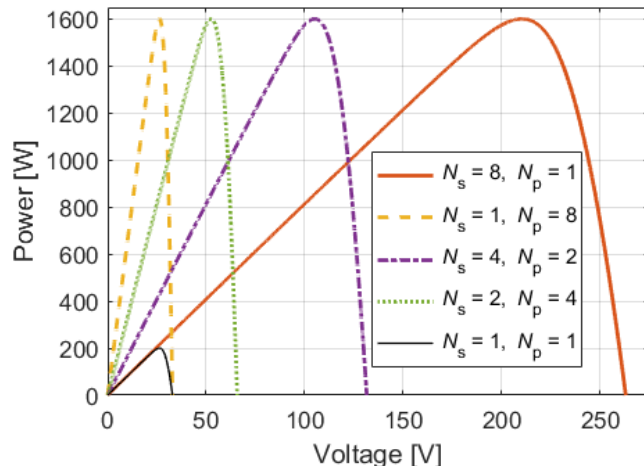


Figure A.1. Power versus voltage curves of arrays of similar sizes but of different configurations, each array consists of eight modules.

Figure A.1 shows that the maximum power of an array does not depend on the configuration (number of modules connected in parallel/series). The configuration is affecting only the voltage of the maximum power point ( $V_m$ ). The system at the maximum power point is found that it has a linear behavior as shown below:

$$P_{m, \text{array}} = P_{m, \text{module}} \times N_{PV} \quad (\text{A.15})$$

$$V_{m, \text{array}} = V_{m, \text{module}} \times N_s \quad (\text{A.16})$$

$$I_{m, \text{array}} = I_{m, \text{module}} \times N_p \quad (\text{A.17})$$

where  $P_m$  is the maximum PV power,  $N_{PV}$  is the total number of modules,  $N_s$  is the number of PV modules connected in series,  $N_p$  is the number of PV modules connected in parallel,  $I_m$  is the current at the maximum power point.

However, the value of the voltage at MPP and the  $I$ - $V$  curves are not the main points of interest in this work. Sections A.1 and A.2 show that the PV array configuration can be decided later on after optimizing the system size. In other words, the optimization algorithm will return only the total number of PV modules without any information about how many modules should be connected in series/parallel.

### A.3. Maximum Power Point Estimation

In the current work, the PV system is assumed to be equipped with a maximum power point tracking controller. The most well-known and simple searching algorithm to estimate the maximum power generated by a solar array is the perturb and observation algorithm (P&O) [40]. In this searching algorithm, we keep changing the operating voltage by a small step-change in one direction. If the voltage-change leads to an increase in the PV array's power, we keep changing the voltage in the same direction. Otherwise, we tune the voltage in the reverse direction. PV-LIB toolbox [41]-[42], an open-source library written in MATLAB and Python, can be also used to estimate the maximum power of PV array for 500 specific PV modules. The library is based on correlations developed in Sandia's laboratory and based on the single diode model. We adopted Sandia's model (See the PV-LIB MATLAB library given in [42]) to estimate the maximum power

produced by a PV module at given solar radiation (Plane-of-array (*POA*) irradiance) and at a given cell temperature. The following two sections show how to calculate these values: plane-of-array irradiance and cell temperature.

#### A.4. Plane-of-array (*POA*) Irradiance

The amount of solar radiation incident on a tilted surface can be estimated using the horizontal solar irradiance measurements/calculations and by the following equations [43]:

$$POA = \text{beam irradiance} + \text{sky-diffuse radiation} + \text{ground-diffuse radiation} \quad (\text{A.18})$$

$$\begin{aligned} POA = DNI \times \cos(\theta) + DHI \times \frac{1 + \cos(\theta)}{2} \\ + GHI \times (0.012 \times \theta_Z - 0.04) \times \frac{1 - \cos(\theta)}{2} \end{aligned} \quad (\text{A.19})$$

The angle of incidence ( $\theta$ ) is obtained as follows (Equation 1.6.3 in [44]):

$$\cos(\theta) = \cos(\theta_Z) \times \cos(\beta) + \sin(\theta_Z) \times \sin(\beta) \times \cos(\gamma_s - \gamma) \quad (\text{A.20})$$

The sun angles, zenith angle ( $\theta_Z$ ) and solar azimuth angle ( $\gamma_s$ ), can be estimated using the equations given in the text book [44] (see Equations 1.6.1, 1.6.5, 1.6.6a – 1.6.6g). Figure A.2 shows the solar sun angles obtained by both SAM software [45] and the equations given in [44] for August 20. The values of irradiance components *DNI*, *DHI*, and *GHI* at a given time and for a given location, can be obtained by SAM software [45], where  $\beta$  is the title angle, and  $\gamma$  is azimuth angle of the PV array. The zenith angle ( $\theta_Z$ ) and the angle of incidence ( $\theta$ ) are higher than 90° at the night (see Figure A.2 and Figure A.3). It is important to mention that the convention used in NREL SAM software [45] (and used here in the current paper) for the azimuth angle is clockwise from due to the

north. The solar book [44] definition is clockwise from due to the south. The angle obtained by the solar book equations has been converted to be in the same convention of SAM software for comparison purposes.

The tilt angle and the azimuth angle of the PV array need to be optimized. These two angles have been optimized for a facility in Texas, and the optimal values to maximize the solar energy captured by the solar array collector over the year are  $\beta = 25.73^\circ$  and  $\gamma = 185.4^\circ$ . Thus, the solar array is facing the south. The optimization of the tilt angle and the azimuth angle was accomplished by the genetic algorithm. However, since the number of optimization variables is small, the optimal angles can be obtained by a simple searching algorithm in a short computation time. It is worth mentioning that the genetic algorithm consumed only 3 seconds to optimize these angles based on historical data of one year.

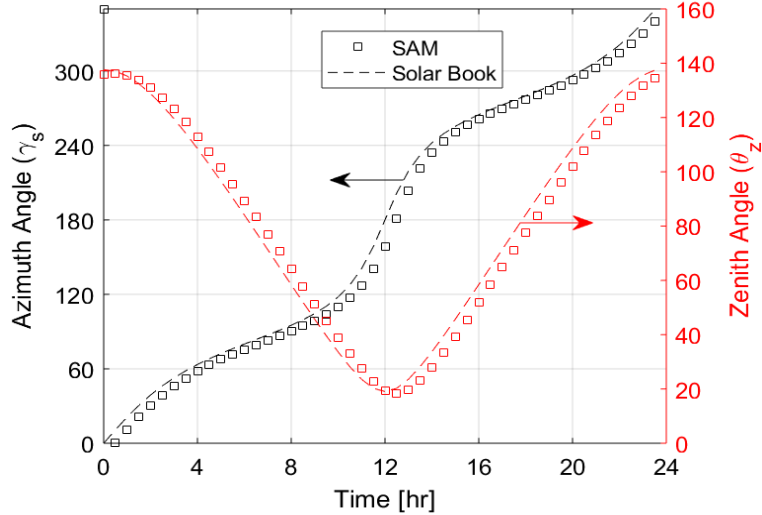


Figure A.2. Sun angles (zenith and azimuth) are obtained by SAM software [45] and calculated using solar book equations [44] for August 20.

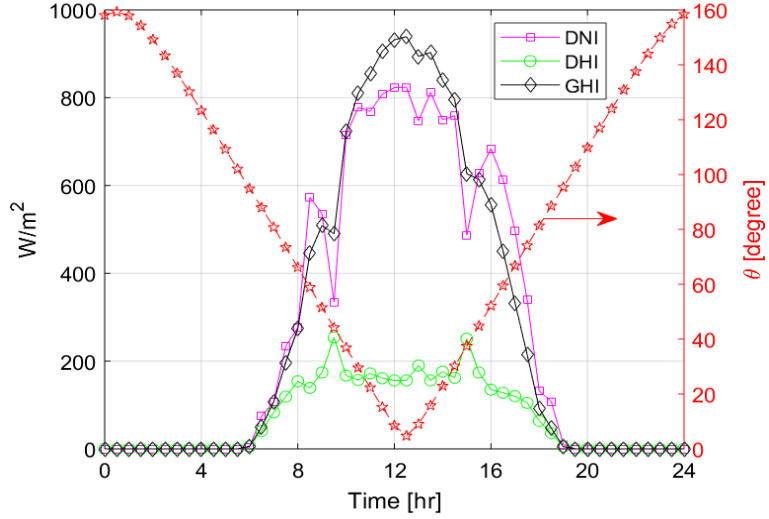


Figure A.3. The solar radiation components and the angle of incidence for August 20.

### A.5. Cell Temperature

The amount of power produced by the solar array is affected by the temperature of the PV cell [46]. The module temperature ( $T_m$ ) can be estimated using Sandia PV module temperature model as shown below [42]:

$$T_m = POA \times (e^{a + b W_s}) + T_a \quad (\text{A.21})$$

The parameters ( $a$  and  $b$ ) depend on the module configuration and materials as well as the method of PV array mounting.  $T_a$  is the ambient temperature and  $W_s$  is the wind speed. The cell temperature is then estimated as shown below [42], [47]:

$$T_c = T_m + \frac{POA}{POA_o} \Delta T \quad (\text{A.22})$$

where  $\Delta T$  is the temperature difference between the cell and the module back surface at the reference irradiance level and  $POA_o$  is reference solar irradiance on module, (1000 W/m<sup>2</sup>).

Another way to estimate the module temperature is by using the nominal operating cell temperature correlations as shown in [48]; however, the Sandia model is adopted for the current work.

#### **A.6. Solar Calculations Flow Chart**

Figure A.4 shows the flow chart used to calculate the maximum power generated by one PV module which is used as input to the optimization algorithm (see Figure 3.2). The optimization algorithm will return the number of PV modules, size of the battery as well as the charging and discharging vector. The genetic algorithm (GA) was used to optimize the mounting angles of the PV array assuming the PV system is fixed. The GA consumed 3 seconds to optimize these angles based on solar radiation historical data of one year.

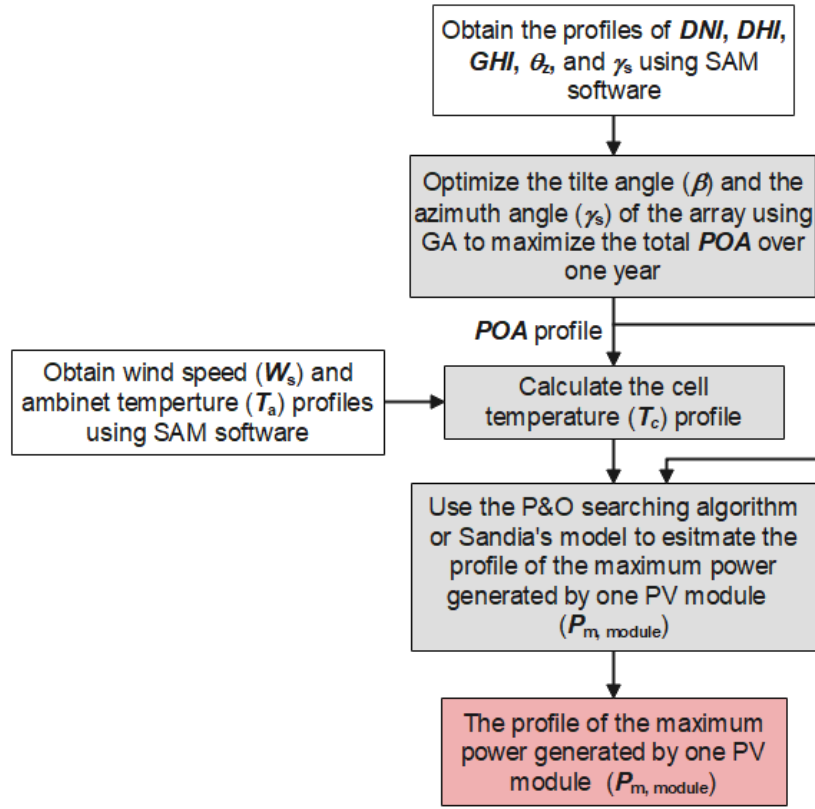


Figure A.4. PV-power calculations (one-time calculation).

## APPENDIX B

### CVX APPLICATION

CVX is a MATLAB application for disciplined convex programming. You can install and import CVX library to your MATLAB at (<http://cvxr.com/>) and obtain the licenses at (<http://cvxr.com/cvx/licensing/>).

The CVX library uses solvers to solve. SDPT3, MOSEK, and GUROBI are examples of solvers CVX library can use. SDPT3 is an academic solver that can solve for continuous variables only. MOSEK and GUROBI are commercial solvers which can be used to solve for both binary and continuous variables or mixed.

Many researchers claimed that GUROBI solver is the fastest solver for convex optimization. However, GUROBI solver was not used in the current work as MOSEK solver was found to be satisfying in terms of the computation cost. MOSEK solver is much faster than the SDPT3 solver. MOSEK can be paired with CVX, more information can be found at (<http://cvxr.com/cvx/doc/mosek.html>).